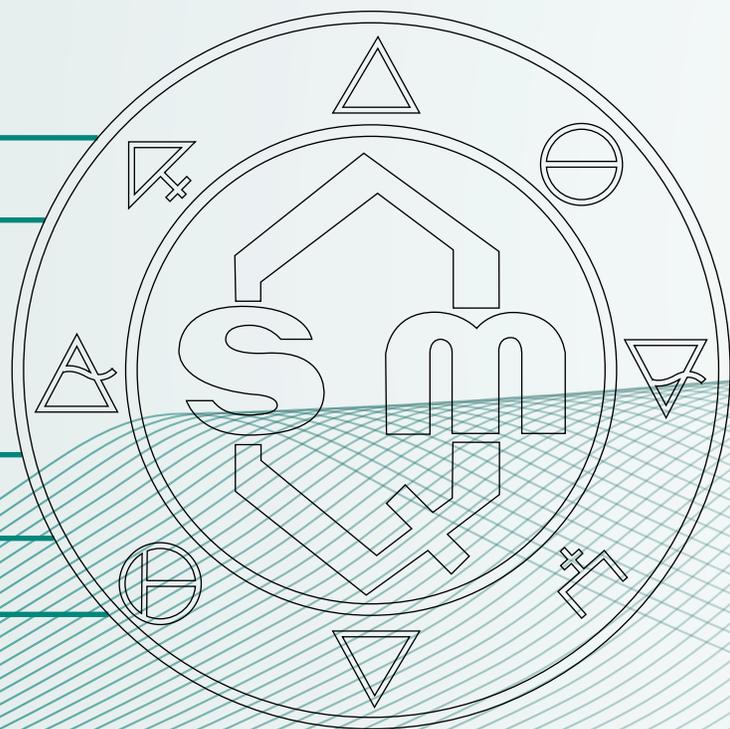




JOURNAL *of the* MEXICAN CHEMICAL SOCIETY

(J. Mex. Chem. Soc.)

Former Revista de la Sociedad Química de México (Rev. Soc. Quím. Mex.)



Special Issue
Dedicated to Prof. Joaquín Tamariz

J. Mex. Chem. Soc.

Volume 68

Issue 1

January-March

Year 2024

Quarterly publication

www.jmcs.org.mx

Mexico City



JOURNAL *of the* MEXICAN CHEMICAL SOCIETY

(J. Mex. Chem. Soc.)

Former Revista de la Sociedad Química de México (Rev. Soc. Quím. Mex.)



Special Issue
Dedicated to Prof. Joaquín Tamariz

J. Mex. Chem. Soc.

Volume 68

Issue 1

January-March

Year 2024

Quarterly publication

www.jmcs.org.mx

Mexico City

The *Sociedad Química de México* was founded in 1956 as a non-profit association to promote the development of the professionals and students of chemistry in education, research, services and industry, and for the diffusion of chemical knowledge. The *Sociedad Química de México* organizes annually the *Mexican Congress of Chemistry* and the *National Congress of Chemical Education*, both congresses include activities of current interest for professionals and students of the chemical sciences. It grants annually the “*Andrés Manuel del Río*” *National Award of Chemistry* in the Academic area (field of research and field of education) and in the Technological area (field of technological development). It also grants each year the *Rafael Illescas Frisbie Best Bachelor, Master and Doctoral Thesis in Chemical Sciences Awards* and the biennial *Award of the Sociedad Química de México in honor of the Doctor Mario J. Molina, directed to the professionals in Chemistry Sciences*.

The *Journal of the Mexican Chemical Society* (*J. Mex. Chem. Soc.*) is the official journal of the *Sociedad Química de México*, it was published as *Revista de la Sociedad Química de México* (*Rev. Soc. Quím. Mex.*) from 1957 to 2003, changing its name in 2004. The *Journal of the Mexican Chemical Society* (*J. Mex. Chem. Soc.*) is a scientific, blind, peer reviewed, and open access, free of charge publication that covers all areas of chemistry and its sub-disciplines (i.e. medicinal chemistry, natural products, electrochemistry, material science, computational chemistry, organic chemistry, bioinorganic chemistry, etc). It is devoted to facilitating the worldwide advancement of our understanding of chemistry. It will primarily publish original contributions of research in all branches of the theory and practice of chemistry in its broadest context as well as critical reviews in active areas of chemical research where the author has published significant contributions. The *J. Mex. Chem. Soc.* is a quarterly publication in which language of submission and publication is English. To be suitable for publication in *J. Mex. Chem. Soc.*, manuscripts must describe novel aspects of chemistry, high quality of results and discussion an excellent bibliographic support, and contribute to the development of the field. Routine or incremental works are not suitable for publication in *J. Mex. Chem. Soc.* Authors are encouraged to send contributions in electronic form. Our online submission system guides you stepwise through the process of entering your article details and uploading your files. The *Sociedad Química de México* also publishes since 2007 articles of general interest in the *Boletín de la Sociedad Química de México*.

La *Sociedad Química de México* fue fundada en 1956 como una agrupación sin fines de lucro para promover el desarrollo de los profesionales y estudiantes de la química en las áreas educativa, investigación, servicios e industria, y para difundir el conocimiento de la química. La *Sociedad Química de México* organiza anualmente el *Congreso Mexicano de Química* y el *Congreso Nacional de Educación Química*, en los cuales se desarrollan diversas actividades de interés para los profesionales y estudiantes de las ciencias químicas. Asimismo, otorga anualmente el *Premio Nacional de Química “Andrés Manuel del Río”* en el área Académica (campos de docencia e investigación) y en el área Tecnológica (campo de Desarrollo Tecnológico). También otorga anualmente el *Premio a las Mejores Tesis de Licenciatura, Maestría y Doctorado en Ciencias Químicas, Rafael Illescas Frisbie*. De manera bienal otorga el *Premio de la Sociedad Química de México en Honor al Doctor Mario J. Molina, dirigido a los profesionistas de las Ciencias Químicas*.

El *Journal of the Mexican Chemical Society* (*J. Mex. Chem. Soc.*), es la revista oficial de la *Sociedad Química de México*. Desde 1957 y hasta 2003 fue publicada como *Revista de la Sociedad Química de México* (*Rev. Soc. Quím. Mex.*), cambiando su nombre en 2004. Es una publicación trimestral que tiene como objetivo coadyuvar al avance del entendimiento de la química; las instrucciones para los autores aparecen en cada fascículo. La *Sociedad Química de México* también publica desde 2007 artículos de interés general en el *Boletín de la Sociedad Química de México*

Journal of the Mexican Chemical Society
(*J. Mex. Chem. Soc.*)

ISSN-e: 2594-0317
ISSN 1870-249X

former

Revista de la Sociedad Química de México
(*Rev. Soc. Quím. Mex.*)

ISSN 0583-7693

Journal of the Mexican Chemical Society (*J. Mex. Chem. Soc.*)

Quarterly publication.

Editor-in-Chief: Prof. Alberto Vela Amieva

Indexed Journal

Certificate of reserved rights granted by the Instituto Nacional del Derecho de Autor (INDAUTOR): 04-2005-052710530600-102

Certificate of lawful title and content: Under procedure

Postal registration of printed matter deposited by editors or agents granted by SEPOMEX: IM09-0312

Copyright © Sociedad Química de México, A.C.

Total or partial reproduction is prohibited without written permission of the right holder.

The Figures/schemes quality and the general contents of this publication are full responsibility of the authors.

Edited and distributed by Sociedad Química de México, A.C.

Barranca del Muerto 26, Col. Crédito Constructor,

Del. Benito Juárez, C.P. 03940, Mexico City.

Phone: +5255 56626837; +5255 56626823

Contact: soquimex@sqm.org.mx

<https://www.sqm.org.mx>

Editorial assistance: jmcs@sqm.org.mx

<https://www.jmcs.org.mx>



Table of Contents

Editorial

A special Issue for an exemplary Professor: Joaquín

i-iii Tamariz Mascarúa

Gabriel Cuevas*

Articles

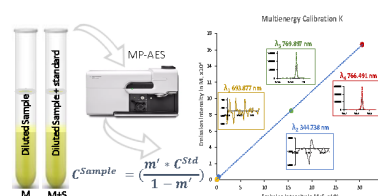
1-17 Carbon Dioxide Capture Using Ionic Liquids Containing Amino Acid-Type Anions. Effect of the Cation, Anion on the Absorption Efficiency

Gabriela Barbosa-Moreno, Nohra V. Gallardo-Rivas*, Rafael Martínez-Palou*



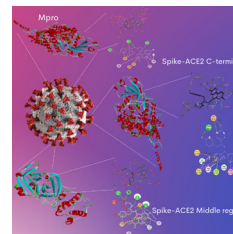
18-28 Determination of Sodium, Potassium, Calcium and Magnesium in Urine, Using Microwave Plasma - Atomic Emission Spectrometry and Multi-Energy Calibration

Tania Lizeth Espinoza Cruz, Kazimierz Wrobel, Eunice Yanez Barrientos, Alma Rosa Corrales Escobosa, Ma Eugenia Garay-Sevilla, Francisco Javier Acevedo-Aguilar, Katarzyna Wrobel*



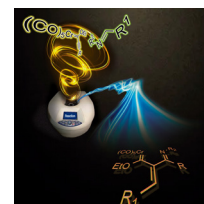
29-55 Synthesis, Characterization, and Molecular Docking of Casiopeinas® with Dipeptides as Secondary Ligand; Potential Inhibitors of SARS-Cov-2 Transmembrane Proteins

Luis Gabriel Talavera-Contreras, Luis Felipe Hernández-Ayala, Virginia Gómez-Vidales, María Lourdes Villar-Cuevas†, Lena Ruiz-Azuara*



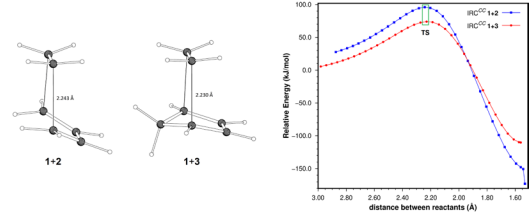
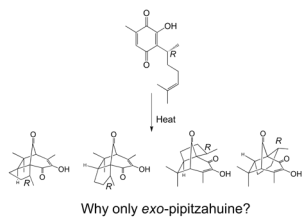
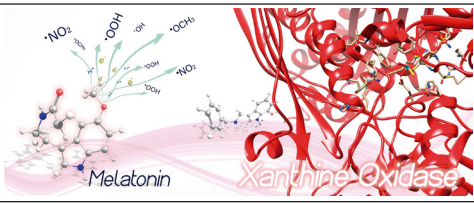
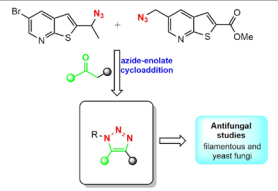
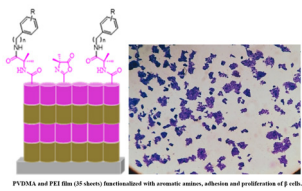
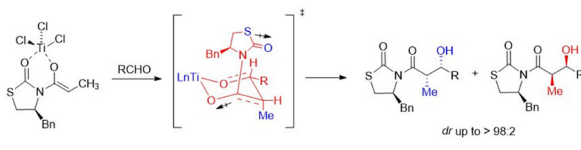
56-72 Microwave-Assisted Reactivity of a Fischer Alkynyl Carbene Complex with Benzylidene Anilines

Alberto Feliciano, Miguel A. Vázquez*, Iván Velazco-Cabral, Julio López, Luis Javier Benítez-Puebla, Salvador Mastachi-Loza, Selene Lagunas-Rivera, Marco A. García-Revilla, Francisco Delgado*



* The asterisk indicates the name of the author to whom inquiries about the paper should be addressed.

Table of Contents

73-87	<p>The Contribution of Dispersion to the Intrinsic Energy Barriers of Neutral Model Diels-Alder Reactions Hugo Alejandro Jiménez-Vázquez*, Luis Almazán, Adriana Benavides</p>	 <p>The figure shows two transition state structures for Diels-Alder reactions, labeled 1+2 and 1+3, with bond lengths of 2.281 Å and 2.284 Å respectively. To the right is a plot of Relative Energy (kJ/mol) versus distance between reactants (Å). The plot shows two curves: a red curve for the 1+2 reaction and a blue curve for the 1+3 reaction. Both curves show a peak at the transition state (TS) around 2.05 Å. The 1+2 reaction has a higher energy barrier than the 1+3 reaction.</p>
88-98	<p>Understanding Experimental Facts for the Transformation of Perezone into α- and β-pipitzols Luis Mauricio Murillo-Herrera, Fátima Soto-Suárez, Eduardo Hernández-Huerta, Karla Ramírez-Gualito, Mariana Ortiz-Reynoso, Ramiro F. Quijano-Quiñones*, Gabriel Cuevas*</p>	 <p>The reaction scheme shows Perezone reacting under heat to form α- and β-pipitzols. The structures of the products are shown with their respective substituents (R' and R'').</p>
99-112	<p>DFT and Molecular Docking Studies of Melatonin and Some Analogues Interaction with Xanthine Oxidase as a Possible Antiradical Mechanism Brenda Manzanilla, Minerva Martínez-Alfaro, Juvencio Robles*</p>	 <p>The figure illustrates the molecular docking of Melatonin and its analogues (with substituents like -NO₂, -OCH₃, -OH, -OCH₂) with Xanthine Oxidase. The protein structure is shown in red, and the ligands are shown in white and blue. The docking site is highlighted in pink.</p>
113-123	<p>Synthesis and Evaluation of the Antifungal Sensibility of Novel Thienopyridine 1,2,3-Triazole Derivatives Ramírez-Villalva Alejandra, Cervantes-Rebolledo Claudia, González-González Carlos A., Mastachi-Loza Salvador*</p>	 <p>The figure shows the synthesis of thienopyridine 1,2,3-triazole derivatives via azide-enolate cycloaddition. The resulting compounds are evaluated for antifungal activity against filamentous and yeast fungi.</p>
124-134	<p>Synthesis, <i>in vitro</i> Antitrichomonal Activity, and Docking Study of <i>N</i>-[(4-substituted phenyl)-1,3-thiazol-2-yl]-4-substituted Benzenesulfonamides Rubén M. Carballo, Héctor A. Peniche-Pavía, Ramiro Quijano-Quiñones, David Cáceres-Castillo, Gumersindo Mirón-López, Manlio Graniel-Sabido, Andrea Reyes-Cuapio, Rosa E. Moo-Puc, Lía Valencia-Chan, Gonzalo J. Mena-Rejón</p>	 <p>The figure shows the synthesis of 13 compounds (7e) where R₁ = R₂ = NO₂. The compounds are evaluated for antitrichomonal activity with IC₅₀ = 0.27 μM / SI > 4500. A molecular docking study is also shown for Trichomonas vaginalis ferredoxin.</p>
135-143	<p>Fabrication of a Reactive Functionalized Microfilm with Aromatic Amines Applied to the Growth of Langerhans Cells Martha Ávila-Cossío, Ignacio A. Rivero*, Victor García-González</p>	 <p>The figure shows the fabrication of a reactive functionalized microfilm (PVDMa and PEG film) with aromatic amines, which is used for the adhesion and proliferation of Langerhans cells.</p>
144-155	<p>4(S)-Benzyl-1,3-thiazolidin-2-one a Novel Chiral Auxiliary for Asymmetric Aldol Coupling through Titanium Enolates Dulce M. Mejía-Nuñez, Salvador Mastachi-Loza, Diego Martínez-Otero, Moisés Romero-Ortega*</p>	 <p>The reaction scheme shows the synthesis of 4(S)-Benzyl-1,3-thiazolidin-2-one as a chiral auxiliary for asymmetric aldol coupling through titanium enolates. The yield is reported as dr up to > 98:2.</p>

* The asterisk indicates the name of the author to whom inquiries about the paper should be addressed.

Table of Contents

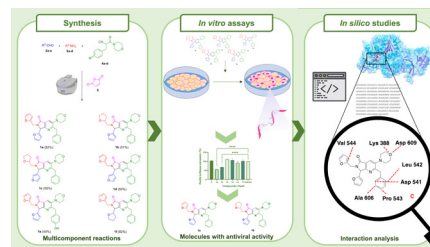
156-169 **Alpha-glucosidase and Alpha-amylase Inhibitors
Derived from Naturally Occurring Prenylated
Isoflavones**

*Brandon Hernández-Gutiérrez, María C. Cruz-López,
Omar Gómez-García, Elvia Becerra-Martínez, Fabiola E.
Jiménez-Montejo, Aarón Mendieta-Moctezuma**



170-183 **In Vitro and In Silico Studies of Bis-furyl-pyrrolo[3,4-b]
pyridin-5-ones on Dengue Virus**

*Ivette Morales-Salazar, Carlos E. Garduño-Albino,
Flora P. Montes-Enríquez, Atilano Gutiérrez-Carrillo,
Yareli Rojas-Aguirre, Nancy Viridiana Estrada-Toledo,
Jorge Sandoval-Basilio, Sofía Lizeth Alcaraz-Estrada*,
Erik Díaz-Cervantes*, Eduardo González-Zamora*,
Alejandro Islas-Jácome**



* The asterisk indicates the name of the author to whom inquiries about the paper should be addressed.

A special Issue for an exemplary Professor: Joaquín Tamariz Mascarúa.*

Gabriel Cuevas^{1*}.

¹ Instituto de Química. Universidad Nacional Autónoma de México. Circuito Exterior, Ciudad Universitaria 04510, Coyoacán.

***Guest editor:** ¹Gabriel Cuevas, email: gecgb@unam.mx

DOI: <http://dx.doi.org/10.29356/jmcs.v68i1.2191>

With a festive tone, but with reflective spirit, let me access to a warmer speech since, through this special issue, the *Journal of the Mexican Chemical Society* (*J. Mex. Chem. Soc.*) thanks Prof. Dr. Joaquín Tamariz Mascarúa for his contributions to the development and welfare of the Mexican Chemical Society. From the point of view of our society, I will point out his omnipresence in our congresses. From the audience's side it must be said that no speaker was spared from his sharp and accurate questions, capable of highlighting the speaker's contributions and allowing the work presented to be assessed. The *Journal of the Mexican Chemical Society* (*J. Mex. Chem. Soc.*) and the *Boletín de la Sociedad Química de México* (*Bol. Soc. Quím. Mex.*), edited by Dr. Mariana Ortiz Reynoso, are benefited from their contributions. I invite you to review his papers and enjoy their scholarship, to value the concepts presented there, and the diversity of scientific problems he addresses. Reading his papers is always stimulating for students and researchers.

Prof. Tamariz has given us his time by participating in countless number of committees to evaluate works, to designate awards winners, and decide on aspects of our society's daily lives. He also was awarded with the Andrés Manuel de Río Prize in 2007 for his Scientific Research, the highest distinction we grant as an association.

Prof. Joaquín was editor-in-chief of the *J. Mex. Chem. Soc.*, just at the time when the *Revista de la Sociedad Química de México* became an indexed Journal and become part of the complex world of periodic evaluation.

Prof. Tamariz decided to address *the problem of the synthesis of new or naturally occurring compounds with relevant properties*. Organic

synthesis is a fascinating field, because through this, the predictive capability of the concepts of Chemistry is manifested, in contrast to considering it, in terms of their explanatory possibilities.



Photograph. 1. Photograph of Prof. Dr. Joaquín Tamariz.

To perform serious research in Mexico is a great due to the inequity in terms of the provision of analytical infrastructure and founding. Joining the Escuela Nacional de Ciencias Biológicas (IPN) as an independent researcher could seem like suicide; but instead, today, Joaquín leaves behind one of the best analytical infrastructures in the country and a solid Organic Chemistry Department.

The first projects in which he participated announced his destiny: Synthetic study to obtain 4'-benzyloxy-6-hydroxy-5,7,3'-trimethoxy-flavone in 1975 and Convergent synthesis of substituted furans in 1977, carried out under the supervision of whom was his professor, colleague and friend, Dr. Gustavo García de la Mora.

Prof. Tamariz is immediately identified with the reaction described for the first time by Otto Diels and Kurt Alder in 1928 with which they won the Nobel Prize in Chemistry in 1950. We owe Joaquín the incorporation of the use of computational methods to explain the origin of the selectivity of this reaction. He ingeniously employed transmission electron and photoelectron spectroscopy to understand the relationship between the energies of the frontier orbitals of dienes, and dienophiles, and their selectivity. He also was interested in the reagents used in this reaction to carry out multiple synthetic transformations and addressed the difficult problem of the reactivity of captodative olefins. Thus, he described conditions in which the selectivity of the transformations increased significantly.

He has also successfully addressed inverse electronic demand reactions and established the effect of commonly used catalytic compounds in this transformation. Joaquín not only used captodative olefins to study cycloaddition reactions, but also, they have allowed him to address the fascinating 1,3-dipolar cycloadditions. Of course, the topic involves extraordinary challenges. To make it more interesting, Dr. Tamariz decided to use nitrones as a dipole, which lead to unsuspected difficulties. Here, the theoretical rationalization required the use of the concepts emanating from the theory of density functionals to predict the selectivity of the reactions.

With his research group, Dr. Tamariz has developed the synthesis of fundamental compounds such as basic derivatives of indol's and carbazols. One of Prof. Tamariz's interesting contributions is the synthesis and study of α -asarone's properties.

Aware of the general national problems, Dr. Joaquín Tamariz has dedicated efforts to control the beetle plague (of the genus *Dendroctonus*) that has had a devastating impact on pine populations in the world's forests, but especially in Mexico. Thus, he has developed the synthesis of some derivatives that have an activity comparable to that of natural pheromones involved in the biochemical processes of communication and reproduction of insects.

The compounds obtained for the study of basic phenomena led him to the preparation of several complex compounds, with fascinating properties. It required the development of new synthetic schemes supported by new strategies, as he showed us in his conference during the scientific congress in 2023:

Synthetic design of aza-heterocycles as building blocks.

Prof. Joaquín Tamariz taught us to publish only when you have something relevant to say, or when fully demonstrated results are rigorously interpreted. He has had careful review when a document falls into his hands. He has known how to resist and assume the consequences of opposing the trend, which has greatly degraded world science with more than 10,000 research papers retracted in 2023 (Van Noorden, R. *Nature*, **2023**, 624, 479-481, DOI: <https://doi.org/10.1038/d41586-023-03974-8>) product of publishing for the sake of publishing, seeking easy citations, or participating in meaningless collaborations accumulating repetitive works and graduating students only for statistical purposes.

Originally from Mexico City, Prof. Dr. Joaquín Tamariz Mascarúa was until a few months ago, Professor at the Escuela Nacional de Ciencias Biológicas (ENCB, IPN). He studied Chemistry and Master's in Organic Chemistry at the Faculty of Chemistry at UNAM he completed doctorate studies in Organic Chemistry at the University of Lausanne (Switzerland) (1983) and his postdoctoral stay with Professor Louis S. Hegedus at Colorado State University (1989-1990). He was visiting Professor at West Virginia University (1997-1998). He has supervised 25 bachelor's theses, 47 master's and 32 doctoral theses, starting at a time when no one was interested in postgraduate studies. He has published 170 papers in indexed journals and has been a member since 1984 of the SNI institution where he has the category of Emeritus. He has been a member of the Mexican Academy of Sciences (since 1989). He has been awarded with the Research Diploma (IPN, 2001), the Andrés Manuel del Río 2007 National Chemistry Prize in Research (SQM, 2007), the Research Prize awarded by the Instituto Politécnico Nacional on three occasions, in 1991, 1993 and 2007, and the Lázaro Cárdenas Prize (IPN, 2008).

He has been a driving force in the postgraduate studies at his Institution and at all the others. I am sure that he has reviewed with rigor and success hundreds of theses of all levels, reports and accompanied many students to obtain degrees and titles through exams, reports, and other university activities.

Joaquín has recently retired. We will miss him because he was always involved in transcendent

scientific discussion. The pen and the brush have earned it for us, and that enormous creative capacity will be expressed in other fields, with the usual rigor and affection that he puts into his contributions.

The Journal of the Mexican Chemical Society (J. Mex. Chem. Soc.), one of his projects, has achieved the success of reaching the Journal Impact Factor of 1.5 (JCR), entering the third quartile in the metrics for evaluating the performance of scientific journals. So, in a festive spirit, we thank our current editor, Prof. Dr. Alberto Vela Amieva, and to the editorial assistants: MVZ. Adriana Vázquez Aguirre and Alejandro Nava Sierra, the members of the editorial

board, the referees evaluating the proposals, and their authors, the talent and efforts invested. A successful great collective effort.

Mexico City, January 2024.

Guest editor

Dr. Gabriel Cuevas

*For additional content, see: Cuevas, G. Semblanza de Joaquín Tamariz. *Bol. Soc. Quim. Mex.* **2007**, 3, 217.

Carbon Dioxide Capture Using Ionic Liquids Containing Amino Acid-Type Anions. Effect of the Cation, Anion on the Absorption Efficiency

Gabriela Barbosa-Moreno¹, Nohra V. Gallardo-Rivas*¹, Rafael Martínez-Palou*²

¹Tecnológico Nacional de México/Instituto Tecnológico de Ciudad Madero. Prol. Bahía de Aldhair y Av. de las Bahías, 89600, Altamira, Tamaulipas, México.

²Instituto Mexicano del Petróleo. Gerencia de Investigación en Desarrollo de Catalizadores y Productos Químicos. Eje Central Lázaro Cárdenas 152. 07730 CDMX, México.

*Corresponding author: Nohra V. Gallardo-Rivas, email: nohvigari@itcm.edu.mx; Rafael Martínez-Palou, email: rpalou@imp.mx

Received June 30th, 2022; Accepted November 15th, 2022.

DOI: <http://dx.doi.org/10.29356/jmcs.v68i1.1827>

Abstract. In this work, the synthesis of twelve ionic liquids (ILs) with imidazolium cation and amino acid-derived anions and their evaluation as carbon dioxide (CO₂) absorbents both, in pure form and aqueous solution (30 % of water) are reported and compared with monoethanolamine (MEA), which is a well-known commercial absorbent with wide application in the Petroleum Industry for capturing acid gases. The effect of both cation substituent features such as length and unsaturation of alkyl chains and amino acid structure at the anion on the CO₂ absorption efficiency was studied. All the ILs displayed good CO₂ absorption efficiency, being the ILs derived from 1-octyl-3-vinylimidazolium the most effective for this purpose, especially with lysinate anion ([OVI][L]); a capture rate of 1501 mg CO₂/mol of IL was achieved when it was diluted in water (30 %).

Keywords: Carbon dioxide; ionic liquids; amino acids type anions; absorption.

Resumen. En este trabajo se reporta la síntesis de doce líquidos iónicos (LIs) con el catión imidazolio y los aniones derivados de aminoácidos y la evaluación de estos compuestos como absorbentes de dióxido de carbono (CO₂), tanto empleando los absorbentes puros, como en solución acuosa (30 % de agua). Los resultados se comparan con los obtenidos con monoetanolamina (MEA), que es un conocido absorbente comercial con amplia aplicación en la Industria del Petróleo en la captura de gases ácidos. Se estudió el efecto de las características de ambos *N*-sustituyentes de los cationes, como la longitud y la presencia de insaturación en las cadenas de alquilo y la estructura de aminoácidos que conforman los aniones de los LIs estudiados, en la eficiencia de absorción de CO₂. Todos los LIs mostraron una buena eficiencia de absorción de CO₂, siendo los LIs derivados del 1-octil-3-vinilimidazolio los más efectivos para este fin, especialmente con el anión lisinato ([OVI][L]); se logró una tasa de captura de 1501 mg CO₂/mol de LIs cuando el absorbente se diluyó en agua (30 %).

Palabras clave: Dióxido de carbono; líquidos iónicos; aniones derivados de aminoácidos; absorción.

Introduction

The main energy source for humanity has arisen from non-renewable fossil compounds, which when used, generate some acid gases, from which CO₂ is the most abundant and contributes greatly to the greenhouse

effect. The production of this gas is not only increased by the point mentioned above, but also by other factors such as the burning of coal in power plants or combustion of diesel in engines and devices based on this fuel type, which turn out to be very frequent and harmful emission sources [1,2].

The economic development of countries, especially those in the process of growth, is closely linked to an increase in energy demand; therefore, projections indicate that the need for fossil fuels will continue growing given the world population soaring trend, which is why the development of novel environmentally and economically efficient technologies is more and more necessary [3].

Among the main options to achieve the reduction of CO₂ emissions, the efficiency improvement of conventional generating plants, better control over energy consumption, use of greater proportions of renewable resources, and capture and storage of CO₂ are found, where the last alternative is the most feasible and possible to develop today, and for this reason, it has been playing an important role in the last century [4-6].

Different processes such as pre-, post-, and oxy-combustion have been developed to capture CO₂ [7,8]. One of the advantages of post-combustion capture is that since it occurs after combustion and before CO₂ is released into the atmosphere, it can be implemented in facilities that are still in operation [9]. In this context, absorption is considered within this capture stage; in this process, chemical solvents trigger an acid-based chemical reaction, where alkanolamines are among the best-known compounds. Primary amines are very reactive with CO₂, but they are also more corrosive and sensitive to degradation, so secondary and tertiary amines are used to reduce these characteristics [10,11].

Ionic liquids (ILs), which are known as “green solvents” due to their low toxicity, practically zero vapor pressure and high solvent capacity, have been noted as promising candidates to remove CO₂ through absorption because of their high thermal stability, negligible steam pressure and adjustable physicochemical properties [12-18]. ILs exhibit strong affinity to CO₂, which stems from the possibility of varying cations or anions by adding functional groups, especially those containing amino groups [19-23]. It has been proven that when functionalized ILs are dissolved, they can greatly reduce viscosity [24]. The absorption capacity of most ILs solutions with a functional group with basic properties has been widely reported with absorption values higher than 0.5 mol of CO₂/mol of IL, including anions derived from amino acids [24-29]. The study of the absorption capacity of some amino acids was previously compiled [1,19,30]. Since 2010, Gurkan et al. showed that methioninate and proline trihexyl(tetradecyl)phosphonium absorb CO₂ in nearly 1:1 stoichiometry [31]. Recently, two reviews have shown the potential of ILs for CO₂ capture and utilization, mechanisms, and nature of interactions between ILs and CO₂ in terms of cation and anion nature, economic analysis, and perspectives of using ILs for this application [32,33].

In this work, the synthesis of ILs with imidazolium cation and amino acid anions is described and the efficiency of these compounds as absorbers performing CO₂ capture is evaluated with the aim of making a comparative study of the effect of the cation and substituents of the amino acid structure (anion) to obtain a prototype with high capture efficiency. In addition, the effect of diluting ILs with water on the absorption efficiency and concomitant cost reduction of the CO₂ capture process is studied by comparing it with the one stemming from using methyl ethyl amine, which is widely used in the Oil Industry as absorbent of acid gases. It was observed that IL [OVI][L] could be regenerated by a simple methodology and reused in several absorption cycles without noticeable absorption capacity loss.

Experimental

Reagents and materials

All reagents (Aldrich) were used without further purification. FT-IR spectra were obtained on a Perkin Elmer Spectrum 100 spectrophotometer with 4 cm⁻¹ spectral resolution and 16 scans using an attenuated total reflection accessory with diamond plate.

The ¹H NMR (400 MHz) and ¹³C NMR (100 MHz) spectra were recorded on an Ascend 400 NMR equipment from Bruker Avance III Console using tetramethylsilane (TMS) as internal standard and deuterated water (D₂O) as solvent at room temperature. EI mass spectra were recorded on GC-Mass Spectrometer Agilent 5973N. For the CO₂ desorption studies, a CEM Discover monomode microwave synthesizer was used [34].

Synthesis of ILs with amino acid anions

The ILs containing an imidazolium-type cation and amino acid anions such as [OMI][AA], [BMI][AA] and [OVI][AA] were synthesized by alkylation reactions of the imidazole derivatives, exchange of the halogenated anion by hydroxyl and subsequent neutralization using the amino acids (AA) Lysine [L], Arginine [A], Glutamine [G], and Histidine [H], which were obtained according to the standard procedure described below.

1-vinyl-3-octylimidazolium bromide [OVI][Br] was prepared by the reaction between 1-vinylimidazole (0.1 mol) and *n*-octylbromide (0.15 mol) in a round-bottom flask with magnetic stirring at 50°C for 4 h without solvent. The resulting IL was washed twice with ethyl acetate (1:4 v/v) and vacuum dried at 50°C for 5 h. The anion exchange of Br by OH was carried out through the equimolar reaction between [OVI][Br] and KOH dissolved in EtOH under stirring at 5°C for 4 h and subsequently filtered to remove the KBr obtained as by-product.

Then, 0.10 mol of [OVI][OH] and the corresponding AA (0.12 mol) were mixed in deionized water (50 mL) at room temperature for 4 h with magnetic stirring. Afterward, water was distilled under vacuum and the product was diluted in ethanol (20 mL) to remove the excess of AA, filtered and ethanol was removed from the solution under vacuum, yielding [OVI][L]. Following the procedure described above with the corresponding reagents, the compounds shown in Table 1 were obtained.

Table 1. ILs synthesized in this study.

Entry	Cation	Anion	Identification
1	1-Butyl-3-methylimidazolium	Lysinate	[BMI][L]
2		Arginate	[BMI][A]
3		Glutamate	[BMI][G]
4		Histidinate	[BMI][H]
5	1-Methyl-3-Octylimidazolium	Lysinate	[OMI][L]
6		Arginate	[OMI][A]
7		Glutamate	[OMI][G]
8		Histidinate	[OMI][H]
9	1-Octyl-3-Vinylimidazolium	Lysinate	[OVI][L]
10		Arginate	[OVI][A]
11		Glutamate	[OVI][G]
12		Histidinate	[OVI][H]

The structure and high purity of the synthesized compounds was confirmed FT-IR spectrometry, ¹H and ¹³C NMR as described below.

[BMI][L]. Following the experimental procedure a viscous light-yellow liquid was obtained (yield: 82 %). FT-IR (neat) ν (cm⁻¹): 3295, 2965, 2931, 2865, 1634, 1592, 1434, 1390, 1368, 1345, 1090, 1050, 879, 782, 729, 663. EI Mass spectrum: C₁₄H₂₉N₄O₂: 284 (Calcd., 284). ¹H NMR (400 MHz, D₂O) δ 8.67 (s, 1H), 7.42 (s, 1H), 7.37 (s, 1H), 4.13 (t, *J* = 7.0 Hz, 2H), 3.83 (s, 3H), 3.21 (t, *J* = 6.9 Hz, 1H), 2.81 (t, *J* = 6.9 Hz, 2H), 1.78 (q, *J* = 7.2 Hz, 2H), 1.54 (m, 6H), 1.28 (m, 2H), 0.84 (t, *J* = 7.0 Hz, 3H) ppm. ¹³C NMR (101 MHz, D₂O) δ 182.41, 135.98, 123.48, 122.23, 55.72, 49.32, 39.74, 35.79, 33.81, 31.33, 28.36, 22.13, 18.83, 12.79 ppm.

[BMI][A]. Following the experimental procedure a viscous light-yellow liquid was obtained (yield: 91 %). FT-IR (neat) ν (cm^{-1}): 3306, 2967, 2929, 2867, 1664, 1601, 1448, 1403, 1379, 1345, 1091, 1052, 878, 783, 730, 663. EI Mass spectrum: $\text{C}_{14}\text{H}_{28}\text{N}_6\text{O}_2$: 312 (Calcd., 312). ^1H NMR (400 MHz, D_2O) δ 8.71 (s, 1H), 7.46 (s, 1H), 7.40 (s, 1H), 4.15 (t, $J = 7.1$ Hz, 2H), 3.85 (s, 3H), 3.18 (m, 1H), 1.79 (q, $J = 7.1$ Hz, 2H), 1.55 (m, 4H), 136 (m, 2H), 0.85 (t, $J = 7.1$ Hz, 3H) ppm. ^{13}C NMR (101 MHz, D_2O) δ 182.95, 157.31, 135.99, 123.53, 122.28, 55.67, 49.36, 41.20, 35.89, 31.37, 24.76, 18.88, 12.86 ppm.

[BMI][G]. Following the experimental procedure a viscous light-yellow liquid was obtained (yield: 88 %). FT-IR (neat) ν (cm^{-1}): 3270, 2967, 2957, 2873, 1640, 1587, 1454, 1433, 1380, 1374, 1091, 1052, 879, 784, 760, 661. EI Mass spectrum: $\text{C}_{13}\text{H}_{24}\text{N}_4\text{O}_3$: 284 (Calcd., 284). ^1H NMR (400 MHz, D_2O) δ 8.69 (s, 1H), 7.44 (s, 2H), 7.39 (s, 2H), 4.15 (t, $J = 7.1$ Hz, 2H), 3.85 (s, 3H), 3.53 (t, $J = 5.9$ Hz, 1H), 2.32 (t, $J = 7.8$ Hz, 2H), 1.96 (q, $J = 6.9$ Hz, 2H), 1.79 (q, $J = 7.1$ Hz, 2H), 1.36–1.13 (m, 2H), 0.86 (t, $J = 7.3$ Hz, 3H) ppm. ^{13}C NMR (101 MHz, D_2O) δ 178.06, 174.29, 135.88, 123.51, 122.26, 54.72, 49.34, 35.83, 31.35, 29.83, 25.45, 18.86, 12.81 ppm.

[BMI][H]. Following the experimental procedure a viscous light-yellow liquid was obtained (yield: 88 %). FT-IR (neat) ν (cm^{-1}): 3284, 2966, 2930, 2865, 1642, 1591, 1444, 1407, 1374, 1371, 1091, 1051, 878, 802, 756, 677, 660. EI Mass spectrum: $\text{C}_{14}\text{H}_{24}\text{N}_5\text{O}_2$: 293 (Calcd., 292). ^1H NMR (400 MHz, D_2O) δ 8.71 (s, 1H), 7.61 (s, 1H), 7.46 (s, 1H), 7.41 (s, 1H), 6.88 (s, 1H), 4.16 (t, $J = 7.1$ Hz, 2H), 3.86 (s, 3H), 3.45–3.55 (m, 1H), 2.90–2.96 (m, 1H), 2.75–2.81 (m, 1H), 1.80 (q, $J = 7.2$ Hz, 2H), 1.24–1.31 (m, 2H), 0.86 (t, $J = 7.1$ Hz, 3H) ppm. ^{13}C NMR (101 MHz, D_2O) δ 174.12, 136.42, 135.79, 132.29, 123.53, 122.29, 116.72, 54.81, 49.36, 35.90, 35.90, 31.38, 28.23, 18.89, 12.87 ppm.

[OMI][L]. Following the experimental procedure a viscous light-yellow liquid was obtained (yield: 78%). FT-IR (neat) ν (cm^{-1}): 3285, 3162, 3064, 2964, 2862, 1656, 1583, 1471, 1372, 1328, 1180, 1101, 1043, 984, 884, 732, 715, 643, 629, 474. EI Mass spectrum: $\text{C}_{18}\text{H}_{37}\text{N}_4\text{O}_2$: 340 (Calcd., 340). ^1H NMR (400 MHz, D_2O) δ 8.82 (s, 1H), 7.47 (s, 1H), 7.45 (s, 1H), 4.17 (t, $J = 7.0$ Hz, 2H), 3.86 (s, 3H), 3.20 (t, $J = 5.6$ Hz, 1H), 2.76 (t, $J = 7.0$ Hz, 2H), 1.78–1.82 (m, 2H), 1.46–1.54 (m, 4H), 1.26–1.34 (m, 2H), 1.15–1.23 (m, 10H), 0.73 (t, $J = 6.1$ Hz, 3H). ^{13}C NMR (101 MHz, D_2O) δ 182.84, 135.96, 123.68, 122.23, 55.80, 49.58, 39.85, 35.93, 34.13, 31.46, 29.63, 28.98, 28.73, 28.60, 25.78, 22.34, 22.19, 13.74.

[OMI][A]. Following the experimental procedure a viscous light-yellow liquid was obtained (yield: 85 %). FT-IR (neat) ν (cm^{-1}): 3280, 3169, 3118, 2961, 2851, 1670, 1574, 1469, 1391, 1286, 1189, 1074, 1044, 1000, 870, 773, 710, 670, 628, 485. EI Mass spectrum: $\text{C}_{18}\text{H}_{36}\text{N}_6\text{O}_2$: 368 (Calcd., 368). ^1H NMR (400 MHz, D_2O) δ 8.68 (s, 1H), 7.41 (s, 1H), 7.37 (s, 1H), 4.11 (t, $J = 7.1$ Hz, 2H), 3.82 (s, 3H), 3.13 (m, 3H), 1.78 (m, 2H), 1.53 (m, 4H), 1.18 (m, 10H), 0.74 (t, $J = 7.1$ Hz, 3H) ppm. ^{13}C NMR (101 MHz, D_2O) δ 183.12, 156.97, 135.60, 123.52, 122.19, 55.51, 49.57, 41.05, 35.73, 31.72, 31.13, 29.31, 29.23, 28.36, 28.19, 25.44, 24.56, 22.10, 13.52 ppm.

[OMI][G]. Following the experimental procedure a viscous light-yellow liquid was obtained (yield: 83 %). FT-IR (neat) ν (cm^{-1}): 3330, 3176, 3107, 2966, 2861, 1658, 1568, 1471, 1383, 1327, 1190, 1099, 1049, 985, 880, 730, 691, 632, 471. EI Mass spectrum: $\text{C}_{17}\text{H}_{32}\text{N}_4\text{O}_3$: 340 (Calcd., 340). ^1H NMR (400 MHz, D_2O) δ 8.64 (s, 1H), 7.3 (s, 3H), 7.35 (s, 3H), 4.10 (t, $J = 7.1$ Hz, 2H), 3.81 (s, 3H), 3.60 (t, $J = 7.0$ Hz, 1H), 2.34 (t, $J = 6.9$ Hz, 2H), 1.98 (q, $J = 6.9$ Hz, 2H), 1.75–1.81 (m, 2H), 1.15–1.21 (m, 10H), 0.75 (t, $J = 7.0$ Hz, 3H) ppm. ^{13}C NMR (101 MHz, D_2O) δ 177.82, 175.29, 135.84, 123.48, 122.18, 54.39, 49.57, 35.67, 31.03, 29.73, 29.21, 28.25, 28.06, 26.99, 25.34, 22.03, 13.46 ppm.

[OMI][H]. Following the experimental procedure a viscous light-yellow liquid was obtained (yield: 81 %). FT-IR (neat) ν (cm^{-1}): 3272, 3138, 3088, 2960, 2860, 1667, 1563, 1443, 1406, 1339, 1169, 1083, 1061, 1000, 880, 750, 706, 655, 620, 482. EI Mass spectrum: $\text{C}_{18}\text{H}_{32}\text{N}_5\text{O}_2$: 349 (Calcd., 348). ^1H NMR (400 MHz, D_2O) δ 8.66 (s, 1H), 7.59 (s, 1H), 7.38 (s, 1H), 7.35 (s, 1H), 6.89 (s, 1H), 4.08 (t, $J = 7.0$ Hz, 2H), 3.79 (s, 3H), 3.72 (m, 1H), 3.03 (m, 1H), 2.90 (m, 1H), 1.74 (m, 2H), 1.14 (m, 10H), 0.71 (t, $J = 7.0$ Hz, 3H) ppm. ^{13}C NMR (101 MHz, D_2O) δ 176.22, 136.21, 135.80, 132.61, 123.52, 122.17, 117.18, 55.24, 49.55, 35.73, 31.15, 29.37, 29.32, 28.38, 28.21, 25.46, 22.11, 13.54 ppm.

[OVI][L]. Following the experimental procedure a viscous light-yellow liquid was obtained (yield: 71 %). FT-IR (neat) ν (cm⁻¹): 3277, 2943, 2926, 2859, 1657, 1595, 1457, 1377, 1349, 1138, 1105, 1092, 1050, 881, 730, 660. EI Mass spectrum: C₁₉H₃₇N₄O₂: 349 (Calcd., 349). ¹H NMR (400 MHz, D₂O) δ 9.13 (s, 1H), 7.79 (s, 1H), 7.58 (s, 1H), 7.12 (dd, J = 3.4, 15.3 Hz, 1H), 5.77 (d, J = 7.1 Hz, 1H), 5.37 (d, J = 6.6 Hz, 1H), 4.21 (t, J = 7.1 Hz, 2H), 3.21 (t, J = 6.0 Hz, 1H), 2.82 (t, J = 7.2 Hz, 2H), 1.82 (m, 2H), 1.52 (m, 4H), 1.37 (m, 2H), 1.18 (m, 10H), 0.73 (t, J = 6.9 Hz, 3H) ppm. ¹³C NMR (101 MHz, D₂O) δ 181.73, 134.35, 128.24, 122.99, 119.59, 109.45, 55.43, 50.02, 39.39, 33.44, 31.26, 29.32, 28.51, 28.36, 27.39, 25.57, 22.19, 21.87, 13.61 ppm.

[OVI][A]. Following the experimental procedure a viscous light-yellow liquid was obtained (yield: 79 %). FT-IR (neat) ν (cm⁻¹): 3287, 2958, 2922, 2858, 1658, 1589, 1459, 1374, 1350, 1164, 1113, 1088, 1049, 882, 764, 663 ppm. EI Mass spectrum: C₁₉H₃₆N₆O₂: 380 (Calcd., 380). ¹H NMR (400 MHz, D₂O) δ 9.17 (s, 1H), 7.82 (s, 1H), 7.58 (s, 1H), 7.17 (dd, J = 3.2, 15.3 Hz, 1H), 5.79 (d, J = 7.2 Hz, 1H), 5.40 (d, J = 6.7 Hz, 1H), 4.22 (t, J = 7.2 Hz, 2H), 3.14 (m, 1H), 3.08 (m, 2H), 1.83 (m, 2H), 1.51 (m, 4H), 1.15-1.25 (m, 10H), 0.74 (t, J = 6.9 Hz, 3H) ppm. ¹³C NMR (101 MHz, D₂O) δ 183.02, 156.73, 134.65, 128.58, 123.37, 119.92, 109.63, 55.64, 50.06, 41.01, 31.65, 31.56, 29.30, 28.53, 28.47, 25.63, 24.50, 22.19, 13.69 ppm.

[OVI][G]. Following the experimental procedure a viscous light-yellow liquid was obtained (yield: 75 %). FT-IR (neat) ν (cm⁻¹): 3301, 2945, 2926, 2860, 1660, 1576, 1452, 1381, 1295, 1175, 1100, 1096, 1054, 876, 725, 672. EI Mass spectrum: C₁₈H₃₂N₄O₃: 352 (Calcd., 352). ¹H NMR (400 MHz, D₂O) δ 9.15 (s, 1H), 7.80 (s, 1H), 7.58 (s, 1H), 7.15 (dd, J = 3.2, 15.1 Hz, 1H), 5.78 (d, J = 7.2 Hz, 1H), 5.39 (d, J = 7.2 Hz, 1H), 4.21 (t, J = 7.0 Hz, 2H), 3.68 (t, J = 6.7 Hz, 1H), 2.36 (t, J = 6.9 Hz, 2H), 2.04 (q, J = 6.9 Hz, 2H), 1.80-1.86 (m, 2H), 1.15-1.24 (m, 10H), 0.73 (t, J = 6.8 Hz, 3H). ¹³C NMR (101 MHz, D₂O) δ 178.62, 174.08, 134.56, 128.41, 123.27, 119.60, 109.54, 54.49, 50.04, 31.37, 30.86, 29.41, 28.51, 28.47, 26.25, 25.60, 22.19, 13.65 ppm.

[OVI][H]. Following the experimental procedure a viscous light-yellow liquid was obtained (yield: 73 %). FT-IR (neat) ν (cm⁻¹): 3301, 2945, 2926, 2860, 1660, 1576, 1452, 1381, 1295, 1175, 1100, 1096, 1054, 876, 725, 672. EI Mass spectrum: C₁₉H₃₂N₅O₂: 361 (Calcd., 361). ¹H NMR (400 MHz, D₂O) δ 9.19 (s, 1H), 7.84 (s, 1H), 7.65 (s, 1H), 7.58 (s, 1H), 7.18 (dd, J = 3.3, 15.2 Hz, 1H), 6.9 (s, 1H), 5.81 (d, J = 7.1 Hz, 1H), 5.42 (d, J = 6.9 Hz, 1H), 4.23 (t, J = 7.1 Hz, 2H), 3.85 (t, J = 6.9 Hz, 1H), 3.07-3.14 (m, 1H), 2.95-3.01 (m, 1H), 1.80-1.90 (m, 2H), 1.20-1.26 (m, 10H), 0.74 (t, J = 7.1 Hz, 3H). ¹³C NMR (101 MHz, D₂O) δ 174.08, 136.43, 134.73, 132.42, 128.65, 123.42, 120.05, 116.73, 109.78, 55.10, 50.10, 31.33, 29.29, 28.51, 28.37, 28.29, 25.66, 22.20, 13.85 ppm.

ILs regeneration and reutilization

The CO₂ could be removed from the saturated ILs (5.0 g) by heating in a microwave oven monomodal (CEM Discover) at 70 °C at 85 W of power for 5 minutes in closed-vessel mode. The CO₂ desorption was verified by ¹H NMR and FT-IR.

Procedure for the quantification of CO₂ absorption using the ILs-AA

The absorption tests were carried out at 303 K using an initial pressure of 3 atm. The apparatus consists of a stainless-steel gas tank equipped with a digital manometer and subjected to constant stirring; the diagram is shown in Fig. 1. The temperature is controlled by a thermostat placed in the heating bath (\pm 0.1 K variation). The variation in gas pressure was approximately \pm 0.001 atm throughout the pressure interval ranging from 1 to 3 atm. 10.0 g of pure ILs or 30 % dissolved in water were introduced into the tank and hermetically sealed. Air was then removed from the system by means of a vacuum pump that was connected to the system for 15 min (ultimate vacuum was $1.3 \cdot 10^{-5}$ atm). Subsequently, CO₂ was loaded into the tank and the absorption process began with stirring (150 rpm). The system was considered in steady state once the pressure remained constant for half an hour. The concentration of absorbed CO₂ was determined using the ideal gas equation of state. Each experiment was performed in triplicate, which had an approximate uncertainty of 0.02 mol CO₂/mol IL. The absorption curves were obtained by measuring the system pressure drop every 2 min. The experiments with ILs and MEA were carried out under the same experimental conditions.

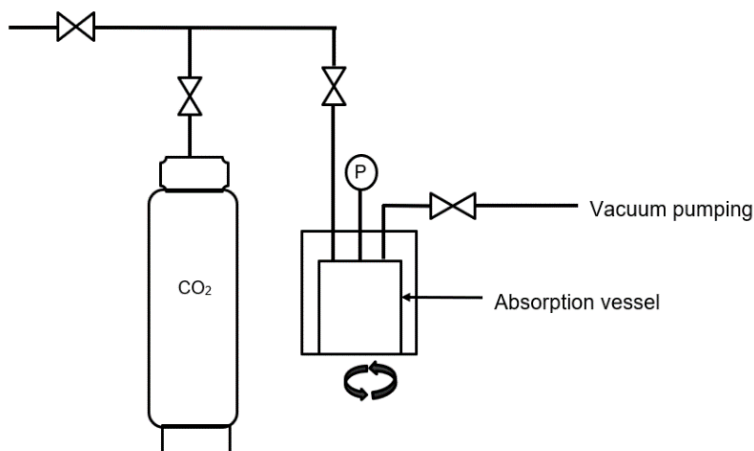


Fig. 1. Schematic representation of the equipment used to determine CO₂ absorption.

Results and discussion

Synthesis of AA functionalized ILs

Table 1 The synthesis general scheme of the ILs functionalized with AA is described in Fig. 2.

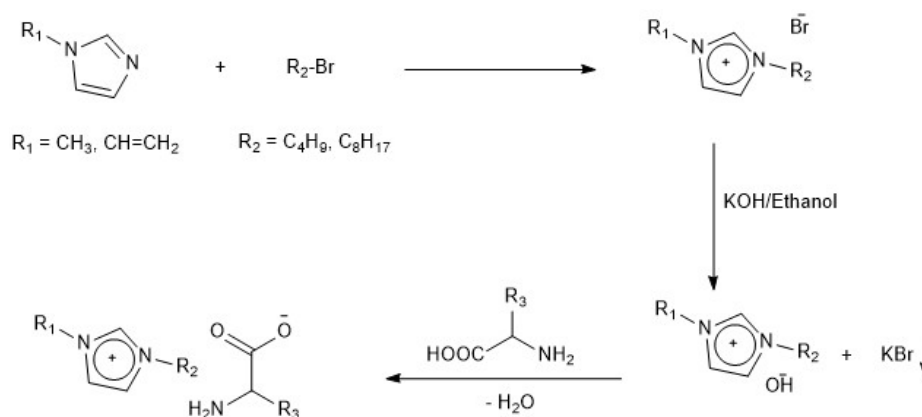


Fig. 2. Synthesis scheme of the ILs functionalized with AA.

The synthesis of the precursor IL [RMI][X] (R = *n*-C₄H₉, *n*-C₈H₁₇ and vinyl; MI = *N*-methylimidazolium; X = Cl, Br) began with the alkylation of 1-methylimidazole (0.1 mol) with the corresponding alkyl halide (0.15 mol) in an inert atmosphere for 48 h with heating and magnetic stirring. The anion exchange reaction to replace the halide by hydroxyl was carried out using potassium hydroxide (KOH) in ethanol at low temperatures to form the precursor IL [RMI][OH], which was subsequently neutralized with AA to obtain the ILs shown in Table 1. The employed amino AAs were selected because they present more than one basic site in their structure, which as expected favors the capture of an acid gas as CO₂ [15,19,22,24].

The results of the IR analysis are shown in Figures 3, 4 and 5.

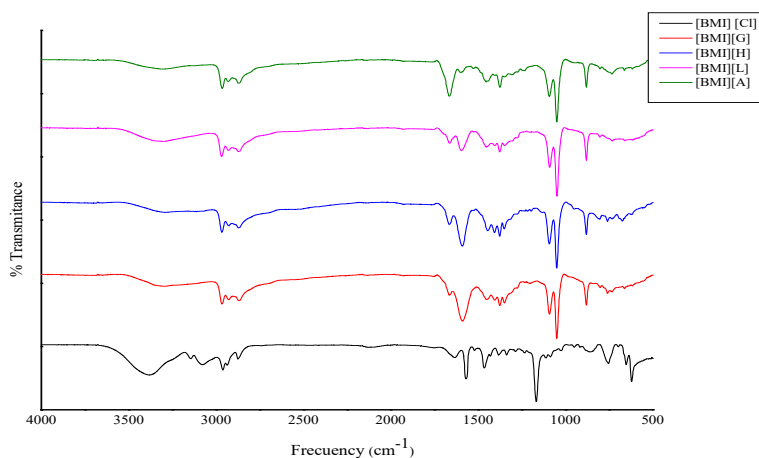


Fig. 3. FTIR spectra of pure ionic liquids corresponding to [BMI][AA] and [BMI][Cl].

Fig. 3 shows a broad peak in the [BMI][Cl] spectrum centered at 3378 cm^{-1} reveals the presence of water in the halogenated IL. Halogens are strong proton acceptors, and this band is the result of the overlapping absorption bands due to symmetric (ν_1) and asymmetric (ν_3) stretching vibrational modes of water molecules, which is strongly red-shifted, reflecting the strong hydrogen bond interaction ($\text{Cl}^- \dots \text{H-O-H} \dots \text{Cl}^-$). The signal centered on 2872 cm^{-1} is due to vibrations of C-H of methylene and methyl groups in the alkyl chains. The bands in the range between $3000\text{-}3200\text{ cm}^{-1}$ are mainly assigned to $+\text{C}(2)\text{-H}$ stretching mode and the intense band at 1166 cm^{-1} correspond to the skeletal vibrational mode of the imidazolium ring [35,36]. The band observed in the AA-containing ILs at $3500\text{-}3100\text{ cm}^{-1}$ is attributed to the -NH groups and is overlapped by the -OH stretching in the AA structure. Also, at 1590 cm^{-1} , a CO_2^- pronounced stretching band was observed in the AA-functionalized ILs. An imidazole C-N stretching peak appeared at $1000\text{-}1100\text{ cm}^{-1}$. Finally, the bands between $3000\text{-}2800\text{ cm}^{-1}$, $1450\text{-}1460\text{ cm}^{-1}$ and around 1350 cm^{-1} correspond to the vibrational modes of C-H the alkyl chains of the cation (symmetric and asymmetric stretching and bending) [37,38].

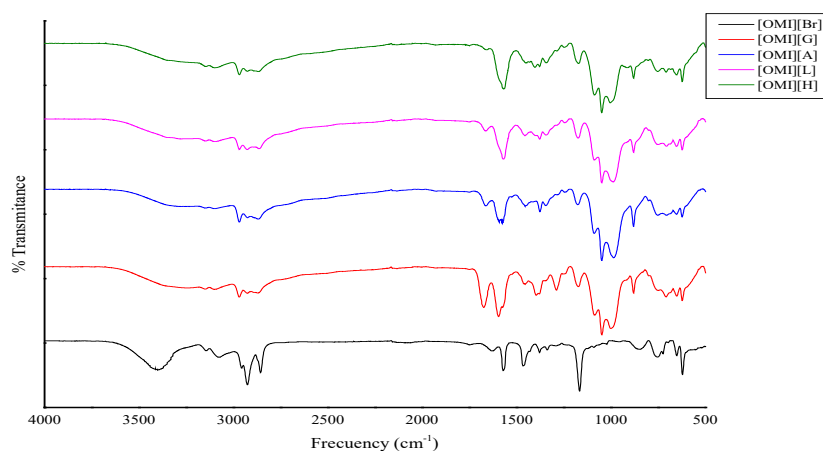


Fig. 4. FTIR spectrum of pure ionic liquids corresponding to [OMI][AA] and [OMI][Br].

Because the only structural difference between of ILs [BMI][AA] (Fig. 3) and [OMI][AA] series (Fig. 4) is the length of the alkyl chain bonded to the Nitrogen-1 of the imidazolium ring, only slight differences between the spectra shown in figures 3 and 4 can be seen in the regions related to the bands in the region 3000-2800 cm^{-1} , 1430-1460 cm^{-1} and 1320-1380 cm^{-1} which correspond to the vibrational C-H modes of the alkyl chains (symmetric and asymmetric stretching and bending) as observed by other authors [37,38]. At 1570 cm^{-1} , a CO_2^- pronounced stretching band was observed in the functionalized AA-functionalized ILs.

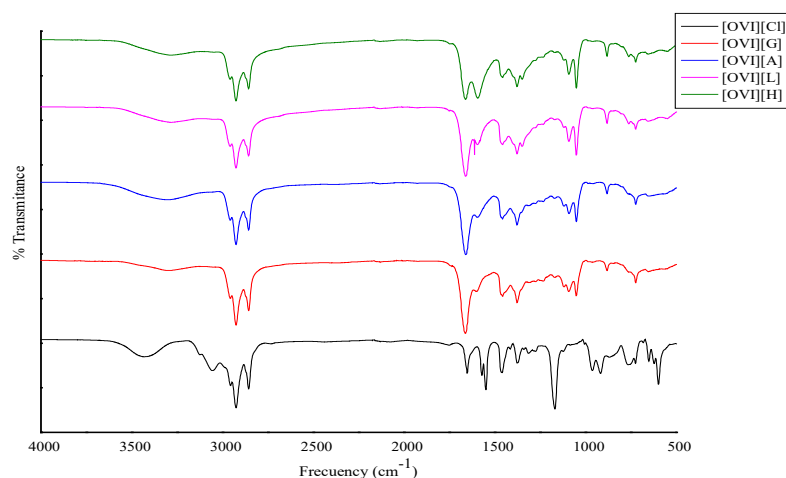


Fig. 5. FTIR spectrum of pure ionic liquids corresponding to [OVI][AA].

Similarly, to Fig. 3 and 4, Fig. 5 shows a broad peak in the [OVI][Cl] spectrum, centered at 3395 cm^{-1} , which corresponds to the overlapping absorption bands due to symmetric (ν_1) and asymmetric (ν_3) stretching vibrational modes of water molecules. A wide band is observed in the AA-functionalized ILs at 3500-3100 cm^{-1} , which is attributed to the -NH groups, and is overlapped with the -OH stretching in the AA structure. The bands located at 3200-3000 cm^{-1} and 1166 cm^{-1} correspond to the vibrational modes of the imidazolium ring (symmetric and asymmetric stretching). At 3045 cm^{-1} , a medium stretching band is observed, which corresponds to the =CH₂ of the vinyl group. The signal situated at 1688 cm^{-1} is attributed to the C=C stretching band of the vinyl group. Also, at 1570 cm^{-1} , a CO_2^- pronounced stretching was observed in the AA-functionalized ILs. Finally, the bands between 3000-2800 cm^{-1} , 1450-1460 cm^{-1} and 1350 cm^{-1} correspond to the vibrational modes of the alkyl chains of the cation (symmetric and asymmetric stretching and bending). As expected, the most noticeable differences between the series of spectra in Fig. 5 with Figures 3 and 4 lie fundamentally in the signals related to =CH₂ of the vinyl group and the C=C bands described previously.

Absorption of CO₂ by the synthesized ILs. Effect of the cation structure

Following the procedure described in the experimental section, the absorption capacity of pure ILs was evaluated at 25 °C and 40 °C. At a temperature of 40 °C, the absorptions follow the same trend than at 25 °C, but the amount of CO₂ absorbed is slightly higher, fundamentally due to the reduction in the viscosity of the ILs, which favors a better interaction between the absorbent and the gas (higher diffusivity). Entries 1-8 shows the absorption results of the functionalized ILs in nitrogen-3 with butyl ([BMI]) and octyl ([OMI]) group with the same four AAs in both cases. It is observed that the absorption values tend to be higher for the AA-functionalized IL with octyl substituent. This result is due to the viscosity of the ILs containing the 1-methyl-3-octylimidazolium cation is lower than the ILs with 3-butyl substituent; this favors the improved interaction efficiency between CO₂ and the IL [3,7].

Feng et al. studied the absorption in AA-functionalized ILs mixture with methyldiethanolamine (MDEA). They found that adding amino acid IL greatly reinforced the CO₂ absorption of MDEA in aqueous solution over a wide range of IL concentration (5-100 %), partial pressure (0.04-4.0 atm) and temperature between 20-40 °C.

Aqueous solution with 15 % IL + 15 % MDEA had higher absorption rate and larger uptake capacity. The higher temperature led to the larger reaction rate and less viscosity [39].

In another study of CO₂ absorption with AA-containing ILs, it was shown that the absorption capacity of the evaluated ILs decreases with increasing temperature between 20 and 80 °C, demonstrating that it is possible to desorb the CO₂ gas under CO₂-rich conditions by temperature-swing absorption [40].

Hiremath et al. have observed a decrease in CO₂ adsorption capacity of silica-supported ILs when the temperature in the experiments was increased from 20 to 100 °C [41].

Table 2. Results of CO₂ absorption by the ILs studied without dilution at 25 °C and 40 °C.

Entry	Identification	Absorption capacity of the ILs without dilution (mmol CO ₂ / mol IL)	
		25 °C	40 °C
1	[BMI][L]	821.47	873.64
2	[BMI][A]	788.58	839.27
3	[BMI][G]	761.94	811.73
4	[BMI][H]	748.32	800.52
5	[OMI][L]	719.25	772.36
6	[OMI][A]	708.47	759.43
7	[OMI][G]	902.62	950.59
8	[OMI][H]	891.55	943.67
9	[OVI][L]	1121.37	1173.85
10	[OVI][A]	1072.84	1124.44
11	[OVI][G]	1042.29	1093.57
12	[OVI][H]	1031.09	1079.63

On the other hand, when comparing the different octyl substituted, it is observed that the vinyl group played a relevant role in the effectiveness of these ILs, which exceeded 1000 mmol CO₂/mol IL in all cases [12]. The effect of the vinyl substituent can probably be explained through the formation of a π - π system between the unsaturated groups of the IL and CO₂, which makes the sorbent-CO₂ interaction more effective. In all cases, a possible electrostatic interaction between the electron rich oxygen atoms in CO₂ and electron deficient heterocycle, that could favor a supramolecular structure between ILs and CO₂, can take place (Fig. 6) [29].

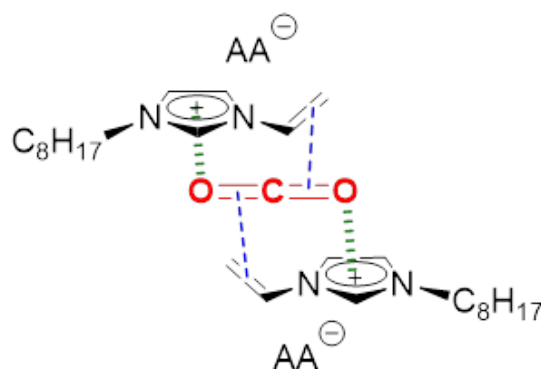


Fig. 6. Possible π - π and electrostatic interaction between [OVI][AA] and CO₂.

Effect of the anion structure on the absorption capacity of the ILs

As shown in Table 2, although the results did not follow the same trend with all the cations, it is evident that the lysinate anion presented the highest adsorption capacity, which seems to be related to the presence of two primary amino groups that result in two strong basic sites capable of interacting more effectively with CO₂, showing that the chemisorption is the more dominant mechanism in our AA-containing ILs.

Fig. 7 shows the ¹³C NMR spectrum of [BMI][L] before and after CO₂ adsorption, where two additional signals appear at 166.74 and 163.75 ppm, respectively, which correspond to the formation of carbamic acids from both amino groups, thus confirming the existence of chemisorption between CO₂ and the IL anion.

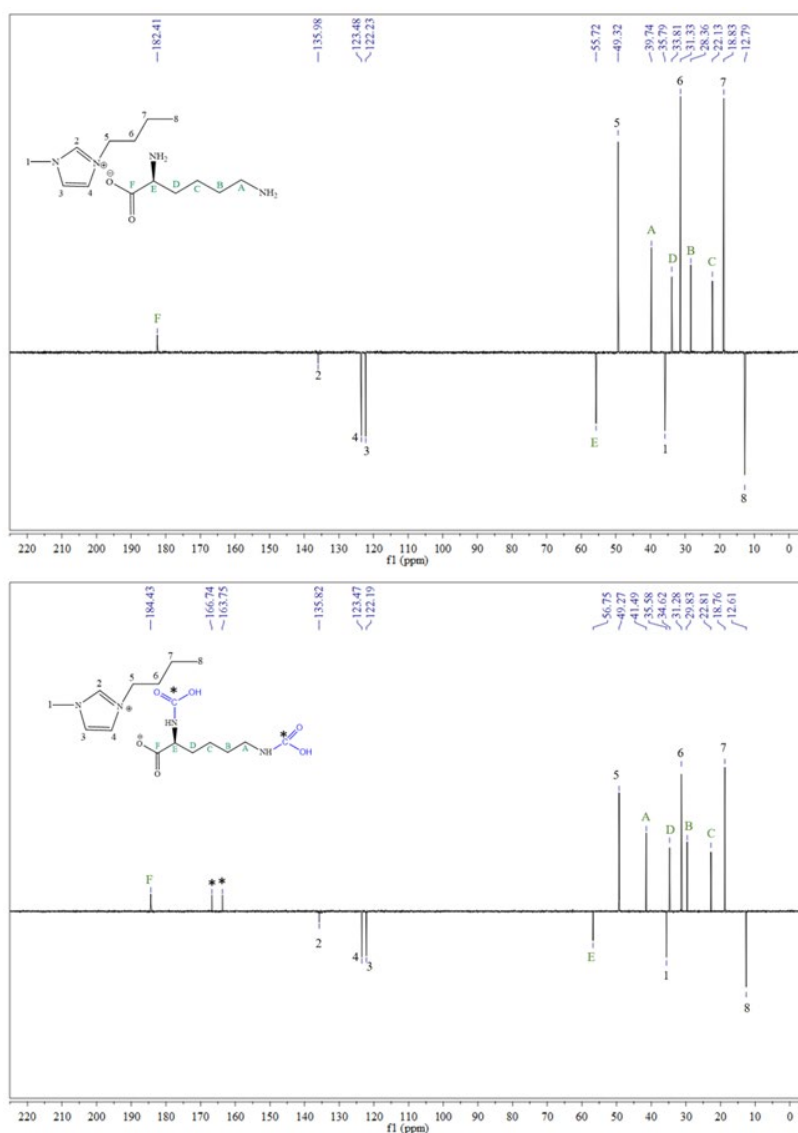


Fig. 7. ¹³C NMR spectrum of [BMI][L] before and after CO₂ absorption.

The chemisorption was also confirmed by the presence of a new FTIR band that appeared after CO₂-IL interaction around 1785 cm⁻¹ and is attributed to the asymmetric C=O vibration of the former carbamate species, as have been observed by us (Fig. 8) and other authors [37,38]. Also, the noticeable decrease in the broad band at 3000–3600 cm⁻¹, assigned to νN–H and νO–H vibrations, and the bands at 1580 and 1400 cm⁻¹ attributed to ν(COO⁻)_{sym.} and ν(COO⁻)_{assym.}, respectively, confirm the carbamate formation [42].

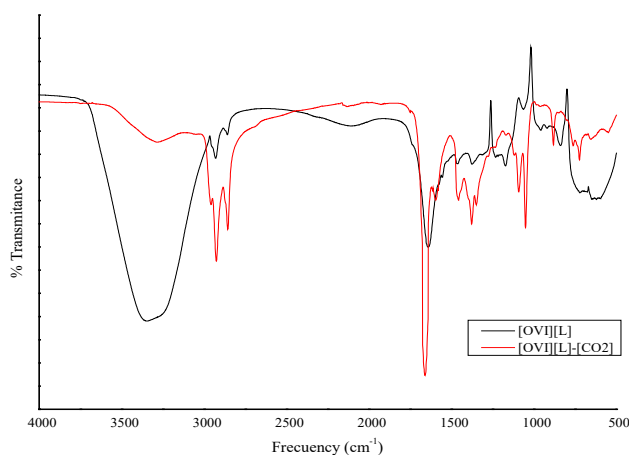


Fig. 8. FT-IR spectrum of [BMI][L] before and after CO₂ absorption.

Effect of dilution on the adsorption capacity of the ILs

Fig. 9 shows a comparison between the absorption capacity of monoethanolamine (MEA) and functionalized ILs-AA diluted at 30 % in water. As can be seen, the solubility of CO₂ is clearly favored after dilution in water even though the solvent absorption under these conditions is practically nil, but in the case of solutions, in addition to chemisorption, the physisorption process is also favored [20,26,30,37].

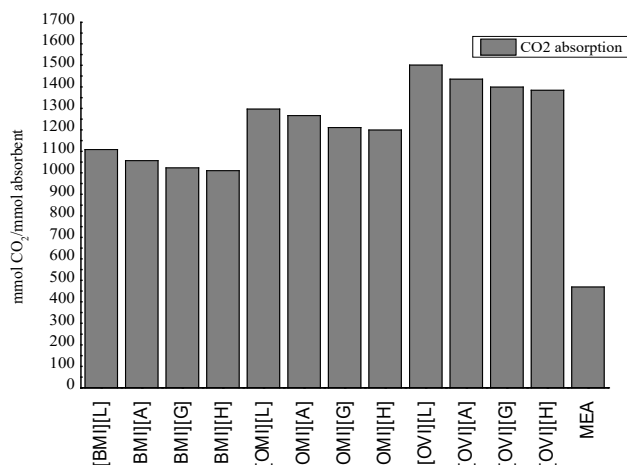


Fig. 9. Absorption capacity of the ILs-AA in 30 % mass of aqueous solution.

Fig.10 shows the CO₂ absorption curves of [OVI][AA] diluted at 30 % wt. in water, which were the most effective ILs.

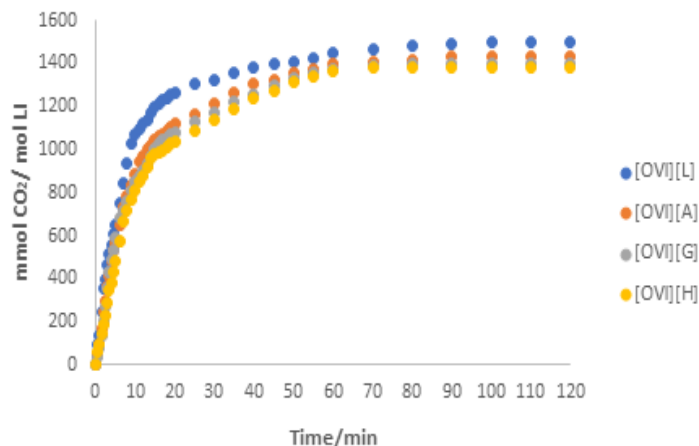


Fig. 10. CO₂ uptake with [OVI] and the different amino acids in 30 % wt. solution.

According to the results shown in Table 2 and Fig. 9, the CO₂ capture efficiency for ILs with the same cation ([BMI], [OMI] or [OVI]), and AAs-containing anions follows the order: [Cation][L] > [Cation][A] > [Cation][G] > [Cation][H]. This order is inversely proportional to the $pK_{a(NH_2)}$ of the corresponding AAs, confirming that the basicity of the amino groups plays a key role the CO₂ capture (Table 3).

Table 3. pK_{NH_2} of the AAs used in this study [42].

AA	$pK_{a(NH_2)}$
Lysine	8.95
Arginine	9.04
Glutamine	9.13
Hystidine	9.17

Fig. 11 shows the CO₂ absorption curves of the different cations with lysinate anion diluted at 30 % wt. in water to appreciate the difference in their activity. The 30 % concentration was selected because it is the concentration commonly applied in the amine-assisted CO₂ capture in Mexican Oil Industry. This concentration achieves an adequate cost/performance ratio of the chemical treatment. On the other hand, it is known that low viscosity obtained after IL dissolution and a weaker cation-anion interaction in the IL solution are the dominant factors responsible of the higher CO₂ capture.

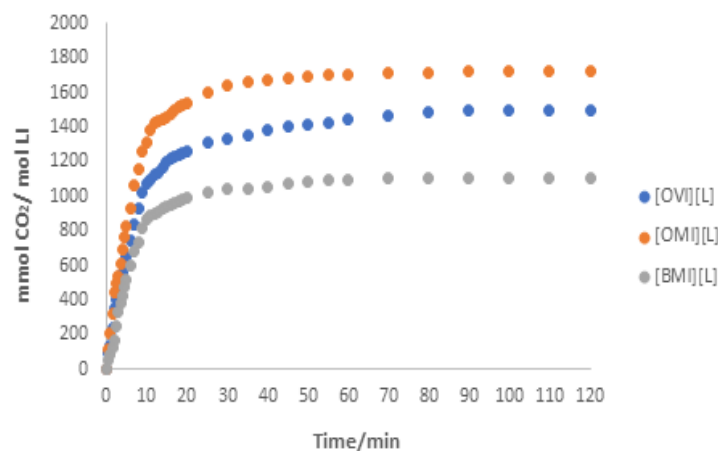


Fig. 11. CO₂ uptake with [L] and the different cations of ILs in 30 % wt. solution.

Fig. 12 shows the CO₂ pressure drop because of the absorption of the lysinate ILs with the different cations, in comparison with MEA at the same dilution. It can be observed that the kinetics of the absorption process is very similar in the case of the ILs, but the highest absorption was obtained in the case of cation with unsaturated substituent ([OVI]).

Considering that the time until a constant pressure was reached is directly linked with the absorption kinetics, the quicker a constant pressure level is reached, the faster is the absorption. Consequently, the absorption kinetics of lysinate-containing ILs was faster than MEA, which is probably due to the presence in the lysinate anion with two amino groups in each molecule of the ILs compared to one amine group in the MEA, coupled with the probable electrostatic π - π interactions that can be favored between the ILs and CO₂ [26].

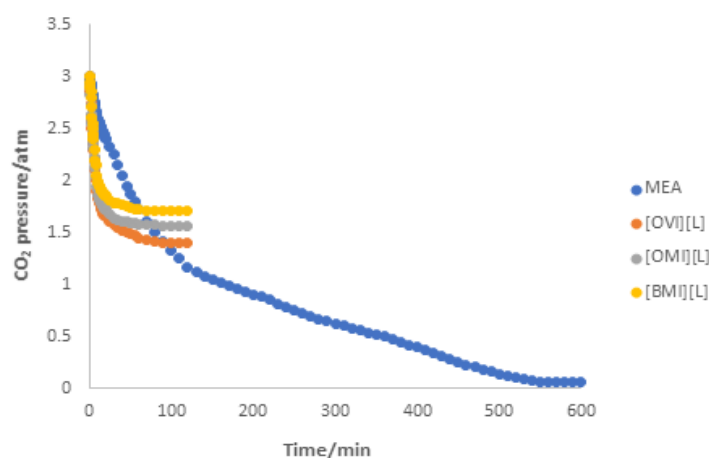


Fig. 12. Absorption kinetics of lysine derivatives compared to MEA (30 % wt. solution).

In the case of dilution experiments, the lysinate ILs showed the highest performance for CO₂ capture, particularly [OVI][L]. The better performance of the lysinate ILs is probably due to the position of the two amino groups in the anion that favor greater basicity and adequate nucleophilicity and a more effective

interaction of these groups with CO₂. Fig. 13 shows the possible interactions that favor the better performance of [OVI][L], even when there is no convincing evidence to confirm this proposal. [29].

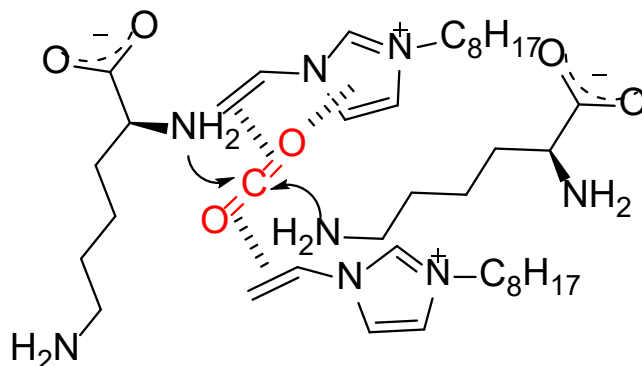


Fig. 13. Probable interactions between CO₂ and [OVI][L].

Chemisorption between CO₂ and carboxylate groups in 1,3-dialkylimidazolium has also been demonstrated, which explains the high performance shown by AA containing ILs [42].

Interestingly, [OVI][L] is a monomer that can be polymerized to obtain the corresponding poly(IL). It has been shown that poly(ILs) are also excellent CO₂ absorbers [43,44]. The study of the absorption properties of poly([OVI][L]) is currently underway in our research group.

According to our observations and those of other authors, the main interactions that favor CO₂ absorption are acid-base interactions (CO₂⋯NH₂, chemisorption), and the electrostatic interactions that can occur between ILs and CO₂. The electrostatic interaction could explain why many non-amino functionalized ILs can absorb a significant amount of CO₂ (physisorption) [1,29,33].

Regeneration and reuse of [OVI][L] after the first adsorption cycle

Following the procedure described in the Experimental Part, it was demonstrated that CO₂ can be desorbed from [OVI][L] and the IL can be reused in five consecutive absorption/desorption cycles without considerable loss of its adsorption capacity (Table 4).

Table 4. Results of CO₂ absorption of [OVI][L] under five cycles of absorption/desorption.

Cycle	Absorption capacity (mmol CO ₂ / mol IL)
1	1121
2	1119
3	1120
4	1114
5	1111
6	1103

Conclusions

Twelve ILs with three imidazole-based cations and four amino acid-derived anions were synthesized and evaluated as CO₂ sorbents. The ILs with the 1-octyl-3-vinylimidazolium cation gave the best adsorption results and the lysinate anion was found to give the ILs the highest adsorption capacity, attributable to the adequate disposition of the primary amino groups that favor a better interaction with CO₂. The performance of the anions correlated inversely with their pK_{a(NH₂)}. The CO₂ solubility was favored with dilution of the ILs in water, which was attributed to the decrease in the medium viscosity, thus favoring the sorbent-CO₂ interaction, and to the combination of chemisorption and physisorption processes. The ¹³C NMR and FT-IR spectrum of [BMI][L] confirmed the chemisorption through the detection of signals corresponding to carbamic acids. [OVI][L] proved to be the best adsorbent, especially after dilution (30 % in water). The better performance of [OVI][L] is probably due to the more adequate distribution of the two amino groups in the aliphatic chain of the amino acid, which favors greater basicity and a more effective acid-base interaction of these groups with CO₂, coupled with the probably π - π and electrostatic interaction between CO₂ and the vinyl group. By comparing the obtained results with those concerning MEA, the ILs-AA displayed faster absorption kinetics. [OVI][L] can be regenerated under microwave irradiation and reutilized in several absorption cycles without appreciable loss of its absorption capacity, so this IL can be considered a viable alternative for application as solvent in post-combustion CO₂ capture from flue gas in fixed emission sources on a large scale.

Acknowledgements

G. Barbosa-Moreno wants to thank to CONACyT-México (511874/287475) for the degree fellowship granted. Furthermore, we appreciate the funding provided by the Tecnológico Nacional de México. The authors want to thank the Instituto Mexicano del Petróleo for the facilities granted in carrying out the experimental part of this work.

References

1. Torralba-Calleja, E.; Skinner, J.; Gutiérrez-Tauste, D. *J. Chem.* **2013**, 1–16. DOI: <http://dx.doi.org/10.1155/2013/473584>.
2. Zambrano-Monserrate, M. A. *Sci. Total Environ.* **2024**, 907, 167853. DOI: <https://doi.org/10.1016/j.scitotenv.2023.167852>.
3. Lecomte, F.; Broutin, P.; Lebas, A. CO₂ Capture Technologies to Reduce Greenhouse Gas Emissions, Ed. Technip, IFP Publications, 2010.
4. Rahman, F. A.; Aziz, M. M.; Saidur, R.; Bakar, W. A. Bakar, Hainin, M.; Putrajaya R.; Hassan, N. A. *Renew. Sustain. Energy Rev.* **2017**, 71, 112-116. DOI: <http://dx.doi.org/10.1016/j.rser.2017.01.011>.
5. Gray, M. L.; Hoffman, J. S.; Hreha, D. C.; Fauth, D. J.; Hedges, S. W.; Hedges, Champagne, K. J.; Pennline, H. W. *Energy Fuels* **2009**, 23, 4840-4844. DOI: <http://dx.doi.org/10.1021/ef9001204>.
6. Koytsoumpa, E. I.; Bergins, C.; Kakaras, E. *J. Supercrit. Fluids.* **2018**, 132, 3-16. DOI: <http://dx.doi.org/10.1016/j.supflu.2017.07.029>.
7. Kenarsari, S. D.; Yang, D.; Jiang, G.; Zhang, S.; Wang, J.; Rusell, A. G.; Wei, Q.; Fan, M. *RSC Adv.* **2013**, 45, 22739. DOI: <http://dx.doi.org/10.1039/C3RA43965H>.
8. Stanger, R.; Wall, T.; Spörl, R.; Paneru, M.; Grathwohl, S.; Weidmann, M.; Schefflmecht, G.; McDonald, D.; Myohanen, K.; Ritvanen, J.; Rahiala, S.; Hyppanen, T.; Mletzco, J.; Kather, A.; Santos, S. *Int. J. Greenhouse Gas Control.* **2015**, 40, 55–125. DOI: <http://dx.doi.org/10.1016/j.ijggc.2015.06.010>.
9. Romano, M. C. *Int. J. Greenhouse Gas Control.* **2013**, 18, 57-67. DOI: <http://dx.doi.org/10.1016/j.ijggc.2013.07.002>.

10. Blauwhoff, P. M.; Versteeg, G. F.; Van Swaaij, W. P. *Chem. Eng. Sci.* **1984**, *39*, 207-225. DOI: [http://dx.doi.org/10.1016/0009-2509\(84\)80021-4](http://dx.doi.org/10.1016/0009-2509(84)80021-4).
11. Vaidya, P. D.; Konduru, P.; Vaidyanathan, M.; Kenig, E. Y. *Ind. Eng. Chem. Res.* **2010**, *49*, 11067-11072. DOI: <http://dx.doi.org/10.1021/ie100224f>.
12. Saravanamurugan, S.; Kunov-Kruse, A. J.; Fehrmann, R.; Riisager, A. *Chem. Sus. Chem.* **2014**, *7*, 897-902. DOI: <http://dx.doi.org/10.1002/cssc.201300691>.
13. Ramdin, M.; De Loos, T. W.; Vlugt, T. J. *Ind. Eng. Chem. Res.* **2012**, *51*, 8149-8177. DOI: <http://dx.doi.org/10.1021/ie3003705>.
14. Luque, R.; Martínez-Palou, R. *Environm. Energy Sci.* **2014**, *7*, 2414-2447. DOI: <http://dx.doi.org/10.1039/c3ee43837f>.
15. Wan, M. M.; Zhu, H. Y.; Li, Y. Y.; Ma, J.; Liu, S.; Zhu, J. H. *ACS Appl. Mat. Interfaces.* **2014**, *6*, 12947-12955. DOI: <http://dx.doi.org/10.1021/am5028814>.
16. Zhang, X.; Zhang, X.; Dong, H.; Zhao, Z.; Zhang, S.; Huang, Y. *Energy Environ. Sci.* **2012**, *5*, 6668-6681. DOI: <http://dx.doi.org/10.1039/C2EE21152A>.
17. Martínez-Palou, R. *J. Mex. Chem. Soc.* **2007**, *51*, 252-264.
18. Bates, E. D.; Mayton, R. D.; Ntai, I.; Davis, J. H. *J. Am. Chem. Soc.* **2002**, *124*, 926-927. DOI: <http://dx.doi.org/10.1021/ja017593>.
19. Guzmán, J.; Ortega-Guevara, C.; De León, R. G.; Martínez-Palou, R. *Chem. Eng. Technol.* **2017**, *40*, 2339-2345. DOI: <http://dx.doi.org/10.1002/ceat.201600593>.
20. Shannon, M. S.; Bara, J. E. *Sep. Sci. Technol.* **2012**, *47*, 178-188. DOI: <http://dx.doi.org/10.1080/01496395.2011.630055>.
21. Carlisle, T. K.; Bara, J. E.; Gabriel, C. J.; Noble, R. D.; Gin, D. L. *Ind. Eng. Chem. Res.* **2008**, *47*, 7005-7012. DOI: <http://dx.doi.org/10.1021/ie8001217>.
22. Chen, X.; Luo, X.; Li, J.; Qiu, R.; Lin, J. *RSC Adv.* **2020**, *10*, 7751-7757. DOI: <http://dx.doi.org/10.1039/c9ra09293e>.
23. Wang, C.; Luo, X.; Zhu, X.; Cui, G.; Jiang, D.; Deng, D.; Li, H.; Dai, S. *RSC Adv.* **2013**, *3*, 15518-15527. DOI: <http://dx.doi.org/10.1039/C3RA42366B>.
24. Zhang, Y.; Wu, Z.; Chen, S.; Yu, P.; Luo, Y. *Ind. Eng. Chem. Res.* **2013**, *52*, 6069-6075. DOI: <http://dx.doi.org/10.1021/ie302928v>.
25. Ren, W.; Sensenich, B.; Scurto, A.M. *J. Chem. Thermodyn.* **2010**, *42*, 305-311. DOI: <http://dx.doi.org/10.1016/j.jct.2009.08.018>.
26. Feng, Z.; Yuan, G.; Xian-Kun, W.; Jing-Wen, M.; You-Ting, W.; Zhi-Bing, Z. *Chem. Eng. J.* **2013**, *223*, 371-378. DOI: <http://dx.doi.org/10.1016/j.cej.2013.03.005>.
27. Jing, G.; Zhou, L.; Zhou, Z. *Chem. Eng. J.* **2012**, *181-182*, 85-95. DOI: <http://dx.doi.org/10.1016/j.cej.2011.11.007>.
28. Sistla, Y. S.; Khanna, A. *Chem. Eng. J.* **2015**, *273*, 268-276. DOI: <http://dx.doi.org/10.1016/j.cej.2014.09.043>.
29. Zeng, S.; Zhang, X.; Bai, L.; Zhang, X.; Wang, H.; Wang, J.; Bao, D.; Li, M.; Liu, X.; Zhang, S. *Chem. Rev.* **2017**, *117*, 9625-9673. DOI: <https://doi.org/10.1021/acs.chemrev.7b00072>.
30. Martínez-Palou, R.; Likhanova, N. V.; Olivares-Xometl, O. *Pet. Chem.* **2014**, *54*, 595-607. DOI: <http://dx.doi.org/10.1134/S0965544114080106>.
31. Gurkan, B. E., de la Fuente, J. C., Mindrup, E. M., Ficke, L. E., Goodrich, B. F., Price, E. A., Schneider, W. F.; Brennecke, J. F. *J. Am. Chem. Soc.* **2010**, *132*, 2116-2117. DOI: <http://dx.doi.org/10.1021/ja909305t>.
32. Shukla, S. K., Khokarale, S. G., Bui, T. Q., Mikkola, J.-P. T. *Front. Mater.* **2019**, DOI: <http://dx.doi.org/10.3389/fmats.2019.00042>.
33. Aghaie, M.; Rezaei, N.; Zendejboudi, S. *Renew. Sustain. Energy Rev.* **2018**, *96*, 502-525. DOI: <http://dx.doi.org/10.1016/j.rser.2018.07.004>.
34. CEM corp. web page: <https://www.cem.com>, accessed in September 2022.
35. Yamada, T.; Tominari, Y.; Tanaka, S.; Mizuno, M. *J. Phys. Chem. B* **2017** *121*, 3121-3129. DOI: <http://dx.doi.org/10.1021/acs.jpcc.7b01429>.

36. Yamada, T.; Tominari, Y.; Tanaka, S.; Mizuno, M.; Fukunaga, K. *Materials*. **2014**, 7, 7409–7422. DOI: <http://dx.doi.org/10.3390/ma7117409>.
37. Saravanamurugan, S.; Kunov-Kruse, A. J.; Fehrmann, R.; Riisager, A. *ChemSusChem*. **2014**, 7, 897–902. DOI: <http://dx.doi.org/10.1002/cssc.201300691>.
38. Ossowicz, P.; Kleboko, J.; Roman, B.; Janus, E.; Rozwadowski, Z. *Molecules*. **2019**, 24, 3252. DOI: <http://dx.doi.org/10.3390/molecules24183252>.
39. Feng, Z.; Cheng-Gang, F.; You-Ting, W.; Yuan-Tao, W.; Ai-Min, L.; Zhi-Bing, Z. *Chem. Eng. J.* **2010**, 160, 691–697. DOI: <http://dx.doi.org/10.1016/j.cej.2010.04.013>.
40. Cammarata, L.; Kazarian, S. G.; Salter, P. A.; Welton, T. *Phys. Chem. Chem. Phys.* **2001**, 3, 5192–5200. DOI: <http://dx.doi.org/10.1039/B106900D>.
41. Hiremath, V.; Jadhav, A. H.; Lee, H.; Kwon, S.; Seo, J. G. *Chem. Eng. J.* **2016**, 287, 602–617. DOI: <http://dx.doi.org/10.1016/j.cej.2015.11.075>.
42. <https://libroelectronico.uaa.mx/capitulo-4-aminoacidos-y/curvas-de-titulacion-de-los.html>, accessed in September 2022.
43. Gurau, G.; Rodriguez, H.; Kelley, S.P.; Janiczek, P.; Kalb, R.S.; Rogers, R.D. *Angew. Chem. Int. Ed.* **2011**, 50, 12024–12026. DOI: <http://dx.doi.org/10.1002/anie.201105198>.
44. Zulfiqar, S.; Sarwar, M. I.; Mecerreyes, D. *Polymer Chem.* **2015**, 6, 6435–6451. DOI: <http://dx.doi.org/10.1039/C5PY00842E>.
45. Shahrom, M. S. R.; Wilfred, C. D.; Taha, A.K.Z. *J. Mol. Liq.* **2016**, 219, 306–312. DOI: <http://dx.doi.org/10.1016/j.molliq.2016.02.046>.

Determination of Sodium, Potassium, Calcium and Magnesium in Urine, Using Microwave Plasma - Atomic Emission Spectrometry and Multi-Energy Calibration

Tania Lizeth Espinoza Cruz¹, Kazimierz Wrobel¹, Eunice Yanez Barrientos¹, Alma Rosa Corrales Escobosa¹, Ma Eugenia Garay-Sevilla², Francisco Javier Acevedo-Aguilar¹, Katarzyna Wrobel^{1*}

¹Departamento de Química, División de Ciencias Naturales y Exactas, Universidad de Guanajuato, Campus Guanajuato, L. de Retana 5, 36000 Guanajuato, Gto., México.

²Departamento de Ciencias Médicas, División de Ciencias de Salud, Universidad de Guanajuato, Campus León, León 37320, México.

*Corresponding author: Katarzyna Wrobel, email: katarzyn@ugto.mx; Phone: +52 473 7327555.

Received November 16th, 2022; Accepted January 11th, 2023.

DOI: <http://dx.doi.org/10.29356/jmcs.v68i1.1906>

Abstract. Microwave plasma - atomic emission spectrometry with multi-energy calibration (MP-AES-MEC) was used for the determination of four major elements in urine. In the family of atomic emission spectrometry, the distinctive features of MP-AES are: (i) nitrogen-based toroidal-shape plasma; (ii) good plasma tolerance to total solids; (iii) exceptionally low operating cost. On the other hand, due to relatively low plasma temperature, this technique is susceptible to spectral interferences and sample-to-sample fluctuating baseline is typical limitation, if previous acid digestion is not performed. MEC is a non-conventional quantification method, not requiring baseline correction and it has been selected in this work to achieve reliable determination of Na, K, Ca and Mg in simply diluted urine. The principle underlying MEC is the proportionality between signal intensity and analyte concentration, occurring at any emission line for given element. Accordingly, for each sample, only two solutions were prepared likewise in the one-point standard addition and two analytical runs were performed, yet four experimental points were generated for calibration according with the number of emission lines utilized. Based on the results obtained by analyzing urines from different subjects, the sample dilution fold was selected to adjust the analyte concentration below half of the calibration range (150 for K, 200 for Na, 50 for Ca and 25 for Mg), while the addition of standard was done roughly doubling natural concentration in the diluted sample. The evaluated instrumental limits of detection were: 0.009 ± 0.005 mg L⁻¹ for K, 0.131 ± 0.011 mg L⁻¹ for Na, 0.050 ± 0.014 mg L⁻¹ for Ca and 0.059 ± 0.010 mg L⁻¹ for Mg (five replicates in different days). Each analysis was performed in triplicate yielding percentage relative standard deviation ≤ 11 %. The percentage recoveries calculated taking the results obtained in acid-digested samples by external calibration as reference values were in the range: 83.3-102 % for K, 88.4-110 % for Na, 82.9-113 % for Ca and 85.8-108 % for Mg. The capability of the proposed MP-AES-MEC procedure for monitoring four elements in different clinical conditions was demonstrated by analyzing ten urines from diabetic patients and ten from non-diabetic control subjects; statistical differences between these two groups was found for Na and K.

Keywords: Microwave plasma - atomic emission spectrometry (MP-AES); multi-energy calibration (MEC); urine; diabetes.

Resumen. La espectrometría de emisión atómica con excitación en plasma de microondas y con el método de calibración multi-energía (MP-AES-MEC) fueron empleados para la determinación de cuatro elementos mayoritarios en orina. Dentro de la familia de técnicas de espectrometría de emisión atómica, las características

distintivas de MP-AES son las siguientes: (i) uso de plasma de nitrógeno con geometría toroidal; (ii) buena tolerancia del plasma a sólidos totales; (iii) excepcionalmente bajo costo de operación. Por otra parte, debido a la relativamente baja temperatura del plasma, una típica limitación de esta técnica es que es susceptible a interferencias espectrales y la fluctuación de línea base entre muestras si estas no son digeridas previamente. El método MEC es un método de cuantificación no-convencional, el cual no requiere corrección de línea base y fue seleccionado en este trabajo para lograr la determinación confiable de Na, K, Ca and Mg después de una simple dilución de orina. MEC se sustenta en la proporcionalidad entre intensidad de la señal y la concentración del analito existente en cualquier línea de emisión de un elemento dado. Para cada una de las muestras, se prepararon dos soluciones, igual que en el método de un punto de adición de estándar y se realizaron dos corridas analíticas, pero se generaron cuatro puntos experimentales para la calibración, correspondientes a cuatro líneas de emisión seleccionadas por elemento. Con base en los resultados obtenidos analizando orinas de diferentes sujetos, el factor de dilución de la muestra fue seleccionado para ajustar la concentración del analito por debajo de la mitad del rango de calibración (150 para K, 200 para Na, 50 para Ca, 25 para Mg), mientras que la adición de estándar se realizó subiéndolo aproximadamente al doble la concentración natural en la muestra diluida. Los límites de detección instrumentales fueron: $0.009 \pm 0.005 \text{ mg L}^{-1}$ para K, $0.131 \pm 0.011 \text{ mg L}^{-1}$ para Na, $0.050 \pm 0.014 \text{ mg L}^{-1}$ para Ca, $0.059 \pm 0.010 \text{ mg L}^{-1}$ para Mg (con base en cinco réplicas realizadas en diferentes días). Cada análisis se realizó por triplicado, obteniéndose valores de desviación estándar relativa $\leq 11 \%$. Los porcentajes de recuperación calculados considerando los resultados obtenidos en muestras digeridas con ácido mediante calibración externa convencional como valores de referencia fueron los siguientes: 83.3-102 % para K, 88.4-110 % para Na, 82.9-113 % para Ca, 85.8-108 % para Mg. La capacidad del procedimiento MP-AES-MEC para monitorear cuatro elementos en diferentes condiciones clínicas se demostró analizando orinas de pacientes diabéticos y orinas de sujetos en un grupo control, encontrándose diferencias estadísticamente significativas para Na y K.

Palabras clave: Espectrometría de emisión atómica con excitación en plasma de microondas (MP-AES); calibración multi-energía (MEC); orina; diabetes.

Introduction

Sodium, potassium, calcium, and magnesium are major cationic urinary electrolytes; their monitoring serves for dietary intake control and as a diagnostic tool in many clinical conditions associated with osmotic balance, renal, muscle and heart functions, among others [1,2]. Given the importance of the four metals in human health and disease, their determination is performed in both, clinical and research laboratories. In routine practice, colourimetric assays, emission flame photometry, flame atomic absorption spectrometry or ion-selective electrodes are in use [3]. Despite meeting the requirements of simplicity, easy implementation, and automation in the analysis of a long series of samples, each of these assays has certain limitations mainly related to the lack of selectivity. For spectrophotometric determination of Ca and Mg, chelating agents such as EDTA, ortho-cresol phthalein or Arsenazo 3 are used; nevertheless, potential interferences must be eliminated by adding masking agents or by the application of multivariate analysis algorithms [4-6]. In the case of ion-selective electrodes, the test provides quantitative data on free ions ("ionized" Ca, Mg); however, the electrodes have a short lifetime, and the measurement is susceptible to interference from organic compounds and/or other ions present in the sample. As to flame emission photometry, it is used only for Na and K with the mandatory installation of interference filters, while the limitation of atomic absorption spectrometry is that only one signal can be acquired per analytical run. In the research laboratories, there is a clear preference for using advanced atomic spectrometry techniques since these are characterized by much greater selectivity, sensitivity and high detection power and are practically free of chemical interferences. Although low limits of quantification are not required for the determination of Na, K, Mg and Ca in clinical samples, the task remains challenging due to spectral and/or ionization interferences. Inductively coupled plasma ionization mass spectrometry (ICP-MS) is considered the gold standard in the determination of metals/metalloids, but it requires a complete mineralization of the sample and an efficient control of spectral interference ($^{40}\text{Ar}^1\text{H}^+$ for K, $^{40}\text{Ar}^+$ for Ca, $^{12}\text{C}_2^+$ for Mg, among

many others)[7]. Another technique of interest in the analysis of the four metals is inductively coupled plasma - atomic emission spectrometry (ICP-OES); in this case, sample mineralization is also preferable since the plasma has a low tolerance to total solids and high loads of organic carbon; other obstacles include spectral interference [8].

Among the different types of atomic emission spectrometers available, the one using in-torch generated microwave plasma (MP-AES) is an interesting option for the determination of major and trace elements in biological samples [9-11]. The important features of MP-AES include: (i) low cost due to the use of nitrogen as a plasma gas; (ii) toroidal-shape plasma; (iii) better plasma tolerance to total solids and organic solvents as compared to ICP; (iv) similar detection power as ICP-AES [9]. On the other hand, due to the lower temperature of microwave plasma, spectral interferences and noisy baseline are typical inconveniences in MP-AES [10,12]. To avoid analytical errors due to the baseline fluctuations often occurring between the samples, acid digestion is highly recommended prior to instrumental analysis. It is noteworthy however that few non-conventional quantification methods, such as multi-energy calibration (MEC) [13] or standard dilution analysis (SDA) [14], do not require baseline correction and provided interference-free results in the analysis of simply diluted samples [10,15].

MEC can be performed in any analytical technique, in which one analyte produces various signals in a single analytical run and several studies informed its successful applications in atomic emission spectrometry [10,13,15,16]. Nonetheless, to the best of our knowledge, there has been only one application of MEC in MP-AES reported so far, in which the determination of Na, K, Mg and Ca in wine was achieved [10]. The rationale underlying MEC in AES is that the relative distribution of spectral lines intensities for given element is constant, independently of element concentration and is determined by specific transition energy, transition probability and excited-state degeneracy related with each line. On the other hand, for each emission line, its intensity is proportional to the analyte concentration in the analyzed sample; therefore, when the sample is prepared as for one-point standard addition, ratios between signals magnitudes acquired at each wavelength are different yet always proportional to the ratio of analyte concentrations in two solutions (sample without and with standard addition). In practice, quantification is performed based on the concentration of added standard and using the slope of the linear regression function, which relates signals intensities acquired in the spiked and non-spiked sample at different wavelengths [13] (respective mathematical equations Eq1S-5S are presented in Supporting Information, SI). It should be stressed that with only two solutions prepared per sample, the number of experimental points used to compute the linear regression function corresponds to the number of emission lines where the signals were acquired [10,13,17]. An additional advantage of MEC is its ability for the detection of wavelengths affected by spectral interferences, since the respective experimental points would present deviation from the linearity of the calibration curve relating intensities of the analyte signals in the spiked and non-spiked samples.

In this work, the interference-free determination of Na, K, Ca, and Mg in urine is proposed, using MP-AES and multi-energy calibration eliminating the requirement for sample digestion and baseline correction.

Experimental

Reagents and samples

All chemicals were of analytical reagent grade. Deionized water (18.2 M Ω cm, Labconco) was used throughout; ultrapure concentrated nitric acid was from Fluka. The standard solutions of Na, K, Ca (1000 mg L⁻¹ each) and Mg (1015 mg L⁻¹) were from Sigma.

The first morning urine samples from ten diabetic patients (D1-D10) and from ten non-diabetic control subjects (C1-C10) were kindly provided by Dra. Ma. E. Garay-Sevilla from the Department of Medical Sciences, University of Guanajuato. The samples were collected in acid-washed 50 mL Falcon tubes; after acidification with ultrapure nitric acid (final concentration 2 % v/v), the tubes were stored at -20 °C. Prior to the analysis, urine samples were thawed and centrifuged (13 000 g, 10 min). Urine from four volunteers (V1-V4) was used for setting the experimental and instrument operating parameters.

Instrumentation and operating conditions

An Agilent 4100 MP-AES atomic emission spectrometer equipped with autosampler SPS3, concentric nebulizer for 4100 MP-AES, a single-pass glass cyclonic spray chamber and controlled by Agilent MP Expert Software (actualized from MP-AES 4200) was used.

For univariate calibration, the instrumental operating conditions were as follows: pump rate of 15 rpm, nitrogen pressure of 140 kPa for Na, K, 200 kPa for Mg and 240 kPa for Ca; plasma viewing position set at 10 for K, Ca, Mg and -5 for Na; stabilization time of 15 s and integration time of 5 s; wavelengths: Na 589.592 nm, K 766.491 nm, Ca 422.673 nm, Mg 285.213 nm. Auto background correction was applied, and for each element, the analytical signal was acquired as peak height (instrumental conditions given in the previous section).

For multi-energy calibration (MEC), the instrumental conditions were not modified except that no baseline correction was applied. The spectral lines were: 330.237 nm, 568.820 nm, 588.995 nm, and 589.592 nm for Na; 693.877 nm, 766.491 nm, 769.897 nm and 344.738 nm for K; 393.366 nm, 396.847 nm, 422.673 nm, and 430.253 nm for Ca; 279.553 nm, 280.271 nm, 285.213 nm and 518.360 nm for Mg. For each diluted sample, all analytical signals corresponding to different wavelengths were acquired in a single run.

Sample digestion and quantification by external calibration (MP-AES-EC)

Multielement standard solutions were prepared in 2 % v/v nitric acid, which was also used as a blank. Six-point calibration covered the concentration ranges: 1.0 - 15 mg L⁻¹ for Na and K; 0.2 - 2.5 mg L⁻¹ for Ca and Mg.

Sample digestion was performed by heating 0.5 mL aliquot of thawed urine with 0.5 mL of nitric acid (90 °C, 2h) and leaving the samples to reach room temperature. The volume was brought to 5 mL in a volumetric flask. An aliquot of each digest was centrifuged in a new 2 mL Eppendorf tube (13 000 g, 10 min) and appropriately diluted with 2 % v/v nitric acid: 10 - 100 times for Na, 10 - 50 times for K, up to 20 times for Ca and Mg.

Each sample were analyzed in triplicate.

Sample dilution and quantification by multi-energy calibration (MP-AES-MEC)

Each urine sample was appropriately diluted and then, the solutions M and M+S were prepared. To do so, 2 mL aliquot of initially diluted sample was mixed with 2 mL of with nitric acid 2 % v/v (solution M) whereas another 2 mL aliquot of diluted sample was mixed with 2 mL of nitric acid containing analyte standard (solution M+S). The total dilution fold was selected to adjust the analyte concentration approximately below the middle of the calibration range and standard addition was performed roughly doubling the natural concentration in the diluted sample. Using four wavelengths per element and instrument operating conditions listed in section of Instrumentation and operating conditions, spectra for M and for M+S were acquired without background correction. Linear regression equation was computed for each analyte, relating the signals obtained for two solutions at each selected wavelength. The analyte concentration in the sample ($c_{A,s}$) was calculated as explained in SI (Equations 1S-5S) [13,15,16,18], according with the following equation:

$$c_{A,s} = \frac{m' * c_{A,std}}{1-m'} \quad \text{Eq.1}$$

where $c_{A,std}$ is the concentration of analyte standard added (solution M+S) and m' is the slope of the linear regression function mentioned above.

Each sample were analyzed in triplicate.

Statistical analysis

The determination results are means obtained for three independent replicates with respective standard deviations. Statistical unpaired *t*-test for independent samples was used to compare the concentrations of four elements in urines from diabetic patients against non-diabetic control subjects. To ensure normal data distribution, the concentration values were transformed to natural logarithms for Na, K and Mg and to square roots for Ca. The software used was Microsoft Excel 2010 and statistical significancy was set at $p < 0.05$.

Results and discussion

In the preliminary experiments it was observed that diluted samples could not be used for elements determination using conventional external calibration; even setting manually background correction individually per each sample, the results were inconsistent with those obtained after acid digestion. The goal of this work was to demonstrate the feasibility of multi-energy calibration (MEC) for interference-free determination of four major elements in urine by MP-AES, avoiding sample digestion and troublesome baseline correction. The attractiveness of such approach lies in the procedural simplicity: only two solutions per sample need to be prepared and two instrumental runs are performed, yet the number of experimental points obtained for computing linear regression function is higher compared to typical one-point standard addition and corresponds to the number of spectral wavelengths selected per given element. It should also be stressed that the same chemical environment of the analyte is preserved in each measurement likewise in the method of standard addition; further, spectral lines affected by interferences can be detected and removed, based on the deviation of corresponding experimental point from the linear regression fit [10,13,15]. In setting-up the MP-AES-MEC procedure, several parameters had to be established; among them, the dilution factor, the concentration of standard added to the sample, the spectral lines and instrument operating conditions. In the next step, analytical performance of the proposed procedure was evaluated, and the results obtained by MP-AES-MEC in diluted urine samples were compared against those attained after acid digestion using typical external calibration (MP-AES-EC). Finally, to demonstrate the procedure utility in the real-world scenarios, the determination of four elements in urines from diabetic patients and non-diabetic control subjects was performed. In the following sections, the above-mentioned points are described in detail.

Setting-up the MP-AES-MEC procedure

The emission lines for K, Na, Mg and Ca were adopted from previous studies [10,15] and these lines are listed in the Experimental section. The selection criteria were: (i) sufficiently high sensitivity enabling for acquisition of analyte signals in M and M+S solutions and (ii) lack of spectral interferences. Instrument operating parameters were not modified from those used for external calibration; however, no baseline correction was applied. As already mentioned before, the dilution factor and the concentration of added standard had to be selected for each element. The assumption was to lower natural analyte concentration upon sample dilution to fit in the lower part of the calibration range and to double this concentration after standard addition. To verify the correctness of this proposal, four urines from volunteers (V1-V4) were acid-digested and the elements were determined by external calibration (analytical parameters evaluated in the calibration process are presented in Table 1S, SI). The results obtained for V1-V4 samples are presented in Table 1 together with the dilution factors proposed for multi-energy calibration. Accordingly, the analyte concentrations in any diluted sample (M) corresponded to about 4 mg L⁻¹ for Na and K; 0.4 mg L⁻¹ for Ca and 0.25 mg L⁻¹ for Mg. The final concentrations of standard added to prepare solutions M+S were set at 8.0 mg L⁻¹ for Na, 6.5 mg L⁻¹ for K, 1.5 mg L⁻¹ for Ca and 0.8 mg L⁻¹ for Mg. Using the above-selected variables, MEC was performed, and the results obtained are included in Table 1. Large differences among concentrations found in four samples, especially for Na and K, should be ascribed to their recent dietary intake; indeed, the samples were randomly obtained from healthy volunteers and did not correspond to the first morning urine. On the other hand, it can be observed in Table 1 that linear regression functions relating analyte signal intensities acquired for M and M+S solutions at different spectral lines presented excellent linearity ($R^2 \geq 0.999$); the slope of this function (m') was used to compute analyte concentration in the sample (Eq. 1 and Eq. 1S-5S in SI). Most importantly, considering the results obtained by EC as reference values, the percentage error of those attained by MEC with respect to EC was in the range (-1.6) – 11 % for K, 7.0 – 19 % for Na, (-6.7) – (-17) % for Ca and (-7.1) – 18 % for Mg; such consistency is indicative of acceptable accuracy of the proposed procedure consisting on simple sample dilution and MP-AES-MEC. It is noteworthy that errors of $\pm 20\%$ were reported in the study by Barros et al., where Na, K, Ca and Mg were determined in urine by MEC, but the analytical technique was inductively coupled plasma-atomic emission spectrometry (ICP-AES) and not MP-AES [15]. As emphasized in the Introduction, nitrogen plasma is used in MP-AES, which makes this technique much cheaper with respect to any other atomic spectrometry technique; however, lower plasma temperature causes higher susceptibility of MP-AES to interferences compared to inductively coupled argon plasma. Therefore, achieving reliable quantification in simply diluted biological samples is more challenging and the results presented in Table 1 confirm the feasibility of MEC for such purpose.

The limits of detection (LOD) for MP-AES-MEC were assessed as reported elsewhere [19,20]. Specifically, blank equivalent concentrations (BEC) were evaluated by taking blank solution as a sample and performing MEC; according with IUPAC's recommendations, limit of detection (LOD) corresponded to three-times multiplied BEC. In five replicates, the obtained LOD values were: $0.009 \pm 0.005 \text{ mg L}^{-1}$ for K, $0.131 \pm 0.011 \text{ mg L}^{-1}$ for Na, $0.050 \pm 0.014 \text{ mg L}^{-1}$ for Ca and $0.059 \pm 0.010 \text{ mg L}^{-1}$ for Mg. Comparing with external calibration, LOD values for MEC were lower for Na and K and similar for Ca and Mg (Table 1S, SI). On the other hand, LOD obtained for MP-AES-MEC were similar to those previously reported for ICP-AES-MEC (0.070 mg L^{-1} K, 0.120 mg L^{-1} Na, 0.015 mg L^{-1} Ca and 0.043 mg L^{-1} Mg) [15].

Table 1. Concentrations of four elements in urine from volunteers (V1-V4), determined in acid-digested samples using external calibration (MP-AES-EC) and in diluted samples using multi-energy calibration (MP-AES-MEC). Means and standard deviations are presented, based on three replicates.

Sample	MP-AES-EC	MP-AES-MEC				
	Mean \pm SD, mg L^{-1}	Dilution ⁽¹⁾	Std., $\text{mg L}^{-1(2)}$	R ²⁽³⁾	m' ⁽⁴⁾	Mean \pm SD, mg L^{-1}
Potassium						
V1	489 \pm 12	60	6.5	0.9998	0.5455	468 \pm 17
V2	3.07 $\cdot 10^3 \pm 0.11 \cdot 10^3$	350		0.9999	0.5749	3.12 $\cdot 10^3 \pm 0.14 \cdot 10^3$
V3	505 \pm 8	60		0.9999	0.5635	503 \pm 9
V4	1.92 $\cdot 10^3 \pm 0.03 \cdot 10^3$	250		0.9998	0.5124	1.71 $\cdot 10^3 \pm 0.10 \cdot 10^3$
Sodium						
V1	708 \pm 7	50	8.0	0.9999	0.6124	634 \pm 12
V2	3.37 $\cdot 10^3 \pm 0.19 \cdot 10^3$	250		0.9999	0.5764	2.72 $\cdot 10^3 \pm 0.05 \cdot 10^3$
V3	740 \pm 32	50		0.9999	0.6323	688 \pm 23
V4	5.05 $\cdot 10^3 \pm 0.12 \cdot 10^3$	400		0.9999	0.5503	4.14 $\cdot 10^3 \pm 0.30 \cdot 10^3$
Calcium						
V1	6.93 \pm 0.41	20	1.5	0.9999	0.2123	8.08 \pm 0.8
V2	30.5 \pm 0.8	35		0.9999	0.3868	33.3 \pm 1.7
V3	13.4 \pm 0.6	20		0.9998	0.3283	14.7 \pm 0.1
V4	150 \pm 6	180		0.9999	0.3714	160 \pm 14
Magnesium						
V1	12.8 \pm 0.2	30	0.8	0.9997	0.3357	12.1 \pm 0.3
V2	42.4 \pm 1.3	75		0.9999	0.4195	42.0 \pm 0.5
V3	10.1 \pm 0.2	30		0.9988	0.2563	8.30 \pm 0.07
V4	44.9 \pm 1.3	100		0.9999	0.3804	48.1 \pm 0.3

⁽¹⁾urine dilution factor corresponds to the final solution prepared for multi-energy calibration (solution M); ⁽²⁾ concentration of the added standard in the final solution used in MEC (M+S); ⁽³⁾regression coefficient on the above function; ⁽⁴⁾slope of linear regression relating signal intensities in M and M+S solutions at different spectral lines, the presented value is a mean from three replicates (Eq. 1).

Analysis of the real-world samples

To explore the capability of the proposed MP-AES-MEC procedure in monitoring urine levels of four major elements in different clinical conditions, ten samples from diabetic patients and ten from non-diabetic control group were analyzed. In the first place, the samples were acid-digested, and the determination was carried out by external calibration. Based on the obtained data, dilution factors were set and MEC was performed using already established standard additions (8.0 mg L⁻¹ Na, 6.5 mg L⁻¹ K, 1.5 mg L⁻¹ Ca and 0.8 mg L⁻¹ Mg). In Table 2S (SI), dilution factors, m' and R^2 values are provided for each sample whereas in Figures 1 and 2, linear regression functions relating intensities acquired in M and M+S for K, Na, Ca and Mg in sample C1 are presented together with spectra registered for both solutions at different spectral lines. The concentrations of four analytes found in urine samples by MP-AES-EC and MP-AES-MEC are given in Table 3S (SI). It should be stressed that precision, evaluated as percentage relative standard deviation in three replicates, did not exceed 5 % for Ca, 6 % for K and Mg, 9 % for Na using external calibration. For MEC, slightly poorer precision was obtained, yet percentage RSD was always below 11 % (Table 3S, SI). Further, percentage recoveries were calculated for MEC, taking the results obtained in acid-digested samples by MP-AES-EC as “reference” values. As can be observed in Table 3S (SI), the obtained recoveries were in the range 83.3-102 % for K, 88.4-110 % for Na, 82.9-113 % for Ca and 85.8-108 % for Mg. In this part of the study, MEC was performed adjusting dilution factors individually for each sample, based on the concentration determined previously by EC. Such approach is of no use when large number of samples need be analyzed; however, more uniform dilution factors can be proposed based on the obtained results, namely 150 for K, 200 for Na, 50 for Ca and 25 for Mg. With such uniformized dilution rates, practically for all samples the analyte concentration falls in the lower range of the calibration and still, the proposed standard additions are adequate.

Mean urine concentrations of four elements in diabetic and in control samples are presented in Table 2 together with means, medians and ranges calculated for each group. Noteworthy is that the almost all results fall within the reference ranges set for random healthy individuals considering different ages and genders yet without restriction of dietary intake: 460 - 4600 mg L⁻¹ for Na, 430 - 6000 mg L⁻¹ for K, 5.0 - 380 mg L⁻¹ for Ca and 6.0 - 230 mg L⁻¹ for Mg [3]. Further, the concentrations determined in this work for control group (Table 2) are consistent with the ranges reported in healthy Pakistan adults for Ca and Mg (39.6 - 78.2 mg L⁻¹ and 42.9 - 82.1 mg L⁻¹, respectively [21]) whereas a tendency toward lower values in this study can be noted for Na and K (3155 - 4039 mg L⁻¹, 1124 - 2068 mg L⁻¹ K, respectively [21]). On the other hand, while comparing the values obtained for diabetic patients against control subjects, means and medians presented in Table 2 are lower for K and Na and higher for Ca in diabetic urines with no apparent change observed for Mg. In the bottom row of Table 2, the results of unpaired *t*-test are shown, indicating that differences for Na and K were statistically significant. In line with the above observations, dysregulation of the major electrolytes urinary excretion has been reported in diabetes, cardiovascular and renal disorders [22]. In particular, the decrease of urinary K levels is well-documented in diabetes, as well as in chronic kidney disease and in cardiovascular diseases [23,24]. In turn, lower sodium concentrations might be indicative of reduced dietary intake in diabetic as compared to healthy subjects [25]; despite clear advantage of lowering blood pressure, several adverse effects of restricted sodium intake and its low urinary levels were discussed, including the increased LDL cholesterol and reduced peripheral insulin sensitivity, among others [25]. When urine electrolytes are monitored, sodium-to-potassium ratio is often reported in relation to dietary intake and blood pressure control [26]; direct association between this parameter and diabetes and renal failure incidence has also been informed [27,28]. In this work, mean sodium-to-potassium ratio was evaluated as 2.5 in diabetic patients and 2.1 in the control group, which is consistent with the above-mentioned effects. Finally, a tendency toward higher urine concentrations of Ca in diabetic urines seems to confirm previously reported loss of Ca due to deterioration of skeletal system and due to dysregulation of the vitamin D pathway, both associated with diabetes [29]. Within the context of the present work, the obtained results and the above discussion support the capability of the proposed procedure for detecting concentration differences of major urine elements in different clinical conditions hence its suitability for routine monitoring purposes.

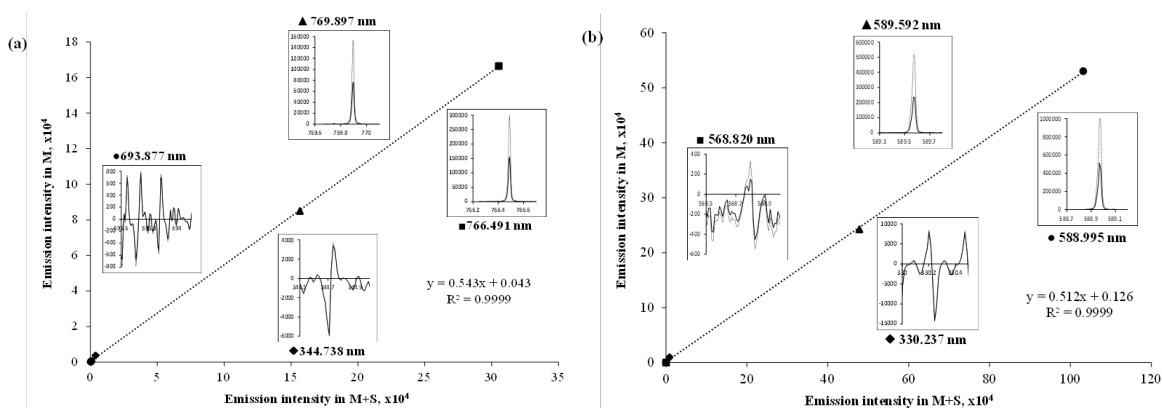


Fig. 1. Linear regression functions relating intensities acquired in solutions M and M+S prepared for sample C1; inserts show emission spectra registered for both solutions at different spectral lines: (a) potassium; (b) sodium.

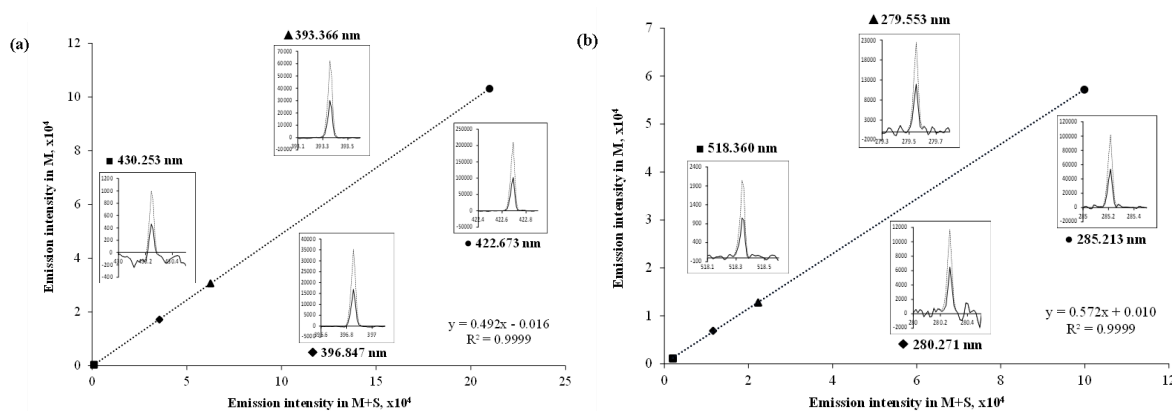


Fig. 2. Linear regression functions relating intensities acquired in solutions M and M+S prepared for sample C1; inserts show emission spectra registered for both solutions at different spectral lines: (a) calcium; (b) magnesium.

Table 2. Concentrations of four elements determined by proposed MP-AES-MEC procedure in urine from diabetic patients (D1-D10) and from non-diabetic control subjects (C1-C10). Mean values based of three replicates of each sample are presented (respective standard deviations are provided in Table 3S, SI), means and median per group and the results of unpaired *t*-test comparing two groups are included in the bottom rows.

Sample	K, mg L ⁻¹		Na, mg L ⁻¹		Ca, mg L ⁻¹		Mg, mg L ⁻¹	
	D	C	D	C	D	C	D	C
1	471.0	1006	1378	1679	155	36.3	26.1	50.6
2	465.6	900.3	915.9	879.0	41.9	31.8	14.2	16.0
3	448.0	1665	1128	1948	71.9	58.2	16.5	27.2
4	984.0	390.7	2696	2045	172	120	79.0	30.9

5	321.3	1076	312.0	3466	24.1	89.4	12.1	41.5
6	197.0	1733	542.4	2294	2.18	28.1	11.3	23.2
7	578.0	437.3	3289	1325	175	41.4	43.2	20.2
8	1099	1338	1070	2442	69.6	24.7	86.0	19.8
9	424.7	1229	1233	1365	28.1	26.1	21.1	22.0
10	371.1	2200	622.1	2059	4.55	20.8	7.46	41.4
Mean	536.0	1198	1319	1950	74.4	47.7	31.7	29.3
Median	456.8	1153	1099	1997	55.8	34.1	18.8	25.2
Range	197- 1099	390.7- 2200	312.0- 3289	879.0- 3466	2.18- 175	20.8- 120	7.46- 86.0	16.0- 50.6
<i>t</i> -test	$T_{\text{exp}} = 3.326$ $T_{\text{crit}} = 1.734$ $p = 0.0019$		$T_{\text{exp}} = 2.162$ $T_{\text{crit}} = 1.761$ $p = 0.0242$		$T_{\text{exp}} = 0.646$ $T_{\text{crit}} = 1.734$ $p = 0.2631$		$T_{\text{exp}} = 0.631$ $T_{\text{crit}} = 1.734$ $p = 0.2681$	

Conclusions

In this work, the feasibility of multi-energy calibration for the determination of Na, K, Ca and Mg in urine by microwave plasma - atomic emission spectrometry has been demonstrated. Specific benefits of the proposed MP-AES-MEC procedure are as follows: (i) simple sample pretreatment consisting of urine dilution with nitric acid 2% v/v; (ii) no need for baseline correction; (iii) chemical matrix of the sample present in all measurements; (iv) two solutions per sample prepared as in one-point standard addition (M and M+S, respectively) and two analytical runs performed, yet four experimental points generated for linear regression function enhancing the quality of linear fit. Four emission lines were selected for each element, the dilution factors were proposed (150 for K, 200 for Na, 50 for Ca, 25 for Mg) to adjust analyte concentration in solution M corresponding to the lower part of calibration range and standard additions used to prepare solution M+S roughly doubled the natural analyte concentration (8.0 mg L⁻¹ Na, 6.5 mg L⁻¹ K, 1.5 mg L⁻¹ Ca, 0.8 mg L⁻¹ Mg). The instrumental limits of detection were similar as those evaluated for conventional external calibration and acceptable precision was obtained for the real-world samples (RSD ≤ 11% based on triplicate analysis). The results obtained by the proposed procedure in urine samples did not present statistical differences as compared to the concentrations determined in acid-digested sample using conventional external calibration (ANOVA, $p < 0.05$). In application of the proposed procedure to the analysis of urine from diabetic patients and from non-diabetic control subjects, statistically lower K and Na concentrations were found in diabetic samples confirming that the sensitivity of MP-AES-MEC allows for detecting differences of major urine electrolytes in different clinical conditions.

Acknowledgements

The financial support from National Council of Science and Technology, Mexico (CONACYT), project A1-S-9671 is gratefully acknowledged.

References

1. Maciel, A. T.; Vitorio, D.; Osawa, E. A. *Front. Med.* **2022**, 9, 2186. DOI: <https://doi.org/10.3389/fmed.2022.912877>.
2. Moulin, F.; Ponte, B.; Pruijm, M.; Ackermann, D.; Bouatou, Y.; Guessous, I.; Ehret, G.; Bonny, O.; Pechère-Bertschi, A.; Staessen, J. A.; Paccaud, F.; Pierre-Yves, M.; Burnier, M.; Vogt, B.; Devuyst, O.; Bochud, M. *Kidney Int.* **2017**, 92, 1536-1543.
3. Tietz, N. W. *Tietz Clinical Guide to Laboratory*. Elsevier, St. Louis MO, 1995.
4. Bazydło, L. A.; Needham, M.; Harris, N. S. *Lab. Med.* **2014**, 45, e44-e50.
5. Wróbel, K.; Wróbel, K.; López-de-Alba, P. L.; López-Martínez, L. *Anal. Lett.* **1997**, 30, 717-737.
6. Parentoni, L. S.; Pozeti, R. C. S.; Figueiredo, J. F.; Faria, E. C. D. *J. Braz. Patol. Med. Lab.* **2001**, 37, 235-238.
7. Agatemor, C.; Beauchemin, D. *Anal. Chim. Acta* **2011**, 706, 66-83.
8. Krejčová, A.; Cernohorsky, T.; Curdova, E. *J. Anal. At. Spectrom.* **2001**, 16, 1002-1005.
9. Balaram, V. *Microchem. J.* **2020**, 159, 105483.
10. Espinoza Cruz, T. L.; Guerrero Esperanza, M.; Wrobel, K.; Barrientos, E. Y.; Acevedo-Aguilar, F. J.; Wrobel, K. *Spectrochim. Acta Part B.* **2020**, 164, 105754.
11. Gonzalez Ibarra, A. A.; Yanez Barrientos, E.; Wrobel, K.; Corrales Escobosa, A. R.; Wrobel, K. *J. Plant Nutr.* **2022**, 1-17. DOI: <https://doi.org/10.1080/01904167.2022.2071733>.
12. Jung, M. Y.; Kang, J. H.; Choi, Y. S.; Lee, J. Y.; Park, J. S. *Food Chem.* 2019, 274, 20-25.
13. Virgilio, A.; Gonçalves, D. A.; McSweeney, T.; Neto, J. A. G.; Nóbrega, J. A.; Donati, G. L. *Anal. Chim. Acta.* **2017**, 982, 31-36.
14. Jones, W. B.; Donati, G. L.; Calloway Jr, C. P.; Jones, B. T. *Anal. Chem.* **2015**, 87, 2321-2327.
15. Barros, A. I.; Pinheiro, F. C.; Nóbrega, J. A. *Anal. Methods.* **2019**, 11, 3401-3409.
16. Machado, R. C.; Silva, A. B. S.; Donati, G. L.; Nogueira, A. R. A. *J. Anal. At. Spectrom.* **2018**, 33, 1168-1172.
17. Donati, G. L.; Amais, R. S. *J. Anal. At. Spectrom.* **2019**, 34, 2353-2369.
18. Tognoni, E.; Hidalgo, M.; Canals, A.; Cristoforetti, G.; Legnaioli, S.; Salvettia, A.; Palleschi, V. *Spectrochim. Acta Part B.* **2007**, 62, 435-443.
19. Virgilio, A.; Gonçalves, D. A.; McSweeney, T.; Neto, J. A. G.; Nóbrega, J. A.; Donati, G. L. *Anal. Chim. Acta.* **2017**, 982, 31-36.
20. Guerrero-Esperanza, M.; Wrobel, K.; Wrobel, K.; Ordaz-Ortiz, J. J. *J. Food Compos. Anal.* **2023**, 115, 104963.
21. Afridi, H. I.; Kazi, T. G.; Kazi, N.; Jamali, M. K.; Arain, M. B.; Jalbani, N.; Sarfaraz, R. A.; Shah, A.; Kandhro, G. A.; Shah, A. Q.; Baig, J. A. *Biol. Tr. Elem. Res.* **2008**, 124, 206-224.
22. Liamis, G.; Evangelos, L.; Fotios, B.; Moses, E. *World J. Clin. Cases.* **2014**, 2, 488-496.
23. Kim, H. W.; Park, J. T.; Yoo, T. H.; Lee, J.; Chung, W.; Lee, K. B.; Chae, D. W.; Ahn, C.; Kang, S. W.; Choi, K. H.; Han, S. H. *Clin. J. Am. Soc. Nephrol.* **2019**, 14, 330-340.
24. Araki, S.; Haneda, M.; Koya, D.; Kondo, K.; Tanaka, S.; Arima, H.; Kume, S.; Nakazawa, J.; Chin-Kanasaki, M.; Ugi, S.; Kawai, H.; Araki, H.; Uzu, T.; Maegawa, H. *Clin. J. Am. Soc. Nephrol.* **2015**, 10, 2152-2158.
25. Ekinci, E. I.; Clarke, S.; Thomas, M. C.; Moran, J. L.; Cheong, K.; MacIsaac, R. J.; Jerums, G. *Diabetes Care* **2011**, 34, 703-709.
26. Perez, V.; Chang, E. T. *Adv. Nutr.* **2014**, 5, 712-741.

27. Siddiqui, K.; Nahla, B.; Scaria Joy, S. *The Scientific World Journal* **2014**, ID 461591. DOI: <http://dx.doi.org/10.1155/2014/461591>.
28. Hattori, H.; Hirata, A.; Kubo, S.; Nishida, Y.; Nozawa, M.; Kawamura, K.; Hirata, T.; Kubota, Y.; Sata, M.; Kuwabara, K.; Higashiyama, A.; Kadota, A.; Sugiyama, D.; Miyamatsu, N.; Miyamoto, Y.; Okamura, T. *Int. J. Environ. Pub. Health* **2020**, 17, 5811. DOI: <https://doi.org/10.3390/ijerph17165811>.
29. Carnevale, V.; Romagnoli, E.; D'Erasmus, E. *Diabetes/Metab. Res. Rev.* **2004**, 20, 196-204.

Synthesis, Characterization, and Molecular Docking of Casiopeinas® with Dipeptides as Secondary Ligand; Potential Inhibitors of SARS-Cov-2 Transcendental Proteins

Luis Gabriel Talavera-Contreras¹, Luis Felipe Hernández-Ayala¹, Virginia Gómez-Vidales², María Lourdes Villar-Cuevas^{1†}, Lena Ruiz-Azuara^{1*}

¹Departamento de Química Inorgánica y Nuclear, Facultad de Química, Universidad Nacional Autónoma de México, Avenida Universidad 3000, Ciudad de México, C.P 04510, México.

²Instituto de Química, Universidad Nacional Autónoma de México, Avenida Universidad 3000, Ciudad de México. C.P. 04510, México.

*Corresponding author: Lena Ruiz-Azuara, email: lenar701@gmail.com, lenar701@quimica.unam.mx; Phone: +52(55)56223529.

Received August 11th, 2022; Accepted March 15th, 2023.

DOI: <http://dx.doi.org/10.29356/jmcs.v68i1.1849>

Abstract. In this work, the synthesis and characterization of fourteen Casiopeinas® are presented, whose general formulae is $[\text{Cu}(\text{N-N})(\text{L-L})]\text{NO}_3$, where N-N are 2,2'-bipyridine and 1,10-phenanthroline and some of its methylated derivatives, L-L represent the dipeptides L-Tyrosil-Glycinate or Glycil-L-Tyrosinate. Spectroscopic characterization and DFT studies determine the square planar geometry for the coordination compounds, as well as the influence of the dipeptide on the molecular arrangement of ternary copper(II) compounds. In addition, a molecular docking study was carried out against transcendental proteins of the SARS-CoV-2 virus such as main protease (M^{pro}) and the RBD Spike-ACE2 complex. Docking studies indicate that all compounds can produce stable adducts with M^{pro} , obtaining ΔG_{U} values (-9.57 to -6.62 Kcal/mol) similar and superior to those presented by the reference inhibitors [boceprevir (-8.44 Kcal/mol) and remdesivir (-6.62 kcal/mol)], while for the RBD Spike-ACE2 complex obtaining ΔG_{U} values of five (-6.69 to -4.61 in C-terminal region) and three (-8.27 to -6.34 in central region) orders of magnitude higher than those presented by the controls (Boceprevir: $\Delta G_{\text{U}}=-1.98$ in C-terminal, $\Delta G_{\text{U}}=-4.97$ in central region, Remdesivir: $\Delta G_{\text{U}}=\text{Non}$ interactions in C-terminal, $\Delta G_{\text{U}}=-3.37$ in central region). π -alkyl interactions, π -cation, π -stacking, as well as hydrogen bonds and salt bridge bonds occur between the proteins and Casiopeinas®. In M^{pro} , interactions occur in aminoacids that are part of the enzymes catalytic site. Casiopeinas® interact at the interface of the RBD Spike-ACE2 complex in both, C-terminal and central regions. The obtained results position Casiopeinas® as potential candidates protein inhibitors of the virus that causes COVID-19.

Keywords: SARS-COV2; Casiopeinas®; metallodrugs; molecular docking; peptides; copper.

Resumen. En este trabajo, se presenta la síntesis y caracterización de 14 Casiopeinas®, cuya fórmula general es $[\text{Cu}(\text{N-N})(\text{L-L})]\text{NO}_3$, donde N-N son 2,2'-bipiridina y derivados metilados o 1,10-fenantrolina y análogos con grupos metilo, L-L representan a los dipéptidos L-Tirosil-Glicinato o Glicil-L-Tirosinato. Mediante estudios espectroscópicos y de DFT determinan la geometría cuadrada de los compuestos sintetizados, así como la influencia del dipéptido en el arreglo molecular de los compuestos ternarios de cobre(II). Complementariamente, se realizó un estudio de docking molecular ante proteínas trascendentales del virus SARS-CoV-2 como lo son la proteasa principal (M^{pro} o nsps-3) y el complejo RBD Spike-ACE2. Estudios de

docking molecular con la M^{Pro} se obtuvieron valores de ΔG_U (-9.57 a -6.629) kcal/mol, valores que son similares y superiores a los presentados por los inhibidores de referencia [boceprevir (-8.44 kcal/mol) y remdesivir (-6.62 kcal/mol)], mientras que para el complejo RBD Spike-ACE2 se obtuvieron valores de ΔG_U de cinco (-6.69 to -4.61 en región C-terminal) y tres (-8.27 to -6.34 en región central) órdenes de magnitud superiores respectivamente a los presentados por los inhibidores de referencia (Boceprevir: ΔG_U = -1.98 en C-terminal, ΔG_U = -4.97 en region central, Remdesivir: ΔG_U = Sin interacciones en C-terminal, ΔG_U = -3.37 en region central). Interacciones π -alquilo, π -catión, apilamiento π , así como enlaces puentes de hidrogeno y puentes de sal se producen entre las proteínas y Casiopeinas® estudiadas. En M^{Pro}, las interacciones ocurren en aminoácidos que forman parte del sitio catalítico de la enzima. Las Casiopeinas® interactúan en la interfase del complejo RBD Spike-ACE2 tanto en la región C-terminal como en la región central. Los resultados obtenidos, posicionan a las Casiopeinas® como potenciales candidatos a inhibidores proteicos del virus causante de la COVID-19.

Palabras clave: SARS-COV2; Casiopeinas®; metalofármacos; acoplamiento molecular; péptidos; cobre.

Introduction

In December 2019 in Wuhan China, a disease like pneumonia of idiopathic origin emerged [1]. Shortly after the causative agent was identified, that illness is transmitted by a virus and spreads in the air. This pathogen belongs to the β -coronavirus family, specifically called SARS-CoV-2 for its 89.1 % analogy with SARS-CoV [2], SARS-CoV-2 produce the COVID-19 disease, which was propagated throughout the world, on March 11, 2020, WHO being declared a pandemic. As of the date of writing, the pandemic still has about 761,071,826 cases and 6,879,677 deaths worldwide [3].

Coronaviruses are single-stranded, positive-sense, enveloped, unsegmented RNA-viruses [4] in which the genomic analysis determined for SARS-CoV-2 presents the following order of genes (5' to 3'): Replicase ORF1a1b, Spike (S), Envelope (E), Membrane (M) and Nucleocapsid (N). ORF1ab encodes 16 non-structural proteins (nsps) and 8 accessory proteins (3a, 3b, p6, 7a, 7b, 8b, 9b and orf14), the genes S, E, M and N encodes structural proteins with the same name. [5].

Considering the natural history of the infection process, the Spike protein is transcendent in the pathogenic process, since it is the antigenic determinant present in SARS-CoV-2, which must interact with the angiotensin-converting enzyme type II (ACE2) to be able to enter the host cells, where it will subsequently replicate the genomic material for the synthesis of viral RNA, structural and non-structural proteins [6]. Spike is a homotrimeric glycoprotein with two subunits (S1 and S2) in each monomer, the S1 subunit contains the receptor binding domain (RBD) that is expressed on the surface of the viral membrane and participates in the cellular recognition of the ACE2. ACE2 is a single-pass transmembrane protein involved in the regulation of vasoconstriction and blood pressure, ACE2 is expressed in cells of the lungs, kidneys, heart, and enterocytes of the small intestinal. [7] Particularly, the contact zones between the Spike protein RBD and ACE2 are divided into three clusters, the N-terminal region Gln498, Thr500 and Asn501 of Spike that bind via hydrogen bridge bond with Tyr41, Gln42, Lys353 and Arg 356 of ACE2. In the central region, Lys417 and Tyr453 of Spike interact with Asp30 and His34 of ACE2. Finally, in the C-terminal region, Gln474 and Phe486 of the RBD join Gln24 and Met 82 of angiotensin-converting enzyme type II [8].

The gene expression of ORF1a1b generates 16 non-structural proteins (nsps). One of them, nsps-5, also known as main protease [M^{Pro}], or 3C-like protease [3CL^{Pro}], is essential for the viral cycle. The M^{Pro} is responsible for the digestion of 11 conserved sites of two polyproteins (pp1a and pp1b) [9]. The functional importance of this enzyme is fundamental to the viral cycle, it is needed for SARS-CoV-2 replication and primary transcription of the viral genetic material [10]. The M^{Pro} active site contains a catalytic dyad (His41 and Cys145) and a substrate union triad (Met49, His163 and Gln189) [11]. This protein has been located at SARS-CoV, human coronavirus (HCoV229E) as well as porcine transmissible gastroenteritis virus (TGEV) [12].

Given the lack of drugs that can inhibit or even eliminate the virus, the scientific community have proposed strategies to be used in viral chemotherapy considering the various molecular targets involved in

the viral cycle, both *in vitro* [13] and *in silico* [14]. Several drugs can be used under recycling to be directed against viral elements such as M^{pro} [15], Spike protein [16], and ACE2, as well as other non-structural proteins such as PL^{pro} [17] and RNA-dependent of RNA polymerase (RdRp) [18]. A powerful tool for the analysis of candidates to be used as potential anti-SARS-CoV-2 drugs is molecular docking in which a diversity of molecules such as boceprevir ($\Delta G_U = -8.3$ Kcal/mol $IC_{50} = 8.0$ μ M, $K_i = 1.19$ μ M) [19-20] as M^{pro} active sites inhibitor [19], remdesivir ($\Delta G_U = -10.1$ Kcal/mol in RdRp) [21-22] (moldock score = -111.07 in Spike Protein central region) [22], Losartan [23], peptide derivatives [24], as well as coordination [25] and organometallics [26] compounds have been analyzed. The importance of targeting molecules to transcendent proteins is crucial to found molecules able to eliminate the SARS-CoV-2, as an example of this kind of compounds is PF-07321332 (PAXLOVID), the first approved drug by FDA, that is a M^{pro} inhibitor [27].

Several authors agree that coordination compounds represent a versatile option for drug development, since its physicochemical features can be tuned depending on the metal center, its oxidation number, the characteristics of ligand, coordination number, geometry around the metal, stereochemistry of the species formed to the aim to improve its biological activity. Medicinal inorganic chemistry has contributed to the development of metallodrugs with compounds that in their chemical structure present the metallic elements to treat various ailments such as cancer, schizophrenia, stomach upset, diabetes, antimicrobials, antiparasitic and antiviral agents [28]. For instance, several metallodrugs have been tested against the proteins involved in the SARS-CoV-2 viral cycle. Gold compounds [29] have presented evidence of inhibition of ACE2 ($IC_{50} = 16.2-25.0$ μ M) and PL^{pro} ($IC_{50} = 0.96 - >100$ μ M). Ebselen [30], a compound of selenium is capable to inhibit M^{pro} ($IC_{50} = 0.67 \pm 0.09$ μ M) and PL^{pro} ($IC_{50} = 2.4$ μ M), while rhenium compounds [31] work as M^{pro} inhibitors in the range of 7.5-9.1 μ M.

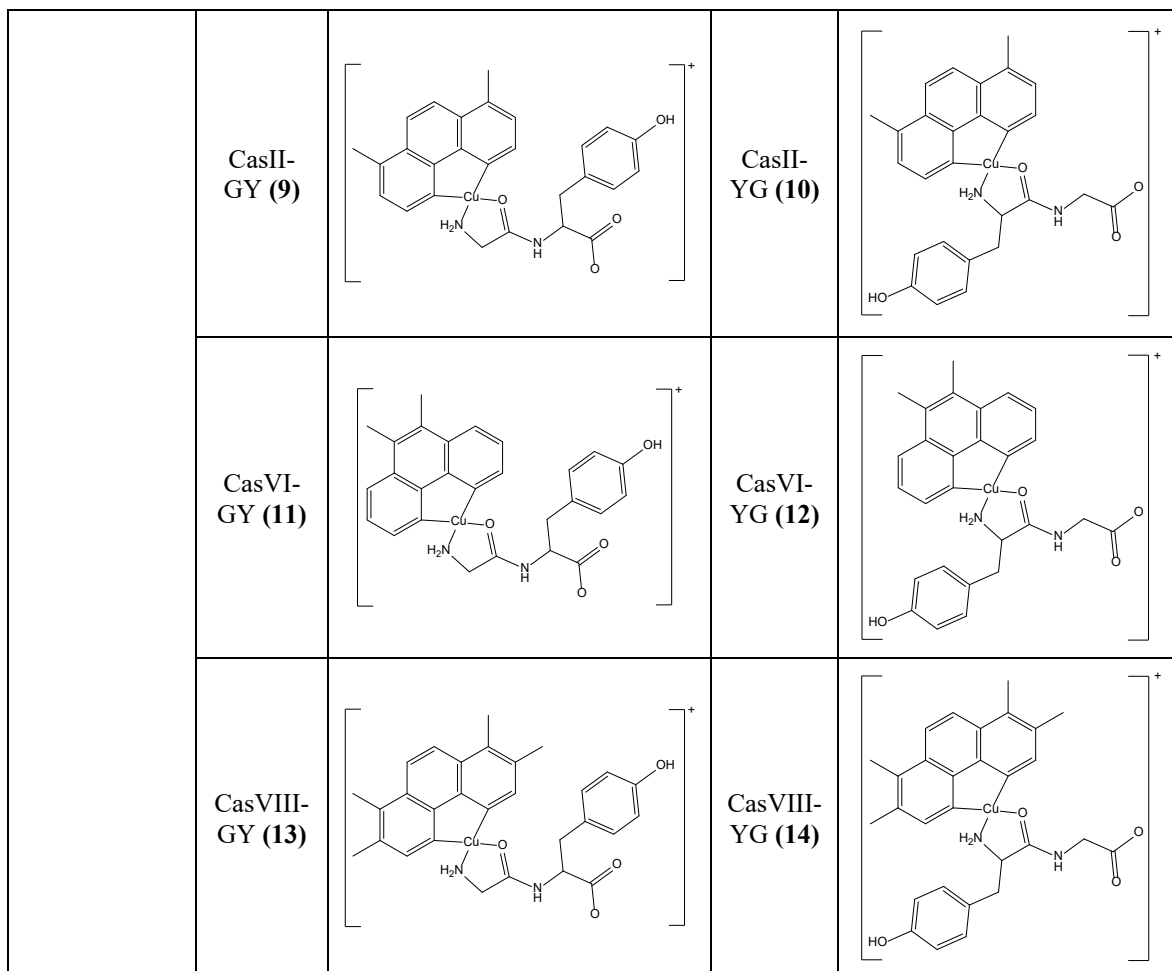
On the other hand, Casiopeinas® are ternary copper(II) compounds with a general formulae [Cu(N-N)(L-L)]ⁿ⁺(NO₃)_n n=1 or 2, where primary donor (N-N fragment) is an aromatic substituted diimine (2,2'-bipyridine or 1,10-phenanthroline) and secondary donors (L-L groups) are several bidentate chelates. These compounds have presented evidence of antitumoral [32], antiparasitic [33] and antimicrobial activity [34]. *In vitro*, *in vivo* [35] and *in silico* studies [36], suggest that Casiopeinas® present diverse mechanisms of action such as cytotoxic and low genotoxic damage, induction of apoptosis [37] and autophagy [38] mediated by interactions with biomolecules as DNA [39], glutathione [40], albumin [32] as well as the generation of reactive oxygen species due to changes in the oxidation number between the redox Cu^{II}/Cu^I pair [41].

Recently we have published a work with the interaction of several Casiopeinas® with proteins such as M^{pro} of SARS-CoV-2. [42] The interactions with biomolecules can be potentiated by incorporating a secondary ligand that have both donor and acceptor groups. For that purpose, dipeptides [43] can be an interesting option, since their physicochemical features can provide structural diversity with the pH-dependent coordination modes [44]; likewise, the nature of the side chain provides donor/acceptor groups capable to enhance their interaction efficiency [45], as well as changes in the metal center oxidation state when interacting with active redox centers [46], favoring several π interactions in residues with aromatic groups (as tyrosine), aliphatic groups (as glycine), cation, stacking [47], they can also present hydrogen bridge and salt bridge bonds [48]. All these interesting features have promoted the flourishing of the field of copper(II)-peptide compounds. These compounds have been developed for diverse therapeutic purposes such as anticancer and antimicrobial agents, care for chronic degenerative diseases such as Alzheimer and Parkinson [49], as well as theranostic agents for imaging studies [50].

In this work, the synthesis and characterization of fourteen compounds with copper(II), diimines derived from 1,10-phenanthroline or 2,2'-bipyridine with the ligands L-Tyrosil-Glycinato (YG) or Glycil-L-Tyrosinate (GY) are presented. Density functional theory (DFT) and molecular docking analysis were performed to investigate the M^{pro} and Spike-ACE2 complex inhibitor behavior of the Casiopeinas®. In the M^{pro}, the catalytic and union sites were analyzed and for Spike-ACE2 complex, the C-terminal and central regions were studied. Table 1 contains Casiopeinas® presented in this work.

Table 1. Casiopeinas[®] synthesized and studied in this work.

Casiopeinas [®]	Glycyl-L-Tyrosinate derivatives (GY ⁻)		L-Tyrosil-Glycinate derivatives (YG ⁻)	
	Name (Code)	Chemical structure	Name Code	Chemical structure
2,2'-bipyridine derivatives	CasX-GY (1)		CasX-YG (2)	
	CasIV-GY (3)		CasIV-YG (4)	
	CasV,V-GY (5)		CasV,V-YG (6)	
1,10-phenanthroline derivatives	CasVII-GY (7)		CasVII-YG (8)	



In all synthesized coordination compounds, nitrate was used as a counterion.

Experimental

Materials and methods

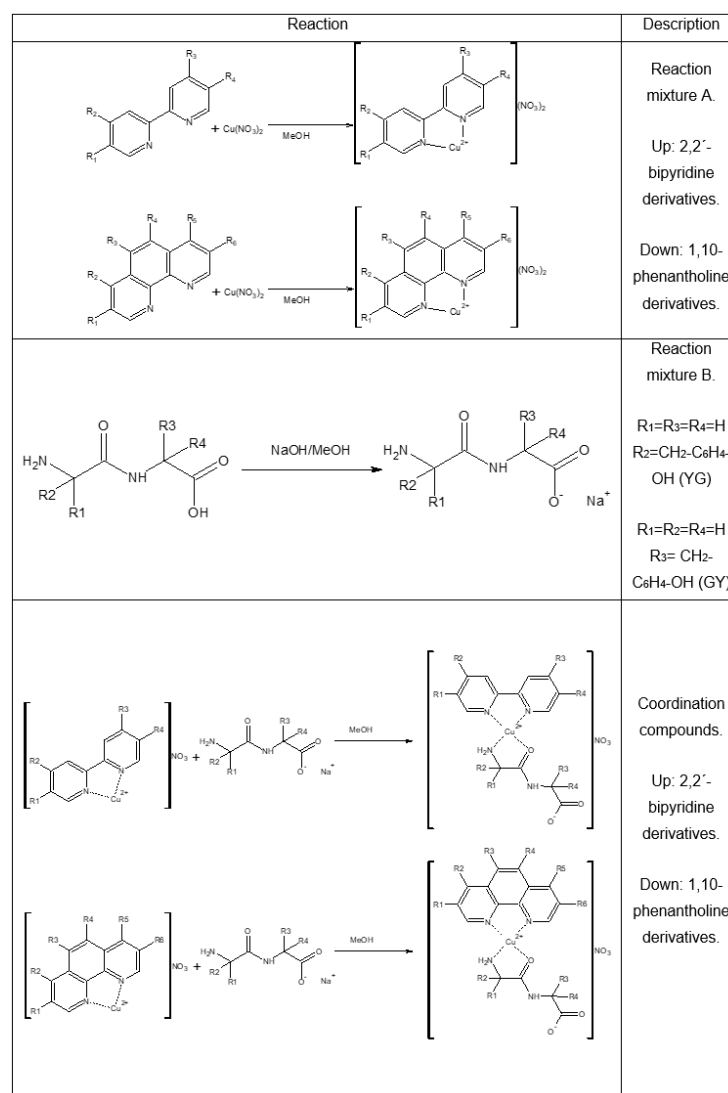
The copper(II) nitrate hemi(pentahydrate) – $\text{Cu}(\text{NO}_3)_2 \cdot 2.5\text{H}_2\text{O}$ -, Glycyl-L-Tyrosine - $\text{C}_{11}\text{H}_{14}\text{N}_2\text{O}_4^-$ (GY), L-Tyrosyl-Glycine - $\text{C}_{11}\text{H}_{14}\text{N}_2\text{O}_4^-$ (YG), 2,2'-bipyridine - $\text{C}_{10}\text{H}_8\text{N}_2^-$ -, 4,4'-dimethyl-2,2'-bipyridine - $\text{C}_{12}\text{H}_{12}\text{N}_2^-$ -, 5,5'-dimethyl-2,2'-bipyridine - $\text{C}_{12}\text{H}_{12}\text{N}_2^-$ -, 1,10-phenanthroline - $\text{C}_{12}\text{H}_8\text{N}_2^-$ -, 4,7-dimethyl-1,10-phenanthroline - $\text{C}_{14}\text{H}_{12}\text{N}_2^-$ -, 5,6-dimethyl-1,10-phenanthroline - $\text{C}_{14}\text{H}_{12}\text{N}_2^-$ -, 3,4,7,8-tetramethyl-1,10-phenanthroline - $\text{C}_{16}\text{H}_{16}\text{N}_2^-$ -, sodium hydroxide and solvents were purchased from Merck were used without further purification.

The FT-IR* spectra of coordination compounds were recorded in KBr pellets in the $4000\text{--}400\text{ cm}^{-1}$ range on Thermo Nicolet Avatar 320 FT-IR Spectrometer. The conductivity of the complexes in water (10^{-3} M) solutions was measured at 298K on a conductivity meter Jenway Conductivity and pH meter 4330, the conductivity cell constant was 1.0 cm^{-1} . FAB (+) mass spectra were recorded on the MStation JMS-700 NBA solutions as a solvent. Magnetic susceptibility measurements were performed on powder samples at 298K on Sherwood-Scientific MK magnetic balance using Gouy's method. The electronic spectra (UV-Vis) were recorded using Cary 60 UV-Vis Spectrophotometer in 200-1000 nm range using water as solvent. Electronic paramagnetic resonance (EPR) spectra were performed on a Jeol JES-TE300, X-band spectrophotometer ($\nu=9.60\text{GHz}$), center field= $300.00\pm 75.00\text{mT}$,

PW=1mW, width=0.1mT, amplitude=250, sweep time=2min, all samples for EPR studies were prepared in methanol solutions glass at 77 K in a cold finger, with a copper(II) ternary compounds concentration of 10^{-3} M.

General procedure for synthesis of Casiopeinas[®]

For the synthesis of ternary copper(II) compounds, a modification was made to the method reported by Ruiz-Azuara and coworkers[51], in which the amount equivalent to 1 mmol of copper(II) nitrate hemihydrate was weighed, which was dissolved in 10 mL of methanol, the equivalent amount to 1 mmol of the diimine was weighed, it was dissolved in 10 mL of methanol. Diimine solution was added under slow drip and stirring at room temperature to the copper(II) nitrate solution, (Reaction mixture A). On the other hand, the equivalent amount to 1mmol of the dipeptide (GY or YG) was weighed, which was dissolved in 10 mL of methanol, under agitation. 1 mL was taken from a 1 M solution of NaOH, which was added under drip and gentle stirring to the dipeptide, to obtain the sodium salt of the dipeptide (Reaction mixture B). Once the reaction mixtures A and B were obtained, we proceeded under stirring and dripping, to add mixture B to mixture A. The solution was vacuum filtered and washed with cold water (3 times with 3 mL). The general synthesis of the complexes **1-14** is shown in Scheme 1.



Scheme 1. Synthesis of Casiopeinas[®].

Synthesis of 1. (2,2'-bipyridine) (Glycyl-L-Tyrosinate) copper(II) nitrate. (CasX-GY). Aqua blue powder; 90 % yield; IR KBr pellets λ_{\max} = 3427 (OH), 3249 (NH₂, NH), 3016, 2948 (CH₂, CH₃), 1608 (C=C), 1685 (CONR), 1631 (C=N), 835, 721 (CH_{ar}), 1384 (NO₃⁻) cm⁻¹; FAB(+)-MS m/z (%Int) 458 [M]⁺; Λ (H₂O) 132.63 Scm²mol⁻¹; μ_{eff} : 1.86 B.M; UV-Vis (H₂O): λ_{\max} (ϵ) 226 nm (29007 M⁻¹cm⁻¹) $\pi \rightarrow \pi^*$, 247 nm (25213 M⁻¹cm⁻¹) $\pi \rightarrow \pi^*$, 311 nm (16074 M⁻¹cm⁻¹) MLCT, 635 nm (105.52 M⁻¹cm⁻¹) $b_{2g} \rightarrow b_{1g}^*$; EPR parameters g_{\parallel} =2.194, g_{\perp} =2.058, A_{\parallel} =153.46x10⁻⁴ cm⁻¹, A_{\perp} =84.24x10⁻⁴ cm⁻¹; elemental analysis calculated for [CuC₂₁H₂₁N₄O₄]NO₃•H₂O (%). 46.97 C, 4.32 H, 13.04 N; found: 46.68 C, 4.39 H, 12.74 N; molecular weight 536.98 g/mol.

Synthesis of 2. (2,2'-bipyridine) (L-Tyrosil-Glycinate) copper(II) nitrate. (CasX-YG). Blue powder; 93 % yield; %yield; IR KBr pellets λ_{\max} = 3430 (OH), 3252, 3222 (NH₂, NH), 3043, 2950 (CH₂, CH₃), 1602 (C=C), 1687 (CONR), 1631 (C=N), 827, 729 (CH_{ar}), 1384 (NO₃⁻) cm⁻¹; FAB(+)-MS m/z 458 [M]⁺; Λ (H₂O) 141.85 Scm²mol⁻¹; μ_{eff} : 1.86 B.M; UV-Vis (H₂O): λ_{\max} (ϵ) 201 nm (611591 M⁻¹cm⁻¹) $\pi \rightarrow \pi^*$, 250 nm (147324 M⁻¹cm⁻¹) $\pi \rightarrow \pi^*$, 311 nm (151624 M⁻¹cm⁻¹) MLCT, 623nm (48.95 M⁻¹cm⁻¹) $b_{2g} \rightarrow b_{1g}^*$; EPR parameters g_{\parallel} =2.189, g_{\perp} =2.059, A_{\parallel} =136.31x10⁻⁴ cm⁻¹, A_{\perp} =115.44x10⁻⁴ cm⁻¹; elemental analysis calculated for [CuC₂₁H₂₁N₄O₄]NO₃•2H₂O (%). 45.45 C, 4.54 H, 12.62 N; found: 45.46 C, 4.61 H, 12.14 N; molecular weight 554.99g/mol.

Synthesis of 3. (4,4'-dimethyl-2,2'-bipyridine) (Glycyl-L-Tyrosinate) copper(II) nitrate. (CasIV-GY). Blue powder; 87 % yield; %yield; IR KBr pellets λ_{\max} = 3419 (OH), 3251 (NH₂, NH), 3026, 2939 (CH₂, CH₃), 1602 (C=C), 1685 (CONR), 1622 (C=N), 827, 729 (CH_{ar}), 1384 (NO₃⁻) cm⁻¹; FAB(+)-MS m/z 485 [M]⁺; Λ (H₂O) 141.49 Scm²mol⁻¹; μ_{eff} : 2.02 B.M; UV-Vis (H₂O): λ_{\max} (ϵ) 207 nm (131656 M⁻¹cm⁻¹) $\pi \rightarrow \pi^*$, 228 nm (58866 M⁻¹cm⁻¹) $\pi \rightarrow \pi^*$, 297 nm (24253 M⁻¹cm⁻¹) $n \rightarrow \pi^*$, 307 nm (22622 M⁻¹cm⁻¹) MLCT, 631nm (43.70 M⁻¹cm⁻¹) $b_{2g} \rightarrow b_{1g}^*$; EPR parameters g_{\parallel} =2.186, g_{\perp} =2.077, A_{\parallel} =123.05x10⁻⁴ cm⁻¹, A_{\perp} =126.22x10⁻⁴ cm⁻¹; elemental analysis calculated for [CuC₂₃H₂₅N₄O₄]NO₃•H₂O (%). 48.85 C, 4.81 H, 12.39 N; found: 48.85 C, 4.81 H, 12.39 N; Molecular weight 565.03 g/mol.

Synthesis of 4. (4,4'-dimethyl-2,2'-bipyridine) (L-Tyrosil-Glycinate) copper(II) nitrate. (CasIV-YG). Blue powder; 85 % yield; IR KBr pellets λ_{\max} = 3467 (OH), 3259, 3222 (NH₂, NH), 2950 (CH₂, CH₃), 1618 (C=C), 1685 (CONR), 1654 (C=N), 827, 727 (CH_{ar}), 1384 (NO₃⁻) cm⁻¹; FAB(+)-MS m/z 485 [M]⁺; Λ (H₂O) 152.99 Scm²mol⁻¹; μ_{eff} : 1.90 B.M; UV-Vis (H₂O): λ_{\max} (ϵ) 208 nm (126201 M⁻¹cm⁻¹) $\pi \rightarrow \pi^*$, 248 nm (26504 M⁻¹cm⁻¹) $\pi \rightarrow \pi^*$, 314 nm (29583 M⁻¹cm⁻¹) MLCT, 637nm (47.34 M⁻¹cm⁻¹) $b_{2g} \rightarrow b_{1g}^*$; EPR parameters g_{\parallel} =2.121, g_{\perp} =2.058, A_{\parallel} =139.77x10⁻⁴ cm⁻¹, A_{\perp} =101.21x10⁻⁴ cm⁻¹; elemental analysis calculated for [CuC₂₃H₂₅N₄O₄]NO₃•H₂O (%). 48.85 C, 4.81 H, 12.39 N; found: 48.62 C, 4.97 H, 12.62 N; Molecular weight 565.03 g/mol.

Synthesis of 5. (5,5'-dimethyl-2,2'-bipyridine) (Glycyl-L-Tyrosinate) copper(II) nitrate. (CasV,V-GY). Blue green powder; 92 % yield; IR KBr pellets λ_{\max} = 3421 (OH), 3251 (NH₂, NH), 3043, 2948 (CH₂, CH₃), 1608 (C=C), 1691 (CONR), 1623 (C=N), 827, 725 (CH_{ar}), 1384 (NO₃⁻) cm⁻¹; FAB(+)-MS m/z 485 [M]⁺; Λ (H₂O) 152.72 Scm²mol⁻¹; μ_{eff} : 1.81 B.M; UV-Vis (H₂O): λ_{\max} (ϵ) 203 nm (128211 M⁻¹cm⁻¹) $\pi \rightarrow \pi^*$, 256 nm (26607 M⁻¹cm⁻¹) $\pi \rightarrow \pi^*$, 319 nm (29583 M⁻¹cm⁻¹) MLCT, 634nm (37.06 M⁻¹cm⁻¹) $b_{2g} \rightarrow b_{1g}^*$; EPR parameters g_{\parallel} =2.176, g_{\perp} =2.059, A_{\parallel} =142.78x10⁻⁴ cm⁻¹, A_{\perp} =77.17x10⁻⁴ cm⁻¹; elemental analysis calculated for [CuC₂₃H₂₅N₄O₄]NO₃•CH₃OH (%). 49.78 C, 5.05 H, 12.09 N; found: 49.51 C, 4.63 H, 11.93 N; molecular weight 579.06 g/mol.

Synthesis of 6. (5,5'-dimethyl-2,2'-bipyridine) (L-Tyrosil-Glycinate) copper(II) nitrate. (CasV,V-YG). Green powder; 88 % yield; IR KBr pellets λ_{\max} = 3473 (OH), 3253, 3222 (NH₂, NH), 3010, 2942 (CH₂, CH₃), 1618 (C=C), 1683 (CONR), 1654 (C=N), 827, 727 (CH_{ar}), 1384 (NO₃⁻) cm⁻¹; FAB(+)-MS m/z 485 [M]⁺; Λ (H₂O) 158.37 Scm²mol⁻¹; μ_{eff} : 2.04 B.M; UV-Vis (H₂O): λ_{\max} (ϵ) 206 nm (120689 M⁻¹cm⁻¹) $\pi \rightarrow \pi^*$, 257 nm (38606 M⁻¹cm⁻¹) $\pi \rightarrow \pi^*$, 319 nm (25904 M⁻¹cm⁻¹) MLCT, 620 nm (49.41 M⁻¹cm⁻¹) $b_{2g} \rightarrow b_{1g}^*$; EPR parameters g_{\parallel} =2.258, g_{\perp} =2.023, A_{\parallel} =149.59x10⁻⁴ cm⁻¹, A_{\perp} =109.61x10⁻⁴ cm⁻¹; elemental analysis calculated for [CuC₂₃H₂₅N₄O₄]NO₃•H₂O (%). 48.85 C, 4.81 H, 12.39 N; found: 48.45 C, 4.47 H, 12.35 N; molecular weight 565.03 g/mol.

Synthesis of 7. (1,10-phenanthroline) (Glycyl-L-Tyrosinate) copper(II) nitrate. (CasVII-GY).

Dark blue powder; 85 % yield; IR KBr pellets λ_{\max} = 3428 (OH), 3253 (NH₂, NH), 3012, 2925 (CH₂, CH₃), 1610 (C=C), 1685 (CONR), 1625 (C=N), 827, 721 (CH_{ar}), 1384 (NO₃⁻) cm⁻¹; FAB(+)-MS m/z 482 [M]⁺; Λ (H₂O) 139.40 Scm²mol⁻¹; μ_{eff} : 1.86 B.M; UV-Vis (H₂O): λ_{\max} (ϵ) 204 nm (175182 M⁻¹cm⁻¹) $\pi \rightarrow \pi^*$, 222 nm (166119 M⁻¹cm⁻¹) $\pi \rightarrow \pi^*$, 272 nm (87823 M⁻¹cm⁻¹) $n \rightarrow \pi^*$, 294 nm (27718 M⁻¹cm⁻¹) MLCT, 631nm (59.78 M⁻¹cm⁻¹) $b_{2g} \rightarrow b_{1g}^*$; EPR parameters g_{\parallel} =2.135, g_{\perp} =2.062, A_{\parallel} =152.28x10⁻⁴ cm⁻¹, A_{\perp} =68.72x10⁻⁴ cm⁻¹; elemental analysis calculated for [CuC₂₃H₂₁N₄O₄]NO₃•0.5H₂O (%). 50.04 C, 4.02 H, 12.69 N; found: 49.94 C, 4.03 H, 12.95 N; molecular weight 551.99 g/mol.

Synthesis of 8. (1,10-phenanthroline) (L-Tyrosil-Glycinate) copper(II) nitrate. (CasVII-YG).

Green jade powder; 92 % yield; IR KBr pellets λ_{\max} = 3442 (OH), 3252, 3223 (NH₂, NH), 3025, 2946 (CH₂, CH₃), 1631 (C=C), 1685 (CONR), 1631 (C=N), 848, 721 (CH_{ar}), 1384 (NO₃⁻) cm⁻¹; FAB(+)-MS m/z 482 [M]⁺; Λ (H₂O) 157.40 Scm²mol⁻¹; μ_{eff} : 2.01 B.M; UV-Vis (H₂O): λ_{\max} (ϵ) 204 nm (164928 M⁻¹cm⁻¹) $\pi \rightarrow \pi^*$, 225 nm (102435 M⁻¹cm⁻¹) $\pi \rightarrow \pi^*$, 276 nm (59436 M⁻¹cm⁻¹) $n \rightarrow \pi^*$, 296 nm (21031 M⁻¹cm⁻¹) MLCT, 631nm (59.78 M⁻¹cm⁻¹) $b_{2g} \rightarrow b_{1g}^*$; EPR parameters g_{\parallel} =2.144, g_{\perp} =2.062, A_{\parallel} =153.13x10⁻⁴ cm⁻¹, A_{\perp} =87.20x10⁻⁴ cm⁻¹; Elemental analysis calculated for [CuC₂₃H₂₁N₄O₄]NO₃•2H₂O(%). 47.71 C, 4.35 H, 12.10 N; found: 47.95 C, 4.73 H, 12.18 N; molecular weight 579.02 g/mol.

Synthesis of 9. (4,7-dimethyl-1,10-phenanthroline) (Glycyl-L-Tyrosinate) copper(II) nitrate. (CasII-GY).

Blue green powder; 91 % yield; IR KBr pellets λ_{\max} = 3419 (OH), 3257 (NH₂, NH), 2998, 2923 (CH₂, CH₃), 1613 (C=C), 1683 (CONR), 1622 (C=N), 827, 723 (CH_{ar}), 1384 (NO₃⁻) cm⁻¹; FAB(+)-MS m/z 510 [M]⁺; Λ (H₂O) 136.10 Scm²mol⁻¹; μ_{eff} : 1.80 B.M; UV-Vis (H₂O): λ_{\max} 204 nm (120466 M⁻¹cm⁻¹) $\pi \rightarrow \pi^*$, 226 nm (60819 M⁻¹cm⁻¹) $\pi \rightarrow \pi^*$, 274 nm (56496 M⁻¹cm⁻¹) $n \rightarrow \pi^*$, 307 nm (10069 M⁻¹cm⁻¹) MLCT, 658nm (42.55 M⁻¹cm⁻¹) $b_{2g} \rightarrow b_{1g}^*$; EPR parameters g_{\parallel} =2.198, g_{\perp} =2.060, A_{\parallel} =155.22x10⁻⁴ cm⁻¹, A_{\perp} =76.99x10⁻⁴ cm⁻¹; elemental analysis calculated for [CuC₂₅H₂₅N₄O₄]NO₃•2H₂O (%). 49.96 C, 4.82 H, 11.66 N; found: 50.23 C, 4.83 H, 12.02 N; molecular weight 607.07 g/mol.

Synthesis of 10. (4,7-dimethyl-1,10-phenanthroline) (L-Tyrosil-Glycinate) copper(II) nitrate. (CasII-YG).

Blue green powder; 93 % yield; IR KBr pellets λ_{\max} = 3436 (OH), 3265 (NH₂, NH), 3014, 2950 (CH₂, CH₃), 1610 (C=C), 1685 (CONR), 1636 (C=N), 848, 723 (CH_{ar}), 1384 (NO₃⁻) cm⁻¹; FAB(+)-MS m/z 510 [M]⁺; Λ (H₂O) 144.80 Scm²mol⁻¹; μ_{eff} : 2.08 B.M; UV-Vis (H₂O): λ_{\max} (ϵ) 208 nm (97547 M⁻¹cm⁻¹) $\pi \rightarrow \pi^*$, 223 nm (54800 M⁻¹cm⁻¹) $\pi \rightarrow \pi^*$, 274 nm (46290 M⁻¹cm⁻¹) $n \rightarrow \pi^*$, 305 nm (8989 M⁻¹cm⁻¹) MLCT, 631nm (50.44 M⁻¹cm⁻¹) $b_{2g} \rightarrow b_{1g}^*$; EPR parameters g_{\parallel} =2.189, g_{\perp} =2.059, A_{\parallel} =156.37x10⁻⁴ cm⁻¹, A_{\perp} =85.27x10⁻⁴ cm⁻¹; elemental analysis calculated for [CuC₂₅H₂₅N₄O₄]NO₃•2.5H₂O (%). 48.74 C, 4.91 H, 11.37 N; found:48.68 C, 4.76 H, 11.44 N; molecular weight 616.08 g/mol.

Synthesis of 11. (5,6-dimethyl-1,10-phenanthroline) (Glycyl-L-Tyrosinate) copper(II) nitrate. (CasVI-GY).

Pale blue powder; 85 % yield; IR KBr pellets λ_{\max} = 3419 (OH), 3245 (NH₂, NH), 3012, 2929 (CH₂, CH₃), 1604 (C=C), 1700 (CONR), 814, 734 (CH_{ar}), 1384 (NO₃⁻) cm⁻¹; FAB(+)-MS m/z 510 [M]⁺; Λ (H₂O) 140.39 Scm²mol⁻¹; μ_{eff} : 2.14 B.M; UV-Vis (H₂O): λ_{\max} (ϵ) 245 nm (84722 M⁻¹cm⁻¹) $\pi \rightarrow \pi^*$, 287 nm (70841 M⁻¹cm⁻¹) $n \rightarrow \pi^*$, 315 nm (21602 M⁻¹cm⁻¹) MLCT, 628nm (51.45 M⁻¹cm⁻¹) $b_{2g} \rightarrow b_{1g}^*$; EPR parameters g_{\parallel} =2.177, g_{\perp} =2.076, A_{\parallel} =140.56x10⁻⁴ cm⁻¹, A_{\perp} =83.09x10⁻⁴ cm⁻¹; elemental analysis calculated for [CuC₂₅H₂₅N₄O₄]NO₃•2CH₃OH (%). 51.06 C, 5.24 H, 11.03 N; found: 51.21 C, 5.38 H, 10.67 N; molecular weight 635.12 g/mol.

Synthesis of 12. (5,6-dimethyl-1,10-phenanthroline) (L-Tyrosil-Glycinate) copper(II) nitrate. (CasVI-YG).

Cobalt blue powder; 89 % yield; IR KBr pellets λ_{\max} = 3429 (OH), 3259, 3216 (NH₂, NH), 3016, 2944 (CH₂, CH₃), 1616 (C=C), 1685 (CONR), 1633 (C=N), 810, 727 (CH_{ar}), 1384 (NO₃⁻) cm⁻¹; FAB(+)-MS m/z 510 [M]⁺; Λ (H₂O) 158.45 Scm²mol⁻¹; μ_{eff} : 1.98 B.M; UV-Vis (H₂O): λ_{\max} (ϵ) 207 nm (172965 M⁻¹cm⁻¹) $\pi \rightarrow \pi^*$, 245 nm (73651 M⁻¹cm⁻¹) $\pi \rightarrow \pi^*$, 285 nm (68066 M⁻¹cm⁻¹) $n \rightarrow \pi^*$, 307 nm (27157 M⁻¹cm⁻¹) MLCT,

627nm ($49.41 \text{ M}^{-1}\text{cm}^{-1}$) $b_{2g} \rightarrow b_{1g}^*$; EPR parameters $g_{\parallel}=2.193$, $g_{\perp}=2.059$, $A_{\parallel}=134.69 \times 10^{-4} \text{ cm}^{-1}$, $A_{\perp}=118.27 \times 10^{-4} \text{ cm}^{-1}$; elemental analysis calculated for $[\text{CuC}_{25}\text{H}_{25}\text{N}_4\text{O}_4]\text{NO}_3 \cdot 2\text{H}_2\text{O}$ (%). 49.46 C, 4.81 H, 11.54 N; found: 49.73 C, 4.41 H, 12.32 N; molecular weight 607.07 g/mol.

Synthesis of 13. (3,4,7,8-tetramethyl-1,10-phenanthroline) (Glycyl-L-Tyrosinate) copper(II) nitrate. (CasVIII-GY). Green powder; IR KBr pellets $\lambda_{\text{max}}=3428$ (OH), 3249 (NH₂, NH), 3016, 2933 (CH₂, CH₃), 1616 (C=C), 1678 (CONR), 1636 (C=N), 823, 721 (CH_{ar}), 1384 (NO₃⁻) cm^{-1} : FAB(+)-MS m/z 538 [M]⁺; Λ (H₂O:MeOH 99:1) $151.28 \text{ Scm}^2\text{mol}^{-1}$; Λ (MeOH) $102.29 \text{ Scm}^2\text{mol}^{-1}$; μ_{eff} : 2.16 B.M; UV-Vis (H₂O): λ_{max} (ϵ) 211 nm ($118383 \text{ M}^{-1}\text{cm}^{-1}$) $\pi \rightarrow \pi^*$, 228 nm ($94981 \text{ M}^{-1}\text{cm}^{-1}$) $\pi \rightarrow \pi^*$, 284 nm ($68173 \text{ M}^{-1}\text{cm}^{-1}$) $n \rightarrow \pi^*$, 307 nm ($17808 \text{ M}^{-1}\text{cm}^{-1}$) MLCT; EPR parameters $g_{\parallel}=2.266$, $g_{\perp}=2.007$, $A_{\parallel}=145.35 \times 10^{-4} \text{ cm}^{-1}$, $A_{\perp}=79.81 \times 10^{-4} \text{ cm}^{-1}$; elemental analysis calculated for $[\text{CuC}_{27}\text{H}_{29}\text{N}_4\text{O}_4]\text{NO}_3 \cdot \text{H}_2\text{O}$ (%). 52.55 C, 5.06 H, 11.35 N; found: 52.37 C, 5.11 H, 11.67 N; molecular weight 617.10 g/mol.

Synthesis of 14. (3,4,7,8-tetramethyl-1,10-phenanthroline) (L-Tyrosil-Glycinate) copper(II) nitrate. (CasVIII-YG). Green powder; 87 % yield; IR KBr pellets $\lambda_{\text{max}}=3454$ (OH), 3279, 3232 (NH₂, NH), 3072, 3000 (CH₂, CH₃), 1609 (C=C), 1675 (CONR), 1625 (C=N), 812, 723 (CH_{ar}), 1384 (NO₃⁻) cm^{-1} : FAB(+)-MS m/z 538 [M]⁺; Λ (H₂O:MeOH 99:1) $158.46 \text{ Scm}^2\text{mol}^{-1}$; Λ (MeOH) $98.27 \text{ Scm}^2\text{mol}^{-1}$; μ_{eff} : 2.06 B.M; UV-Vis (H₂O): 212 nm ($29705 \text{ M}^{-1}\text{cm}^{-1}$) $\pi \rightarrow \pi^*$, 227 nm ($19940 \text{ M}^{-1}\text{cm}^{-1}$) $\pi \rightarrow \pi^*$, 284 nm ($16744 \text{ M}^{-1}\text{cm}^{-1}$) $n \rightarrow \pi^*$, 312 nm ($12080 \text{ M}^{-1}\text{cm}^{-1}$) MLCT; EPR parameters $g_{\parallel}=2.164$, $g_{\perp}=2.078$, $A_{\parallel}=136.74 \times 10^{-4} \text{ cm}^{-1}$, $A_{\perp}=95.16 \times 10^{-4} \text{ cm}^{-1}$; elemental analysis calculated for $[\text{CuC}_{27}\text{H}_{29}\text{N}_4\text{O}_4]\text{NO}_3 \cdot \text{CH}_3\text{OH}$ (%). 53.28 C, 5.27 H, 11.10 N; found: 53.14 C, 5.05 H, 10.86 N; molecular weight 631.14 g/mol.

Computational methods

Geometry optimization and atomic charge estimation

Computational calculations were conducted in Gaussian 09 [52] using density functional theory (DFT) calculations. 2nd generation of Minnesota M06 functional [53] and Los Alamos LanL2DZ [54] basis set were used to compute all compounds. X-ray diffraction preliminary results for [CasVII-YG] (compound **8**) were considered, planar arrangements were observed, those were used as a starting point geometry. Remaining compounds were constructed manually in GaussView6. To simulate solvent (H₂O) effects, a SMD Model [55] was achieved. No imaginary frequencies were detected confirming that the optimized geometry correspond to a local minimum on the potential energy surface. NBO analysis was used to estimate the required atomic charges for molecular docking experiments. Molar volume was obtained as single point calculations from optimized geometries.

Molecular docking

The crystallographic structures of main protease (M^{pro}) and RBD^{Spike}-ACE2 complex were obtained from Protein Data Bank with the ID: 6LU7 [11], 6M17 [7] respectively. These proteins were used as controls because their inhibition capacity was previously reported as well as the interactions it presents. [19, 22] Prior to docking studies M^{pro}, and complex RBD Spike-ACE2 and Casiopeinas® were prepared as follows. In the proteins, extra units, water molecules, cofactors and inhibitors were removed then, polar hydrogens and Gasteiger charges were added using MGL Tools 1.5.6 software [55]. The modified structure was saved as pdbqt file. The optimized structures of copper complexes, remdesivir and boceprevir were employed as ligands, and the estimated atomic charges (QM: M06-LanL2DZ) were added manually in the Autodock4 pdbqt files. Constraints of copper atom as VdW radii, solvation volume, VdW well dept were included in the software parameters to handle the metal ion in the simulations. The docking studies were carried out using AutoDock 4.2 software [56]. A genetic algorithm study inside of the complex protein-Casiopeina® centered as seen in the table 2, 150 individuals in population with 2.5×10^3 evaluations to result in 10 docked poses. For the most stable conformation, energy stabilization (ΔG_U) and inhibition constant (K_i) were reported. Finally, the docked conformation was analyzed with Discovery Studio 2021 [57] graphic interface.

Table 2. Experimental parameters of molecular docking.

PDB ID	M ^{pro}	RBD Spike-ACE2			
		C-terminal Domain		Middle Domain	
	6LU7	6M17			
Target amino acids	His41, Met49, Cys145, Met165, Gln189	ACE2	Spike	ACE2	Spike
		Gln24, Met82	Gln474, Phe486	Asp30, His34	Lys417, Tyr453
Gridbox coordinates	X=14.925 Y=15.964 Z=60.009	X=185.797 Y=109.037 Z=235.465		X=168.884 Y=107.368 Z=235.465	
Gridbox dimensions	40x40x40 Å ³	40x34x44 Å ³		40x40x40 Å ³	

Results and discussion

Synthesis of ternary copper(II) compounds

The preparation of the coordination compounds is a modification to the synthetic methodology of the Casiopeinas® [51, 58]. The change consists of deprotonate the dipeptide in a separate way, and then add this solution to mixture reaction, those was made considering the pH dependence of the dipeptides, since they can present in union modes to metallic center and the charge of the complexes [59], these ensuring coordination sphere that resembles to Casiopeinas®. The compounds are soluble in water, except **13** and **14**, all compounds are soluble in MeOH, MeCN and DMSO. Coordination compounds decompose above 120 °C. The yields obtained were in the range of 85-93%. The powders obtained present colors in the scale from blue to green, being mostly blue when the primary ligand is bipyridine derivatives, while in the compounds that present 1,10-phenanthroline derivatives they are mostly green.

Physicochemical characterization

The synthesized compounds 1-14 (Table 1) present in the elementary analysis a minimum formula that agrees with the proposed formulas adjusted with solvent reaction molecules such as a methanol and water. Comparative analysis of the selected vibration frequencies in the FT-IR spectrum shows the presence of the characteristic functional groups. In the spectrum (Fig. S1 and Table S1) there are changes in the vibration frequencies attributed to the coordination of the central metal to the ligands used in this work, shifts in the vibration frequencies attributed to the carbonyl and amine groups are appreciable, so that in the IR spectra it is considered that coordination bonding occurs by the above mention functional groups, being noticeable in the signals belonging to the C=N (1610-1654 cm⁻¹), O-H (3419-3473 cm⁻¹), C-H_{ar} (723-734 and 810-848 cm⁻¹), N-H and NH₂ (3222-3279 cm⁻¹) C=O (1675-1700 cm⁻¹), C-H_{aliph} (2923-3072 cm⁻¹) and NO₃⁻ groups (1384 cm⁻¹) [60]. In the FAB (+) spectra, the m/z signal corresponds to the cation complex. The conductivity measurements (Table S2) indicate 1:1 electrolytic ratio (H₂O 132.63—158.45 Scm²mol⁻¹ range), (MeOH 80.00—115.00 Scm²mol⁻¹ range) type electrolyte [61], observed in various coordination compounds similar. The techniques of FAB (+) (Fig. S2 and table 2) and conductivity are consistent with the proposed molecular formulas. Magnetic susceptibility values are in the range of 1.80-2.16 B.M (Table S2), values that characteristic for an electronic configuration d⁹ (Cu^{II}) with an unpaired electron [62]; UV-Vis spectra have various absorbance maxima that are determined by the presence of various types of bond that make up the chemical structures of the synthesized compounds, such as the electronic transitions π→π* (201-257nm) presented mainly by aromatic groups, n→π* transitions (272-287nm) presented in groups with pairs of non-bonding electrons such as C=O and NH, metal

to ligand charge transfer (MLCT) absorption band in the range of 294-219nm ($d \rightarrow \pi^*$), as well a maximum absorption in the visible region (620-637nm) assigned for the $b_{2g} \rightarrow b_{1g}$ transition in square planar geometry around the metal ion in the coordination compounds [63], this geometry would imply that the coordination bonding to the metal center is performed both by the nitrogen atoms of the diimines, as well as by the terminal amino and carbonyl groups of the peptide bond. Fig. 1. Show the UV-Vis spectrum for compound **8**. The coordination compounds are stable in 1×10^{-3} M aqueous solution. Stability tests (Fig. S3) for compounds **3**, **4**, **9** and **10** were performed at 0.0, 0.5, 1.0, 2.0, 4.0, 6.0, 12.0, 24.0, 48.0 and 72.0 hours. These show that no change around the metal center involving a change in the coordination were observed. The decrease of absorbance values may be due to slight precipitation of the compounds, and then a dilution effect is seen in the electronic spectra.

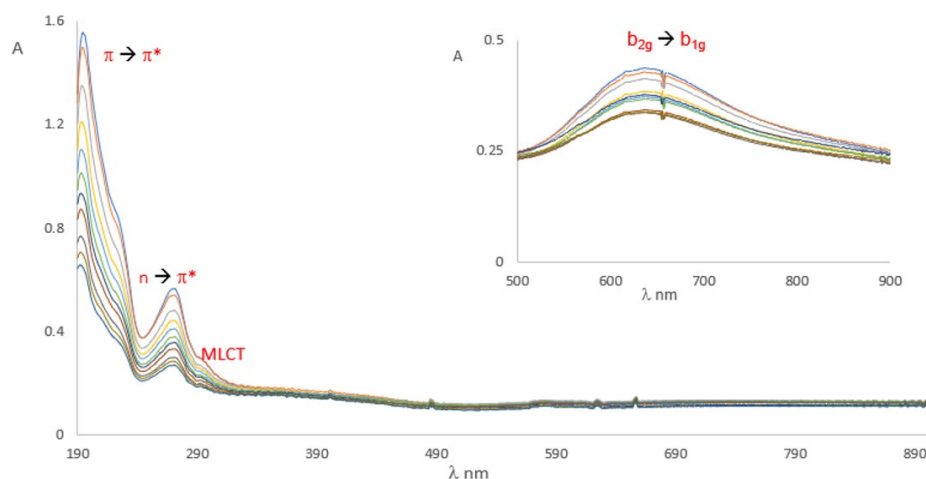


Fig. 1. UV-Vis spectrum of **8**. Solvent: water. Acquired UV region [0.1-1.0] mM; Vis region (top) acquired [1.0-3.0] mM.

The EPR spectra obtained in methanol at 77K at 9.6GHz (X-Band), present the characteristic pattern of copper(II) compounds, in which an axial type spectrum is observed where $g_{\parallel} > g_{\perp}$, with a hyperfine coupling in the g_{\parallel} region that has a multiplicity ($M=2nI+1$) of four due to nuclear spin ($I=3/2$) ^{63}Cu or ^{65}Cu ; in the g_{\perp} region [60-62], it can be seen in Fig. 2, belonging to CasX-GY (**1**) and CasVII-GY (**7**) that the signals presents a multiplicity of 7 due to superhyperfine coupling with ^{14}N ($I=1$) [63]. Fig. 2 shows the comparative EPR spectrum for compounds **1** and **7**, as well as shows the A_{iso} vs g_{iso} diagram [64-66] (Fig 3) in which Casiopeinas® synthesized in the region of the square planar geometry are located agree with the values of g_{iso} (Equation 1) and A_{iso} (Equation 2) obtained, a square planar geometry reported in the literature [67-68]. Table 3 shows Hamiltonian spin parameters for the compounds 1-14. The experimental and simulated EPR spectra of compound **1** are presented in Fig. S4.

$$g_{\text{iso}} = \frac{(2g_{\perp} + g_{\parallel})}{3} \quad \text{Equation 1}$$

$$A_{\text{iso}} = \frac{A_{\perp} + A_{\parallel}}{2} \quad \text{Equation 2}$$

Considering the analysis performed in the spectroscopic techniques (IR, UV-Vis and EPR), it is proposed that the dipeptide is functionalized as a dipeptide ligand with the amino and carbonyl groups bonded to the copper(II) atom forming a 5-membered rings; the basic characteristics as a Pearson soft base of the primary amine and the peptide carbonyl, would imply a higher affinity to the metallic center that other donor groups present in the dipeptide as the secondary amine and carboxylate groups, which are Pearson hard bases.

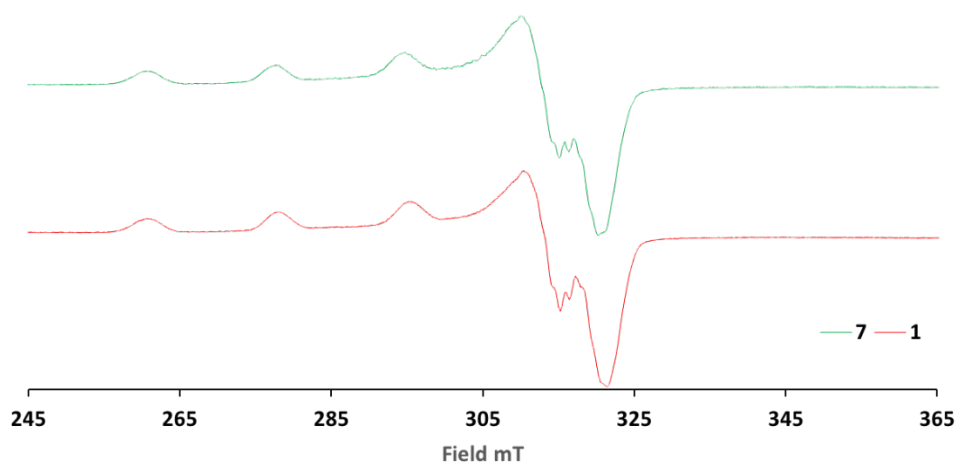


Fig. 2. Comparative EPR spectra for the compounds **1** and **7**. EPR spectra were acquired at 77K from a MeOH solution of final concentration 1mM. EPR spectra acquired using X-Band.

Table 3. Hamiltonian Spin parameters derived from the methanol glass spectra.

Compound	A_{\parallel} (10^{-4} cm $^{-1}$)	A_{\perp} (10^{-4} cm $^{-1}$)	g_{\parallel}	g_{\perp}	A_{iso} (10^{-4} cm $^{-1}$)	g_{iso}
1	153.47	84.24	2.20	2.06	79.23	2.10
2	136.31	115.544	2.19	2.06	83.92	2.10
3	123.05	126.22	2.19	2.08	83.09	2.11
4	139.77	101.21	2.12	2.06	80.33	2.08
5	142.78	77.17	2.18	2.06	73.32	2.10
6	149.59	109.61	2.26	2.02	86.40	2.10
7	152.28	68.72	2.14	2.06	73.67	2.09
8	153.13	108.48	2.14	2.06	87.20	2.09
9	155.22	75.76	2.20	2.06	76.99	2.11
10	156.37	99.45	2.19	2.06	85.27	2.10
11	140.56	83.09	2.18	2.08	74.55	2.11
12	134.69	118.28	2.19	2.06	84.32	2.10
13	145.35	79.81	2.27	2.00	75.05	2.09
14	136.74	95.16	2.16	2.08	77.3	2.11

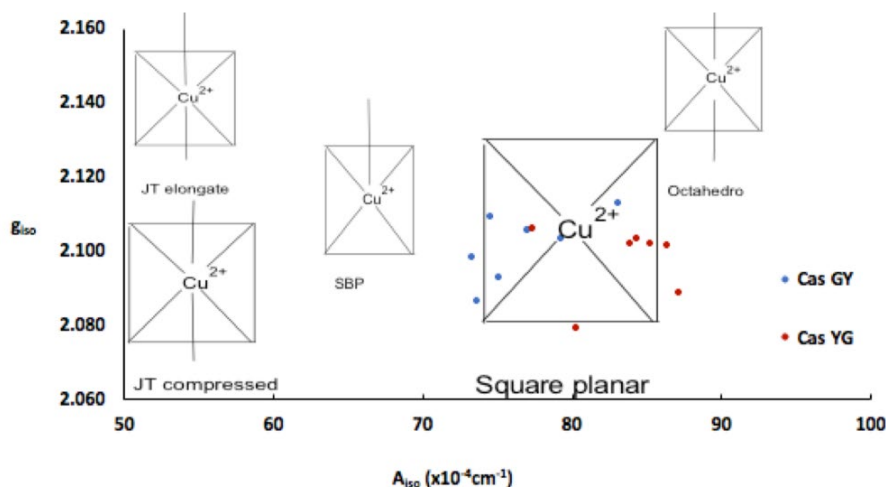
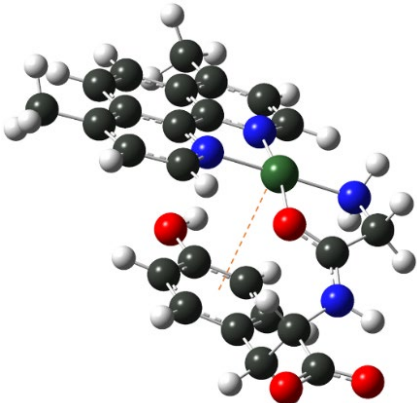
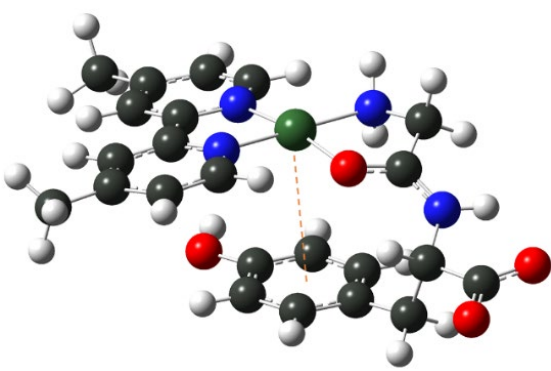
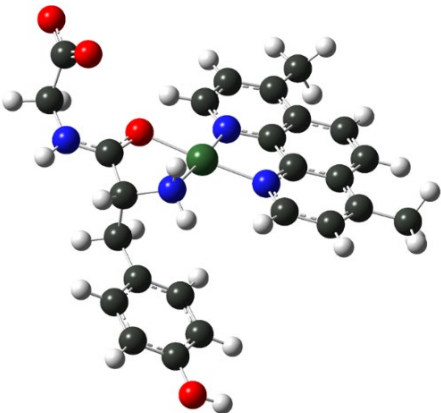
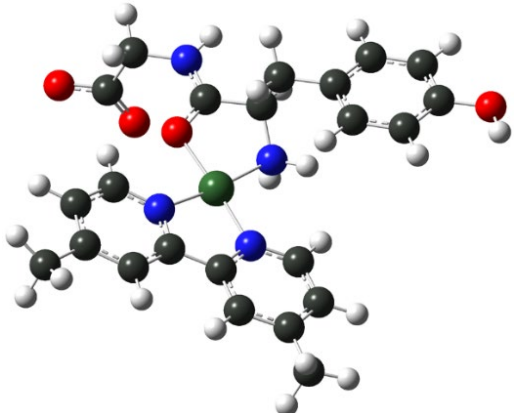


Fig. 3. A_{iso} vs g_{iso} diagram. Comparison of several copper(II) coordination compounds with different geometries, compounds studied in this work appear as square planar.

Geometry optimization

Prior to molecular docking studies, all Casiopeinas® were optimized using M06 functional and LanL2DZ pseudopotential. All copper(II) coordination compounds were optimized as $[Cu(N-N)(L-L)]^+$ square planar complexes and were optimized employing DFT protocols. Finally, boceprevir and remdesivir were also optimized with the same computational methodology. Optimized geometries of CasII-GY, CasIV-GY and their analogues of YG are presented in Table 4. The formation of coordination bonds occurs through the nitrogen's of the diimine, as well as the amino terminal of the dipeptide and the carbonyl group belonging to the peptide bond. This coordination mode agrees with the FT-IR and EPR characterization. DFT results suggests that the side chain present in tyrosine has an important effect on the chemical structure, as well as on the intramolecular interactions that the ternary copper(II) compounds can present. Since in the YG family the aromatic ring present in the dipeptide is in a position far from the copper atom, while in GY, the chemical structure is twisted so that there is an approach and a π -cation interaction (≈ 3.5 Å) between the phenyl and the central metal. Due to the structural similarity of both peptides, there is not separate cause for this behavior. Nevertheless, the steric hindrance, generated by the tertiary carbon of GY peptide, can be diminished by the formation of these intramolecular interaction. This trend is repeated in all studied Casiopeinas®. All Casiopeinas® (1-14) present a square planar arrangement around the metal center. In some cases, geometrical deviations were observed. Angles and distances estimated are in the range of the reported ones for some Casiopeinas® [72]. Generally, Casiopeinas® present an octahedral or square pyramidal geometries in solid state [73], completing with nitrate (NO_3^-) donors in the axial positions. However, in physiological conditions, the axial ligands can be substituted by aquo or other relevant biological molecules as nucleotides [74], glutathione or protein heteroatoms [75]. The optimizations presented here emulated the solution behavior of the coordination compounds and they are in according to the EPR experiments and the aqueous behavior of these class of compounds [32]. Energies, atomic coordinates and the remaining optimized geometries can be found in Table S3 and Scheme S1 of Supporting Information File.

Table 4. Optimized M06/LanL2DZ structures of **3**, **4**, **9** and **10**.

 <p style="text-align: center;">CasII-GY (3)</p>				 <p style="text-align: center;">CasIV-GY (4)</p>			
Bond	Distance (Å)	Bonds	Angle (°)	Bond	Distance (Å)	Bonds	Angle (°)
Cu-N _{NN} -N	2.00	N _{NN} -Cu-N' _{NN} -N	83.3	Cu-N _{NN} -N	1.99	N _{NN} -Cu-N' _{NN} -N	82.5
Cu-N' _{NN} -N	1.98	N _{NN} -Cu-N _{GY}	100.0	Cu-N' _{NN} -N	1.98	N _{NN} -Cu-N _{GY}	100.1
Cu-N _{GY}	2.02	N _{NN} -Cu-O _{GY}	92.6	Cu-N _{GY}	2.02	N _{NN} -Cu-O _{GY}	93.8
Cu-O _{GY}	1.99	N _{GY} -Cu-O _{GY}	84.3	Cu-O _{GY}	2.00	N _{GY} -Cu-O _{GY}	83.8
 <p style="text-align: center;">CasII-YG (9)</p>				 <p style="text-align: center;">CasIV-YG (10)</p>			
Bond	Distance (Å)	Bonds	Angle (°)	Bond	Distance (Å)	Bonds	Angle (°)
Cu-N _{NN} -N	2.02	N _{NN} -Cu-N' _{NN} -N	83.2	Cu-N _{NN} -N	1.99	N _{NN} -Cu-N' _{NN} -N	82.7
Cu-N' _{NN} -N	1.98	N _{NN} -Cu-N _{YG}	101.5	Cu-N' _{NN} -N	1.98	N _{NN} -Cu-N _{YG}	102.5
Cu-N _{GY}	2.01	N _{NN} -Cu-O _{YG}	93.3	Cu-N _{GY}	2.01	N _{NN} -Cu-O _{YG}	90.0
Cu-O _{GY}	2.03	N _{GY} -Cu-O _{YG}	82.0	Cu-O _{GY}	2.02	N _{GY} -Cu-O _{YG}	81.8

Molecular docking

All compounds were docked to the M^{pro} enzyme as well as the RBD^{Spike}-ACE2 complex in the RBD C-terminal and middle region. The values of binding energy (ΔG_U), inhibition (K_i) for the 5 best rated compounds were analyzed and boceprevir and remdesivir were presented for comparative purposes. The major inhibitor systems are those that have a more negative ΔG_U value, which is indicative of a stable interaction, a lower K_i value corresponds to the minimum amount to inhibit the protein efficiently. The objective is to focus on the Casiopeinas® that presents a greatest potential to be used as metallodrugs, particularly as anti-SARS-CoV-2 agents. In addition, the protein residues that interact with the coordination compounds are presented and the interactions obtained from the best molecular docking simulation were analyzed.

M^{pro}:Cas adduct

Table 5 presents the predicted ΔG_U to evaluate the affinity to M^{pro} and the K_i for compounds **14**, **10**, **5**, **3**, **8**, which exert the protein, as well as the interacting amino acids. Results with M^{pro} for compounds **3** and **9** as well as Casiopeinas® controls with amino acids (CasII-Tyr, CasIV-Tyr, CasII-gly and CasIV-gly) and without amino acids (CasIII-ia) were previous published [41]. Fig. 4 shows the comparative graph for all compounds analyzed. ΔG_U values for the better pose are in the range of (-6.62 to -9.57) Kcal/mol. The calculated values of K_i present a range of 0.10-14.00 μ M. For a wide range, log K_i is a better descriptor of the inhibition of M^{pro}. In general, Casiopeinas® can produce stable complexes with M^{pro}, that is expected from the structural diversity of the compounds, i. e., Casiopeinas® primary and secondary ligands are capable to form stabilizing interactions with the key residues of M^{pro} catalytic site. **14** and **10** have better ΔG_U and K_i values. **5**, **3**, **8** have values in the same magnitude order and slightly less stable compared to boceprevir [76]. The remain copper compounds have higher stabilization and inhibition values compared to remdesivir. Considering that stable adducts are predicted from docking simulations, the catalytic site of the protein is blocked with a high specificity. As observed in Fig. 2, the K_i values are less than 10 μ M, even presenting values in nanomolar order. Remained M^{pro}:Cas ΔG_U , K_i and interactions can be found in Scheme S2 of supporting information file.

Table 5. Binding affinities, predicted inhibition constants and potential interactions for the best rated M^{pro}:Cas adducts.

Compound	ΔG_U (Kcal/mol)	K _i (μ M) [log K _i]	AA's (M ^{pro} -Cas)
14	-9.57	(0.10) [-1.01]	Leu27, His41, Met49, Tyr54, Gly143, Cys145, His163, Met165, Glu166, Asp187, Arg188, Gln189, Thr190, Gln192
10	-9.02	(0.25) [-0.61]	His41, Met49, Phe140, Cys145, Met165, Glu166, Gln189
5	-8.41	(0.69) [-0.16]	His41, Tyr54, Cys145, Gly143, His163, Met165, Glu166, His172, Gln189
3	-8.38	(0.72) [-0.15]	Thr26, His41, Met49, Asn142, Gly143, Ser144, Cys145, Met165
8	-8.21	(0.72) [-0.14]	Cys44, Met49, Cys145, His163, His164, Glu166, Thr190, Gln192
Boceprevir	-8.44	(0.65*) [-0.19]	His41, Met49, Asn142, Ser144, Gly143, Cys145, His164, Met165, Glu166, Gln189
Remdesivir	-7.17	(5.53) [0.74]	His 41, Met49, Leu141, Gly143, His164, Met165, Glu166.

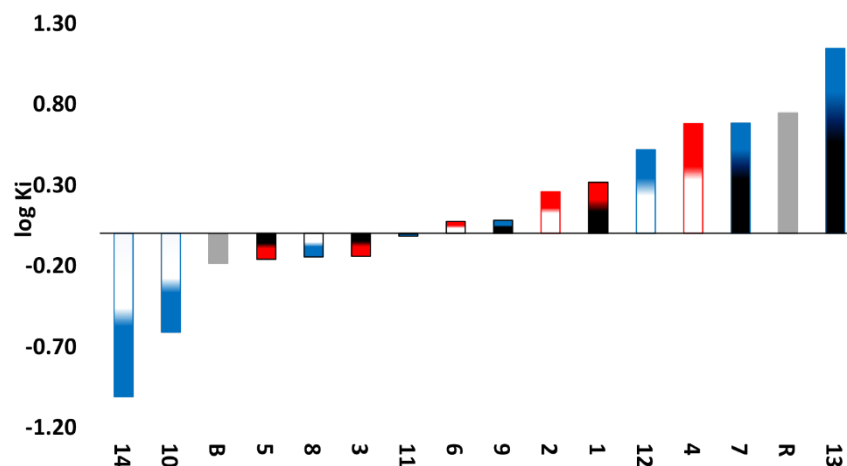
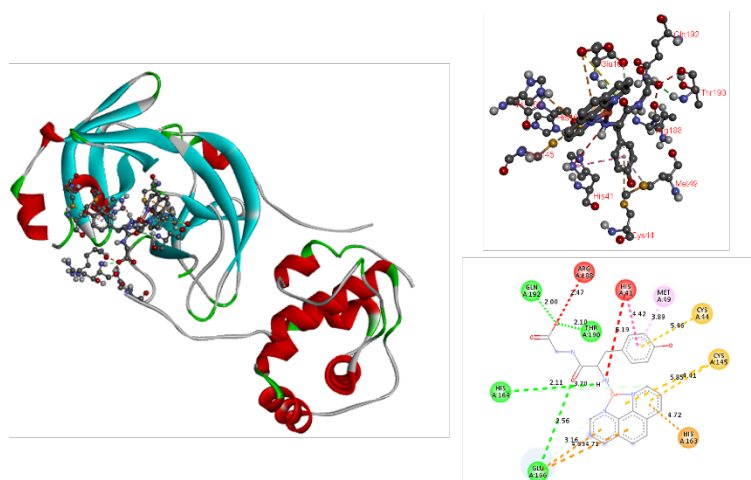


Fig. 4. Graph of predicted values of M^{Pro} inhibition constants for all compounds. Red: Compounds derived from 2,2'-bipyridine. Blue: Compounds derived from 1,10-phenanthroline. White: Compounds derived from YG. Black: Compounds derived from GY. Grey. Controls. B: boceprevir. R: remdesivir.

Several interactions can stabilize the Casiopeina- M^{Pro} adducts. The complex predicted between M^{Pro} and **14**, the best rated compound, is shown in Fig. 5. In the same figure, the pocket close-up and 2D diagrams can be observed to facilitate the localization of the stabilizing interactions.



residues belonging to the polypeptide chain of the protein. π -cation interactions are presented by the aromatic N-N ligand with His41, also π - π stacking between this residue and the tyrosine fragment of L-L ligand can be observed. Several π -alkyl interactions between the methyl substituents of 1,10-phenanthroline and Leu27, His41, His163. Hydrogen bonds between the amino and carboxylate groups of the dipeptide with Glu166, Gln189, Thr190, Gln192 were founded. The π -sulfur interaction of the diimine ligand with Met49, also occurs. Finally, π -sulfur interaction and hydrogen bond between the N-N ligand and Cys145 were observed. Similar interactions have been reported between M^{Pto} and several species such as organic [77] and inorganic compounds [78], particularly with N3 peptide [79], as well as with rhenium and selenium coordination compounds [80] respectively. Compounds **10** and **5** presented in Fig. 6 offer value information regarding to the interactions provided by both the diimine ligand and the dipeptide moiety. Similar interactions occur due to the chemical structure of these 14 Casiopeinas® that favor the interaction with M^{Pto} , and its potential inhibition. Inhibition of this protein may be satisfactory to prevent viral replication and transcription [81].

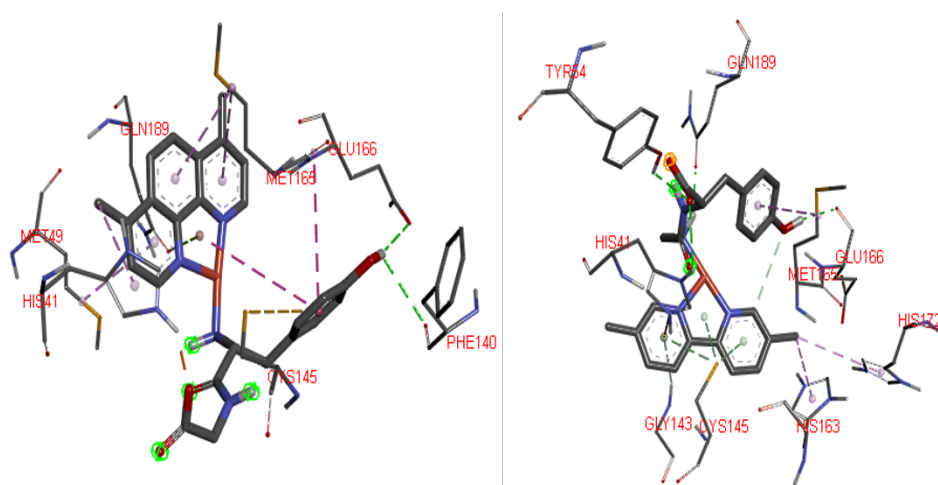


Fig.6. Possible 3D interaction diagrams of **10**: M^{Pto} (Left) and **5**: M^{Pto} (right) adducts, To recognize principal interactions, most the protein was removed. Only the main interactions predicted were presented.

Spike-ACE2 complex

The study of the molecular docking of the Spike-ACE2 complex was carried out to determine if the Casiopeinas® can block the formation of protein complex. All compounds can interact with the C-terminal and central regions. Tables 6 (RBD C-terminal) and 7 (RBD-bridge) present the values of predicted ΔG_U , K_i , as well as the amino acids of the B chain belonging to the Spike protein and the residues of the E chain of the human ACE2 protein. It is worth mentioning that in several cases they bind to the amino acids that participate in the assemble of the complex. That provokes that the virus enters to the human cells. The amino acids involved in assemble are Gln24 and Met82 located in the E chain of the ACE2, Gln474 and Phe486 of the Spike protein, belong to the C-terminal region. In the central region the targets are Asp30 and Hys34 from the ACE2, Lys417 and Tyr453 for Spike [7]. The details of the interactions are broken down separately for each region of the RBD Spike-ACE2 complex. The test compounds present significantly better values of ΔG_U and K_i (Tables 6 and 7) than those shown by the controls, they are comparable with those evidenced by other potential inhibitors of RBDSpike-ACE2 complex [82]; there is currently no drug that has this protein complex as a molecular target [23]. Remained Spike-ACE2-Cas ΔG_U , K_i and interactions can be found in Scheme S3 (C-terminal region) and Scheme S4 (central region) of Supporting Information File.

Table 6. Binding affinities predicted inhibition constants and potential interactions for the best rated Spike-ACE2 RBD Domain C-terminal-Cas-adducts.

Compound	ΔG_U (Kcal/mol)	K_i (μ M) [log K_i]	AA's (Spike-ACE2 complex-Cas)	
			Spike Chain E	ACE2 Chain B
6	-6.69	(12.47) [1.10]	Ala475A, Thr478, Cys480, Phe486, Asn487, Cys488	Ile21, Met82
7	-5.28	(133.98) [2.13]	Ala475, Gly476, Thr478, Cys480, Phe486, Asn487, Cys488	Ile21, Met82
9	-5.27	(137.53) [2.14]	Thr478, Phe486, Asn487	Ile21, Gln24, Tyr83, Pro84, Glu87
4	-5.01	(214.45) [2.33]	Ala475, Ser477, Cys480, Cys488	Ile21, Pro84, Glu87
5	-4.61	(421.15) [2.62]	Ala475, Gly476, Ser477, Thr478, Cys480, Phe486, Asn487, Cys488	Ile21, Pro84
Boceprevir	-1.98	(35280) [4.55]	Thr478, Phe486	Gln24, Ala25, Met82, Tyr83, Pro84, Glu87, Ile88
Remdesivir	>0	---	---	---

Table 7. Binding affinities, inhibition constants and potential interactions for the best rated Spike-ACE2 RBD Domain Bridge-Cas-adducts.

Compound	ΔG_U (Kcal/mol)	K_i (μ M) [log K_i]	AA's (Spike-ACE2 complex-Cas)	
			Spike Chain E	ACE2 Chain B
13	-8.27	(0.86) [-0.07]	Arg403, Asp 405, Tyr453, Tyr505	Asp30, Glu37, Gln388, Pro389, Arg393
9	-6.78	(10.7) [1.03]	Arg403, Asp405, Lys417, Tyr453, Tyr495, Tyr505	Asn33, His34, Glu37, Pro389, Arg393
3	-6.45	(18.75) [1.27]	Arg402, Asp405, Glu406	Asn33, Glu37, Ala387, Gln388, Pro389, Arg393
8	-6.34	(22.38) [1.35]	Non interactions	Lys26, Leu29, Asn33, Glu37, Thr92, Val93, Ala387, Pro389
12	-6.34	(22.63) [1.35]	Arg403, Lys417	Leu29, Asp30, Asn33, His34, Glu37, Gln388, Pro389
Boceprevir	-4.97	(227.27) [2.36]	Arg403, Glu406, Lys417, Tyr453, Tyr505	Asp30, His34, Pro389
Remdesivir	-3.37	(3400) [3.53]	Arg403, Asp405, Glu406, Gln409, Lys417	Non interactions

a) C-terminal region

The inhibition of this zone of the RBD of the Spike-ACE2 complex is centered in the amino acids Gln24 and Met82 of the ACE2, Gln474 and Phe486 of Spike protein [7]. The predicted values of ΔG_U and K_i presented in table 6, which can be seen its visual representation in Fig. 7. Remdesivir control cannot inhibit the complex formation. On the other hand, Boceprevir control has a K_i value of 35.28 mM ($\log K_i=4.55$), which is very high compared to that observed by compound **6**, the difference is 3 orders of magnitude ($K_i=12.47 \mu\text{M}$, $\log K_i=1.10$) value, **6** has the highest affinity to the Spike-ACE2 complex in the RBD at C-terminal domain. Most compounds have $\log K_i$ values in the range of 2.00 to 4.00.

The potential high affinity of compound **6** to the Spike-ACE2 complex is due to highest number of potential interactions. The contacts presented this compound are Ile21 and Met82 (involved in the assemble of Spike-ACE2 complex), both in the ACE2, they are interactions of hydrogen bonds, salt bridge interaction between the carboxylate anion and the protonated amine of Ile21 (see Fig. 8). Regarding the E chain of the Spike, it should be noted that the amino acids that are part of the binding are with Gln474 and Phe486, the last amino acid interacts with Met82 of ACE2 to form the Spike-ACE2 complex. Compound **6** interacts with Phe486 (Spike) and Met82 (ACE2) by blocking the binding site to RBD; it interacts through a hydrogen bond, Phe486 forms the interaction by π - π stacking with one of the aromatic rings belonging of N-N ligand. Other interactions determined with the Spike E chain by molecular docking are π -sulfur (Cys480 and Cys488), π -alone pair (Asn487), π -donor hydrogen bond (Gly476 and Thr478) and π -alkyl (Ala475), between an aromatic ring of the 2,2'-bipyridine derivative with the residues described. **7** and **9** interacts in the same way that **6**. The principal interactions of these compounds to be observed in Fig. 9. They allow the interaction with RBD-Spike-ACE2 C-terminal domain, as well as its potential inhibition.

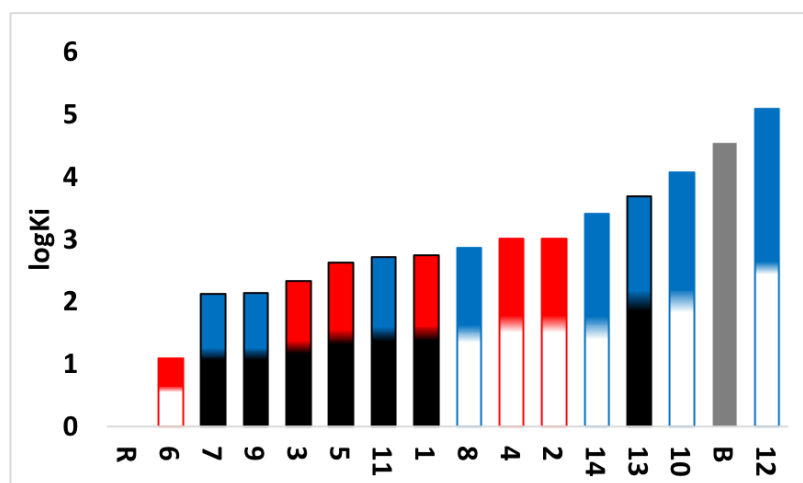


Fig. 7. Graph of predicted values of RBD-C terminal Spike-ACE2 complex inhibition constants for all compounds. Red: Compounds derived from 2,2'-bipyridine. Blue: Compounds derived from 1,10-phenanthroline. White: Compounds derived from YG. Black: Compounds derived from GY. Grey: Controls. B: Boceprevir. R: Remdesivir.

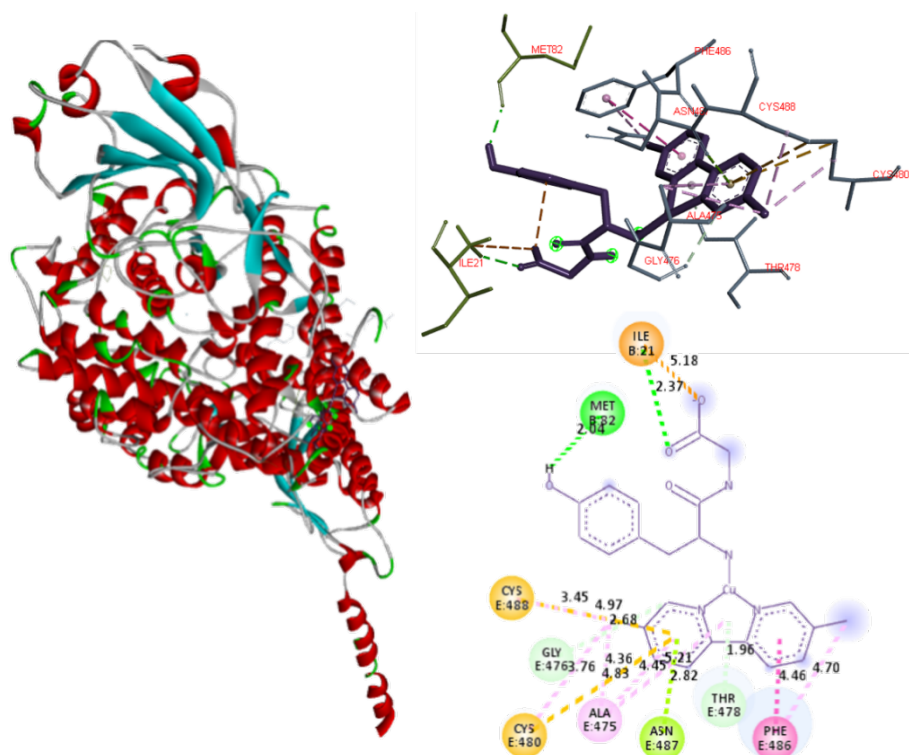


Fig. 8. Docked simulations of 6:Spike-ACE2 complex, C-terminal region. In the left side can be founded the complete complex. Red: Chain B of ACE2. Blue: Chain E of Spike. In the top right is showed a 3D diagram with the principal interactions between 6 and Spike-ACE2 complex. 2D diagrams is in the bottom of the right side.

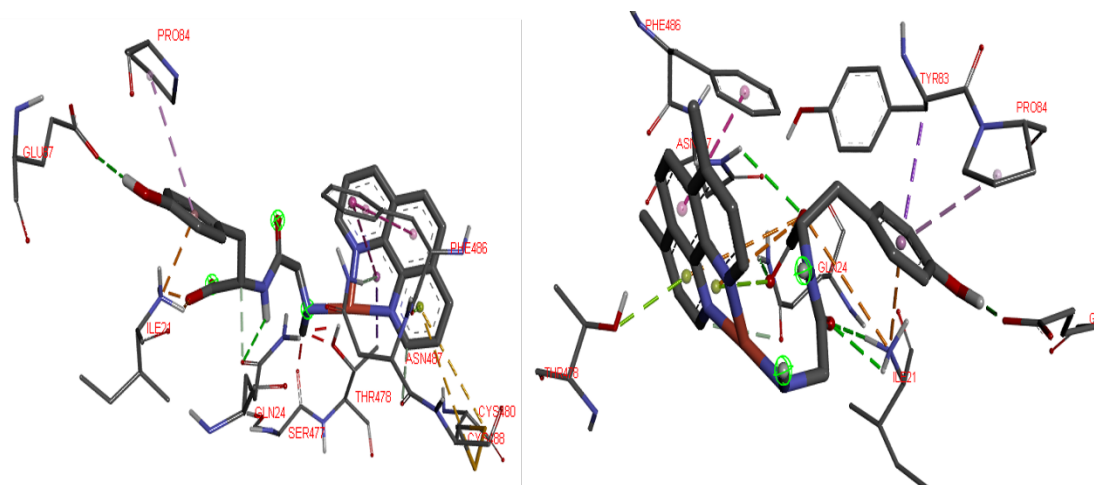


Fig. 9. Possible 3D interactions of 7-Complex Spike-ACE2 (left) and 9-Complex Spike-ACE2 (right) adducts. To recognize principal interactions, most the protein was removed. Only the main interactions were presented.

b) Central region

In this region, molecular docking is focused on the amino acids Asp30 and Hys34 of the ACE2 and the Lys417 and Tyr453 residues of the Spike protein, which are the amino acids that comprise the RBD Spike-ACE2 complex [7]. As denoted in table 7, Casiopinas® present interaction with the residues of the E chain of the Spike protein and the B chain of the ACE2 with values of ΔG_U $-$ (4.76 to 8.27 Kcal/mol) and K_i (0.86 to 326.37 μ M) better than those presented by the controls up to 4 orders of magnitude (Fig. 10), it should be mentioned that boceprevir presents interaction with the 4 amino acids that comprise the RBD Spike-ACE2, but the affinity is low compared to 13 of the proposed ternary copper(II) compounds. Compound **13** has the highest affinity to the Spike-ACE2 complex in the RBD at central region.

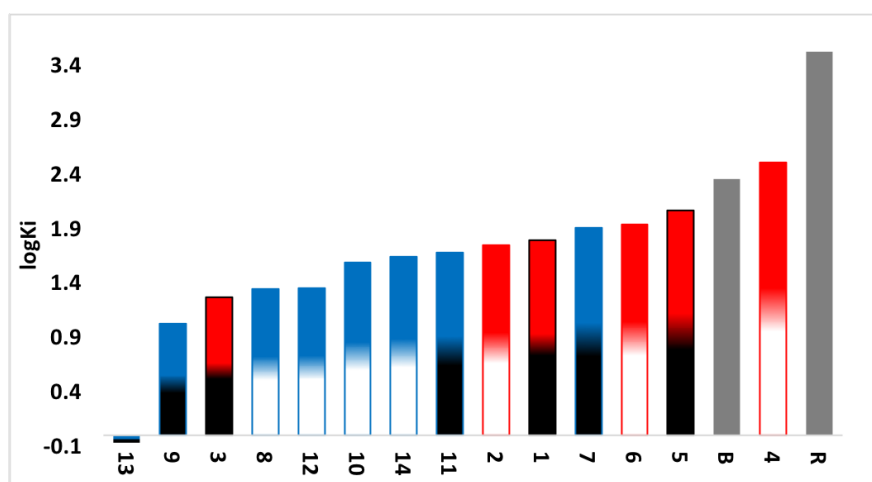


Fig. 10. Graph of predicted values of RBD-middle region Spike-ACE2 complex inhibition constants for all compounds. Red: Compounds derived from 2,2'-bipyridine. Blue: Compounds derived from 1,10-phenanthroline. White: Compounds derived from YG. Black: Compounds derived from GY. Grey: Controls. B: boceprevir. R: remdesivir.

The interactions that stabilized RBD SPIKE-ACE2 adducts involve the amino acids Asp30 and His34 interacts with Lys417 and Tyr453 respectively, the effect of blocking these contacts is important to inhibit the interaction of SARS-CoV-2 with the human host cells that express the ACE2 protein. As can be seen in table 7, compounds **3**, **8**, **9**, **12** and **13** exhibits at least one of the four interactions mentioned, so inherently these compounds can inhibit the formation of the Spike-ACE2 complex in the bridge domain. Particularly, compound **13** has interactions with the amino acids Asp30 of the E chain of ACE2 and Tyr453 of the Spike protein [8], the inhibition action is performed through the formation of hydrogen bonds between carbonyl group of Asp30 and primary amine group of L-L. Other interaction occurs between hydroxyl group of Tyr453 and secondary amine on dipeptide. Other interesting interactions observed are due to the steric effects that can be allows the inhibition of RBD Spike-ACE2 in the bridge domain. These interactions are hydrogen bonds between Asp405 (Spike) and hydroxyl group of Tyrosine. Amide- π interactions (Arg393-N-N ligand and Arg403-Tyr of L-L ligand), π -alkyl interactions between the methyl groups with the amino acids Pro389 and Tyr505 in the ACE2 (Fig. 11) also were founded. Compounds **9** and **3** presented in Fig. 12 have similar interactions than **13**, again all of these favors the interaction with RBD-Spike-ACE2 bridge domain and its potential inhibition.

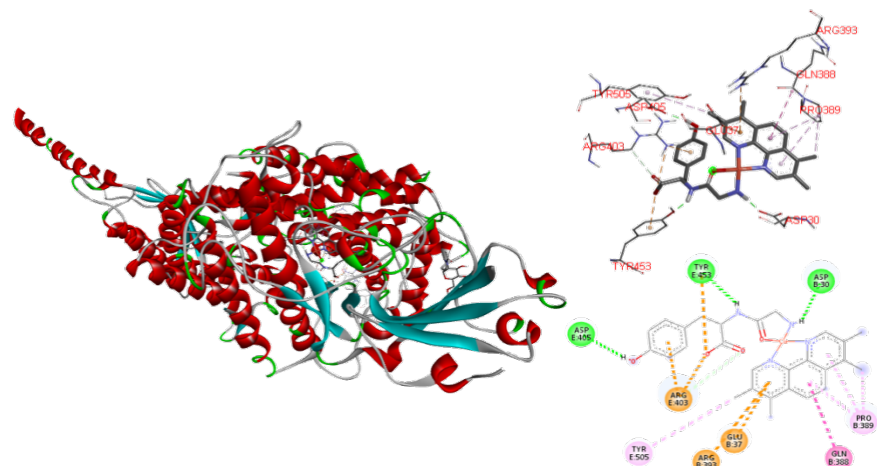


Fig. 11. Docked simulations of **13**:Spike-ACE2 complex middle region. In the left side can be founded the complete complex, Red: Chain B of ACE2. Blue: Chain E of Spike. In the top right is showed a 3D diagram with the principal interaction between **6** and Spike-ACE2 complex. 2D diagrams is in the bottom of the right side.

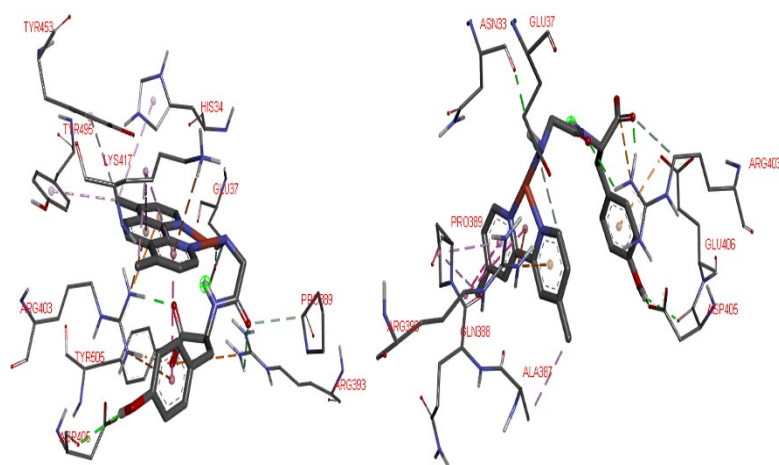


Fig. 12. 3D interactions of **9**-Spike-ACE2 complex (left) and **3**-Spike-ACE2 complex (right) adducts. To recognize principal interactions, most the protein was removed. Only the main interactions were presented.

Conclusions

The 14 coordination compounds with diimine ligands and dipeptides Casiopeinas® synthesized were composed as monocationic coordination sphere according to the analysis obtained by the FAB(+), as well as with the values obtained in the conductivity. Ternary copper(II) compounds are paramagnetic with an unpaired electron. EPR studies suggest a planar square geometry and DFT calculations are in according with this geometry proposal and with the structural parameters informed for other Casiopeinas® and their solution behavior. The values obtained from ΔG_U and K_i position the Casiopeinas® as potential inhibitory agents of SARS-CoV-2 transcendental proteins, since in the study with the M^{pro} , similar and even better values are presented with respect to the controls used in this work, in terms of the 2 regions analyzed in the RBD Spike-ACE2, the potential copper metallodrugs present significantly better values compared to those obtained for

boceprevir and remdesivir. The potential inhibitory effect of Casiopeinas® may be due to the various components (copper[II], diamine and dipeptide) that form the ternary coordination compounds, which interact with the amino acid residues present in SARS-COV2 proteins, through hydrogen bonding, various π -interactions, as well as by electrostatic attraction. Casiopeinas® may stabilize the formation of adducts with amino acids belonging to the catalytic site of M^{PRO} or with those involved in the formation of RBD Spike-ACE2 in the domains analyzed.

Acknowledgements

This work was supported by UNAM-PAPIIT IN218013; Project Grant UNAM-PAPIIT 230020; UNAM-FQ 5000-9047; UNAM-DGTIC (projects LANCAD-UNAM-DGTIC-358 and UNAM-DGTIC-COVID-005). LGTC thanks to CONACYT-CVU 689679 for the PhD scholarship. To Dra. Laura Padierna and M. Karyna Pérez from the Laboratorios de Especialidades Inmunológicas S.A. de C.V. for the donating material. To M. in C. Adrian Espinoza Guillén for the technical support in the LQIM. †MLVC died on April 28, 2009, her expertise in the chemical synthesis of peptides inspired this work, as well as she was a disciple of Professor Joaquín Tamariz who is honored with this special issue. Dedicated to all people who died from this emerging disease.

References

1. Zhou, P.; Yang, X. L.; Wang, X. G.; Hu, B.; Zhang, L.; Zhang, W.; Si, H. R.; Zhu, Y.; Li, B.; Huang, C. L.; Chen, H. D.; Chen, J.; Luo, Y.; Guo, H.; Jiang, R. D.; Liu, M. Q.; Chen, Y.; Shen, R.; Wang, X.; Zheng, X. S.; Zhao, K.; Chen, Q. J.; Deng, F.; Liu, L. L.; Yan, B.; Zhan, F. X.; Wang, Y. Y.; Xiao, G. F.; Shi, Z. L. *Nature* **2020**, *579*, 270-273. DOI: <https://doi.org/10.1038/s41586-020-2012-7>
2. Wu, F.; Zhao, S.; Yu, B.; Wang, W.; Song, Z. G.; Hu, Y.; Tao, Z. W.; Tlan, J. H.; Pel, Y. Y.; Yuan, M. L.; Zhang, Y. L.; Dal, F. H.; Liu, Y.; Yang, Q. M.; Zheng, J. J.; Xu, L.; Holmes, E. C.; Zhang, Y. Z. *Nature* **2020**, *579*, 265-269. DOI: <https://doi.org/10.1038/s41586-020-2008-3>
3. <http://covid19.who.int/>, accessed in March 2023.
4. Guarner, J. *Am. J. Clin. Pathol.* **2020**, *153*, 420-421. DOI: <https://doi.org/10.1093/AJCP/AQAA029>
5. V'koski, P.; Kratzel, A.; Steiner, S.; Stalder, H.; Thiel, V. *Nat. Rev. Microbiol.* **2020**, *19*, 155-170. DOI: <https://doi.org/10.1038/s41579-020-00468-6>
6. Wu, A.; Peng, Y.; Huang, B.; Ding, X.; Wang, X.; Niu, P.; Meng, J.; Zhu, Z.; Zhang, Z.; Wang, J.; Sheng, J.; Quan, L.; Xia, Z.; Tan, W.; Cheng, G.; Jiang, T. *Cell Host Microbe.* **2020**, *27*, 325-328. DOI: <https://doi.org/10.1016/j.chom.2020.02.001>
7. Yan, R.; Zhang, Y.; Li, Y.; Xia, L.; Guo, Y.; Zhou, Q. *Science.* **2020**, *367*, 1444-1449. DOI: <https://doi.org/10.1126/science.abb2762>
8. Lan, J.; Ge, J.; Yu, J.; Shan, S.; Zhou, H.; Fan, S.; Zhang, Q.; Shi, X.; Wang, Q.; Zhang, L.; Wang, X. *Nature* **2020**, *581*, 215-220. DOI: <https://doi.org/10.1038/s41586-020-2180-5>
9. Zhou, X.; Zhang, Y.; Zhong, F.; Lin, C.; McCormick, P. J.; Jiang, F.; Luo, J.; Zhou, H.; Wang, Q.; Fu, Y.; Duan, J.; Zhang, J. *Chin. Sci. Bull.* **2021**, *66*, 661-663. DOI: <https://doi.org/10.106/j.scib.2020.10.018>
10. Finkel, Y.; Mizrahi, O.; Nachshon, A.; Weingarten-Gabbay, S.; Morgenstern, D.; Yahalom-Ronen, Y.; Tamir, H.; Achdout, H.; Stein, D.; Israeli, O.; Beth-Din, A.; Melamed, S.; Weiss, S.; Israely, T.; Paran, N.; Schwartz, M.; Ginossar, S. *Nature.* **2020**, *589*, 125-130. DOI: <https://doi.org/10.1038/s41586-020-2739-1>
11. Jin, Z.; Du, X.; Xu, Y.; Deng, Y.; Liu, M.; Zhao, Y.; Zhang, B.; Li, X.; Zhang, L.; Peng, C.; Duan, Y.; Yu, J.; Wang, L.; Yang, K.; Liu, F.; Jiang, R.; Yang, X.; You, T.; Liu, X.; Yang, X.; Bai, F.; Liu,

- H.; Liu, X.; W, Guddat.; Xu, W.; Xiao, G.; Qin, C.; Shi, Z.; Jlang, H.; Rao, Z.; Yang, H. *Nature*. **2020**, 582, 289-293. <https://doi.org/10.1038/s41586-020-2233-y>
12. Xu, T.; Ooi, A.; Lee, H. C.; Wilmouth, R.; Liu, D. X.; Lescar. J. *Acta Crystallogr., Sect. F: Struct. Biol. Cryst. Commun.* **2005**, F61, 964-966. DOI: <https://doi.org/10.1107/s1744309105033257>
13. Parvez, S. A.; Karim, A.; Hasan, M.; Jaman, J.; Karim, Z.; Tahsin, T.; Hasan, N.; Hozen, M. *Int. J. Biol. Macromol.* **2020**, 163, 1787-1797. DOI: <https://doi.org/10.1016/j.ijbiomac.2020.09.098>
14. Naveja, J. J.; Madariaga-Mazón, A.; Flores-Murrieta, F.; Granados-Montiel, J.; Madariaga-Ceceña, M.; Duarte-Alaniz, V.; Maldonado-Rodríguez, M.; García-Morales, J.; Senosiain-Peláez, J. P.; Martínez-Mayorga, K. *Drug Discovery Today*. **2021**, 26, 229-239. DOI: <https://doi.org/10.1016/j.drudis.2020.10.018>
15. Domínguez-Villa, F. X.; Durán-Iturbide, N. A.; Ávila-Zarraga, J. G. *Bioorg. Chem.* **2021**, 106, 104497. DOI: <https://doi.org/10.1016/j.bioorg.2020.104497>
16. Wu, C.; Liu, Y.; Yang, Y.; Zhang, P.; Zhong, W.; Wang, Y.; Wang, Q.; Xu, Y.; Li, M.; Li, Z.; Zheng, M.; Chen, L.; Li, H. *Acta Pharm. Sin. B.* **2020**, 10, 766-788. DOI: <https://doi.org/10.1016/j.apsb.2020.02.008>
17. Krumm, Z. A.; Lloyd, G. M.; Francis, C. P.; Nasif, L. H.; Mitchell, D. A.; Golde, T. E.; Giasson, B. I.; Xia, Y. *Virology*. **2021**, 18. DOI: <https://doi.org/10.1186/s12985-021-01526-y>
18. Guedes, I. A.; Costa, L. S. C.; Dos Santos, K. N.; Karl, A. L.; Rocha, G. K.; Teixeira, I. M.; Galheigo, M. M.; Medeiros, V.; Krempser, E.; Custódio, F. L.; Barbosa, H. J. C.; Nicolas, M. F.; Dardenne, L. E. *Sci. Rep.* **2021**, 11, 5543. DOI: <https://doi.org/10.1038/s41598-021-84700-0>
19. Ahamad, S.; Kanipakam, H.; Birla, S.; Ali, M. S.; Gupta, D. *Eur. J. of Pharm.* **2021**, 890, 173664. DOI: <https://doi.org/10.1016/j.ejphar.2020.173664>
20. Fu, L.; Ye, F.; Feng, Y.; Yu, F.; Wang, Q.; Wu, Y.; Zhao, C.; Shun, H.; Huang, B.; Niu, P.; Song, H.; Shi, Y.; Li, X.; Tan, W.; Qi, J.; Gao, G. F. *Nat. Commun.* **2020**, 11, 4417, 1-8. DOI: <https://doi.org/10.1038/s41467-020-18233-x>
21. Ali, A.; Sepay, N.; Afzal, M.; Alarifi, A.; Shadid, M.; Ahmad, M. *Bioorg. Chem.* **2021**, 110, 104772. DOI: <https://doi.org/10.1016/j.bioorg.2021.104772>
22. Eweas, A. F.; Alhossary, A. A.; Abdel-Moneim, A. S. *Front. Microbiol.* **2021**, 11, 1-15. DOI: <https://doi.org/10.3389/fmicb.2020.592908>
23. Gil-Moles, M.; Türck, S.; Basu, U.; Pettenuzzo, A.; Bhattacharya, S.; Rajan, A.; Ma, X.; Büssing, R.; Wölker, J.; Burmeister, H.; Hoffmeister, H.; Schneeberg, P.; Prause, A.; Lippmann, P.; Kusi-Nimarko, J.; Hassell-Hart, S.; McGown, A.; Guest, D.; Lin, Y.; Notaro, A.; Vinck, R.; Karges, J.; Cariou, K.; Peng, K.; Qin, X.; Wang, X.; Skiba, J.; Szczupak, L.; Kowalski, K.; Schatzschneider, U.; Hemmert, C.; Gornitzka, H.; Milaeva, E. R.; Nazarov, A. A.; Gasser, G.; Spencer, J.; Ronconi, L.; Kortz, U.; Cinatl, J.; Bojkova, D.; Ott, I. *Chem. Eur. J.* **2021**, 27, 17928-17940. DOI: <https://doi.org/10.1002/chem.202103258>
24. Pal, M.; Musib, D.; Roy, M. *New. J. Chem.* **2020**, 10, 1039. DOI: <https://doi.org/10.1039/D0NJ04578K>
25. Geromichalou, E. G.; Trafalis, D. T.; Dalezis, P.; Malis, G.; Psomas, G.; Geromichalos, G. D. *J. Inorg. Biochem.* **2022**, 231, 111805. DOI: <https://doi.org/10.1016/j.jinorgbio.2022.111805>
26. Karges, J.; Cohen, S. M. *Chem. Biochem.* **2021**, 22, 1-9. DOI: <https://doi.org/10.1002/cbic.202100186>
27. Owen, D. R.; Allerton, C. M. N.; Anderson, A. S.; Aschenbrenner, L.; Avery, M.; Berrit, S.; Boras, B.; Cardin, R. D.; Carlo, A.; Coffman, K. J.; Dantonio, A.; Di, L.; Eng, H.; Ferre, R. A.; Gajiwala, K. S.; Gibson, S. A.; Greasley, S. E.; Hurst, B. L.; Kadar, E. P.; Kalgutkar, A. S.; Lee, J. C.; Lee, J.; Liu, W.; Mason, S. W.; Noell, S.; Novak, J. J.; Obach, R. S.; Ogilvie, K.; Patel, N. C.; Pettersson, M.; Rai, D. K.; Reese, M. R.; Sammons, M. F.; Sathish, J. G.; Singh, R. S. P.; Steppan, C. M.; Stewart, A. E.; Tuttle, J. B.; Updyke, L.; Verhoest, P. R.; Wei, L.; Yang, Q.; Zhu, Y. *Science*. **2021**, 374, 1586-1593. DOI: <https://doi.org/10.1126/science.aba4784>

28. Anthony, E. J.; Bolitho, E. M.; Bridgewater, H. E.; Carter, O. W. L.; Donnelly, J. M.; Imberty, C.; Lant, E. C.; Lermite, F.; Needham, R. J.; Palau, M.; Sadler, P. J.; Shi, H.; Wang, F. X.; Zhang, W. Y.; Zhang, Z. *Chem. Sci.* **2020**, *11*, 12888-12917. DOI: <https://doi.org/10.1039/d0sc04082g>
29. Cirri, D.; Pratesi, A.; Marzo, T.; Messori, L. *Expert. Opin. Drug. Discovery.* **2020**, *16*, 39-46. DOI: <https://doi.org/10.1080/17460441.2020.1819236>
30. Karges, J. *Chem. Bio. Chem.* **2020**, *21*, 1-4. DOI: <https://doi.org/10.1002/cbic.202000397>
31. Ioannou, K.; Vlasidou, M. *Biometals.* **2022**, *35*, 639-652. DOI: <https://doi.org/10.1007/s10534-022-00386-5>
32. Correia, I.; Borovic, S.; Cavaco, I.; Matos, C. P.; Roy, S.; Santos, H. M.; Fernández, L.; Capelo, J. L.; Ruiz-Azuara, L.; Costa Pessoa, J. *J. Inorg. Biochem.* **2017**, *175*, 284-297. DOI: <https://doi.org/10.1016/j.jinorgbio.2017.07.025>
33. Rufino-González, Y.; Ponce-Macotela, M.; García-Ramos, J. C.; Martínez-Gordillo, M. N.; Galindo-Murillo, R.; González-Maciel, A.; Reynoso-Robles, R.; Tovar-Tovar, A.; Flores-Álamo, M.; Toledano-Magaña, Y.; Ruiz-Azuara, L. *J. Inorg. Biochem.* **2019**, *195*, 83-90. DOI: <https://doi.org/10.1016/j.jinorgbio.2019.03.012>
34. Larios-Cervantes, A. A.; Chávez-Cortéz, E. G.; Martínez-Hernández, M.; Talavera-Contreras, L. G.; Espinoza-Guillen, A.; Carrillo-Ávila, B. A.; Ruiz-Azuara, L.; Álvarez-Pérez, M. A.; Martínez-Aguilar, V. M. *Braz. J. Microbiol.* **2022**, *53*, 179-184. DOI: <https://doi.org/10.1007/s42770-021-00648-3>
35. Ruiz-Azuara, L.; Bravo-Gómez, M. E. *Curr. Med. Chem.* **2010**, *17*, 3606-3615. DOI: <https://doi.org/10.2174/092986710793213751>
36. Ramírez-Palma, L. G.; García-Jacas, C. R.; García-Ramos, J. C.; Almada-Monter, R.; Galindo-Murillo, R.; Cortés, F. *J. Molec. Struct.* **2020**, *1204*, 127480. DOI: <https://doi.org/10.1016/j.molstru.2019.127480>
37. Trejo-Solís, C.; Jiménez-Farfan, D.; Rodríguez-Enriquez, S.; Fernández-Valverde, F.; Cruz-Salgado, A.; Ruiz-Azuara, L.; Sotelo, J. *BMC. Cancer.* **2012**, *12*, 156.
38. Gutiérrez, A. G.; Vázquez-Aguirre, A.; García-Ramos, J. C.; Flores-Alamo, M.; Hernández-Lemus, E.; Ruiz-Azuara, L.; Mejía, C. *J. Inorg. Biochem.* **2013**, *126*, 17-25. DOI: <https://doi.org/10.1016/j.jinorgbio.2013.05.001>
39. Figueroa-DePaz, Y.; Resendiz-Acevedo, K.; Dávila-Manzanilla, S. G.; García-Ramos, J. C.; Ortiz-Frade, L.; Serment-Guerrero, J.; Ruiz-Azuara, L. *J. Inorg. Biochem.* **2022**, *231*, 111772. DOI: <https://doi.org/10.1016/j.jinorgbio.2022.111772>
40. Kachadourian, R.; Brechbuhl, H. M.; Ruiz-Azuara, L.; Gracia-Mora, I.; Day, B. J. *Toxicol.* **2010**, *268*, 176-183. DOI: <https://doi.org/10.1016/j.tox.2009.12.010>
41. García-Ramos, J. C.; Galindo-Murillo, R.; Tovar-Tovar, A.; Alonso-Sáenz, A. L.; Gómez-Vidales, V.; Flores-Álamo, M.; Ortiz-Frade, L.; Cortés-Guzmán, F.; Moreno-Esparza, R.; Campero, A.; Ruiz-Azuara, L. *Chem. Eur. J.* **2014**, *20*, 13730-13741. DOI: <https://doi.org/10.1002/chem.201402775>
42. Reyna, M.; Talavera Contreras, L. G.; Figueroa de Paz, Y.; Ruiz-Azuara, L.; Hernández Ayala, L. F. *New. J. Chem.*, **2022**, *46*, 12500-12511. DOI: <https://doi.org/10.1039/d2nj01480g>
43. Erxleben, A. *Coord. Chem. Rev.* **2018**, *360*, 92-121. DOI: <https://doi.org/10.1016/j.ccr.2018.01.008>
44. Grenács, Á.; Kaluha, A.; Kállay, C.; Józai, V.; Sanna, D.; Sóvago, I. *J. Inorg. Biochem.* **2013**, *128*, 17-25. DOI: <https://dx.doi.org/10.1016/j.jinorgbio.2013.07.008>
45. Oliveira-Brett, A. M.; Diculescu, V. C.; Enache, T. A.; Fernandes, I. P. G.; Chiorcea-Paquim, A. M.; Oliveira, S. C. B. *Curr. Opin. Electrochem.* **2019**, *14*, 173-179. DOI: <https://doi.org/10.1016/j.coelec.2019.03.008>
46. Arcos-López, T.; Qayyum, M.; Rivilas-Acevedo, L.; Miotto, M. C.; Grande-Aztatzi, R.; Fernández, C. O.; Hedman, B.; Hodgson, K. O.; Vela, A.; Solomon, E. I.; Quintanar, L. *Inorg. Chem.* **2016**, *55*, 2909-2922. DOI: <https://doi.org/10.1021/acs.inorgchem.5b02794>
47. Brasún, J.; Cebat, M.; Sochacka, A.; Gladysz, O.; Swiatek-Kozloska, J. *Dalton. Trans.* **2008**, 4978-4980. DOI: <https://doi.org/10.1039/b807799a>

48. Kotynia, A.; Czyżnikowska, Z.; Cebrat, M.; Jaremko, L.; Gladysz, O.; Jaremko, M.; Marciniak, A.; Brasún, J. *Inorg. Chim. Acta.* **2013**, *396*, 40-48. DOI: <https://dx.doi.org/10.1016/j.ica.2012.09.035>
49. Atrián-Blanco, E.; González, P.; Santoro, A.; Alies, B.; Faller, P.; Hureau, C. *Coord. Chem. Rev.* **2018**, *371*, 38-55. DOI: <https://doi.org/10.1016/j.ccr.2018.04.007>
50. McGivern, T. J. P.; Afsharpour, S.; Marmion, C. J. *Inorg. Chim. Acta.* **2018**, *472*, 12-39. DOI: <https://doi.org/10.1016/j.ica.2017.08.043>
51. Ruiz-Azuara, L. 07/628,628 Re 35,458, Feb 18 (1997) U.S. Patent 1992, in 1992. Ruiz-Azuara, L. 07/628,628: 5,576,326 U.S. Patent 1996 in 1996.
52. Frisch, M. J.; Trucks, G. W.; Schlegel, H. B.; Scuseria, G. E.; Robb, M. A.; Cheeseman, J. R.; Scalmani, G.; Barone, V.; Mennucci, B.; Petersson, G. A.; Nakatsuji, H.; Caricato, M.; Li, X.; Hratchian, H. P.; Izmaylov, A. F.; Bloino, J.; Zheng, G.; Sonnenberg, J. L.; Hada, M.; Ehara, M.; Toyota, K.; Fukuda, R.; Hasegawa, J.; Ishida, M.; Nakajima, T.; Honda, Y.; Kitao, O.; Nakai, H.; Vreven, T.; Montgomery, J. A.; Peralta, J. E.; Ogliaro, F.; Bearpark, M. J.; Kudin, K. N.; Staroverov, V. N.; Kobayashi, R.; Normand, J.; Raghavachari, K.; Rendell, A. P.; Burant, J. C.; Iyengar, S. S.; Tomasi, J.; Cossi, M.; Rega, N.; Millam, N. J.; Klene, M.; Knox, J. E.; Cross, J. B.; Bakken, V.; Adamo, C.; Jaramillo, J.; Gomperts, R.; Stratmann, R. E.; Yazyev, O.; Austin, A. J.; Cammi, R.; Pomelli, C.; Ochterski, J. W.; Martin, R. L.; Morokuma, K.; Zakrzewski, V. G.; Voth, G. A.; Salvador, P.; Dannenberg, J. J.; Dapprich, S.; Daniels, A. D.; Farkas, O.; Foresman, J. B.; Ortiz, J. V.; Cioslowski, J.; Fox, D. J. Gaussian 09, Gaussian Inc, Wallingford, **2009**.
53. Zhao, Y.; Truhlar, D.G. *Theor. Chem. Acc.*, **2008**, *120*, 215-241. DOI: <https://doi.org/10.1007/s00214-007-0310-x>
54. Dolg, M.; Wedig, U.; Stoll, H. *J. Chem. Phys.*, **1989**, *90*, 1730-1734. DOI: <https://doi.org/10.1063/1.456066>
55. Marenich, A. V.; Cramer, C. J.; Truhlar, D. G. *J. Phys. Chem. B*, **2009**, *113*, 6378-6396. DOI: <https://doi.org/10.1021/jp810292n>
56. Morris, G.; Huey, R.; Lindstrom, W.; Sanner, M.; Belew, R.; Goodsell, D.; Olson, A. *J. Comput. Chem.*, **2009**, *30*, 2785-2791. DOI: <https://doi.org/10.1002/jcc.21256>
57. BIOVIA, Dassault Systèmes, Discovery Studio 2021, V.21 1.0, San Diego: Dassault Systèmes, 2020.
58. Título de Marca Reg. 407543 SECOFI (1992), (2002), (2012).
59. Sóvago, I.; Várnagy, K.; Lihi, N.; Gregnács, Á. *Coord. Chem. Rev.* **2016**, *327-328*, 43-54. DOI: <http://dx.doi.org/10.1016/j.ccr.2016.04.015>
60. Pretsch, E.; Bühlmann, P.; Badertscher, M. *Structure determination of organic compounds*. 4th Ed. Springer-Verlag, Berlin, **2009**.
61. Pethybridge, A. D.; Spiers, D. J. *J. Chem. Soc., Chem Commun.* **1974**, 423-424. DOI: <https://doi.org/10.1039/C39740000423>
62. Drago, R. S. *Physical methods for chemists*. 2nd Ed. W.B. Saunders Company, Philadelphia, **1977**.
63. Hagen, W. H. *Dalton Trans.* **2006**, 4415-4436. DOI: <https://doi.org/10.1039/B608163K>
64. Fielding, A. J.; Fox, S.; Millshauser, G. L.; Chattopadhyay, M.; Kroneck, P. M. H.; Fritz, G.; Eaton, G. R.; Eaton, S. S. *J. Magn. Reson.* **2006**, *179*, 92-104. DOI: <https://doi.org/10.1016/j.jmr.2005.11.011>
65. Garriba, E.; Micera, G. *J. Chem. Ed.* **2006**, *83*, 1229-1232. DOI: <https://doi.org/10.1021/ed083p1229>
66. Kivelson, D.; Neiman, R. *J. Chem. Phys.* **1961**, *35*, 149. DOI: <http://dx.doi.org/10.1063/1.1731880>
67. Sawada, T.; Fukumaru, K.; Sakurai, H. *Chem. Pharm. Bull.* **1996**, *44*, 1009-1016.
68. Kwik, W. L.; Ang, K. P. *J. Inorg. Nucl. Chem.* **1980**, *42*, 303-313.
69. Yokoi, H.; Addison, W. *Inorg. Chem.* **1977**, *16*, 1341-1349.
70. Peisach, J.; Blumberg, W. E. *Arch. Biochem. Biophys.* **1974**, *165*, 691-708. DOI: [https://doi.org/10.1016/0003-9861\(74\)90298-7](https://doi.org/10.1016/0003-9861(74)90298-7)
71. Gembus, A.; Corzilius, B.; Eichel, R. A.; Dinse, K. P.; Immel, S.; Stumm, D.; Flauaus, M. & Plenio, H. *J. Phys. Chem. B*. **2006**, *110*, 15012-15020. DOI: <https://doi.org/10.1021/jp062158x>

72. Bravo-Gómez, M. E.; Dávila-Manzanilla, S.; Flood-Garibay, J.; Muciño-Hernández, M. A.; Mendoza, A.; García-Ramos, J. C.; Moreno-Esparza, R.; Ruiz-Azuara, L. *J. Mex. Chem. Soc.*, **2012**, *56*, 85-92. DOI: <https://doi.org/10.29356/jmcs.v56i1.280>
73. Tovar-Tovar, A.; García-Ramos, J. C.; Flores-Álamo, M.; Ruiz-Azuara, L. *Acta Cryst.*, **2011**, *E67*, m1796–m1797. DOI: <https://doi.org/10.1107/S1600536811047398>
74. García-Ramos, J. C.; Tovar-Tovar, A.; Hernández-Lima, J.; Cortés-Guzman, F.; Moreno-Esparza, R.; Ruiz-Azuara, L. *Polyhedron*, **2011**, *30*, 2697-2703. DOI: <https://doi.org/10.1016/j.poly.2011.07.022>
75. Ugone, V.; Pisanu, F.; Sana, D.; Garriba, E. *J. Inorg. Biochem.*, **2021**, *224*, 111566. DOI: <https://doi.org/10.1016/j.jinorgbio.2021.111566>
76. Ma, C.; Sacco, M. D.; Hurst, B.; Townsend, J. A.; Hu, Y.; Szeto, T.; Zhang, X.; Tarbet, B.; Marty, M. T.; Chen, Y.; Wang, J. *Cell. Res.* **2020**, *30*, 678-692. DOI: <https://doi.org/10.1038/s41422-020-0356-z>
77. Zhang, L.; Lin, D.; Sun, X.; Curth, U.; Drosten, C.; Sauerhering, L.; Becker, S.; Rox, K.; Hilgenfeld, R. *Science*. **2020**, *368*, 409-412. DOI: <https://doi.org/10.1126/science.abb3405>
78. Buitrón-González, I.; Aguilera-Durán, G.; Romo-Mancillas, A. *Results. Chem.* **2021**, *3*, 100094. DOI: <https://doi.org/10.1016/j.rechem.2020.100094>
79. Yuan, S.; Wang, R.; Fuk-Woo Chan, J.; Zhang, A. J.; Cheng, T.; Ka-Heng Chik, K.; Ye, Z. W.; Wang, S.; Chak-Yiu Lee, A.; Jin, L.; Li, H.; Jin, D. Y.; Yuen, K. Y.; Sun, H. *Nat. Microbiol.* **2020**, *5*, 1439-1448. DOI: <https://doi.org/10.1038/s41564-020-00802-x>
80. Griffin, J. W. D. *J. Struct. Biol.* **2020**, *211*, 107575. DOI: <https://doi.org/10.1016/j.jsb.2020.07575>
81. Weglarz-Tomczak, E.; Tomczak, J. M.; Talma, M.; Burda-Grabowska, M.; Giurg, M.; Brul, S. *Sci. Rep.* **2021**, *11*, 3640. DOI: <https://doi.org/10.1038/s41598-021-83229-6>
82. Alkhatip, A. A. A. M. M.; Georgakis, M.; Montero Valenzuela, L. R.; Hamza, M.; Farag, E.; Hodgkinson, J.; Hosny, H.; Kamal, A. M.; Wagih, M.; Naguib, A.; Yassin, H.; Algameel, H.; Elayashy, M.; Abdelhaq, M.; Younis, M. I.; Mohamed, H.; Abdulshafi, M.; Elramely, M. A. *Int.J.Mol. Sci.* **2021**, *22*, 2977. DOI: <https://doi.org/10.3390/ijms22062977>
83. Gil-Moles, M.; Basu, U.; Büssing, R.; Hoffmeister, H.; Türck, S.; Varchmin, A.; Ott, I. *Chem. Eur. J.* **2020**, *26*, 15140-15144. DOI: <https://doi.org/10.1002/chem.202004112>

Microwave-Assisted Reactivity of a Fischer Alkynyl Carbene Complex with Benzyldene Anilines

Alberto Feliciano^{1,3}, Miguel A. Vázquez^{1*}, Iván Velazco-Cabral¹, Julio López³, Luis Javier Benítez-Puebla¹, Salvador Mastachi-Loza¹, Selene Lagunas-Rivera², Marco A. García-Revilla¹, Francisco Delgado^{3*}

¹Departamento de Química, DCNyE, Universidad de Guanajuato, Noria Alta S/N, 36050, Guanajuato, Gto., México.

²Cátedra-CONAHCYT, Departamento de Química, DCNyE, Universidad de Guanajuato, Noria Alta s/n, 36050, Guanajuato, Gto., México.

³Departamento de Química Orgánica, Escuela Nacional de Ciencias Biológicas, Instituto Politécnico Nacional, ProL. Carpio y Plan de Ayala S/N, 11340, Cd. de México, México.

*Corresponding author: Miguel A. Vázquez, email: mvazquez@ugto.mx; Francisco Delgado, email: jfdelgado@gmail.com

Received September 26th, 2022; Accepted April 25th, 2023.

DOI: <http://dx.doi.org/10.29356/jmcs.v68i1.1863>

This article is dedicated to Professor Joaquín Tamariz as a tribute for his 40 years as a Mexican researcher.

Abstract. The reaction between the Fischer carbene complex $(\text{CO})_5\text{Cr}=\text{C}(\text{OEt})\text{C}\equiv\text{CPh}$ and various benzyldene anilines $\text{RCH}=\text{NR}^1$ was promoted by microwave irradiation, generating stable cross-conjugated metallahexatrienes in 45-70 % yield. Compared to conventional heating, the present conditions provided shorter reaction times with moderate yields. The geometrical configuration and the most stable conformation for each of the Fischer carbene complexes and their oxidation products were established by NMR and DFT analysis. The reaction mechanism was explored by DFT calculations of the potential energy surface, suggesting a 1,4-addition/ring closure/electrocyclic opening cascade process.

Keywords: Fischer carbene complexes; benzyldene anilines; microwave irradiation; DFT analysis; electronic effect.

Resumen. Se reporta la reactividad entre el carbeno de Fischer $(\text{CO})_5\text{Cr}=\text{C}(\text{OEt})\text{C}\equiv\text{CPh}$ y las bencilidén anilinas, $\text{RCH}=\text{NR}^1$, empleando irradiación de microondas. Los resultados indican que el calentamiento por microondas generó metalohexatrienos cruzados estables en rendimientos de 45-70 %, mostrando además, que los nuevos complejos se obtienen en tiempos de reacción más cortos y rendimientos moderados en comparación con las condiciones de calentamiento convencional. La configuración geométrica y la conformación más estable para los complejos carbénicos de Fischer y de sus derivados oxidados fueron establecidos por medio de RMN y DFT. La exploración de la superficie de energía potencial por cálculos DFT mostró que el proceso consistió en una reacción en cascada incluyendo una secuencia de adición-1,4, cierre de anillo y apertura electrocíclica.

Palabras clave: Complejos carbénicos de Fischer; bencilidén anilinas; irradiación de microondas; análisis DFT; efecto electrónico.

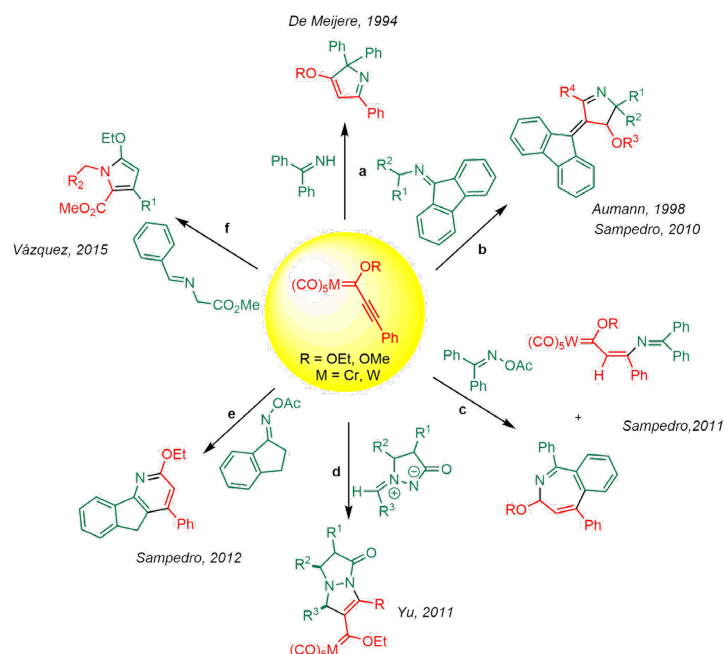
Introduction

Transition metal Fischer carbene complexes undergo cycloaddition reactions with a variety of substrates, and the growing body of research on their use is creating a broad new field in chemistry [1-8]. Even the simplest carbene complexes have exhibited great versatility[9]. The scope of the reaction increases in the event of the formation of an unsaturated system and is controlled by the type of substituents[10-14]. As a result, these organometallic complexes are capable of reacting with imines and many other molecules. Imines are important building blocks because they can contain not only nucleophilic or electrophilic sites but also a combination of the two, thus allowing for different reaction pathways in some cases[15-17]. Usually, this reactivity favours the synthesis of cyclic compounds in a few steps[15,16,18-23].

The reactivity of imines and carbene complexes has been reported by various authors. Imines were reacted with simple Fischer-type carbenes by Hegedus via thermal and photochemical routes, leading to new carbenic complexes and lactam nuclei, respectively [23]. On the other hand, de Meijere found that chromium alkynyl carbene complexes react with imines to produce the Michael adduct, which undergoes cyclization in thermal conditions to generate 2*H*-pyrroles (Scheme 1(a)) [24]. Meanwhile, Aumman [15] obtained Michael adducts and mesoionic pyrrolium carbonyl tungstates by the reaction of imines with alkynyl chromium(0) carbene complexes (Scheme 1(b)). Subsequently, Sampedro's group [16,25] conducted a complete computational mechanistic study of the same reaction to afford potential molecular switches and motors. In a later publication, this group documented the reaction of oxime derivatives and alkynyl Fischer carbene complexes to furnish four distinct types of nitrogenated heterocycles [26,27] (Scheme 1(c) and (e)). Yu achieved [28] the regioselective [3+2] annulation of azomethine imines with 1-alkynyl Fischer carbene complexes to synthesize versatile functionalized *N,N*-bicyclic pyrazolidin-3-ones (Scheme 1(d)). Along the same lines, our group has described the reaction of alkynyl Fischer carbene complexes with α -imino glycine methyl esters to provide 1,2,3,5-tetrasubstituted pyrroles (Scheme 1(f)) [11].

A search of the literature revealed few reports on energy sources other than conventional heating to test the reactivity of Fischer-type carbenes, except for the extensive investigation on the photochemistry of these complexes[29-33]. In 2002, Magennis *et al.* [34] established an advantage for a Dötz reaction when assisted by microwave energy versus the traditional thermal heating method. This reaction was also carried out by utilizing resin-bound Fischer carbenes subjected to microwave irradiation, followed by an oxidative reaction to generate 1,4-naphthoquinones [35]. Uracil-containing Fischer carbenes [36,37] and 1,3-dienol esters [38] have been prepared with microwave irradiation as well.

Therefore, investigating the behavior of Fischer carbenes in chemical reactions promoted by microwave energy is a relevant approach. In the methodologies developed by our group for the reaction of alkynyl and vinyl(alkoxy)carbene complexes under thermal conditions, substituents proved to play an important role in reactivity and selectivity during the synthesis of a variety of compounds, such as *ortho*- and *para*-quinones [39], phenols [12,40,41], furans, pyran-2-ones [42], 4-amino-1-azadienes [14], and pyrroles. The aim of the current contribution was to explore the reactivity of alkynyl(ethoxy)carbene complex **1** with benzylidene anilines **2a-p** under microwave irradiation.



Scheme 1. Synthesis of a variety of heterocyclic compounds with alkynyl(alkoxy)carbene complexes.

Experimental

Chemistry

All solvents and reagents were purchased from Sigma-Aldrich and used without further purification. The products were purified by column chromatography with silica gel (MN Kieselgel 60, 230-400 mesh), employing ethyl acetate and *n*-hexane as eluents in different proportions. To identify the compounds, the mixture was submitted to thin-layer chromatography (TLC, utilizing aluminum sheets and silica gel 60 F/UV₂₅₄) visualized with UV light. Melting points were measured on a digital Electrothermal 90100 melting point apparatus. ¹H and ¹³C nuclear magnetic resonance (NMR) spectra were recorded on a Bruker Ascend 500 MHz or a Bruker Ultrashield 600 MHz spectrometer with CDCl₃ or DMSO-*d*₆ as the solvent. Chemical shifts are expressed in ppm, relative to tetramethylsilane as the internal reference. Infrared (IR) spectra were captured on potassium bromide plates with a Perkin-Elmer Spectrum 100 FT-IR spectrophotometer. Spectra from high-resolution mass spectrometry (HRMS) were acquired by carrying out electrospray ionization on a Bruker micrOTOF-Q II device, electron nebulization ionization on a Bruker QTOF mass spectrometer, and electron ionization techniques (70 eV) on a Jeol JSM-GC Mate II. X-ray data were collected on an Oxford Diffraction Gemini 'A' diffractometer with a CCD area detector. Microwave irradiation was performed in a Discover SP CEM microwave apparatus. The alkynyl(ethoxy)carbene complex of chromium **1** and the benzylidene anilines **2a-p** were prepared by the reported methods [43].

General method

Alkynyl(ethoxy)carbene complex **1** and one of the benzylidene anilines **2a-p** (1.5:1 mol equiv) were added to a reaction vessel containing anhydrous tetrahydrofuran (THF) (5 mL) under nitrogen atmosphere. Subsequently, the mixture was heated at 66 °C with microwave irradiation (150 W) for 5 h. The reaction was monitored by TLC until completion. Purification of the crude mixtures by column chromatography over silica gel (*n*-hexane/EtOAc, 99:1) gave the corresponding products **3a-n**. Compounds **5** and **6** were identified by NMR, and the results were compared to information in the literature [14,44,45].

Pentacarbonyl-(Z)-2-phenyl-2-[(E)-(phenyl)(phenylimino)methyl] (ethoxy)carbene chromium(0) (3a).

According to the general method, the reaction between **1** (0.30 g, 0.85 mmol) and imine **2a** (0.10 g, 0.57 mmol) provided **3a** (0.18 g, 60 %) as a red oil. FT-IR (CH₂Cl₂) ν_{\max} 2061, 1988, 1936, 1712, 1593 cm⁻¹. ¹H NMR (CDCl₃, 600 MHz): δ 1.74 (t, *J* = 6.6 Hz, 3H, H-18), 4.68 (bs, 1H, H-17), 4.86 (bs, 1H, H-17), 6.28 (s, 1H, H-3), 6.62 (d, *J* = 7.8 Hz, 2H, H-6), 6.87-6.92 (m, 1H, H-8), 7.06-7.11 (m, 2H, H-7), 7.14-7.17 (m, 2H, H-14), 7.22-7.26 (m, 2H, H-10), 7.30-7.38 (m, 6H, H-11, H-12, H-15, H-16). ¹³C NMR (150 MHz, CDCl₃): δ 14.7 (C-18), 75.5 (C-17), 120.9 (C-6), 123.8 (C-8), 128.3 (C-11), 128.3 (C-7), 128.7 (C-15), 129.0 (C-9), 129.2 (C-10), 129.5 (C-16), 130.2 (C-12, C-14), 130.3 (C-3), 134.1 (C-13), 149.5 (C-2), 149.7 (C-5) 166.0 (C-4), 216.6 (CO_{cis}), 224.3 (CO_{trans}), 353.4 (Cr = Ccarb). HRMS (EI) calcd for C₂₉H₂₁NO₆Cr [M]⁺ 531.0774, found 531.0766.

Pentacarbonyl-(Z)-2-[(E)-(4-methoxyphenylimino)(phenyl)methyl]-3-phenyl(ethoxy)carbene chromium(0) (3b).

According to the general method, the reaction between **1** (0.30 g, 0.856 mmol) and imine **2b** (0.12 g, 0.571 mmol) delivered **3b** (0.20 g, 65 %) as a red solid (mp 92-94 °C). FT-IR (CH₂Cl₂) ν_{\max} 2061, 1988, 1932, 1605, 1566 cm⁻¹. ¹H NMR (CDCl₃, 600 MHz): δ 1.72 (t, *J* = 7.2 Hz, 3H, H-18), 3.70 (s, 3H, OMe) 4.65 (bs, 1H, H-17), 4.82 (bs, 1H, H-17), 6.22 (s, 1H, H-3), 6.60 (d, *J* = 9.0 Hz, 2H, H-7), 6.64 (d, *J* = 9.0 Hz, 2H, H-6), 7.15 (d, *J* = 6.6 Hz, 2H, H-14), 7.24-7.29 (m, 2H, H-10), 7.30-7.35 (m, 3H, H-15, H-16), 7.36-7.41 (m, 3H, H-11, H-12). ¹³C NMR (150 MHz, CDCl₃): δ 14.7 (C-18), 55.3 (OMe), 75.5 (C-17), 113.6 (C-6), 123.2 (C-7), 128.5 (C-11), 128.7 (C-12, C-15), 129.0 (C-16), 129.2 (C-3), 129.3 (C-10), 130.1 (C-14), 133.7 (C-13), 134.6 (C-9), 142.5 (C-5), 150.0 (C-2), 156.6 (C-8), 164.6 (C-4) 216.6 (CO_{cis}), 224.4 (CO_{trans}), 353.5 (Cr = Ccarb). HRMS (EI) calcd for C₃₀H₂₃CrNO₇ [M]⁺ 561.0880, found 561.0873.

Pentacarbonyl-(Z)-2-[(E)-(4-chlorophenylimino)(phenyl)methyl]-3-phenyl(ethoxy)carbene chromium(0) (3c).

According to the general method, the reaction between **1** (0.30 g, 0.856 mmol) and imine **2c** (0.12 g, 0.571 mmol) afforded **3c** (0.14 g, 45 %) as a red oil. FT-IR (CH₂Cl₂) ν_{\max} 2061, 1989, 1933, 1583, 1567 cm⁻¹. ¹H NMR (CDCl₃, 600 MHz): δ 1.73 (t, *J* = 7.2 Hz, 3H, H-18), 4.66 (bs, 1H, H-17), 4.81 (bs, 1H, H-17), 6.29 (s, 1H, H-3), 6.55 (d, *J* = 8.4 Hz, 2H, H-6), 7.05 (d, *J* = 8.4 Hz, 2H, H-7), 7.14-7.19 (m, 2H, H-14), 7.21-7.26 (m, 2H, H-10), 7.30-7.39 (m, 6H, H-11, H-12, H-15, H-16). ¹³C NMR (150 MHz, CDCl₃): δ 14.7 (C-18), 75.5 (C-17), 122.3 (C-6), 128.5 (C-11), 128.5 (C-7), 128.7 (C-15), 129.1 (C-10), 129.2 (C-12), 129.7 (C-16), 130.2 (C-14), 130.7 (C-3), 133.4 (C-13), 133.8 (C-9), 148.2 (C-5), 149.2 (C-2), 166.6 (C-8), 166.6 (C-4), 216.6 (CO_{cis}), 224.1 (CO_{trans}), 353.2 (Cr = Ccarb). HRMS (EI) calcd for C₂₉H₂₀ClCrNO₆ [M]⁺ 565.0384, found 565.0377.

Pentacarbonyl-(Z)-3-(fluorophenyl)-2-[(E)-(phenylimino)(phenyl)methyl] (ethoxy)carbene chromium(0) (3d).

According to the general method, the reaction between **1** (0.30 g, 0.856 mmol) and imine **2d** (0.113 g, 0.571 mmol) furnished **3d** (0.20 g, 66 %) as a red oil. FT-IR (CH₂Cl₂) ν_{\max} 2061, 1988, 1940, 1704, 1599 cm⁻¹. ¹H NMR (CDCl₃, 600 MHz): δ 1.73 (t, *J* = 7.0 Hz, 3H, H-18), 4.65 (bs, 1H, H-17), 4.86 (bs, 1H, H-17), 6.24 (s, 1H, H-3), 6.62 (d, *J* = 8.5 Hz, 2H, H-6), 6.87-6.92 (m, 1H, H-8), 7.00-7.05 (m, 2H, H-15), 7.06-7.11 (m, 2H, H-7), 7.12-7.16 (m, 2H, H-14) 7.21-7.25 (m, 2H, H-10), 7.30-7.35 (m, 3H, H-11, H-12). ¹³C NMR (150 MHz, CDCl₃): δ 14.7 (C-18), 75.6 (C-17), 115.9 (C-15, *J* = 25.8 Hz), 120.8 (C-6), 123.8 (C-8), 128.2 (C-7), 128.3 (C-11), 128.7 (C-13, *J* = 1.2 Hz) 128.8 (C-3), 129.0 (C-12), 129.1 (C-10), 132.0 (C-14, *J* = 10.0 Hz), 134.0 (C-9), 149.4 (C-2), 149.6 (C-5), 164.3 (C-16, *J* = 300.7 Hz), 165.9 (C-4), 216.5 (CO_{cis}), 224.0 (CO_{trans}), 353.3 (Cr = Ccarb). HRMS (EI) calcd for C₂₉H₂₀FNO₆Cr [M]⁺ 549.0680, found 549.0686.

Pentacarbonyl-(Z)-3-(4-chlorophenyl)-2-[(E)-(phenyl)-(phenylimino)methyl] (ethoxy)carbene chromium(0) (3e).

According to the general method, the reaction between **1** (0.30 g, 0.856 mmol) and imine **2e** (0.12g, 0.571 mmol) produced **3e** (0.17 g, 53 %) as a red solid (mp 101-103 °C). FT-IR (CH₂Cl₂) ν_{\max} 2061, 1989, 1940, 1716, 1582 cm⁻¹. ¹H NMR (CDCl₃, 600 MHz): δ 1.73 (t, *J* = 7.2 Hz, 3H, H-18), 4.64 (bs, 1H, H-17), 4.85 (bs, 1H, H-17), 6.21 (s, 1H, H-3), 6.61 (d, *J* = 7.8 Hz, 2H, H-6), 6.88-6.93 (m, 1H, H-8), 7.07-7.12 (m, 4H, H-7, H-14), 7.21-7.25 (m, 2H, H-10), 7.30-7.37 (m, 5H, H-11, H-12, H-15). ¹³C NMR (150 MHz, CDCl₃): δ 14.8 (C-18), 75.6 (C-17), 120.9 (C-6), 124.0 (C-8), 127.7 (C-12), 128.3 (C-7), 128.5 (C-3), 129.0 (C-11), 129.1 (C-10), 131.2 (C-15), 131.2 (C-15), 132.1 (C-13), 133.9 (C-9), 135.7 (C-16), 149.6 (C-5), 165.9 (C-

2), 167.4 (C-4), 216.4 (CO_{cis}), 224.0 (CO_{trans}), 352.9 (Cr = C_{carb}). HRMS (EI) calcd for C₂₉H₂₀CrNO₆Cr [M]⁺ 565.0384, found 565.0370.

Pentacarbonyl-(Z)-3-(4-methoxyphenyl)-2-[(E)-(phenyl)(phenylimino)methyl](ethoxy)carbene chromium(0) (3f).

According to the general method, the reaction between **1** (0.30 g, 0.856 mmol) and imine **2f** (0.12 g, 0.571 mmol) provided **3f** (0.20 g, 64 %) as a red oil. FT-IR (CH₂Cl₂) ν_{\max} 2060, 1938, 1601 cm⁻¹. ¹H NMR (CDCl₃, 600 MHz): δ 1.72 (t, *J* = 6.6 Hz, 3H, H-18), 3.81 (s, 3H, OMe), 4.64 (bs, 1H, H-17), 4.84 (bs, 1H, H-17), 6.22 (s, 1H, H-3), 6.61 (d, *J* = 7.2 Hz, 2H, H-6), 6.82-6.93 (m, 3H, H-8, H-14), 7.05-7.13 (m, 4H, H-7, H-15), 7.20-7.25 (m, 2H, H-10), 7.28-7.34 (m, 3H, H-11, H-12). ¹³C NMR (150 MHz, CDCl₃): δ 14.7 (C-18), 55.3 (OMe), 75.3 (C-17), 114.2 (C-14), 120.9 (C-6), 123.6 (C-8), 126.3 (C-13), 128.2 (C-11), 128.3 (C-7), 128.9 (C-12), 129.2 (C-10), 129.9 (C-3), 131.9 (C-15), 134.2 (C-9), 147.7 (C-2), 149.9 (C-5), 160.8 (C-16), 165.9 (C-4), 216 (CO_{cis}), 224.4 (CO_{trans}), 354.4 (Cr = C_{carb}). HRMS (EI) calcd for C₃₀H₂₃CrNO₇ [M]⁺ 561.0880, found 561.0883.

Pentacarbonyl-(Z)-3-(4-methylphenyl)-2-[(E)-(phenyl)(phenylimino)methyl](ethoxy)carbene chromium(0) (3g).

According to the general method, the reaction between **1** (0.30 g, 0.856 mmol) and imine **2g** (0.11 g, 0.571 mmol) generated **3g** (0.16 g, 52 %) as a red oil. FT-IR (CH₂Cl₂) ν_{\max} 2060, 1986, 1939, 1715, 1605 cm⁻¹. ¹H NMR (CDCl₃, 600 MHz): δ 1.72 (t, *J* = 7.2 Hz, 3H, H-18), 2.34 (s, 3H, Me), 4.65 (bs, 1H, H-17), 4.84 (bs, 1H, H-17), 6.24 (s, 1H, H-3), 6.61 (d, *J* = 7.8 Hz, 2H, H-6), 6.86-6.92 (m, 1H, H-8), 7.02-7.11 (m, 4H, H-7, H-14), 7.15 (d, *J* = 7.8 Hz, 2H, H-15), 7.22-7.26 (m, 2H, H-10), 7.29-7.35 (m, 3H, H-11, H-12), ¹³C NMR (150 MHz, CDCl₃): δ 14.7 (C-18), 21.3 (Me), 75.4 (C-17), 120.9 (C-6), 123.7 (C-8), 128.2 (C-11), 128.3 (C-7), 128.9 (C-12), 129.2 (C-10), 129.5 (C-15), 130.2 (C-3), 130.3 (C-14), 130.8 (C-13), 134.2 (C-9), 140.0 (C-16), 148.7 (C-2), 149.8 (C-5), 165.9 (C-4), 216.7 (CO_{cis}), 224.4 (CO_{trans}), 353.9 (Cr = C_{carb}). HRMS (EI) calcd for C₃₀H₂₃CrNO₆ [M]⁺ 545.0930, found 545.0925.

Pentacarbonyl-(Z)-3-(furan-2-yl)-2-[(E)-(phenyl)(phenylimino)methyl](ethoxy)carbene chromium(0) (3h).

According to the general method, the reaction between **1** (0.30 g, 0.856 mmol) and imine **2h** (0.09 g, 0.571 mmol) promoted the formation of **3h** (0.14 g, 49 %) as a red solid (mp 95-97 °C). FT-IR (CH₂Cl₂) ν_{\max} 2059, 1986, 1929, 1580 cm⁻¹. ¹H NMR (CDCl₃, 600 MHz): δ 1.66 (t, *J* = 6.0 Hz, 3H, H-18), 4.60 (bs, 1H, H-17), 4.71 (bs, 1H, H-17), 6.01 (s, 1H, H-3), 6.43 (s, 1H, H-16), 6.45 (s, 1H, H-15), 6.61 (d, *J* = 7.8 Hz, 2H, H-6), 6.87-6.92 (m, 1H, H-8), 7.04-7.11 (m, 2H, H-7), 7.20-7.26 (m, 2H, H-10), 7.28-7.35 (m, 3H, H-11, H-12), 7.53 (s, 1H, H-14). ¹³C NMR (150 MHz, CDCl₃): δ 14.7 (C-18), 75.1 (C-17), 112.8 (C-15), 115.0 (C-3), 115.3 (C-16), 121.0 (C-6), 123.8 (C-8), 128.3 (C-11), 128.3 (C-7), 129.0 (C-12), 129.2 (C-10), 133.8 (C-9), 146.1 (C-16), 146.2 (C-2), 149.7 (C-5), 149.8 (C-13), 165.0 (C-4), 216.8 (CO_{cis}), 224.6 (CO_{trans}), 350.0 (Cr = C_{carb}). HRMS (EI) calcd for C₂₇H₁₉CrNO₇ [M]⁺ 521.0567, found 521.0557.

Pentacarbonyl-(Z)-3-(furan-2-yl)-2-[(E)-(4-methoxyphenylimino)(phenyl)methyl](ethoxy)carbene chromium(0) (3i).

According to the general method, the reaction between **1** (0.30 g, 0.856 mmol) and imine **2i** (0.11 g, 0.571 mmol) led to **3i** (0.21 g, 69%) as a red oil. FT-IR (CH₂Cl₂) ν_{\max} 2059, 1986, 1931, 1603, 1578 cm⁻¹. ¹H NMR (CDCl₃, 600 MHz): δ 1.57 (t, *J* = 6.0 Hz, 3H, H-18), 3.61 (s, 3H, OMe), 4.50 (bs, 1H, H-17), 4.61 (bs, 1H, H-17), 5.88 (s, 1H, H-3), 6.32 (s, 1H, H-16), 6.37 (s, 1H, H-15), 6.51 (d, *J* = 9.0 Hz, 2H, H-7), 6.55 (d, *J* = 9.0 Hz, 2H, H-6), 7.14-7.22 (m, 2H, H-10), 7.25-7.33 (m, 3H, H-11, H-12), 7.43 (s, 1H, H-14). ¹³C NMR (150 MHz, CDCl₃): δ 14.6 (C-18), 55.2 (OMe), 75.0 (C-17), 112.7 (C-15), 113.6 (C-6), 114.2 (C-3), 114.9 (C-16), 123.3 (C-7), 128.5 (C-11), 128.9 (C-12), 129.1 (C-10), 134.3 (C-9), 142.5 (C-5), 145.8 (C-14), 146.6 (C-2), 149.9 (C-13), 156.6 (C-8), 163.6 (C-4), 216.9 (CO_{cis}), 224.7 (CO_{trans}), 350.0 (Cr = C_{carb}). HRMS (EI) calcd for C₂₈H₂₁CrNO₈ [M]⁺ 551.0672, found 551.0660.

Pentacarbonyl-(Z)-3-(4-bromophenyl)-2-[(E)-(4-methoxyphenylimino)(phenyl)methyl](ethoxy)carbene chromium(0) (3j).

According to the general method, the reaction between **1** (0.30 g, 0.856 mmol) and imine **2j** (0.16 g, 0.571 mmol) resulted in **3j** (0.19 g, 53 %) as a red oil. FT-IR (CH₂Cl₂) ν_{\max} 2061, 1989, 1934, 1605, 1584 cm⁻¹. ¹H NMR (CDCl₃, 600 MHz): δ 1.72 (t, *J* = 6.6 Hz, 3H, H-18), 3.70 (s, 3H, OMe), 4.60 (bs, 1H, H-17), 4.81 (bs, 1H, H-17), 6.13 (s, 1H, H-3), 6.58 (d, *J* = 7.0 Hz, 2H, H-7), 6.64 (d, *J* = 7.0 Hz, 2H, H-6), 7.02 (d, *J* = 6.5 Hz,

2H, H-14), 7.22- 7.28 (m, 2H, H-10), 7.36-7.42 (m, 3H, H-11, H-12), 7.46 (d, $J = 6.5$ Hz, 2H, H-15). ^{13}C NMR (150 MHz, CDCl_3): δ 14.7 (C-18), 55.2 (OMe), 75.6 (C-17), 113.6 (C-6), 123.3 (C-7), 123.9 (C-16), 127.6 (C-3), 128.6 (C-11), 129.1 (C-12), 129.1 (C-10), 131.3 (C-14), 131.9 (C-15), 132.6 (C-13), 134.5 (C-9), 142.3 (C-5), 150.4 (C-2), 156.7 (C-8) 164.5 (C-4), 216.6 (CO_{cis}), 224.2 (CO_{trans}), 353.0 (Cr = C_{carb}). HRMS (EI) calcd for $\text{C}_{30}\text{H}_{22}\text{BrNO}_7\text{Cr}$ $[\text{M}]^+$ 638.9985, found 638.9980.

Pentacarbonyl-(Z)-3-(4-chlorophenyl)-2-[(E)-(4-methoxyphenylimino)(phenyl)methyl](ethoxy)carbene chromium(0) (3k). According to the general method, the reaction between **1** (0.30 g, 0.856 mmol) and imine **2k** (0.139 g, 0.571 mmol) gave **3k** (0.17 g, 50 %) as a red oil. FT-IR (CH_2Cl_2) ν_{max} 2061, 1989, 1935, 1605 cm^{-1} . ^1H NMR (CDCl_3 , 600 MHz): δ 1.72 (t, $J = 6.6$ Hz, 3H, H-18), 3.70 (s, 3H, OMe) 4.61 (bs, 1H, H-17), 4.81 (bs, 1H, H-17), 6.15 (s, 1H, H-3), 6.58 (d, $J = 8.4$ Hz, 2H, H-7), 6.64 (d, $J = 9.0$ Hz, 2H, H-6), 7.08 (d, $J = 8.4$ Hz, 2H, H-14), 7.23-7.27 (m, 2H, H-10), 7.29-7.34 (m, 2H, H-15), 7.36-7.40 (m, 3H, H-11, H-12). ^{13}C NMR (150 MHz, CDCl_3): δ 14.7 (C-18), 55.3 (OMe), 75.6 (C-17), 113.6 (C-6), 123.3 (C-7), 127.6 (C-3), 128.6 (C-11), 128.9 (C-15), 129.0 (C-12), 129.1 (C-10), 131.1 (C-14), 132.2 (C-16), 134.5 (C-9), 135.5 (C-13), 142.3 (C-5), 150.3 (C-2), 156.7 (C-8), 164.4 (C-4) 216.6 (CO_{cis}), 224.2 (CO_{trans}), 353.1 (Cr = C_{carb}). HRMS (EI) calcd for $\text{C}_{30}\text{H}_{22}\text{ClCrNO}_7$ $[\text{M}]^+$ 595.0490, found 595.0489.

Pentacarbonyl-(Z)-3-(4-methoxyphenyl)-2-[(E)-(4-methoxyphenylimino)(phenyl)methyl](ethoxy)carbene chromium(0) (3l). According to the general method, the reaction between **1** (0.30 g, 0.856 mmol) and imine **2l** (0.13 g, 0.571 mmol) delivered **3l** (0.23 g, 70 %) as a red solid (mp 46-48 °C). FT-IR (CH_2Cl_2) ν_{max} 2060, 1932, 1604 cm^{-1} . ^1H NMR (CDCl_3 , 600 MHz): δ 1.70 (t, $J = 7.2$ Hz, 3H, H-18), 3.69 (s, 3H, OMe), 3.80 (s, 3H, OMe), 4.61 (bs, 1H, H-17), 4.81 (bs, 1H, H-17), 6.16 (s, 1H, H-3), 6.57 (d, $J = 9.0$ Hz, 2H, H-7), 6.63 (d, $J = 9.0$ Hz, 2H, H-6), 6.85 (d, $J = 8.4$ Hz, 2H, H-15), 7.09 (d, $J = 8.4$ Hz, 2H, H-14), 7.23-7.27 (m, 2H, H-10), 7.34-7.38 (m, 3H, H-11, H-12). ^{13}C NMR (150 MHz, CDCl_3): δ 14.8 (C-18), 55.3 (OMe, OMe), 75.3 (C-17), 113.6 (C-6), 114.2 (C-15), 123.1 (C-7), 126.5 (C-13), 128.4 (C-11), 128.8 (C-3), 129.0 (C-12), 129.2 (C-10), 131.8 (C-14), 134.7 (C-9), 142.7 (C-5), 148.2 (C-4), 156.4 (C-8), 160.7 (C-16), 164.6 (C-2), 216.8 (CO_{cis}), 224.4 (CO_{trans}), 354.4 (Cr = C_{carb}). HRMS (EI) calcd for $\text{C}_{31}\text{H}_{25}\text{NO}_8\text{Cr}$ $[\text{M}]^+$ 591.0985, found 591.0972.

Pentacarbonyl-(Z)-3-(4-methylphenyl)-2-[(E)-(4-methoxyphenylimino)(phenyl)methyl](ethoxy)carbene chromium(0) (3m). According to the general method, the reaction between **1** (0.30 g, 0.856 mmol) and imine **2m** (0.12 g, 0.571 mmol) afforded **3m** (0.20 g, 62 %) as a red oil. FT-IR (CH_2Cl_2) ν_{max} 2060, 1987, 1932, 1606 cm^{-1} . ^1H NMR (CDCl_3 , 500 MHz): δ 1.71 (t, $J = 7.0$ Hz, 3H, H-18), 2.34 (s, 3H, Me), 3.69 (s, 3H, OMe), 4.62 (bs, 1H, H-17), 4.80 (bs, 1H, H-17), 6.19 (s, 1H, H-3), 6.58 (d, $J = 8.5$ Hz, 2H, H-7), 6.63 (d, $J = 9.0$ Hz, 2H, H-6), 7.05 (d, $J = 8.0$ Hz, 2H, H-14), 7.14 (d, $J = 8.0$ Hz, 2H, H-15), 7.24-7.28 (m, 2H, H-10), 7.34-7.39 (m, 3H, H-11, H-12). ^{13}C NMR (125 MHz, CDCl_3): δ 14.7 (C-18), 21.3 (Me), 55.3 (OMe), 75.3 (C-17), 113.6 (C-6), 123.2 (C-7), 128.4 (C-11), 128.9 (C-12), 129.2 (C-10), 129.3 (C-3), 129.4 (C-15), 130.1 (C-14), 130.9 (C-13), 134.7 (C-9), 139.8 (C-16), 142.5 (C-5), 149.1 (C-2), 156.5 (C-8) 164.6 (C-4), 216.7 (CO_{cis}), 224.4 (CO_{trans}), 353.9 (Cr = C_{carb}). HRMS (EI) calcd for $\text{C}_{31}\text{H}_{25}\text{NO}_7\text{Cr}$ $[\text{M}]^+$ 575.1036, found 575.1045.

Pentacarbonyl-(Z)-2-[(E)-(4-chlorophenylimino)(phenyl)methyl]-3-(4-methoxyphenyl)(ethoxy)carbene chromium(0) (3n). According to the general method, the reaction between **1** (0.30 g, 0.856 mmol) and imine **2n** (0.13 g, 0.571 mmol) furnished **3n** (0.170 g, 50 %) as a red oil. FT-IR (CH_2Cl_2) ν_{max} 2060, 1931, 1604, 1580 cm^{-1} . ^1H NMR (CDCl_3 , 600 MHz): δ 1.71 (t, $J = 6.6$ Hz, 3H, H-18), 3.82 (s, 3H, OMe) 4.62 (bs, 1H, H-17), 4.80 (bs, 1H, H-17), 6.22 (s, 1H, H-3), 6.54 (d, $J = 8.4$ Hz, 2H, H-6), 6.86 (d, $J = 9$ Hz, 2H, H-15), 7.04 (d, $J = 8.4$ Hz, 2H, H-7), 7.10 (d, $J = 8.4$ Hz, 2H, H-14), 7.20-7.24 (m, 2H, H-10), 7.32-7.37 (m, 3H, H-11, H-12). ^{13}C NMR (150 MHz, CDCl_3): δ 14.7 (C-18), 55.4 (OMe), 75.3 (C-17), 114.3 (C-15), 122.4 (C-6), 128.4 (C-7), 128.4 (C-11), 129.0 (C-8), 129.1 (C-12), 129.2 (C-10), 130.4 (C-3), 132.0 (C-14), 133.9 (C-9), 144.9 (C-13), 147.4 (C-2), 148.3 (C-5), 160.9 (C-16), 166.6 (C-4), 216.7 (CO_{cis}), 224.1 (CO_{trans}), 354.1 (Cr = C_{carb}). HRMS (EI) calcd for $\text{C}_{30}\text{H}_{22}\text{ClCrNO}_7$ $[\text{M}]^+$ 595.0490, found 595.0490.

Ethyl (E)-3-(4-methoxyphenyl)-2-[(E)-(4-methoxyphenylimino)(phenyl)methyl]acrylate (10b). Compound **31** (0.25g, 0.422 mmol) in THF (5 mL) was irradiated with visible light (fluorescent lamp, 22 watts, Osram) at room temperature for 48 h. The solvent was then removed under vacuum and the residue was separated by flash column chromatography (*n*-hexane/EtOAc, 99:1), obtaining **10b** (0.1 g, 59 %) as a pale-yellow solid. FT-IR (CH₂Cl₂) ν_{max} 2934, 1731, 1689, 1238, 1168 cm⁻¹. ¹H NMR (500 MHz, CDCl₃) δ 1.06 (t, *J* = 7.1 Hz, 3H, H-18), 3.66 (s, 3H, OMe), 3.71 (s, 3H, OMe), 4.06 (m, *J* = 7.1 Hz, 2H, H-17), 6.75-6.56 (m, 6H, Ar), 7.45-7.26 (m, 5H, Ar), 7.69 (s, 1H, H-3), 7.92 (d, *J* = 7.5 Hz, 2H, Ar). ¹³C NMR (126 MHz, CDCl₃) δ 14.1 (C-18), 16.0 (C-17), 55.5 (OMe), 55.6 (OMe), 76.8, 77.0, 77.3, 114.3, 114.4, 114.8, 115.1, 125.5, 125.6, 128.5, 128.8, 129.7, 131.7, 132.0, 132.9, 133.7, 190.8 (C-1). HRMS (ESI) calcd for C₂₆H₂₆NO₄ [M+H]⁺ 416.1862 found 416.1865.

X-ray structure determination

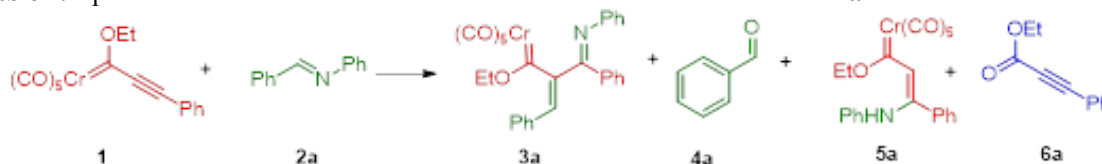
Crystal data and refinement details for **10b** are included in supplementary information. Single crystals were generated by the slow diffusion of *n*-hexane in a CHCl₃ solution with **10b** at 4 °C. The pale-yellow crystal of compound **10b** was mounted on glass fibers. Data was collected at 20 °C on an Agilent SuperNova (single source at offset, Eos) S2 diffractometer using Mo K α radiation (graphite crystal monochromator, λ 0.71073 Å). Hydrogen atoms were placed in idealized positions, and their atomic coordinates refined. An empirical absorption correction was applied based on spherical harmonics (implemented in SCALE3 ABSPACK scaling algorithm). The structure was solved with the SHELXT program package [46-48] running under the OLEX2 1.5 environment [49]. CCDC 2192850 contains the supplementary crystallographic data for this paper, which can be acquired free of charge from the Cambridge Crystallographic Data Centre via www.ccdc.cam.ac.uk/structures.

Computational details

All the stationary points along the reaction mechanisms were established by the density functional theory (DFT) at the M06-L level of theory [50] on the Gaussian 09 suite of programs [51], with the 6-311++G** basis set [52] for non-heavy atoms and the LANL2TZ effective core potential [53] for Cr atoms. The level of theory herein employed provides a good description of the thermochemistry, chemical kinetics (transition state energy), non-covalent interactions, and dissociation energy for organometallic compounds [51,54]. All the stationary points and transition state points were re-optimized with a non-explicit solvent model by means of the polarizable continuum model (PCM) [55,56]. The solvent considered for all the calculations was THF. The minima and transition states along the potential energy surface were optimized by performing a frequency calculation for each compound. The intrinsic reaction coordinate (IRC) was computed with Berny optimization to confirm the connection along a minimum energy path of reactants, intermediates, adducts, and products. Free energies at 363.15 K were calculated by including the corresponding thermal corrections to Gibbs free energies (TCGE).

Results and discussion

To initiate the reactivity study, benzylidene aniline **2a** [43] and Fischer carbene complex **1** were utilized as model reagents [57]. Four anhydrous solvents (toluene, benzene, methyl *t*-butyl ether (MTBE), and THF) were tested to avoid the hydrolysis of **2a** (Table 1, entries 1-4). Under thermal conditions, various products were detected by ¹H NMR. For example, ester **6a** resulted from the oxidation of **1** [44,45], benzaldehyde **4a** from the hydrolysis of **2a**, and enamine **5a** from the 1,4-addition of aniline to **1** [14].

Table 1. Optimization of the reaction conditions of Fischer carbene **1** and imine **2a**.^a

Entry	Solvent	t (h)	T (°C)	Source	3a(%)	4a(%)	5a(%)	6a(%)
1	toluene	24	111	thermal	traces	traces	40	20
2	benzene	2	80	thermal	18	traces	28	10
3	MTBE	17	55	thermal	17	traces	20	15
4	THF	1	66	thermal	20	traces	30	25
5 ^b	neat	1	111	thermal	22	traces	15	30
6 ^b	neat	1	80	IR/25 Volts	15	traces	10	10
7 ^b	neat	9	80	MW	trace	traces	30	50
8	THF	5	66	MW	60	traces	10	5
9	CH ₃ CN	5	82	MW	30	traces	10	15
10	toluene	5	111	MW	traces	traces	25	30

^aComplex **1** (1.5 equiv) and **2a** (1 equiv), N₂, 5 mL of solvent. ^bNo solvent.

The spectroscopy data (HPLC and NMR) of the isolated product **3a** were different than the expected result [15,25]. The ¹H NMR spectrum of **3a** showed signals for three aromatic rings located between 7.38 and 6.62 ppm, as well as a singlet at 6.28 ppm attributed to a vinyl proton. In the ¹³C NMR spectrum, a signal at 353.4 ppm indicated the existence of a carbene carbon (Cr = C_{carb}), and the signals in 216.6 and 224.3 ppm evidenced the presence of CO_{cis} and CO_{trans} groups. Hence, the structure of **3a** corresponds to a new vinyl chromium carbene complex α -substituted by an (*E*)-phenyl(phenylimino)methyl group (*i.e.*, a cross-conjugated metallatriene system, Table 1). Furthermore, the HRMS analysis is in agreement with the proposed structure of **3a**.

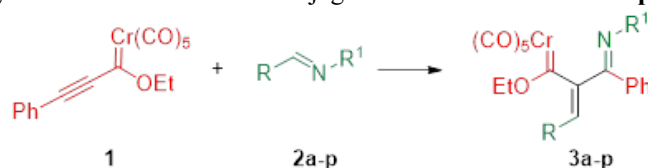
Other experiments were carried out to improve the yield of **3a**. With thermal heating and THF (entry 4), the low yield at 1 h did not improve when the reaction was monitored over the next few hours. Under neat conditions, infrared irradiation as the source of heat afforded a mixture of products comparable to those found with the thermal procedure, while microwave irradiation promoted the formation of only traces of the same (Table 1, entries 5-7). With microwave energy as the source of heat, the reactions performed in a sealed vessel furnished **3a** in yields of 60 % and 30 % when using polar solvents (THF and CH₃CN, respectively), and only a trace amount with toluene (Table 1, entries 8-10). This outcome may be due to the main properties of microwave energy, being dipolar polarization and ionic conduction [58]. Accordingly, the polar solvents probably provoke an efficient dipolar polarization effect over the generation and stabilization of polar species during the proposed reaction mechanism (Scheme 4).

Under the optimized conditions, the scope of the methodology was explored by modifying the aromatic substituents of the benzyldene aniline (**2a-p**) while keeping **1** as the phenyl alkyne carbene complex (Table 2). The new complexes **3a-n** were achieved in 45-70 % yields. Prolonging the irradiation time led to the decomposition of the carbene complex and only traces of the target compound.

The products were separated by column chromatography over silica gel, and their structures were established by ¹H, ¹³C, 2D, and nuclear Overhauser effect (NOE) NMR experiments as well as IR and HRMS.

In all cases, complexes **3a-n** were obtained as single *Z* (double bond)/*E* (imino group) isomers, along with the corresponding by-products indicated in Table 1.

Table 2. Scope of the synthesis of the new cross-conjugated metallahexatrienes **3a-p**^a



Entry	Benzylidene aniline	R	R ¹	Yield (%)
1	2a	C ₆ H ₅	C ₆ H ₅	3a (60)
2	2b	C ₆ H ₅	<i>p</i> -OMeC ₆ H ₄	3b (65)
3	2c	C ₆ H ₅	<i>p</i> -ClC ₆ H ₄	3c (45)
4	2d	<i>p</i> -FC ₆ H ₄	C ₆ H ₅	3d (66)
5	2e	<i>p</i> -ClC ₆ H ₄	C ₆ H ₅	3e (53)
6	2f	<i>p</i> -OMeC ₆ H ₄	C ₆ H ₅	3f (64)
7	2g	<i>p</i> -MeC ₆ H ₄	C ₆ H ₅	3g (52)
8	2h	C ₄ H ₃ O	C ₆ H ₅	3h (49)
9	2i	C ₄ H ₃ O	<i>p</i> -OMeC ₆ H ₄	3i (69)
10	2j	<i>p</i> -BrC ₆ H ₄	<i>p</i> -OMeC ₆ H ₄	3j (53)
11	2k	<i>p</i> -ClC ₆ H ₄	<i>p</i> -OMeC ₆ H ₄	3k (50)
12	2l	<i>p</i> -OMeC ₆ H ₄	<i>p</i> -OMeC ₆ H ₄	3l (70)
13	2m	<i>p</i> -MeC ₆ H ₄	<i>p</i> -OMeC ₆ H ₄	3m (62)
14	2n	<i>p</i> -OMeC ₆ H ₄	<i>p</i> -ClC ₆ H ₄	3n (50)
15	2o	C ₆ H ₅	<i>p</i> -NO ₂ C ₆ H ₄	3o (0)
16	2p	<i>p</i> -NO ₂ C ₆ H ₄	C ₆ H ₅	3p (0)

^aComplex **1** (1.5 equiv) and **2a-p** (1 equiv) in THF (5 mL) under N₂, MW (150 W), 66 °C, 5h.

The impact of the electronic effect of the different aromatic groups of the imines on the efficiency of the reaction is illustrated in Table 2, although a quantitative structure-reactivity relationship was not established. A relatively low yield of complex **3c** resulted from the presence of the chlorine atom (a weak electron donating group) in imine **2c** (Table 2, entry 3) compared to a greater yield of complex **3b** derived from the methoxy group (a stronger electron donating group) in the imine of **2b** (Table 2, entry 2). The yield of complexes **3a** and **3b** were 60 % and 65 %, respectively (Table 2, entries 1 and 2), despite the lack of substituents in the phenyl rings of **2a** (*vide infra*). On the other hand, electron donor groups in the imines **2l** and **2m** (R and R¹) increased the yield of complexes **3l** and **3m** (Table 2, entries 12 and 13). The combination of electron donating and electron withdrawing groups in the imines **2j**, **2k**, and **2n** afforded slightly lower yields of **3j**, **3k**, and **3n** (53, 50, and 50%, respectively) compared to **3a** (60 %), the latter furnished by the reaction with the unsubstituted imine **2a**. In contrast, when the imine bore a strong electron withdrawing group, such as **2o** and **2p** (R = *p*-

$\text{NO}_2\text{C}_6\text{H}_4$, $\text{R}^1 = p\text{-NO}_2\text{C}_6\text{H}_4$), the reaction did not occur. Due to these differences in reactivity, the electronic effects of the substituents in imines **2** were analyzed by theoretical studies (*vide infra*).

Even though it was not possible to obtain the crystalline structures of **3a-n** by single crystal X-ray diffraction, NOE spectroscopy (NOESY and ROESY) experiments provided sufficient evidence to determine the conformation. Accordingly, complex **3j** exhibited a NOE effect of the vinyl proton H-3 and the $\text{CH}_3\text{CH}_2\text{O}$ group (protons H-17 and H-18) by irradiating the aromatic proton H-14 (7.02 ppm) (Fig. 1), indicating a Z configuration of the double bond C-C. Neither proton H-17 nor H-18 showed a NOE effect with H-6 or H-7, which suggests that the *N*-anisyl ring of the imine moiety remains distant from the metal center.

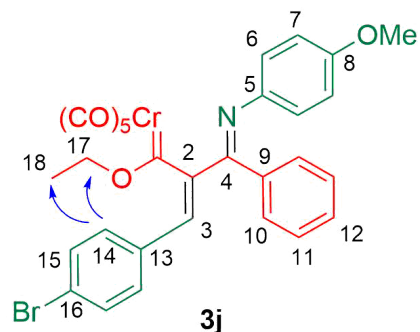
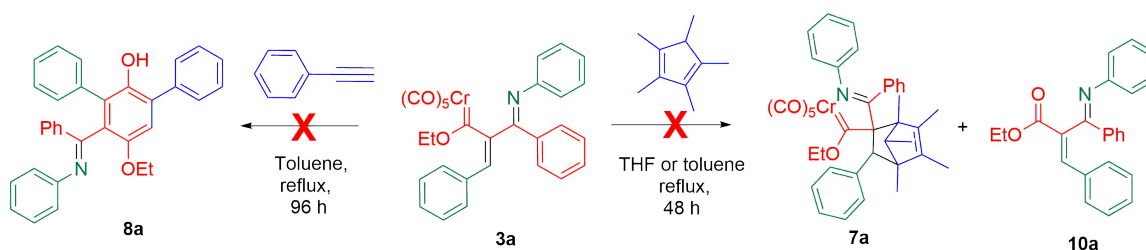


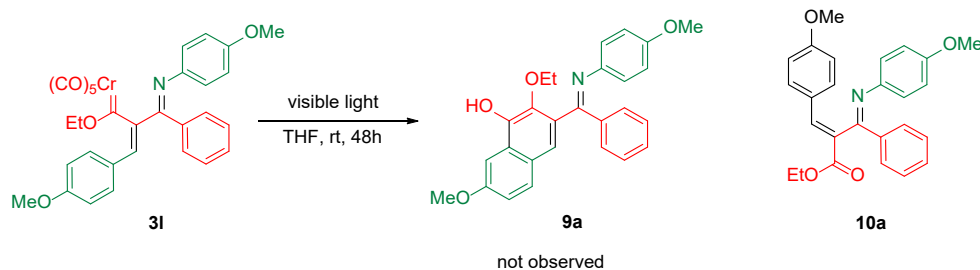
Fig. 1. NOESY for complex **3j**.

It is reported that metallatrienes are precursors of cyclopentadienes [58], indenenes [59], naphthalenes [60], homopyrroles [61], and other carbo- and heterocycles [22]. Hence, some experiments were conducted to evaluate the reactivity of the new metallatrienes **3a-n**. The reaction of **3a** and pentamethylcyclopentadiene was attempted under the [4+2] cycloaddition conditions previously described. The reaction did not proceed in THF or toluene at reflux for 48 h, and a consequence, the starting materials were recovered. The results of the Dötz reaction of phenylacetylene with **3a** in toluene was also examined after refluxing for 96 h. The ^1H NMR analysis of the crude reaction mixture did not show the expected transformation, but the oxidation product **10a** was detected (Scheme 2).



Scheme 2. Exploration of the reactivity of complex **3a**.

With the objective of forming a six-membered cycle in complex **3l**, further experiments were performed with UV and visible light irradiation to attain the insertion of CO and the subsequent cyclization to phenol **9a**. Nevertheless, the desired product was not found and only the oxidized compound **10b** was isolated, afforded in a moderate yield of 59 % (Scheme 3). Despite there being an α,β -unsaturated system in complexes **3a-n**, indicating susceptibility to Dötz benzannulation, such a reaction did not take place for **3l**, probably because of the steric effect of the bulky substituents.



Scheme 3. Conversion of **31** into ethyl acrylate **10b**.

A crystal sample was obtained by the slow diffusion of *n*-hexane in a CHCl_3 solution with **10b** at 4 °C. The crystallized compound fits in the monocyclic crystal system. The space group P21/c and unit cell parameters are $a = 17.0269(12)$ Å, $b = 9.6109(5)$ Å, and $c = 14.1952(8)$ Å, as well as $\alpha = 90^\circ$, $\beta = 104.895(7)^\circ$, $\gamma = 90^\circ$, and a volume of $2244.9(2)$ Å³. According to the crystalline structure of **10b**, oxidation of **31** and removal of the steric hindrance of the bulky $\text{Cr}(\text{CO})_5$ group leads to isomerization of the double bond of this compound to the *E* configuration [torsion angle: C1-C2-C6-C21 = 72.78°]. Moreover, the ester group adopts the *s-cis* conformation and the imino moiety is orthogonal to the double bond (Fig. 2).

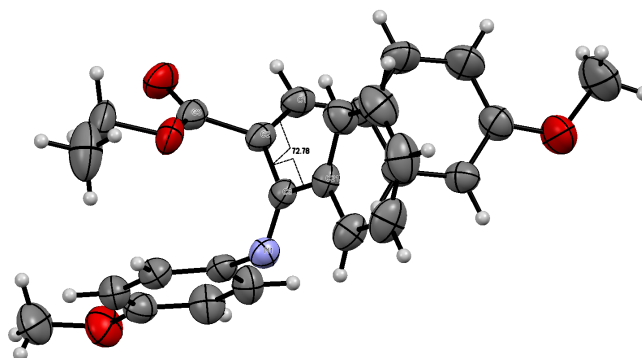


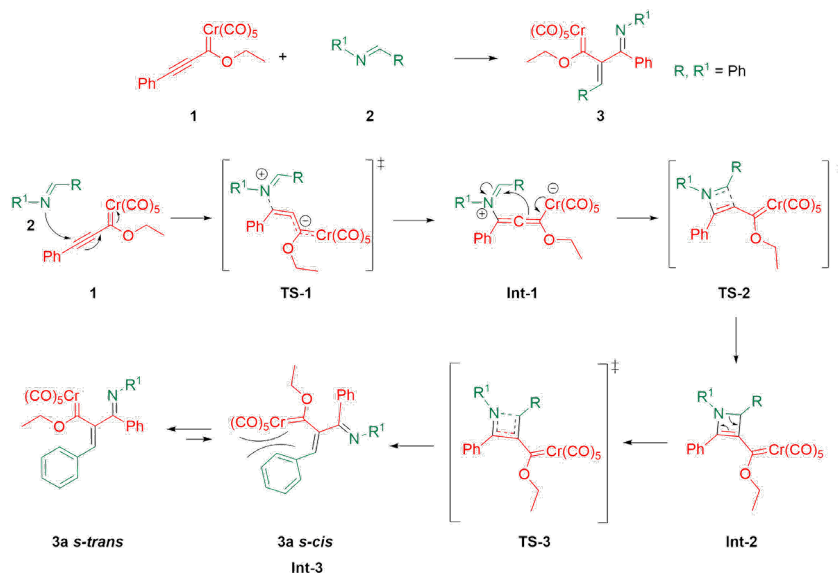
Fig. 2. Molecular structure of **10b** with 50 % probability ellipsoids.

Computational analysis

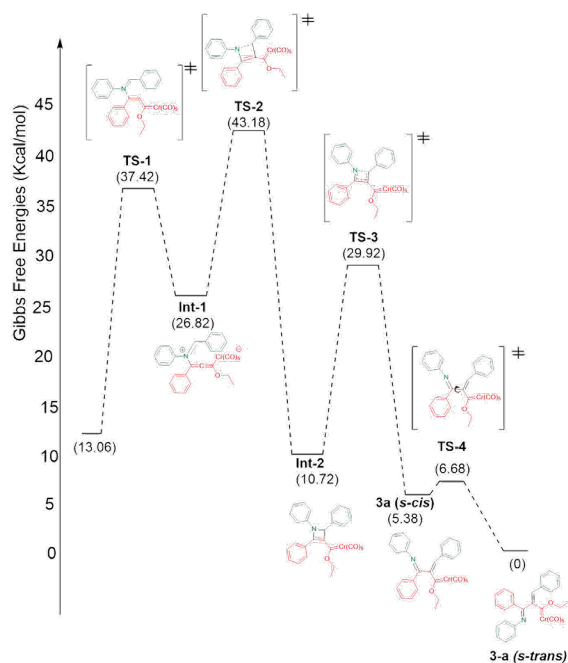
Reaction between the Fischer alkynyl carbene complex and benzylidene anilines

Considering the experimental findings, a computational study was performed to account for the mechanism of formation of the new compounds **3a-n**. The potential energy surface was calculated for the proposed four-step mechanism (Scheme 4), involving three intermediates and three transition states (Scheme 5). The first step consists of the 1,4-addition of the nitrogen atom of the imine to the alkynyl Fischer carbene, leading to transition state **TS-1** with an N-C_β bond distance of 1.95 Å and an activation energy (ΔG^\ddagger) of 37.42 kcal/mol. Afterwards, intermediate 1 (**Int-1**) is generated, with a reactant energy (ΔG°) of 13.76 kcal/mol. **Int-1** undergoes an intramolecular attack by the carbenic anion and is converted into the iminium moiety by passing through the cyclic **TS-2**, which is the rate-determining step ($\Delta G^\ddagger = 43.18$ kcal/mol). The distance of the C-C_β bond formed is 2.24 Å for **Int-1** but only 1.40 Å for intermediate 2 (**Int-2**). The latter exhibits much greater stability than **Int-1** ($\Delta G^\circ = 16.10$ kcal/mol). Subsequently, the thermally allowed electrocyclic opening of the aza-cyclobutene of **Int-2** brings about transition state 3 (**TS-3**) with an activation barrier (ΔG^\ddagger) of 29.92 kcal/mol, which in turn evolves into **3a** (*s-cis*) with a dihedral angle of 68.83° (Figures 3 and 4). Interestingly, greater stability (-5.38 kcal/mol) was found for the *s-trans* than the *s-cis* conformation of **3a**. To find the

transition state barrier associated with the rotation, a SCAN of the dihedral rotation was performed (Scheme 6), using 18 steps spanning an interval of 0-180 degrees (consisting of 10 degrees for each step), starting from the *s-cis* and arriving to the *s-trans* conformation. The energetic profile shows two minima: the **3a** *s-cis* structure at 68.83° and the more stable **3a** *s-trans* conformer with an activation energy (ΔG^\ddagger) of 1.30 kcal/mol between both rotamers. The stability of the *s-trans* conformer is in agreement with the experimental results for compound **3a**.



Scheme 4. Proposed reaction mechanism for the generation of **3a**.



Scheme 5. Energetic profile of the Gibbs free energies (kcal/mol) relative to the energy of product at the M06L/6311++G**/Cr=LANL2TZ/SCRF=THF level of theory.

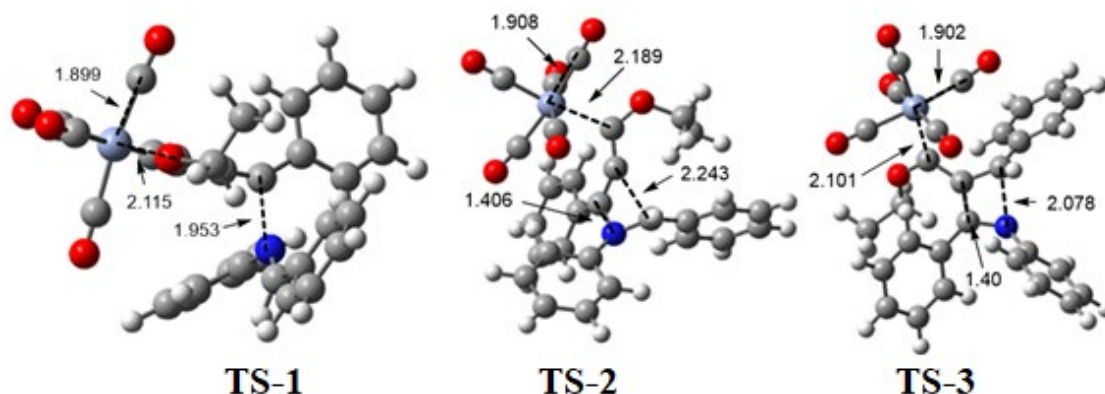


Fig. 3. Structures corresponding to the transition states **TS-1**, **TS-2**, and **TS-3** at the M06-L/6-311++G**/Cr=LANL2TZ/SCRF=THF level of theory. Bond distances are given in Å. Color code of the spheres pictured: hydrogen atoms in white, carbon atoms in grey, nitrogen atoms in blue, oxygen atoms in red, and chromium atoms in light blue.

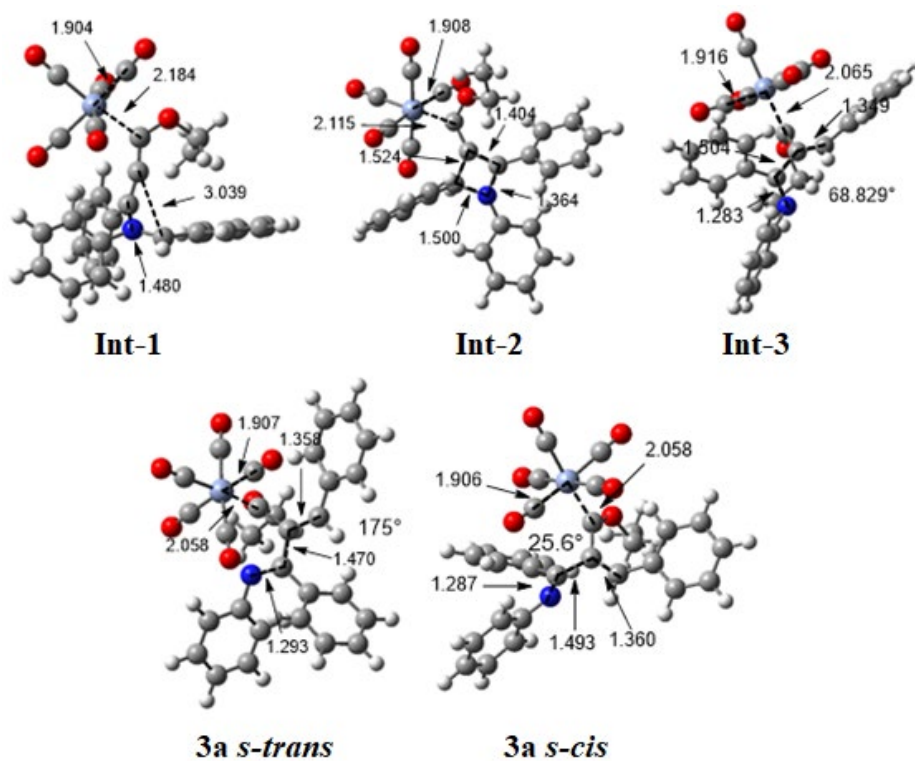
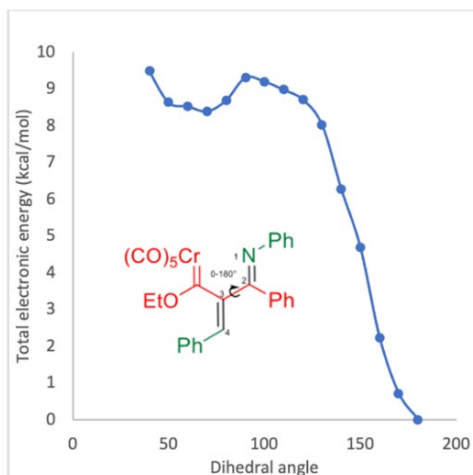


Fig. 4. Optimized structures of intermediates **Int-1**, **Int-2**, and **Int-3**, as well as products **3a** (*s-cis*) and **3a** (*s-trans*) at the M06-L/6-311++G**/Cr=LANL2TZ/SCRF=THF level of theory. Bond distances are given in Å. Color code of the spheres depicted: hydrogen atoms in white, carbon atoms in grey, nitrogen atoms in blue, oxygen atoms in red, and chromium atoms in light blue.



Scheme 6. Energetic profile of the scan of dihedral rotation for the *cis-trans* transformation.

A comparative study was carried out to explore the impact of the R and R¹ substituents on the aromatic system of benzylidene anilines **2a-p**. Apparently, the R¹ substituent did not have any relevant effect on the 1,4-addition, and the electronic effect of the R substituent was not relevant in the reactivity of the entire process (see supplementary data).

Conclusions

Microwave irradiation promoted the reaction between the Fischer carbene complex of Cr(0) (**1**) and benzylidene anilines **2a-n**, obtaining moderate yields of new, stable, and polysubstituted Fischer carbenes with a cross-conjugated system. In all cases, complexes **3a-n** were afforded as single *Z* (double bond)/*E* (imino group) isomers, while the oxidation product **10a** changed to the *E* (double bond)/*E* (imino group) configuration. The computational study of the reaction mechanism revealed that the formation of the dihydroazete intermediate (**Int-2**) is the rate-determining step of the reaction. The proposed mechanism involves a 1,4-addition/ring closure/electrocyclic opening cascade reaction. The reaction did not proceed in any of the compounds **2** that had an electron withdrawing group in the aromatic ring of the imine moiety. Even though complexes **3a-n** did not evolve into the Diels-Alder or the Dötz products (probably because of the great steric effects exhibited by the organometallic compounds), these kinds of structures are interesting from a synthetic and theoretical point of view. Further research on Fischer carbene complexes of W(0) and Mo(0) with different substituents is currently under way, and the results will be reported in due course.

Acknowledgements

This research was funded by the Consejo Nacional de Humanidades Ciencias y Tecnologías (CONAHCYT) (grant A1-S-27694) and DAIP-UG (grant 058/2023). A.F. thanks CONAHCYT for a postdoctoral grant (472610). E.I.V. appreciates CONAHCYT for graduate scholarships (926323). J.L. is grateful to CONAHCYT for postdoctoral grant (329994). S.M. is beholden to PRODEP: DAIP-0132-2020 for postdoctoral support. F.D. gratefully acknowledges CONAHCYT (grant 282033) and SIP-IPN (grants 20210851 and 20221003) for financial support. The authors are indebted to the Guanajuato National Laboratory

(UG-UAA- CONAHCYT 316011) for their generous allocation of analytical and computing resources. We are also thankful to the Unit for Industry and Research Support (USAI) at the School of Chemistry of the UNAM and to Dr. Marcos Flores-Álamo and Dr. Gerardo González for the X-ray analysis, as well as to Adán Bazán-Jiménez for the supercomputing technical support.

References

1. de Meijere, A. *Pure Appl. Chem.* **1996**, 68, 61–72. DOI: <https://doi.org/10.1351/pac199668010061>.
2. de Meijere, A.; Schirmer, H.; Duetsch, M. *Angew. Chem.* **2000**, 39, 3965–4002. DOI: [https://doi.org/10.1002/1521-3773\(20001117\)39:22<3964::aid-anie3964>3.0.co;2-c](https://doi.org/10.1002/1521-3773(20001117)39:22<3964::aid-anie3964>3.0.co;2-c).
3. Wu, Y.-T.; de Meijere, A. *Top. Organomet. Chem.* **2004**, 13, 21–57. DOI: <https://doi.org/10.1007/b98762>.
4. Barluenga, J.; Santamaría, J.; Tomás, M. *Chem. Rev.* **2004**, 104, 2259–2283. DOI: <https://doi.org/10.1021/cr0306079>.
5. Dötz, K. H.; Stendel, J. *J. Chem. Rev.* **2009**, 109, 3227–3274.
6. Santamaría, J.; Aguilar, E. *Org. Chem. Front.* **2016**, 3, 1561–1588. DOI: <https://doi.org/10.1039/c6qo00206d>.
7. Fernández-Rodríguez, M. Á.; García-García, P.; Aguilar, E. *Chem. Commun.* **2010**, 46, 7670–7687. DOI: <https://doi.org/10.1039/c0cc02337j>.
8. Feliciano, A.; Vázquez, J. L.; Benítez - Puebla, L. J.; Velazco - Cabral, I.; Cruz Cruz, D.; Delgado, F.; Vázquez, M. A. *Chem. - A Eur. J.* **2021**, 27, 8233–8251. DOI: <https://doi.org/10.1002/chem.202005434>.
9. Dötz, K. H. in: *Verlag chemie; Fischer*, E. O., Ed.; Weinheim, **1983**.
10. Chan, K. S.; Wulff, W. D. *J. Am. Chem. Soc.* **1986**, 108, 5229–5236.
11. de La Cruz, F. N.; López, J.; Jiménez-Halla, J. Ó. C.; Flores-Álamo, M.; Tamariz, J.; Delgado, F.; Vázquez, M. A. *Org. Biomol. Chem.* **2015**, 13, 11753–11760. DOI: <https://doi.org/10.1039/c5ob01655j>.
12. López, J.; de la Cruz, F. N.; Flores-Conde, M. I.; Flores-Álamo, M.; Delgado, F.; Tamariz, J.; Vázquez, M. A. *Eur. J. Org. Chem.* **2016**, 2016, 1314–1323. DOI: <https://doi.org/10.1002/ejoc.201501211>.
13. Reyes, L.; Mendoza, H.; Vázquez, M. A.; Ortega-Jiménez, F.; Fuentes-Benites, A.; Flores-Conde, M. I.; Jiménez-Vázquez, H.; Miranda, R.; Tamariz, J.; Delgado, F. *Organometallics*. **2008**, 27, 4334–4345. DOI: <https://doi.org/10.1021/om8002416>.
14. Benítez-Puebla, L. J.; López, J.; Flores-Álamo, M.; Cruz, D. C.; Peña-Cabrera, E.; Delgado, F.; Tamariz, J.; Vázquez, M. A. *Eur. J. Org. Chem.* **2019**, 2019, 6571–6578. DOI: <https://doi.org/10.1002/ejoc.201901047>.
15. Aumann, R.; Yu, Z.; Fröhlich, R.; Zippel, F. *Eur. J. Inorg. Chem.* **1998**, 1998, 1623–1629. DOI: [https://doi.org/10.1002/\(SICI\)1099-0682\(199811\)1998:11<1623::AID-EJIC1623>3.0.CO;2-P](https://doi.org/10.1002/(SICI)1099-0682(199811)1998:11<1623::AID-EJIC1623>3.0.CO;2-P).
16. Rivado-Casas, L.; Campos, P. J.; Sampedro, D. *Organometallics*. **2010**, 29, 3117–3124. DOI: <https://doi.org/10.1021/om100219h>.
17. Aumann, R.; Yu, Z.; Fröhlich, R. *J. Organometallic Chem.* **1997**, 549, 311–318. DOI: [https://doi.org/10.1016/S0022-328X\(97\)00526-3](https://doi.org/10.1016/S0022-328X(97)00526-3).
18. Herndon, J. W. *Coord. Chem. Rev.* **2018**, 356, 1–114. DOI: <https://doi.org/10.1016/j.ccr.2017.09.003>.
19. Barluenga, J.; Aguilar, E. in: *Advances in Organometallic Chemistry*; Elsevier Inc., **2017**; 67, 1–150. DOI: <https://doi.org/10.1016/bs.adomc.2017.04.001>.

20. Barluenga, J.; Tomás, M.; López-Pelegrín, J. A.; Rubio, E. *Tetrahedron Lett.* **1997**, 38, 3981–3984. DOI: [https://doi.org/10.1016/S0040-4039\(97\)00737-5](https://doi.org/10.1016/S0040-4039(97)00737-5).
21. Aumann, R.; Yu, Z.; Fröhlich, R. *Organometallics*. **1998**, 17, 2897–2905. DOI: <https://doi.org/10.1021/om980068b>.
22. Aumann, R. *Eur. J. Org. Chem.* **2000**, 17–31. DOI: [https://doi.org/10.1002/\(SICI\)1099-0690\(200001\)2000:1<17::AID-EJOC17>3.0.CO;2-T](https://doi.org/10.1002/(SICI)1099-0690(200001)2000:1<17::AID-EJOC17>3.0.CO;2-T).
23. Hegedus, L. S.; McGuire, M. A.; Schultze, L. M.; Yijun, C.; Anderson, O. P. *J. Am. Chem. Soc.* **1984**, 106, 2680–2687. DOI: <https://doi.org/10.1021/ja00321a032>.
24. Funke, F.; Duetsch, M.; Stein, F.; Noltemeyerl, M.; De Meijere, A. *Chem. Ber.* **1994**, 127, 911–920.
25. Rivado-casas, L.; Sampedro, D.; Campos, P. J.; Fusi, S.; Zanirato, V.; Olivucci, M. *J. Org. Chem.* **2009**, 74, 4666–4674. DOI: <https://doi.org/10.1021/jo802792j>
26. Blanco-Lomas, M.; Caballero, A.; Campos, P. J.; González, H. F.; López-Sola, S.; Rivado-Casas, L.; Rodríguez, M. A.; Sampedro, D. *Organometallics*. **2011**, 30, 3677–3682. DOI: <https://doi.org/https://doi.org/10.1021/om200438y>.
27. González, H. F.; Blanco-Lomas, M.; Rivado-Casas, L.; Rodríguez, M. A.; Campos, P. J.; Sampedro, D. *Organometallics*. **2012**, 31, 6572–6581. DOI: <https://doi.org/https://doi.org/10.1021/om300570q>.
28. Luo, N.; Zheng, Z.; Yu, Z. *Org. Lett.* **2011**, 13, 3384–3387. DOI: <https://doi.org/10.1021/ol201139w>.
29. Fernandez, I.; Cossío, F. P.; Sierra, M. A. *Acc. Chem. Res.* **2011**, 44, 479–490.
30. Rivero, A. R.; Fernández, I.; Sierra, M. A. *Chem. Eur. J.* **2014**, 20, 1359–1366. DOI: <https://doi.org/10.1002/chem.201302029>.
31. Hegedus, L. S.; Weck, G. De; D'Andrea, S. *J. Am. Chem. Soc.* **1988**, 110, 2122–2126. DOI: <https://doi.org/10.1021/ja00215a019>.
32. Su, M. *Der. ACS Omega*. **2017**, 2, 5395–5406. DOI: <https://doi.org/10.1021/acsomega.7b00766>.
33. Arrieta, A.; Cossio, F. P.; Fernandez, I.; Gomez-Gallego, M.; Lecea, B.; Mancheño, M. J.; Sierra, M. A. *J. Am. Chem. Soc.* **2000**, 122, 11509–11510. DOI: <https://doi.org/10.1021/ja000706t>.
34. Hutchinson, E. J.; Kerr, J.; Magennis, E. *J. Chem. Commun.* **2002**, 2262–2263. DOI: <https://doi.org/10.1039/B206981B>
35. Shanmugasundaram, M.; Garcia-Martinez, I.; Li, Q.; Estrada, A.; Martinez, N. E.; Martinez, L. E. *Tetrahedron Lett.* **2005**, 46, 7545–7548. DOI: <https://doi.org/10.1016/j.tetlet.2005.08.158>.
36. Artillo, A.; Sala, G. Della; De Santis, M.; Llordes, A.; Ricart, S.; Spinella, A. *J. Organomet. Chem.* **2007**, 692, 1277–1284. DOI: <https://doi.org/10.1016/j.jorganchem.2006.08.097>.
37. Spinella, A.; Caruso, T.; Pastore, U.; Ricart, S. *J. Organomet. Chem.* **2003**, 684, 266–268. DOI: [https://doi.org/10.1016/S0022-328X\(03\)00756-3](https://doi.org/10.1016/S0022-328X(03)00756-3).
38. Kashinath, D.; Mioskowski, C.; Falck, J. R.; Goli, M.; Meunier, S.; Baati, R.; Wagner, A. *Org. Biomol. Chem.* **2009**, 7, 1771–1774. DOI: <https://doi.org/10.1039/b903244b>.
39. Vázquez, M. A.; Reyes, L.; Miranda, R.; García, J. J.; Jiménez-Vázquez, H. A.; Tamariz, J.; Delgado, F. *Organometallics*. **2005**, 24, 3413–3421. DOI: <https://doi.org/10.1021/om050159q>.
40. Montenegro, M. M.; Vega-Báez, J. L.; Vázquez, M. A.; Flores-Conde, M. I.; Sánchez, A.; González-Tototzin, M. A.; Gutiérrez, R. U.; Lazcano-Seres, J. M.; Ayala, F.; Zepeda, L. G.; Tamariz, J.; Delgado, F. *J. Organomet. Chem.* **2016**, 825–826, 41–54. DOI: <https://doi.org/10.1016/j.jorganchem.2016.10.017>.
41. Feliciano, A.; Padilla, R.; Escalante, C. H.; Herbert-Pucheta, E.; Vázquez, M. A.; Tamariz, J.; Delgado, F. *J. Organometallic Chem.* **2020**, 923, 121360. DOI: <https://doi.org/10.1016/j.jorganchem.2020.121360>

42. Flores-Conde, M. I.; de la Cruz, F. N.; Lopez, J.; Jiménez-Halla, J. Ó. C.; Peña-Cabrera, E.; Flores-Álamo, M.; Delgado, F.; Vázquez, M. Á. *Appl. Organomet. Chem.* **2017**, *e4202*, 1–12. DOI: <https://doi.org/https://doi.org/10.1002/aoc.4202>.
43. Vázquez, M. Á.; Landa, M.; Reyes, L.; Miranda, R.; Tamariz, J.; Delgado, F. *Synth. Commun.* **2004**, *34*, 2705–2718. DOI: <https://doi.org/10.1081/SCC-200026190>.
44. Lee, S. Y. A.; Yang, H. C.; Su, F. Y. *Tetrahedron Lett.* **2001**, *42*, 301–303. DOI: [https://doi.org/10.1016/S0040-4039\(00\)01954-7](https://doi.org/10.1016/S0040-4039(00)01954-7).
45. Wang, X.; Yang, Y.; Zhao, Y.; Wang, S.; Hu, W.; Li, J.; Wang, Z.; Yang, F.; Zhao, J. *J. Org. Chem.* **2020**, *85*, 6188–6194. DOI: <https://doi.org/10.1021/acs.joc.0c00485>.
46. Sheldrick, G. M. *Acta Crystallogr. Sect. A Found. Crystallogr.* **2008**, *64*, 112–122. DOI: <https://doi.org/10.1107/S0108767307043930>.
47. Sheldrick, G. M. *Acta Crystallogr. Sect. C Struct. Chem.* **2015**, *71*, 3–8. DOI: <https://doi.org/10.1107/S2053229614024218>.
48. Sheldrick, G. M. *Acta Crystallogr. Sect. A Found. Crystallogr.* **2015**, *71*, 3–8. DOI: <https://doi.org/10.1107/S2053273314026370>.
49. Dolomanov, O. V.; Bourhis, L. J.; Gildea, R. J.; Howard, J. A. K.; Puschmann, H. *J. Appl. Crystallogr.* **2009**, *42*, 339–341. DOI: <https://doi.org/10.1107/S0021889808042726>.
50. Zhao, Y.; Truhlar, D. G. *J. Chem. Phys.* **2006**, *125*. DOI: <https://doi.org/10.1063/1.2370993>.
51. M. J. Frisch, G. W. Trucks, H. B. Schlegel, G. E. Scuseria, M. A. Robb, J. R. Cheeseman, G. Scalmani, V. Barone, G. A. Petersson, H. Nakatsuji, X. Li, M. Caricato, A. Marenich, J. Bloino, B. G. Janesko, R. Gomperts, B. Mennucci, H. P. Hratchian, J. V. Ort, D. J. F. Gaussian Inc: Wallingford CT 2016.
52. Clark, T.; Chandrasekhar, J.; Spitznagel, G. W.; Schleyer, P. V. R. *J. Comput. Chem.* **1983**, *4*, 294–301. DOI: <https://doi.org/10.1002/jcc.540040303>.
53. Hay, P. J.; Wadt, W. R. *J. Chem. Phys.* **1985**, *82*, 270–283. DOI: <https://doi.org/10.1063/1.448799>.
54. Zhao, Y.; Truhlar, D. G. *Theor. Chem. Acc.* **2008**, *120*, 215–241. DOI: <https://doi.org/10.1007/s00214-007-0310-x>.
55. Tomasi, J.; Mennucci, B.; Cammi, R. *Chem. Rev.* **2005**, *105*, 2999–3093. DOI: <https://doi.org/10.1021/cr9904009>.
56. Cammi, R.; Mennucci, B.; Tomasi, J.; Generale, C.; Uni, V.; Scienze, V.; Industriale, C.; Uni, V. *J. Phys. Chem. A* **2000**, *104*, 5631–5637.
57. Vázquez, M. A.; Cessa, L.; Vega, J. L.; Miranda, R.; Herrera, R.; Jiménez-Vázquez, H. A.; Tamariz, J.; Delgado, F. *Organometallics*. **2004**, *23*, 1918–1927. DOI: <https://doi.org/10.1021/om0343317>.
58. Aumann, R.; Heinen, H.; Hinterding, P.; Strater, N.; Krebs, B. *Chem Ber.* **1991**, *124*, 1229–1236.
59. Aumann, R.; Jasper, B.; Fröhlich, R. *Organometallics*. **1995**, *14*, 231–237. DOI: <https://doi.org/10.1021/om00001a035>.
60. Merlic, C. A.; Xu, D. *J. Am. Chem. Soc.* **1991**, *113*, 7418–7420. DOI: <https://doi.org/10.1021/ja00019a047>.
61. Aumann, R.; Michael, K.; Roths, K.; Frohlich, R. *Synlett.* **1994**, 1041–1044. DOI: <https://doi.org/10.1055/s-1994-23079>

The Contribution of Dispersion to the Intrinsic Energy Barriers of Neutral Model Diels-Alder Reactions

Hugo Alejandro Jiménez-Vázquez*, Luis Almazán, Adriana Benavides

Departamento de Química Orgánica. Escuela Nacional de Ciencias Biológicas. Instituto Politécnico Nacional. Prol. Carpio y Plan de Ayala. Col. Plutarco Elías Calles. Ciudad de México, CP 11350. México.

*Corresponding author: Hugo A. Jiménez-Vázquez, email: hjimenezv@ipn.mx; Tel: +52(55)5729-6000×62562.

Received June 30th, 2022; Accepted November 15th, 2022.

DOI: <http://dx.doi.org/10.29356/jmcs.v68i1.1867>

Respectfully dedicated to Prof. Joaquín Tamariz, an exemplary colleague, on the occasion of his retirement.

Abstract. The intrinsic reaction coordinates for the cycloadditions between ethene and 1,3-butadiene, and ethene and cyclopentadiene, were determined at the SCS-MP2/*aug-cc-pVTZ* level of theory. The energy contents of the points determined for both coordinates were decomposed into their deformation and interaction contributions. From this analysis it is concluded that the higher reaction barrier for the butadiene-ethene cycloaddition can be attributed primarily to the conformational change of butadiene required by the reaction (higher deformation energy). There is also a minor contribution of the interaction term, which is more stabilizing for the cyclopentadiene-ethene reaction. An additional decomposition of these terms into their Hartree-Fock and SCS-MP2 correlation components suggests that the higher stabilization of the transition state of the cyclopentadiene-ethene cycloaddition is mostly due to stronger dispersion interactions between reactants, resulting from the larger contact surface between them, and not to stabilizing electronic effects.

Keywords: Diels-Alder reaction; activation barrier; intrinsic reaction coordinate; dispersion interactions; deformation/interaction model.

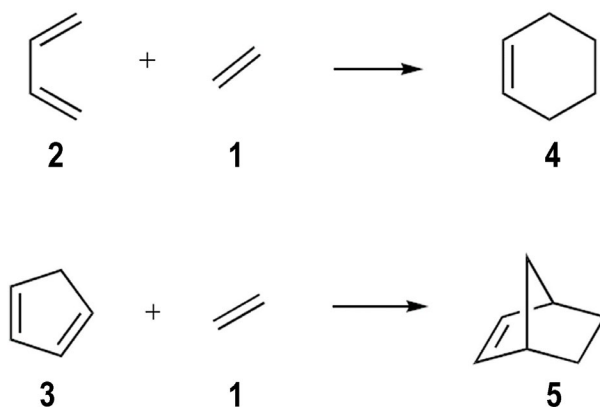
Resumen. Se determinaron las coordenadas intrínsecas de reacción para las cicloadiciones entre eteno y 1,3-butadieno, y eteno y ciclopentadieno al nivel de teoría SCS-MP2/*aug-cc-pVTZ*. La energía de los puntos obtenidos en ambas coordenadas se descompuso en sus contribuciones de deformación e interacción. A partir de este análisis se concluye que la mayor barrera energética para la cicloadición eteno-butadieno puede atribuirse, principalmente, al cambio conformacional del butadieno requerido por la reacción (mayor energía de deformación). También se encuentra que el término de interacción es más estabilizante para la reacción entre ciclopentadieno y eteno, aunque la contribución de este término es menor. La descomposición adicional de las energías de interacción de estas reacciones en sus componentes de Hartree-Fock y de correlación SCS-MP2, sugiere que la mayor estabilización del estado de transición en la reacción entre ciclopentadieno y eteno, se debe principalmente a la interacción de dispersión más fuertemente estabilizante entre estos reactantes, resultado de la mayor superficie de contacto entre ellos y no a efectos electrónicos estabilizantes.

Palabras clave: Reacción de Diels-Alder; barrera de activación; coordenada de reacción intrínseca; interacciones de dispersión; modelo de deformación/interacción.

Introduction

The concerted nature and stereospecificity of the Diels-Alder cycloaddition reaction have been rationalized in terms of the Woodward-Hoffmann rules of conservation of orbital symmetry. [1-3] According to these rules, and to Frontier Molecular Orbital (FMO) theory, [4-7] the reaction takes place through the interaction of the HOMO of one of the reactants (usually the diene) and the LUMO of the other (usually the alkene or dienophile). The energy difference between these orbitals, which is in turn altered by the presence of substituents in both reactants, [8] can be taken as a parameter indicative of the magnitude of the energy barrier for the process, although other parameters have been proposed. [9-11]

The cycloaddition of ethene (**1**) to 1,3-butadiene (**2**) is the simplest Diels-Alder reaction that can be carried out. The reactants contain the minimum number of atoms and double bonds required by the $[4\pi_s + 2\pi_s]$ process. The reaction between cyclopentadiene (**3**) and **1** (Scheme 1) can also be considered as a simple cycloaddition with two differences with respect to the former: (a) the diene is locked in the *s-cis* conformation required for the concerted reaction [12] and (b) the C5 methylene of **3** is a substituent that should alter the steric and electronic properties of the dienic π system. According to FMO theory, however, both reactions would be considered “neutral” in terms of the energy differences of the interacting orbitals of these essentially unperturbed systems. [13] Thus, the cycloadditions of **1** to **2** and **3** have relatively high activation barriers and are known to require high temperatures and pressures. [14-16]



Scheme 1. Model Diels-Alder reactions under study

A large number of experimental [15-23] and theoretical [10-11, 23-60] studies have been devoted to the analysis of these simple reactions, particularly to the study of the cycloaddition between **1** and **2**. Nevertheless, herein we present a theoretical study of the intrinsic kinetics and thermodynamics of these reactions carried out at the SCS-MP2(FC)/*aug-cc-pVTZ* level of theory, with the goal of comparing the reaction coordinates and energy barriers of both reactions according to known energy partition schemes, and considering the role of dispersion in the interaction energy of the reactants, an issue that has not been addressed previously. Dispersion forces should be particularly important for these cycloadditions due to the non-polar nature of the reactants, and their contribution to the interaction energy along the reaction coordinate is expected to be brought out through the MP2 correlation energies. Because MP2 theory has been criticized on the grounds of its overestimation of the correlation energy, [61-62] we have carried out spin-component-scaled (SCS) MP2 calculations attempting to correct this deficiency. [63-67] An ever-growing number of reports suggest that this methodology yields more accurate interaction energies, even in complexes interacting through weak intermolecular forces. [68-74]

Theoretical methods

All the calculations described in this work were carried out at the SCS-MP2/*aug-cc-pVTZ* level of theory with the Gaussian 09 (G09) program package. [75] Geometries for the minima and transition states (TSs) were first obtained at the HF/6-31+G(d,p) level of theory and used as starting points for successive optimizations at the MP2/6-31+G(d,p), and SCS-MP2/*aug-cc-pVTZ* levels of theory. All SCS-MP2 calculations were carried out within the frozen-core approximation. The SCS-MP2 calculations were achieved by including the MP2 and IOp(3/125=0333312000) options of G09 in the corresponding input files, which applied Grimme's original scaling factors [63] of 1/3 (truncated to 0.3333) and 6/5 to the second-order parallel ($\alpha\alpha + \beta\beta$), and antiparallel ($\alpha\beta$) spin-pair contributions to the correlation energy, respectively. The TSs were located with the QST2 or QST3 G09 optimization options. Most stationary points were optimized within the C_s point-group symmetry; for all of them vibrational frequency analyses were carried out after optimization. A single imaginary frequency was located for each TS; all frequencies were real for the minima. The electronic energies (E) of minima and TSs were corrected by the inclusion of zero-point energies (E_0); ZPE's were obtained by applying a scaling factor of 0.9586 (determined for the SCS-MP2/*aug-cc-pV(T+d)Z* level of theory) to the vibrational frequencies. [76] The IRCs were determined from the corresponding transition states using the IRC G09 keyword. In each case the FORWARD and REVERSE sections of the IRCs were determined independently with a STEPSIZE of 30 (3.0 bohr/amu^{1/2}); in all cases the USE=L115 G09 keyword was employed. Counterpoise corrections [77] for basis-set superposition errors were applied to all IRC points, including the adducts (see text); these corrections were determined with the COUNTERPOISE G09 keyword. Hartree-Fock, and MO energies were obtained from the G09 output files. The partition of the reaction coordinate energies into their deformation and interaction components was carried out as described below and extended to the analysis of molecular orbital interactions and to the partition of the interaction energy into the Hartree-Fock and SCS-MP2 correlation terms.

Deformation/Interaction energy partition scheme

For a bimolecular concerted reaction, the complex [Note 1] $\mathbf{A}^* \cdots \mathbf{B}^*$, formed by the interaction of the reactants at any given point i along the reaction coordinate (Fig. 1), has an absolute electronic energy content that we will define as $E_{(i)}$. In addition, this complex has a *complexation energy* $\Delta E_{(i)}$ relative to the *isolated reactants* \mathbf{A} and \mathbf{B} , at their electronic and conformational ground states, energy that we will define at this moment in the standard way (eq 1):

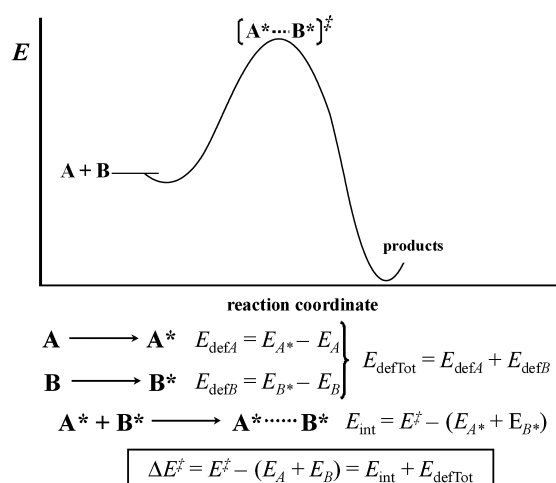


Fig. 1. Thermodynamic cycle employed for the decomposition of the complexation energy into interaction (E_{int}) and deformation (E_{def}) energies. The point of the reaction coordinate corresponding to the transition state (‡) is used as an example; however, this decomposition can be extended to any point along the reaction coordinate. \mathbf{A} and \mathbf{B} describe the geometries of the isolated reactants at their electronic and conformational ground states, while \mathbf{A}^* and \mathbf{B}^* correspond to the distorted geometries of the reactants at the point being considered.

$$\Delta E_{(i)} = E_i - (E_A + E_B) \quad (1)$$

where E_A and E_B are the electronic energies of the isolated reactants.

Within the deformation energy-interaction energy formalism we can define an interaction energy for the complex at each point of the reaction coordinate ($E_{\text{int}(i)}$), deformation energies for each one of the reactants, and a total deformation energy ($E_{\text{def A}(i)}$, $E_{\text{def B}(i)}$, and $E_{\text{def Tot}(i)}$) at these points.

The deformation energy corresponds to the energy increase arising from the change in geometry required by the isolated reactants (**A** and **B**) to reach the geometry they have within the complex (**A*** and **B***), at any given point i of the reaction coordinate. Thus, if $E_{A^*(i)}$ is the electronic energy of the distorted isolated reactant **A*** at point i , and similarly we define $E_{B^*(i)}$ for reactant **B***, we can write eqs 2–4.

$$E_{\text{def A}(i)} = E_{A^*(i)} - E_A \quad (2)$$

$$E_{\text{def B}(i)} = E_{B^*(i)} - E_B \quad (3)$$

$$E_{\text{def Tot}(i)} = E_{\text{def A}(i)} + E_{\text{def B}(i)} \quad (4)$$

The interaction energy at point i , $E_{\text{int}(i)}$, is defined as the change in energy that takes place when the distorted isolated reactants **A*** and **B*** reach the geometry of the complex (**A*...B***) at that point of the reaction coordinate (eq 5). According to the thermodynamic cycle, the sum of both $E_{\text{int}(i)}$ and $E_{\text{def Tot}(i)}$ terms should amount to the complexation energy at point i with respect to the isolated reactants (eq 6).

$$E_{\text{int}(i)} = E_{(i)} - (E_{A^*(i)} + E_{B^*(i)}) \quad (5)$$

$$\Delta E_{(i)} = E_{(i)} - (E_A + E_B) = E_{\text{int}(i)} + E_{\text{def Tot}(i)} \quad (6)$$

If the analysis is carried out with MP2 energies (E_{MP2}), a further decomposition can be carried out considering that these energies correspond to the sum of the Hartree-Fock (E_{HF}) and correlation E_{corr} terms (eq 7).

$$E_{\text{MP2}} = E_{\text{HF}} + E_{\text{corr}} \quad (7)$$

As the MP2 calculation provides both, it is a simple matter to carry out the deformation/interaction energy partition considering each term independently.

Results and discussion

For the sake of brevity, from now on we will refer to the cycloaddition between ethene (**1**) and 1,3-butadiene (**2**) as the **1+2** cycloaddition and to the cycloaddition between ethene (**1**) and cyclopentadiene (**3**) as the **1+3** cycloaddition. To calibrate our methodology, we present in Table 1 the relative energies of the stationary points obtained in this work (reaction energies and energy barriers) with the SCS-MP2 methodologies, with and without the inclusion of counterpoise corrections.

Table 1. SCS-MP2/*aug-cc-pVTZ* relative energies^a (kJ/mol) of the stationary points (SP) optimized in this work.^b On the the right side of the table counterpoise-corrected (CC) values are presented.

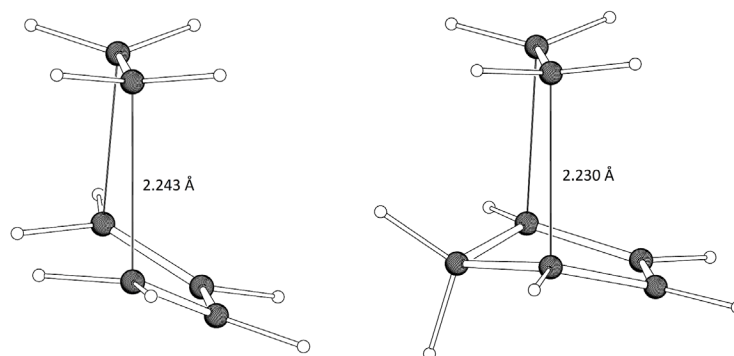
SP	ΔZPE	ΔE	ΔE_0	ΔH	ΔG	<i>cc</i>	ΔE^{CC}	ΔE_0^{CC}	ΔH^{CC}	ΔG^{CC}
TS 1+2	9.3	86.9	96.2	90.5	141.2	9.1	96.0	105.7	99.8	150.3
TS 1+3	8.9	62.9	71.8	66.7	117.2	11.0	74.0	83.2	77.9	128.2
4 ^c	27.7	-191.5	-163.9	-172.2	-114.6	18.6	-173.0	-144.1	-152.5	-96.0
5	24.3	-130.4	-106.0	-113.6	-58.1	20.3	-110.1	-84.7	-92.4	-37.9

^aRelative to the isolated reactants at their most stable geometries; for **2** this corresponds to the *s-trans* conformer.

^b*E*: electronic energy, ZPE: zero-point energy, *E*₀: ZPE-corrected electronic energies, *H*: enthalpies at 298.15 K, *G*: Gibbs free energies at 298.15 K, *cc*: magnitude of the counterpoise correction and *CC* values. TS: transition state.

^c Corresponds to the half-chair conformer of cyclohexene.

From the table we can see that the energy barrier for the **1+2** cycloaddition is between 21.8 and 25.9 kJ/mol higher than that for the **1+3** reaction. The geometries of the transition states, in terms of the distance between reactants at the reacting centers, which is 2.243 Å for the former and 2.230 Å for the latter, are very similar for both reactions. However, the diene is more “parallel” to the dienophile in the **1+3** reaction, probably because of steric repulsion between the methylene of cyclopentadiene with the two *syn* hydrogens of ethene (Fig. 2). The reaction energies favor the formation of cyclohexene (**4**) much more than the formation of norbornene (**5**). In terms of the inclusion of vibrational energies relative to the isolated reactants, the effect is about the same for both transition states; for the products, the zero-point vibrational energy is higher for **4** by 3.5 kJ/mol. The magnitude of the counterpoise correction is modest for the transition states (~10 kJ/mol), and about twice as high for the products, in such a way that energy barriers and reaction energies become more positive with respect to the uncorrected values.

**Fig. 2.** SCS-MP2/*aug-cc-pVTZ* transition states for the concerted cycloadditions of ethene to 1,3-butadiene (left) and cyclopentadiene (right).

The reaction energies can be compared to those obtained from the experimental heats of formation of reactants and products which can be found in the NIST Chemistry Webbook. [78] From here we gathered the data for the heats of formation ($\Delta_f H_g^\circ$, kJ/mol) of: **1**, 52.3; **2**, 108.8; **3**, 138.9; **4**, -4.2; **5**, 90.0. From these values the following gas-phase heats of reaction (kJ/mol) are calculated: $\Delta_r H_g^\circ$ (**1+2**) = -165.3; $\Delta_r H_g^\circ$ (**1+3**) = -101.3. We can see in Table 1 that the theoretical reaction enthalpy values (ΔH) with the inclusion of counterpoise corrections have a very good agreement with the thermochemical values. The experimental activation energies

for these reactions have also been determined. For the **1+2** cycloaddition $E_a = 115.1$ kJ/mol (~ 800 K); [17,19-20,22] while for the **1+3** process $E_a = 99.2$ kJ/mol (~ 550 K). [16] From these values and the known relationship $E_a = \Delta H^\ddagger - RT$ we can estimate $\Delta H^\ddagger = 108.5$ kJ/mol (800 K) and $\Delta H^\ddagger = 94.6$ kJ/mol (550 K). Again, we can see a better agreement with the counterpoise-corrected (CC) SCS-MP2 values of the corresponding transition states, considering temperature differences. Thus, at least for these two reactions, the inclusion of counterpoise corrections gives better results for both, ΔH^\ddagger and ΔH values, at least at the level of theory we used. [79] In Table 1 we also included the ΔG^\ddagger and ΔG values for the **1+2** and **1+3** reactions, which are about 50–55 kJ/mol higher than the corresponding enthalpies and lead to very similar activation and reaction entropies (ΔS^\ddagger and ΔS) for all cases (~ -175 J/K·mol).

In view of the above results, we decided to carry out the theoretical analysis of the energetics of these processes using the CC SCS-MP2 data. The IRCs for these reactions are shown in Fig. 3 as a function of the distance between the two reacting fragments (“bond-length” of the forming C-C bonds), considering that the symmetry point group of the reacting complexes along most of the IRCs is C_s . In both cases the energies are relative to those of the isolated reactants at their lowest-energy geometries; for 1,3-butadiene this corresponds to the *s-trans* conformer.

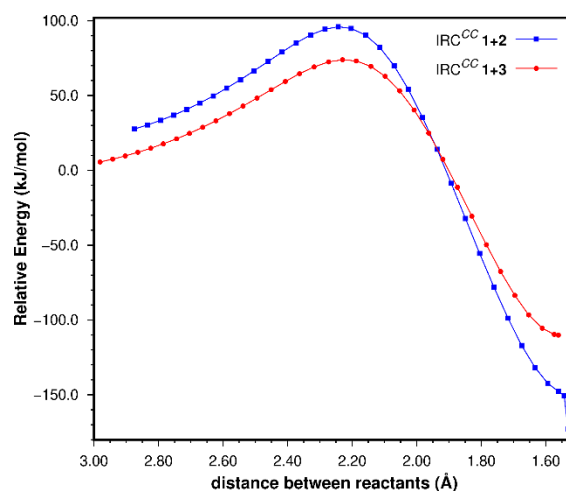


Fig. 3. SCS-MP2 counterpoise-corrected reaction coordinates for the **1+2** and **1+3** cycloadditions. For the former the last point on the right corresponds to the half-chair conformer of cyclohexene (see text).

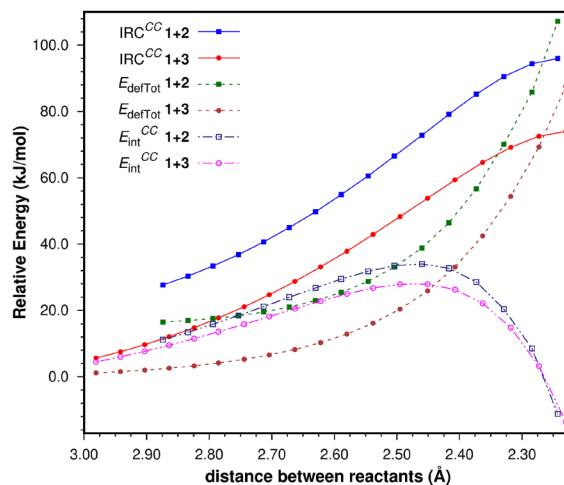
There are several features worth noting. The IRC for the **1+2** cycloaddition runs a few kJ/mol higher than that for the **1+3** process up to a point beyond the TS. From there on, the former IRC goes down in energy more rapidly, leading to a product that is more stable (relative to the corresponding reactants) than the strained bicyclic norbornene, product of the **1+3** cycloaddition. We should not forget that the **1+2** cycloaddition takes place through the C_s geometry of the reactants along the reaction coordinate which leads, in the first place, to cyclohexene in the boat conformation. However, the boat is a conformation with an energy higher than the two half-chair conformers. Thus, the last two IRC points for the **1+2** cycloaddition correspond to the boat and half-chair conformations, respectively; no IRC was determined for the conversion to the half-chair.

With respect to the intrinsic kinetics of these reactions, the relative difference in energy barriers between both reactions (22.0 kJ/mol) was analyzed in terms of the decomposition of the energy contents of the reacting complexes into their deformation (E_{defTot}) and interaction components (E_{int}) up to the TSs (Fig. 4), according to the distortion/interaction model, [80-87] also known as the Activation Strain Model. [87-93] Although this methodology has been used mainly for the comparison between isomeric transition states, it allowed us to make a direct comparison between the reaction coordinates of our two related reactions. The values obtained from this analysis at the TS geometries are presented in Table 2.

Table 2. SCS-MP2/*aug-cc-pVTZ* deformation and interaction energies (kJ/mol) of the TSs of the reactions under study.^a

SP	$\Delta E^{\ddagger CC}$	$E_{\text{def } 1}$	$E_{\text{def diene}}$	E_{defTot}	E_{int}^{CC}	E_{HF}^{CC}	E_{corr}^{CC}
TS 1+2	96.0	30.3	76.9	107.2	-11.2	59.6	-70.8
TS 1+3	74.0	27.1	60.5	87.6	-13.6	60.9	-74.5
Δ^b	22.0	3.2	16.4	19.6	2.4	-1.3	3.7

^aSP: Stationary point, $\Delta E^{\ddagger CC}$: CC electronic activation energy, $E_{\text{def } 1}$: Deformation energy of ethene, $E_{\text{def diene}}$: deformation energy of **2** or **3**, E_{defTot} : Total deformation energy of the reactants, E_{int}^{CC} : CC interaction energy, E_{HF}^{CC} : CC Hartree-Fock component of E_{int}^{CC} , E_{corr}^{CC} : CC correlation component of E_{int}^{CC} . ^b Difference between the 1+2 and 1+3 energy values.

**Fig. 4.** CC SCS-MP2 deformation and interaction components of the IRC energy (kJ/mol) for the 1+2 and 1+3 reactions. The last points on the right correspond to the TSs.

It is readily seen that the major component of the differences along the first stage of both reaction coordinates is E_{defTot} ($\Delta E_{\text{defTot}} = 19.6$ kJ/mol at the TSs favoring the 1+3 cycloaddition). Very early on the study of cycloaddition reactions the issue of the *s-trans* conformational preference of 1,3-butadiene, and its effect on their rates was analyzed by a number of authors. [94-96] In particular, Eisler and Wassermann concluded that the conformational change of **2** from the more stable *s-trans* conformation to the *s-cis* geometry required for the reaction to take place, is the main reason why the activation energies of the cycloadditions of **2** are higher than those of **3** with the same dienophiles. [94,95] Thus, the E_{defTot} term is more destabilizing for the 1+2 process as a result of the conformational change required of **2** for the reaction to take place; note that the difference is even higher at the beginning of the reaction. E_{defTot} was further decomposed into the contributions of the individual reactants (e.g. $E_{\text{defTot}(1+2)} = E_{\text{def}(1)} + E_{\text{def}(2)}$), as can be seen in Fig. 5.

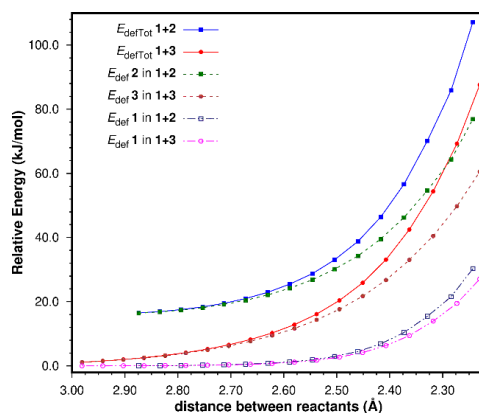


Fig. 5. Total deformation energies E_{defTot} and individual deformation (E_{def}) energies for each reactant (kJ/mol) in the 1+2 and 1+3 cycloadditions. The last points on the right correspond to the TSs.

In both reactions, the major component of E_{defTot} is the deformation energy of the dienes. Again, the conformational change of 1,3-butadiene alone accounts for most of E_{defTot} (see Table 2), [Note 2] although at the TSs, ethene is slightly more distorted in the 1+2 cycloaddition than it is in the 1+3 process, despite the fact that in the latter TS the contact between the reactants is slightly tighter.

Regarding E_{int} , Fig. 4 shows that for both reactions this term is repulsive along most of the first stage of the IRCs although it is more so for the 1+2 reaction. However, at the TS, where E_{int} is becoming attractive, the difference between the two interaction energies is relatively small with respect to the relative difference in activation barriers ($\Delta\Delta E^{\ddagger CC}$, 22.0 kJ/mol); $\Delta E_{\text{int}}^{CC} = 2.4$ kJ/mol [Note 3] (Table 2), thus being slightly more stabilizing for the 1+3 cycloaddition. The fact that E_{int} is repulsive in most of this region of the reaction coordinates can be attributed to the neutrality (in terms of Electron Demand) of the reactants, and contrasts with the attractive values of E_{int} determined by our research group in reactions that take place by Normal Electron Demand.

To gain further insight into the origin of ΔE_{int} , we took a quick look at the energies of the six electrons involved in the cycloaddition. Fig. 6 presents the MO energies of the distorted, isolated reactants at the geometry corresponding to the first point of the IRC, as well as the MOs of the interacting complex for the 1+2 cycloaddition. According to the diagram, the main contributor to the HOMO of the 1+2 complex (ψ_3) is the HOMO of 2 (π_2). Similarly, the main contributors to the HOMO-1 (ψ_2) and HOMO-2 (ψ_1) orbitals of the complex are the HOMO of 1 (π) and the HOMO-1 of 2 (π_1), respectively.

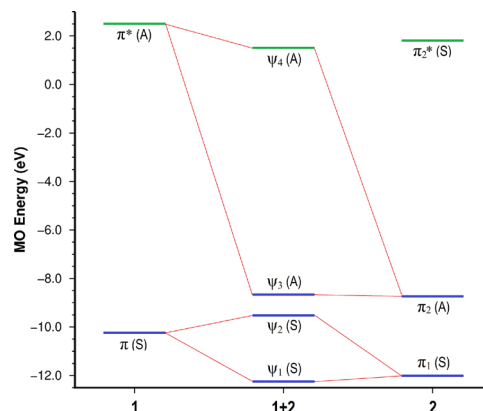


Fig. 6. MO perturbation diagram at first point of the IRC of the 1+2 cycloaddition showing the orbitals involved in the [4+2] interaction. Orbital symmetries are shown in parentheses. The orbital energies shown for the MOs of 1 and 2 correspond to those of the isolated reactants at the geometry of the reacting complex. Orbitals in blue are occupied, orbitals in green are unoccupied.

In Fig. 7 we present the MO energies of the orbitals shown in Fig. 6, along the reaction coordinates. [Note 4] From typical FMO arguments we could anticipate the 1+3 to be stronger, because the electron-donor effect of the CH₂ group of cyclopentadiene. Thus, the orbitals of **3** would be expected to be higher in energy than those of **2**, giving rise to a stronger interaction with the LUMO of **1** (for the 1+2 cycloaddition, the strongest HOMO-LUMO interaction is HOMO(2)-LUMO(1) by 0.80 eV while for the 1+3 reaction the HOMO(3)-LUMO(1) interaction is even more favoured by 2.01 eV). Fig. 7(a) contains the MOs of the interacting complex, while Fig. 7(b) shows the MO energies of the relevant orbitals for the isolated reactants as they distort along the reaction coordinates; the effect of the C5 methylene of **3** can be clearly seen here. If we assume from Fig. 5 that the HOMO of **2** (or **3**) becomes the HOMO of the complex, that the HOMO-1 of **2** (or **3**) becomes the HOMO-2 of the complex, and that the HOMO of **1** becomes the HOMO-1 of the complex, we can relate the plot in Fig. 7(a) to that in Fig. 7(b). We can see that between the two reactions the largest differences in MO energies can be found in the HOMO-2 orbitals of the interacting complexes and in the HOMO-1 orbitals of the dienes. We can also see that deformation of the reactants causes small, continuous changes in the MO energies of the isolated reactants (Fig. 7(b)), being the HOMO-1 orbitals of the dienes the least affected.

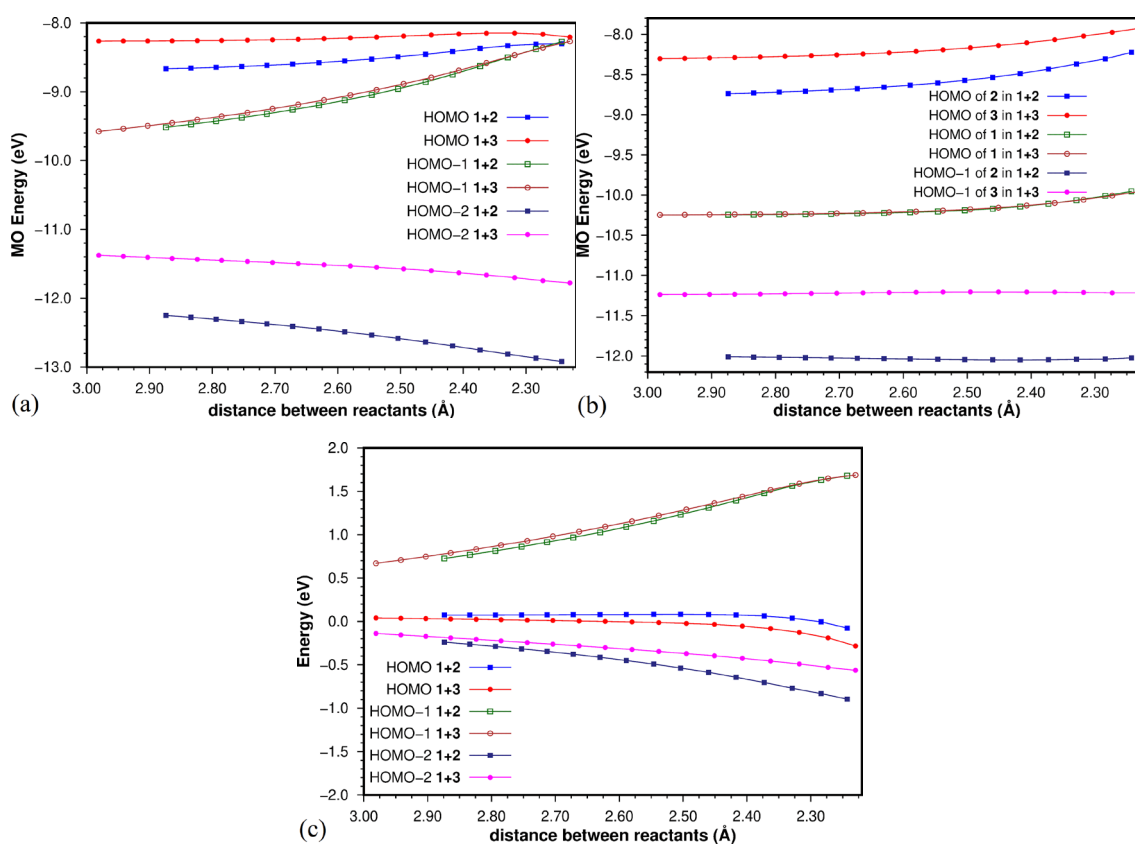


Fig. 7. MO energies (eV) along the first stage of the reaction coordinates for (a) the interacting complex and (b) the isolated reactants at the complex geometries. In (c) we present the subtraction of (b) from (a), which leaves only the effect of the interaction between reactants on the MO energies of the complex. The last points on the right correspond to the TSs.

As the MOs of the complexes contain both, deformation, and interaction effects, we subtracted the effect of deformation (subtraction of the data in Fig. 7(b) from that in Fig. 7(a)), at least of the MO that is the

major contributor to the MOs of the complex. This exercise led to the results shown in Fig. 7(c), which essentially should display the effect of the interaction (perturbation) between reactants on the MO energy. We can see that the MO of the complex most affected by the interaction is the HOMO-1, which becomes more destabilized as the reaction proceeds. It is also interesting to note that the effect is about the same for both reactions, although this should not surprise us, as this orbital corresponds essentially to the perturbed HOMO of ethene. The other two orbitals of the complex, HOMO and HOMO-2 become slightly destabilized the former and slightly stabilized the latter for both reactions. However, the HOMO of the **1+3** reaction becomes less destabilized, and the HOMO-2 of the **1+2** reaction becomes more stabilized. According to the energy differences of these orbitals alone, if E_{int} were composed only by the contributions of the MO interactions between the reactants (charge transfer effects), one would expect an overall stronger stabilizing interaction for the **1+2** reaction, which is not the case. Thus, it is not a good idea to assume that the energy changes of only these three orbitals will be the major contributors to the interaction energy between two reactants, when there are many other orbitals that are not considered in this analysis.

In a final attempt to explain the differences in $E_{\text{int}}^{\text{CC}}$ between both reactions, we carried out a further partition of the SCS-MP2 interaction energies into their Hartree-Fock (HF) and correlation (corr) components; the results of this exercise are shown in Fig. 8 and in Table 2.

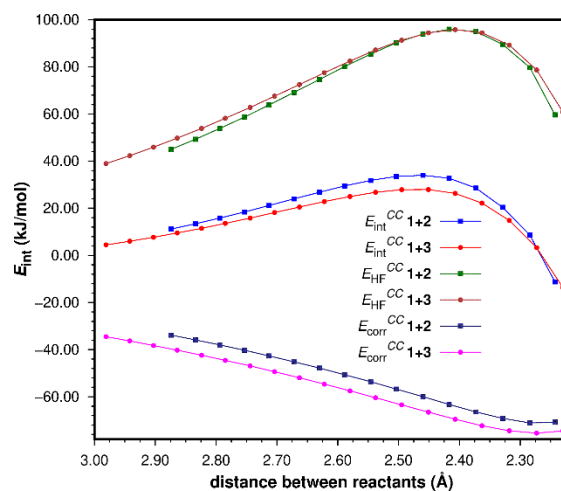


Fig. 8. Partition of the CC SCS-MP2 interaction energy (E_{int}) into its Hartree-Fock (HF) and correlation (corr) components.

We can see that the HF components are quite a bit repulsive along the first stage of both reaction coordinates, although they are very similar for both reactions. At the transition states the difference between both HF components is only 1.3 kJ/mol, suggesting that for both reactions the HF contribution to E_{int} is about the same; however, it is slightly less repulsive for the **1+2** reaction. On the other hand, the correlation components tell us a different story: first, they are rather stabilizing; second, there is a clear difference between the correlation terms of both reactions along the first part of the reaction coordinate. At the TSs the difference in the $E_{\text{corr}}^{\text{CC}}$ terms amounts to 3.7 kJ/mol favoring the **1+3** process, thus representing the main contribution to the more stabilizing $E_{\text{int}}^{\text{CC}}$ of the **1+3** TS with respect to that of the **1+2** cycloaddition. [Note 5]

As the HF component of the interaction energy corresponds to energy terms such as electrostatic interactions, charge transfer, exchange, and polarization, [97,98] Fig. 8 suggests that all these terms contribute to a similar extent in both reactions. On the other hand, the MP2 correlation term essentially corresponds to the effects of dispersion. In our interacting complexes this translates primarily into differences in the effect of van der Waals/London interactions between the reactants. The results we obtained suggest that the **1+3** TS is more stabilized because of the larger contact surface between these reactants due to the additional molecular surface

of the CH₂ moiety in cyclopentadiene. This can be better rationalized by looking again at the TSs in Fig. 2. The C5 methylene in **3** gives rise to a nonbonding interaction with the *exo* hydrogens of **1**. The repulsion between these atoms causes the C2/C3 atoms of **3** to come closer to the *endo* hydrogens of **1** than the C2/C3 atoms of **2**, thus creating a larger contact surface between the reactants.

Conclusions

The more stabilizing reaction energy for the **1+2** reaction can be attributed to the formation of a product (**4**) with less strain with respect to that obtained in the **1+3** reaction (**5**). The higher energy barrier for the **1+2** cycloaddition with respect to the **1+3** process (22 kJ/mol) is mostly due to the deformation that the reactants (19.6 kJ/mol), particularly 1,3-butadiene, must suffer for the cycloaddition to take place; in other words, to the mandatory adoption of the *s-cis* geometry of 1,3-butadiene. Only a fraction (2.4 kJ/mol) of the total difference in energy barriers between both reactions can be attributed to differences in the interaction energies between reactants at the corresponding transition states (Table 2).

Although a qualitative MO perturbation analysis supports the idea that the C5 methylene of **3** would lead to a better orbital interaction between reactants in the **1+3** cycloaddition, by increasing the energy of the π MOs of the diene, our overall results indicate that this is not relevant in terms of the interaction energies. A further partition of the SCS-MP2 interaction energies into their Hartree-Fock and correlation components indicates that electronic effects (which should be accounted for by the HF component), including MO perturbations, play a minor role in the differences observed in the systems under study. The $\Delta E_{\text{HF}}^{\text{CC}}$ term favors the **1+2** cycloaddition by 1.3 kJ/mol, while the $\Delta E_{\text{corr}}^{\text{CC}}$ term favors the **1+3** cycloaddition by 3.7 kJ/mol. This difference suggests that dispersion is the most important factor determining the overall difference in interaction energies. Thus, we conclude that for the **1+3** reaction dispersion interactions between reactants are stronger because of the larger surface area of **3**. This agrees with other results obtained by our research group and supports the idea that the contact surface between reactants at the TS can play a significant role in determining the height of reaction barriers.

Acknowledgements

HJV thanks the Consejo Nacional de Ciencia y Tecnología (CONACYT, grant 61272) and the Secretaría de Posgrado e Investigación-IPN (grants 20082577, 20091360, 20113361, and 20221854) for financial support. LA thanks CONACYT for a M.Sc. scholarship. HJV is a fellow of the EDI and COFAA programs of the IPN.

Notes

Note 1. In this particular case we will define "complex" as any geometry involving the interaction between both reactants, regardless of its position along the reaction coordinate.

Note 2. Note that at the level of theory employed in our work, for the planar *s-cis* conformation (which is not a minimum) $\Delta E_0 = 14.7$ kJ/mol with respect to the *s-trans* conformer.

Note 3. A similar trend is observed when uncorrected energies are used for the analysis.

Note 4. A simpler analysis of these MOs was carried out in Ref. 28 for the **1+2** reaction.

Note 5. Similar results are obtained when no *CC* corrections are applied.

References

1. Hoffmann, R.; Woodward, R. B. *J. Am. Chem. Soc.* **1965**, 87, 4388-4389. DOI: <https://doi.org/10.1021/ja00947a033>.
2. Hoffmann, R.; Woodward, R. B. *Acc. Chem. Res.* **1968**, 1, 17-22. DOI: <https://doi.org/10.1021/ar50001a003>.
3. Woodward, R. B.; Hoffmann, R., *The Conservation of Orbital Symmetry*. Academic Press: New York, 1970.
4. Fukui, K.; Yonezawa, T.; Shingu, H. *J. Chem. Phys.* **1952**, 20, 722-725. DOI: <https://doi.org/10.1063/1.1700523>.
5. Fukui, K. *Acc. Chem. Res.* **1971**, 4, 57-64. DOI: <https://doi.org/10.1021/ar50038a003>.
6. Houk, K. N. *Acc. Chem. Res.* **1975**, 8, 361-369. DOI: <https://doi.org/10.1021/ar50095a001>.
7. Fleming, I. *Frontier Orbitals and Organic Chemical Reactions*. John Wiley & Sons: Chichester, 1976.
8. Robiette, R.; Marchand-Brynaert, J.; Peeters, D. *J. Org. Chem.* **2002**, 67, 6823-6826. DOI: <https://doi.org/10.1021/jo025796u>.
9. Domingo, L. R.; Aurell, M. J.; Pérez, P.; Contreras, R. *Tetrahedron.* **2002**, 58, 4417-4423. DOI: [https://doi.org/10.1016/S0040-4020\(02\)00410-6](https://doi.org/10.1016/S0040-4020(02)00410-6).
10. Domingo, L. R.; Saez, J. A. *Org. Biomol. Chem.* **2009**, 7, 3576-3583. DOI: <https://doi.org/10.1039/B909611F>.
11. Domingo, L. R.; Chamorro, E.; Perez, P. *Org. Biomol. Chem.* **2010**, 8, 5495-5504. DOI: <https://doi.org/10.1039/C0OB00563K>.
12. Sauer, J.; Lang, D.; Mielert, A. *Angew. Chem., Int. Ed.* **1962**, 1, 268-269. DOI: <https://doi.org/10.1002/anie.196202683>.
13. Carey, F. A.; Sundberg, R. J. *Advanced Organic Chemistry Part A: Structure and Mechanism*. Fifth ed.; Springer: New York, 2007.
14. Bartlett, P. D.; Schueller, K. E. *J. Am. Chem. Soc.* **1968**, 90, 6071-6077. DOI: <https://doi.org/10.1021/ja01024a024>.
15. Joshel, L. M.; Butz, L. W. *J. Am. Chem. Soc.* **1941**, 63, 3350-3351. DOI: <https://doi.org/10.1021/ja01857a033>.
16. Walsh, R.; Wells, J. M. *J. Chem. Soc., Perkin Trans. 2* **1976**, 52-55. DOI: <https://doi.org/10.1039/P29760000052>.
17. Rowley, D.; Steiner, H. *Discuss. Faraday Soc.* **1951**, 10, 198-213. DOI: <https://doi.org/10.1039/DF9511000198>.
18. Smith, S. R.; Gordon, A. S. *J. Phys. Chem.* **1961**, 65, 1124-1128. DOI: <https://doi.org/10.1021/j100825a008>.
19. Skinner, J. L.; Sliepcevich, C. M. *Ind. Eng. Chem. Fundam.* **1963**, 2, 168-172. DOI: <https://doi.org/10.1021/i160007a002>.
20. Uchiyama, M.; Tomioka, T.; Amano, A. *J. Phys. Chem.* **1964**, 68, 1878-1881. DOI: <https://doi.org/10.1021/j100789a036>.
21. Van Sickle, D. E.; Rodin, J. O. *J. Am. Chem. Soc.* **1964**, 86, 3091-3094. DOI: <https://doi.org/10.1021/ja01069a024>.
22. Tardy, D. C.; Ireton, R.; Gordon, A. S. *J. Am. Chem. Soc.* **1979**, 101, 1508-1514. DOI: <https://doi.org/10.1021/ja00500a024>.
23. Houk, K. N.; Lin, Y. T.; Brown, F. K. *J. Am. Chem. Soc.* **1986**, 108, 554-556. DOI: <https://doi.org/10.1021/ja00263a059>.
24. Burke, L. A.; Leroy, G.; Sana, M. *Theor. Chem. Acc.* **1975**, 40, 313-321. DOI: <https://doi.org/10.1007/bf00668337>.
25. Townshend, R. E.; Ramunni, G.; Segal, G.; Hehre, W. J.; Salem, L. *J. Am. Chem. Soc.* **1976**, 98, 2190-2198. DOI: <https://doi.org/10.1021/ja00424a031>.
26. Burke, L. A.; Leroy, G. *Theor. Chem. Acc.* **1977**, 44, 219-221. DOI: <https://doi.org/10.1007/bf00549104>.

27. Jug, K.; Krüger, H. W. *Theor. Chem. Acc.* **1979**, *52*, 19-26. DOI: <https://doi.org/10.1007/bf00581697>.
28. Bernardi, F.; Bottoni, A.; Robb, M. A.; Field, M. J.; Hillier, I. H.; Guest, M. F. *J. Chem. Soc., Chem. Commun.* **1985**, 1051-1052. DOI: <https://doi.org/10.1039/C39850001051>.
29. Dewar, M. J. S.; Olivella, S.; Stewart, J. J. P. *J. Am. Chem. Soc.* **1986**, *108*, 5771-5779. DOI: <https://doi.org/10.1021/ja00279a018>.
30. Bernardi, F.; Bottoni, A.; Field, M. J.; Guest, M. F.; Hillier, I. H.; Robb, M. A.; Venturini, A. *J. Am. Chem. Soc.* **1988**, *110*, 3050-3055. DOI: <https://doi.org/10.1021/ja00218a009>.
31. Bach, R. D.; McDouall, J. J. W.; Schlegel, H. B.; Wolber, G. J. *J. Org. Chem.* **1989**, *54*, 2931-2935. DOI: <https://doi.org/10.1021/jo00273a029>.
32. Houk, K. N.; Loncharich, R. J.; Blake, J. F.; Jorgensen, W. L. *J. Am. Chem. Soc.* **1989**, *111*, 9172-9176. DOI: <https://doi.org/10.1021/ja00208a006>.
33. Jorgensen, W. L.; Lim, D.; Blake, J. F. *J. Am. Chem. Soc.* **1993**, *115*, 2936-2942. DOI: <https://doi.org/10.1021/ja00060a048>.
34. Li, Y.; Houk, K. N. *J. Am. Chem. Soc.* **1993**, *115*, 7478-7485. DOI: <https://doi.org/10.1021/ja00069a055>.
35. Herges, R.; Jiao, H.; Schleyer, P. v. R. *Angew. Chem., Int. Ed.* **1994**, *33*, 1376-1378. DOI: <https://doi.org/10.1002/anie.199413761>.
36. Houk, K. N.; Li, Y.; Storer, J.; Raimondi, L.; Beno, B. *J. Chem. Soc., Faraday Trans.* **1994**, *90*, 1599-1604. DOI: <https://doi.org/10.1039/FT9949001599>.
37. Bernardi, F.; Celani, P.; Olivucci, M.; Robb, M. A.; Suzzi-Valli, G. *J. Am. Chem. Soc.* **1995**, *117*, 10531-10536. DOI: <https://doi.org/10.1021/ja00147a014>.
38. Jursic, B.; Zdravkovski, Z. *J. Chem. Soc., Perkin Trans. 2* **1995**, 1223-1226. DOI: <https://doi.org/10.1039/P29950001223>.
39. Goldstein, E.; Beno, B.; Houk, K. N. *J. Am. Chem. Soc.* **1996**, *118*, 6036-6043. DOI: <https://doi.org/10.1021/ja9601494>.
40. Torrent, M.; Durán, M.; Solà, M. *SCIENTIA gerundensis*. **1996**, *22*, 123-131.
41. Branchadell, V. *Int. J. Quantum Chem.* **1997**, *61*, 381-388. DOI: [https://doi.org/10.1002/\(sici\)1097-461x\(1997\)61:3<381::aid-qua3>3.0.co;2-s](https://doi.org/10.1002/(sici)1097-461x(1997)61:3<381::aid-qua3>3.0.co;2-s).
42. Jiao, H.; Schleyer, P. v. R. *J. Phys. Org. Chem.* **1998**, *11*, 655-662. DOI: [https://doi.org/10.1002/\(SICI\)1099-1395\(199808/09\)11:8/9<655::AID-POC66>3.0.CO;2-U](https://doi.org/10.1002/(SICI)1099-1395(199808/09)11:8/9<655::AID-POC66>3.0.CO;2-U).
43. Spino, C.; Pesant, M.; Dory, Y. *Angew. Chem., Int. Ed.* **1998**, *37*, 3262-3265. DOI: [https://doi.org/10.1002/\(sici\)1521-3773\(19981217\)37:23<3262::aid-anie3262>3.0.co;2-t](https://doi.org/10.1002/(sici)1521-3773(19981217)37:23<3262::aid-anie3262>3.0.co;2-t).
44. Bradley, A. Z.; Kociolek, M. G.; Johnson, R. P. *J. Org. Chem.* **2000**, *65*, 7134-7138. DOI: <https://doi.org/10.1021/jo000916o>.
45. Sakai, S. *J. Phys. Chem. A*. **2000**, *104*, 922-927. DOI: <https://doi.org/10.1021/jp9926894>.
46. Huang, C.-H.; Tsai, L.-C.; Hu, W.-P. *J. Phys. Chem. A*. **2001**, *105*, 9945-9953. DOI: <https://doi.org/10.1021/jp012740f>.
47. Dinadayalane, T. C.; Vijaya, R.; Smitha, A.; Sastry, G. N. *J. Phys. Chem. A*. **2002**, *106*, 1627-1633. DOI: <https://doi.org/10.1021/jp013910r>.
48. Guner, V.; Khuong, K. S.; Leach, A. G.; Lee, P. S.; Bartberger, M. D.; Houk, K. N. *J. Phys. Chem. A*. **2003**, *107*, 11445-11459. DOI: <https://doi.org/10.1021/jp035501w>.
49. Lischka, H.; Ventura, E.; Dallos, M. *ChemPhysChem* **2004**, *5*, 1365-1371. DOI: <https://doi.org/10.1002/cphc.200400104>.
50. Sakai, S. *J. Phys. Chem. A*. **2006**, *110*, 6339-6344. DOI: <https://doi.org/10.1021/jp0560011>.
51. Hirao, H. *J. Comput. Chem.* **2008**, *29*, 1399-1407. DOI: <https://doi.org/10.1002/jcc.20899>.
52. Murray, J. S.; Yepes, D.; Jaque, P.; Politzer, P. *Comput. Theor. Chem.* **2015**, *1053*, 270-280. DOI: <https://doi.org/10.1016/j.comptc.2014.08.010>.
53. Scarborough, D. L. A.; Kobayashi, R.; Thompson, C. D.; Izgorodina, E. I. *Int. J. Quantum Chem.* **2015**, *115*, 989-1001. DOI: <https://doi.org/10.1002/qua.24933>.
54. Sexton, T.; Kraka, E.; Cremer, D. *J. Phys. Chem. A* **2016**, *120*, 1097-1111. DOI: <https://doi.org/10.1021/acs.jpca.5b11493>.

55. Domingo, L. R.; Ríos-Gutiérrez, M.; Pérez, P. *Tetrahedron*. **2017**, *73*, 1718-1724. DOI: <https://doi.org/10.1016/j.tet.2017.02.012>.
56. Chakraborty, D.; Das, R.; Chattaraj, P. K. *ChemPhysChem*. **2017**, *18*, 2162-2170. DOI: <https://doi.org/10.1002/cphc.201700308>.
57. Chen, B.; Hoffmann, R.; Cammi, R. *Angew. Chem., Int. Ed.* **2017**, *56*, 11126-11142. DOI: <https://doi.org/10.1002/anie.201705427>.
58. Casals-Sainz, J. L.; Francisco, E.; Martín Pendás, Á. Z. *Anorg. Allg. Chem.* **2020**, *646*, 1062-1072. DOI: <https://doi.org/10.1002/zaac.202000038>.
59. Jara-Cortés, J.; Leal-Sánchez, E.; Hernández-Trujillo, J. J. *Phys. Chem. A*. **2020**, *124*, 6370-6379. DOI: <https://doi.org/10.1021/acs.jpca.0c04171>.
60. Ayarde-Henríquez, L.; Guerra, C.; Duque-Noreña, M.; Rincón, E.; Pérez, P.; Chamorro, E. *J. Phys. Chem. A*. **2021**, *125*, 5152-5165. DOI: <https://doi.org/10.1021/acs.jpca.1c01448>.
61. McLachlan, A. D.; Ball, M. A. *Rev. Mod. Phys.* **1964**, *36*, 844-855. DOI: <https://doi.org/10.1103/RevModPhys.36.844>.
62. Jurečka, P.; Šponer, J.; Černý, J.; Hobza, P. *Phys. Chem. Chem. Phys.* **2006**, *8*, 1985-1993. DOI: <https://doi.org/10.1039/b600027d>.
63. Grimme, S. *J. Chem. Phys.* **2003**, *118*, 9095-9102. DOI: <https://doi.org/10.1063/1.1569242>.
64. Gerenkamp, M.; Grimme, S. *Chem. Phys. Lett.* **2004**, *392*, 229-235. DOI: <https://doi.org/10.1016/j.cplett.2004.05.063>.
65. Goumans, T. P. M.; Ehlers, A. W.; Lammertsma, K.; Würthwein, E.-U.; Grimme, S. *Chem. - Eur. J.* **2004**, *10*, 6468-6475. DOI: <https://doi.org/10.1002/chem.200400250>.
66. Piacenza, M.; Grimme, S. *J. Comput. Chem.* **2004**, *25*, 83-99. DOI: <https://doi.org/10.1002/jcc.10365>.
67. Grimme, S.; Mück-Lichtenfeld, C.; Würthwein, E.-U.; Ehlers, A. W.; Goumans, T. P. M.; Lammertsma, K. *J. Phys. Chem. A* **2006**, *110*, 2583-2586. DOI: <https://doi.org/10.1021/jp057329x>.
68. Hill, J. G.; Platts, J. A.; Werner, H.-J. *Phys. Chem. Chem. Phys.* **2006**, *8*, 4072-4078. DOI: <https://doi.org/10.1039/B608623C>.
69. Antony, J.; Grimme, S. *J. Phys. Chem. A*. **2007**, *111*, 4862-4868. DOI: <https://doi.org/10.1021/jp070589p>.
70. Takatani, T.; David Sherrill, C. *Phys. Chem. Chem. Phys.* **2007**, *9*, 6106-6114. DOI: <https://doi.org/10.1039/B709669K>.
71. Bates, D. M.; Anderson, J. A.; Oloyede, P.; Tschumper, G. S. *Phys. Chem. Chem. Phys.* **2008**, *10*, 2775-2779. DOI: <https://doi.org/10.1039/B718720C>.
72. Takatani, T.; Hohenstein, E. G.; Sherrill, C. D. *J. Chem. Phys.* **2008**, *128*, 124111-124117. DOI: <https://doi.org/10.1063/1.2883974>.
73. King, R. A. *Mol. Phys.* **2009**, *107*, 789-795. DOI: <https://doi.org/10.1080/00268970802641242>.
74. Riley, K. E.; Platts, J. A.; Řezáč, J.; Hobza, P.; Hill, J. G. *J. Phys. Chem. A*. **2012**, *116*, 4159-4169. DOI: <https://doi.org/10.1021/jp211997b>.
75. Frisch, M. J.; Trucks, G. W.; Schlegel, H. B.; Scuseria, G. E.; Robb, M. A.; Cheeseman, J. R.; Scalmani, G.; Barone, V.; Mennucci, B.; Petersson, G. A.; Nakatsuji, H.; Caricato, M.; Li, X.; Hratchian, H. P.; Izmaylov, A. F.; Bloino, J.; Zheng, G.; Sonnenberg, J. L.; Hada, M.; Ehara, M.; Toyota, K.; Fukuda, R.; Hasegawa, J.; Ishida, M.; Nakajima, T.; Honda, Y.; Kitao, O.; Nakai, H.; Vreven, T.; Montgomery, J., J. A.; Peralta, J. E.; Ogliaro, F.; Bearpark, M.; Heyd, J. J.; Brothers, E.; Kudin, K. N.; Staroverov, V. N.; Keith, T.; Kobayashi, R.; Normand, J.; Raghavachari, K.; Rendell, A.; Burant, J. C.; Iyengar, S. S.; Tomasi, J.; Cossi, M.; Rega, N.; Millam, J. M.; Klene, M.; Knox, J. E.; Cross, J. B.; Bakken, V.; Adamo, C.; Jaramillo, J.; Gomperts, R.; Stratmann, R. E.; Yazyev, O.; Austin, A. J.; Cammi, R.; Pomelli, C.; Ochterski, J. W.; Martin, R. L.; Morokuma, K.; Zakrzewski, V. G.; Voth, G. A.; Salvador, P.; Dannenberg, J. J.; Dapprich, S.; Daniels, A. D.; Farkas, O.; Foresman, J. B.; Ortiz, J. V.; Cioslowski, J.; Fox, D. J. *Gaussian 09, Revision D.01*, Gaussian, Inc.: Wallingford, CT, 2013.
76. Kesharwani, M. K.; Brauer, B.; Martin, J. M. L. *J. Phys. Chem. A*. **2015**, *119*, 1701-1714. DOI: <https://doi.org/10.1021/jp508422u>.

77. Boys, S. F.; Bernardi, F. *Mol. Phys.* **1970**, *19*, 553-566. DOI: <https://doi.org/10.1080/00268977000101561>.
78. NIST Chemistry Webbook. <http://webbook.nist.gov>, accessed in June 2022.
79. Alvarez-Idaboy, J. R.; Galano, A. *Theor. Chem. Acc.* **2010**, *126*, 75-85. DOI: <https://doi.org/10.1007/s00214-009-0676-z>.
80. Xidos, J. D.; Poirier, R. A.; Pye, C. C.; Burnell, D. J. *J. Org. Chem.* **1998**, *63*, 105-112. DOI: <https://doi.org/10.1021/jo9712815>.
81. Houk, K. N.; Gandour, R. W.; Strozier, R. W.; Rondan, N. G.; Paquette, L. A. *J. Am. Chem. Soc.* **1979**, *101*, 6797-6802. DOI: <https://doi.org/10.1021/ja00517a001>.
82. Coxon, J. M.; Grice, S. T.; Maclagan, R. G. A. R.; McDonald, D. Q. *J. Org. Chem.* **1990**, *55*, 3804-3807. DOI: <https://doi.org/10.1021/jo00299a021>.
83. Ess, D. H.; Houk, K. N. *J. Am. Chem. Soc.* **2007**, *129*, 10646-10647. DOI: <https://doi.org/10.1021/ja0734086>.
84. Ess, D. H.; Houk, K. N. *J. Am. Chem. Soc.* **2008**, *130*, 10187-10198. DOI: <https://doi.org/10.1021/ja800009z>.
85. Jones, G. O.; Houk, K. N. *J. Org. Chem.* **2008**, *73*, 1333-1342. DOI: <https://doi.org/10.1021/jo702295d>.
86. Hayden, A. E.; Houk, K. N. *J. Am. Chem. Soc.* **2009**, *131*, 4084-4089. DOI: <https://doi.org/10.1021/ja809142x>.
87. Bickelhaupt, F. M.; Houk, K. N. *Angew. Chem., Int. Ed.* **2017**, *56*, 10070-10086. DOI: <https://doi.org/10.1002/anie.201701486>.
88. Bickelhaupt, F. M. *J. Comput. Chem.* **1999**, *20*, 114-128. DOI: [https://doi.org/10.1002/\(SICI\)1096-987X\(19990115\)20:1<114::AID-JCC12>3.0.CO;2-L](https://doi.org/10.1002/(SICI)1096-987X(19990115)20:1<114::AID-JCC12>3.0.CO;2-L).
89. Diefenbach, A.; Bickelhaupt, F. M. *J. Phys. Chem. A* **2004**, *108*, 8460-8466. DOI: 10.1021/jp047986+.
90. De Jong, G. T.; Bickelhaupt, F. M. *ChemPhysChem* **2007**, *8*, 1170-1181. DOI: <https://doi.org/10.1002/cphc.200700092>.
91. Van Zeist, W.-J.; Bickelhaupt, F. M. *Org. Biomol. Chem.* **2010**, *8*, 3118-3127. DOI: <https://doi.org/10.1039/B926828F>.
92. Fernández, I.; Bickelhaupt, F. M. *Chem. Soc. Rev.* **2014**, *43*, 4953-4967. DOI: <https://doi.org/10.1039/C4CS00055B>.
93. Wolters, L. P.; Bickelhaupt, F. M. *Wiley Interdiscip. Rev.: Comput. Mol. Sci.* **2015**, *5*, 324-343. DOI: <https://doi.org/10.1002/wcms.1221>.
94. Eisler, B.; Wassermann, A. *Discuss. Faraday Soc.* **1951**, 235. DOI: <https://doi.org/10.1039/DF9511000213>.
95. Eisler, B.; Wassermann, A. *J. Chem. Soc.* **1953**, 979-982. DOI: <https://doi.org/10.1039/JR9530000979>.
96. Craig, D.; Shipman, J. J.; Fowler, R. B. *J. Am. Chem. Soc.* **1961**, *83*, 2885-2891. DOI: <https://doi.org/10.1021/ja01474a023>.
97. Morokuma, K. *J. Chem. Phys.* **1971**, *55*, 1236-1244. DOI: <https://doi.org/10.1063/1.1676210>.
98. Kitaura, K.; Morokuma, K. *Int. J. Quantum Chem.* **1976**, *10*, 325-340. DOI: <https://doi.org/10.1002/qua.560100211>.

Understanding Experimental Facts for the Transformation of Perezone into α - and β -pipitzols

Luis Mauricio Murillo-Herrera^{1,2}, Fátima Soto-Suárez¹, Eduardo Hernández-Huerta¹, Karla Ramírez-Gualito³, Mariana Ortiz-Reynoso⁴, Ramiro F. Quijano-Quiñones^{5*}, Gabriel Cuevas^{1*}

¹Instituto de Química. Universidad Nacional Autónoma de México. Circuito Exterior, Ciudad Universitaria 04510, Coyoacán.

²Current address: Department of Chemistry, University of York, Heslington, York YO10 5DD, United Kingdom.

³Facultad de Ingeniería, Universidad Anáhuac México. Avenida Universidad Anáhuac 46, Col. Lomas Anáhuac, Huixquilucan, 52786, Estado de México, México.

⁴Facultad de Química, Universidad Autónoma del Estado de México, Paseo Colón esq. Paseo Tollocan. 50120, Residencial Colón, Toluca, Estado de México. México.

⁵Facultad de Química, Universidad Autónoma de Yucatán, Calle 43 No 613 por calle 90, Colonia Inalámbrica. 97069. Mérida, Yucatán, México.

*Corresponding author: Ramiro F. Quijano-Quiñones, email: ramiro.quijano@correo.uady.mx; Gabriel Cuevas, email: gecgb@unam.mx

Received December 11th, 2022; Accepted May 29th, 2023.

DOI: <http://dx.doi.org/10.29356/jmcs.v68i1.1926>

This paper is dedicated to Prof. Joaquín Tamariz Mascarua, who is an example of dedication oriented to the development of Mexican chemistry. He served as editor-in-chief of this Journal right around the time it acquired the impact index.

Abstract. Under thermal conditions perezone, a sesquiterpene quinone, forms an equimolar amount of α - and β -pipitzol through an intermolecular cycloaddition reaction. Computational calculations at M06-2x/6-311++G(2d,2p) level of theory of the transition states and the associated reaction paths allow justifying the experimental observations. Only *exo* adducts are observed experimentally, which is in line with the calculated energy difference of 6.5 kcal/mol between the transition states associated with the *endo* and *exo* adducts. Activation free energy was accurately predicted, those the uncatalyzed thermal process of cycloaddition requires 37.0 kcal/mol. The study of the potential energy surface allows to establish the existence of folded conformers of perezone in the potential energy surface.

Keywords: Perezone; α -pipitzol; β -pipitzol; reaction mechanism; concerted reaction.

Resumen. En condiciones térmicas la perezona, una quinona sesquiterpénica, forma, cantidades equimolares de α - y β -pipitzoles a través de una reacción de cicloadición intramolecular. A nivel M06-2x/6-311++G(2d,2p) el cálculo de los estados de transición y de las trayectorias de reacción asociadas permiten justificar los resultados observados. Desde el punto de vista experimental sólo se forman los aductos *exo* y no los *endo* pues los estados de transición relacionados muestran una diferencia energética de 6.5 kcal/mol. La energía de activación calculada para el procedo desprovisto de catálisis es de 37.0 kcal/mol. El estudio de la superficie de energía potencial permite establecer la existencia de conformeros plegados de la perezona.

Palabras clave: Perezona; α -pipitzol; β -pipitzol; mecanismo de reacción; reacción concertada.

Introduction

It is well known that depending on the time of year in which the pipitzahuac roots are collected, it is possible to isolate predominantly perezone [1] (**1**, Fig. 1) or a homogeneous mixture of α - (**2-a**) and β -pipitzols (**2-c**, Fig. 1) that naturally co-crystallize. [2-4] The extracts of this plant of the *Acourtia* genus have been used in traditional Mexican medicine since pre-Columbian times. The genus *Perezia* has been reconsidered as *Acourtia* and some synonyms for this plant are *Acourtia humboldtoii*, (BL Robinson & Green Reveal & RM King), formerly *Perezia cuernavacana* (BL Rob & Green), and initially *Trixis pipitzahuac*, (Schaff. Ex Herrera) Asteracea (Herrera).

In 1852 the Mexican pharmacist Leopoldo Río de la Loza isolated perezone in its crystalline form from a crude extract that had been provided to him by Pascual Díaz Leal by sublimation from the dried root, or by alcohol extraction followed by recrystallization from gasoline.[5] He reported the first elemental analysis developed in Mexico using the method implemented by Professor Justus von Liebig in Germany. [6] Río de la Loza analysis turned out to be erroneous, as a nitrogen atom was incorrectly assigned to the molecular formula, [7] nonetheless this assay should be considered a historical milestone, being the first attempt to carry out Liebig's method for organic elemental analysis in America.

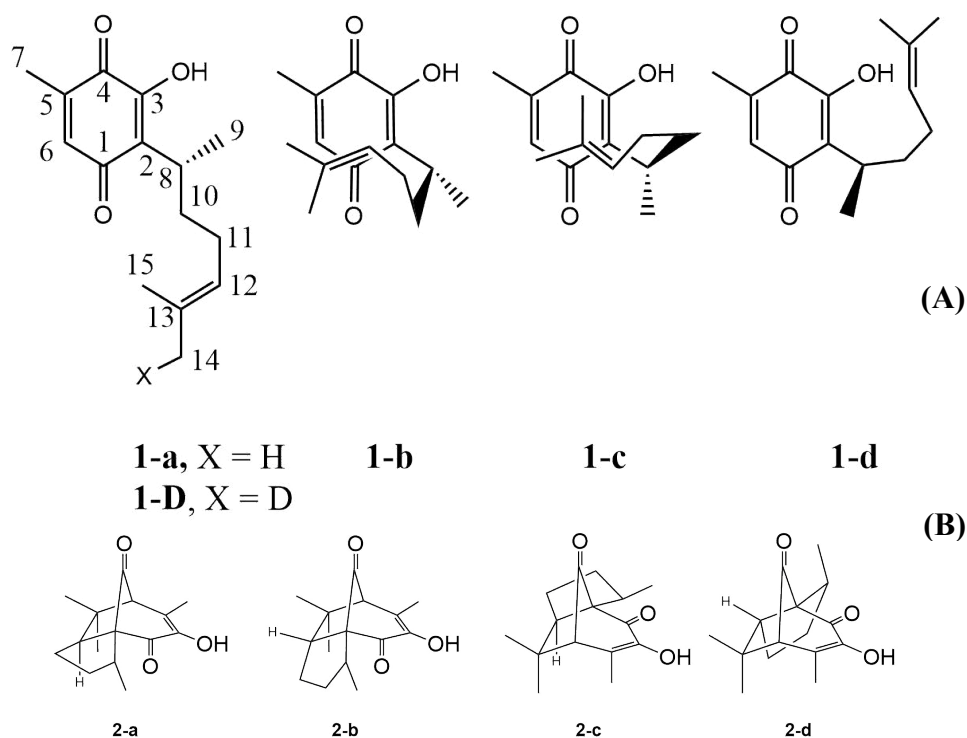


Fig. 1. (A) Perezone molecular structure with extended (**1-a** and **1-d**) and folded (**1-b** and **1-c**) conformers (See Fig. S1). (B) Four possible cycloaddition adducts: α -pipitzols (*exo*: **2-a** and *endo* **2-b**) and β -pipitzols (*exo*: **2-c** and *endo*: **2-d**).

In 1857 Severiano Pérez reported the finding of a white and crystalline substance as a component of the pipitzahuac resin, which he initially called fructicosina and later pipitzahuina,[8,9] two ways for naming pipitzols that were lost over time. Pérez described the first isolation of pipitzols through the accidental thermal transformation of perezone, obtaining them as a crystalline by-product of its purification using sublimation, however, Pérez only described some physical properties and did not delve the molecular composition of this by product. Pérez considered that Río de la Loza's perezone was a mixture formed by pipitzoles contaminated by colored compounds that imparted its color to the mixture. A serious mistake.

At the turn of the century, Remfry[10] obtained pipitzols by a thermal reaction of perezone but it was until 1965 when the first mechanism for this transformation was proposed, [1,11] in order to support perezone's connectivity proposal, which resulted to be wrong. This mechanism, suggested the intermediation of a cyclobutane, followed by two alkyl group migrations for the formation of the pipitzols. [1]

The connectivity of prerezone (**1**) was established the same year when four independent works were published. By means of ^1H NMR analysis, it was finally established that the correct connectivity of quinone substituents exhibits a methyl group and a hydrogen atom on the same side of the quinone.[12-15] With the connectivity described, it was possible to report the first total synthesis of perezone.[16] The determination of the chemical structure of perezone allowed to propose an adequate mechanism for the formation of pipitzols, whose structure had been determined shortly before by Romo *et al.* [1] Initially they established that the product of the reaction consisted of a mixture of two diastereomers, in which all the stereogenic centers formed in the reaction had opposite configurations, but since the stereogenic center at C8 (of *R* configuration, Fig. 1) is kept constant, diastereoisomers are formed.

Experimentally, the selective oxidation of the methyl vinyl group at position 14, located *trans* with respect to the alkyl chain of **1** using selenium oxide, produced a pair of reaction products from which the aldehyde was isolated, and subsequently reduced with sodium borodeuteride and deoxygenated.[17] In this way, it was possible to prepare monodeuterated perezone at only one methyl group. When subjected to the thermal conditions of cycloaddition, pipitzols were formed, in which there were no scattering labels, so this mechanism was interpreted to correspond to a class B cycloaddition [$\pi 4s + \pi 2s$][18] or as a sigmatropic reaction of [1,9] order.[17] Furthermore, it was observed that in thermal conditions the proportion of the obtained pipitzols was similar, without induction of the stereogenic center. [17]

Because pipitzols have their biogenetic origin in perezone and both are natural products, their study is part of our interest in the terminal biogenesis of terpenes. [19,20]

Results and discussion

Concerted cycloaddition of perezone (**1**)

The folded conformers of perezone which are the precursors of pipitzols, present two easily differentiable arrangements according to the face of the quinone on which the side chain approaches, and each of them presents two possible orientations of the double bond; this is whether the side chain approaches *exo* (**1-a** and **1-c**, Fig. 2) or *endo* (**1-b** and **1-d**). It is important to notice that to date only compounds originating from the *exo* approach have been isolated from the plant and obtained by synthesis.[1-4,16,18] Deuterium labeling experimentation on perezone's C14 methyl group (structure **1-d**, Fig. 1), demonstrated complete preservation of deuterium on methyl C14 of the *endo* adduct, thus assuring the concerted mechanism nature.[16,21,22]

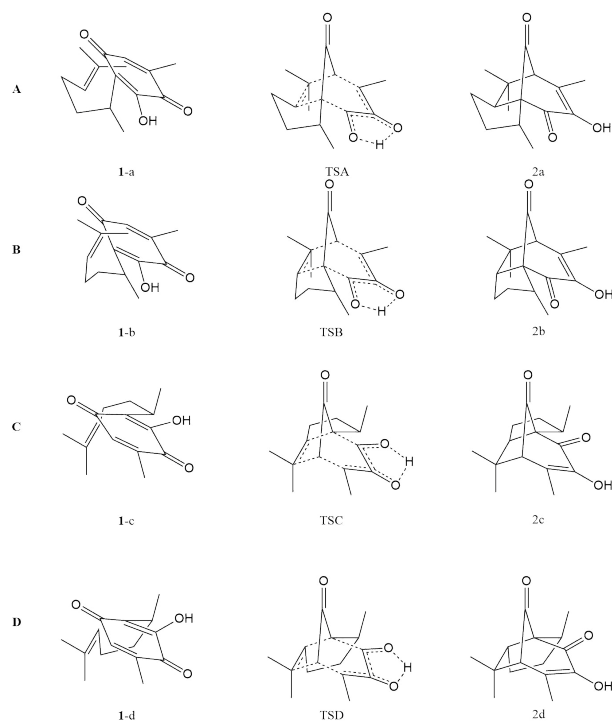


Fig. 2. Transition states in the formation of the four isomeric pipitzols **1-a** – **2-d**.

With the available conformers and the structure of the two isolable diastomeric pipitzols, the search for the transition states associated with the four possible approaches was undertaken. (See Table S3) All four transition states are characterizable and are presented in Fig. 3.

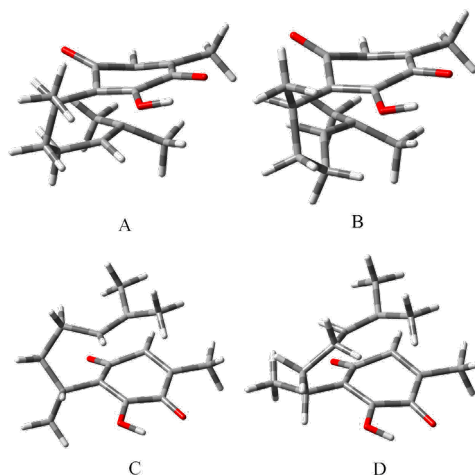


Fig. 3. Geometries of the transition-states **A**, **B** and **C**, **D** of the cycloaddition path to produce α - and β -pipitzols, respectively.

The mere existence of a transition state formally concludes the problem of the existence of the folded conformers of perezona as in this case, it has allowed the characterization of the four transition states associated with the formation of the four possible pipitzol diastereoisomers. On a surface of any nature, (potential energy in this case, and electron density or coulombic potential as an example), the existence of a point of (3, -1) curvature, (associable with a transition state) in which two curvatures are negative and one positive, the energy reaches a maximum within the plane defined by the corresponding axes and a minimum along the third axis which, is perpendicular to the previous plane. The existence of a transition state is a necessary and sufficient condition for the associated minima and maxima to exist, regardless of its vibrational nature.

The forming sigma bond distances and the pyramidalization (Δ) of the involved carbon atoms are presented in Table 1. In the transition state that leads to the formation of *exo*- β -pipitzol, the C2-C12 bond distance is the largest in all cases (see entry C, Table 1), while C6-C13 is the shortest. A larger bond could diminish the angular strain and allow for a more synchronous approximation of the two olefin carbon atoms towards the quinone center, affecting the experimented vibrational degrees of freedom. This can be understood in terms of the greater participation of the second bond in the stability (or the shorter length of the C6-C13 bond).

Table 1. Bond distances (\AA) and pyramidalization (Δ , in \AA) are associated to the formation of C2-C12 and C6-C13 bonds in their transition states.

Structure	DC ₂ -C ₁₂	DC ₆ -C ₁₃	Δ C ₂	Δ C ₁₂	Δ C ₆	Δ C ₁₃
A α -Exo	1.9956	2.1305	0.20378	0.12886	0.21279	0.17533
B α -Endo	2.0164	2.0856	0.15240	0.14404	0.18772	0.16608
C β -Exo	2.1398	2.0070	0.17319	0.12073	0.17573	0.14644
D β -Endo	1.9899	2.0946	0.14741	0.13233	0.16969	0.14645

Table 2 shows the energy parameters for the formation of the four possible products of cycloaddition using tetralin as an implicit solvent.[1] In terms of the stability of the adducts, the transition states that lead to the *exo* isomers are *ca.* 6.0 kcal/mol more stable than the *endo* ones, being enthalpy as the major contributor term. The angular strain on *endo* products, causes a stability loss reflected mainly on the enthalpic term, with values matching the T Δ S term (T = 480 K), while for the *exo* products the T Δ S term represents 40 % of the enthalpy value. Lastly, the *exo* adduct derived α - and β -pipitzols are 10.8 and 11.8 kcal/mol more stable with respect to their parent conformer.

Table 2. Kinetic and thermodynamic data for intramolecular cycloaddition [5 + 2] of perezona at 480 K, 1 atm and tetralin dielectric constant. The free energy (G) and enthalpy (H) values are in kcal/mol while those of entropy (S) are in cal/K·mol.

Reaction*	Kinetic data			Thermodynamic data		
	ΔH^\ddagger	ΔS^\ddagger	ΔG^\ddagger	ΔH°	ΔS°	ΔG°
A α -Exo	30.4	-14.5	37.4	-18.0	-15.0	-10.8
B α -Endo	36.6	-15.2	43.8	-7.4	-17.2	0.8
C β -Exo	32.5	-11.8	38.2	-19.0	-15.3	-11.8
D β -Endo	38.6	-12.3	44.4	-7.3	-12.9	-1.1

See Fig. 2

Data presented in Fig. 4, allowed us to quickly conclude on why, neither α - nor β - adducts generated by the side chain *endo* approximation have ever been observed. The activation energy for the former is 6.5 kcal/mol while for the latter is 6.3 kcal/mol higher with respect to the corresponding transition states for the formation of *exo* products. The formation of β -pipitzol requires overpassing an activation energy barrier of $\Delta G^\ddagger = 37.4$ kcal/mol, while for α -pipitzol this energy is of 38.3 kcal/mol. Therefore, a resulting energy difference of $\Delta\Delta G^\ddagger = 0.8$ kcal/mol led to an approximate proportion of 70/30. [23]

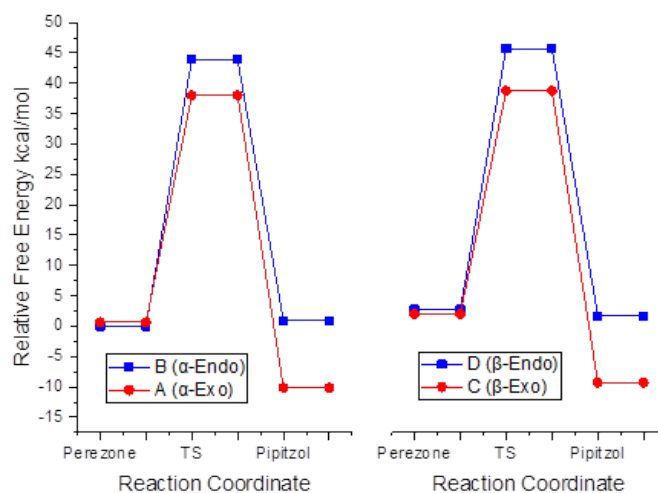


Fig. 4. Intramolecular [5+2] cycloaddition paths of perezone to produce α - and β -pipitzols at M06–2X/6-311++G(2d,2p) level of theory in tetralin as implicit solvent.

Activation enthalpy favors the formation of stable *exo* adducts, since angular strain is larger in *endo* adducts. Selectivity towards *exo* adducts can be explained in terms of steric compression. Careful observation of the *endo* adducts allows to identify a severe deformation in the environment at C12 carbon. The steric demand that the five-membered ring closure requires is responsible for hindering the *endo* isomers formation. These isomers have not been observed, not even by heating methods in which the vibrationally excited states would be feasible, as it has been proposed as mechanisms without the existence of folded conformers. [24]

The sigma bond formation process is asynchronous since the C2-C12 bond is shorter than the C6-C13 one and the stability of C13 is attributable to its tertiary carbocation character. Nevertheless, the pyramidization degree is larger on C6 than C2, as it is with the C13 and C12 pair, probably originated from the intense angular tension upon the formation of the second bond and the bicycle closure.

The stability of C13 is originated as well by the hyperconjugation arising from two vicinal hydrogen atoms oriented in such a way that σ_{C-H} is held perpendicular to the carbon atom plane. The hyperconjugation contribution to stability is not ideal since C13 has a certain degree of pyramidization.

The approximation of the lateral chain towards the quinone group is defined by the dihedral angle C1-C2-C8-C18, with values of 98.1° and 52.0° for the transition states of *exo* adducts A and C (which lead to the formation of α - and β -pipitzol), respectively and the *endo* adducts with values of 129.4° and 122.4° for B and D, respectively (Table 1). The lateral chain folding entails the consecutive *gauche* conformation along that segment, with an ideal dihedral angle of 60°. In this regard, the *endo* transition states show an intense twisting concerning *exo* ones. The C2-C8-C10-C12 dihedral angle has values of 30.8° and 30.5° for A and C, respectively and 24.5° and 12.4° for *endo* B and D transition states, respectively. Nevertheless, the C8-C10-C11-C12 segment has a more relaxed geometry in transition state A of 56.6°, while the same

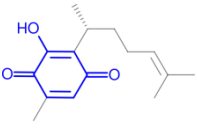
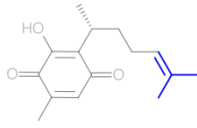
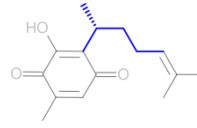
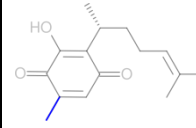
segment in transition state C shows a high degree of eclipsed conformation with a value of 3.9°. The same segment on B and D transition states show dihedral angles of 19.9° and 30.2° revealing the angular tension generated on these systems. Finally, the *endo* and *exo* orientations are described by the C10-C11-C12-C13 dihedral angle which has values of 152.5°, 133.4°, 157.6° and 160.5° for A, C, B and D transition states, respectively.

Topological analysis of the electron density

According to Professor Houk intermolecular interactions as well as deformations experimented by the reacting fragments in transition states determine both the favored products and the activation energies.[25] Since the fragments involved in the formation of pipitzols belong to the same molecule, carrying out deformation energy analysis is not possible. Instead, it was decided to obtain atomic properties under the framework of Bader's Quantum Theory of Atoms in Molecules (QTAIM).[26,27]

Table 3 shows the energetic differences corresponding to the evolution of 4 fragments of perezone: (F1) the quinoid ring, (F2) the isopropenyl group (F3) the alkyl chain bonding the first two, and (F4) the methyl group. The process comprises the change of the reagents to the corresponding transition states. This data indicates the isopropenyl group is responsible for the increase in energy required to reach the transition states of the 4 isomers. Charge transfer to the quinoid ring and pyramidalization accounts for the destabilization. The reduction in stability of F2 is compensated by the quinoid ring, which is increasingly stabilized when F2 approximates in *endo* fashion. The *exo* configuration, observed experimentally, is explained by the contributions of F3, since the steric compression which deforms the fragment is decisive as for the *exo* conformers, F3 is strongly stabilizing with contributions of -11.67 and -11.60 kcal/mol for the α - and β conformers respectively. The α -*endo* conformer is destabilizing with a contribution of 6.33 kcal/mol (18.00 kcal/mol overall with respect to the α -*exo* isomer). β -*endo* contribution of -2.64 kcal/mol is only slightly stabilizing. Hence, the steric compression of the lateral chain is decisive for the stereoselectivity of the *exo* isomers over the *endo*.

Table 3. Change in Potential Energy related to four fragments of perezone. Values in kcal/mol. (F indicates fragment)

					
	$\Delta\epsilon^\ddagger(\mathbf{F1})$	$\Delta\epsilon^\ddagger(\mathbf{F2})$	$\Delta\epsilon^\ddagger(\mathbf{F3})$	$\Delta\epsilon^\ddagger(\mathbf{F4})$	$\Delta\epsilon^\ddagger$
A α -Exo	-19.54	69.82	-11.67	-8.84	29.77
B α -Endo	-25.67	64.83	6.33	-6.65	38.85
C β -Exo	-19.57	70.15	-11.60	-9.24	29.74
D β -Endo	-25.10	72.22	-2.64	-6.36	38.12

Experimentally, the formation of α -pipitzol is similar to the formation of the β -isomer, in that the two adducts are obtained in the same proportion. The contributions to free energy show this behavior has its origin in the activation enthalpy, since in all cases the activation entropy maintains similar values and points towards the decrease of the well-known degrees of freedom common to cycloaddition reactions. Additionally, entropy is highly relevant for α -isomers with respect to β -isomers.

To study the influence of the steric clash as the energy barrier of the compounds studied here, a calculation of the non-covalent interactions (NCI) based on the reduced density gradient $s(r)$ was performed.

$$s(r) = \frac{1}{2(3\pi^2)^{1/3}} \frac{|\vec{\nabla}\rho(R)|}{\rho(r)^{4/3}}$$

The reduced density gradient $s(r)$ is a dimensionless quantity especially suited to identify noncovalent interactions that show the inhomogeneity of the electronic density. The capability of $s(r)$ to recognize chemical hallmarks is reflected by the positions of its critical points (CP). The CP in $s(r)$ is located at critical points in the electron density ($\nabla\rho(r)=0$), and at points where a complex balance between $\rho(r)$ and von Weizsäcker kinetic exists.[28] The latter are blind to QTAIM theory and correspond to intramolecular weak interactions. In this approach, the classification of the NCI is done in terms of the maximum variations in the contributions to the Laplacian, along with the axes, corresponding to the eigenvalues (λ_i) of the electron-density Hessian matrix. The sign of λ_2 enables us to distinguish between the different types of weak interactions, attractive and repulsive (such as steric repulsions), while the electron density lets us assess the interaction strength. To gain a deeper understanding of factors controlling the selectivity trends, we performed an analysis of NCI in TSs based on the study of the density reduced gradient.

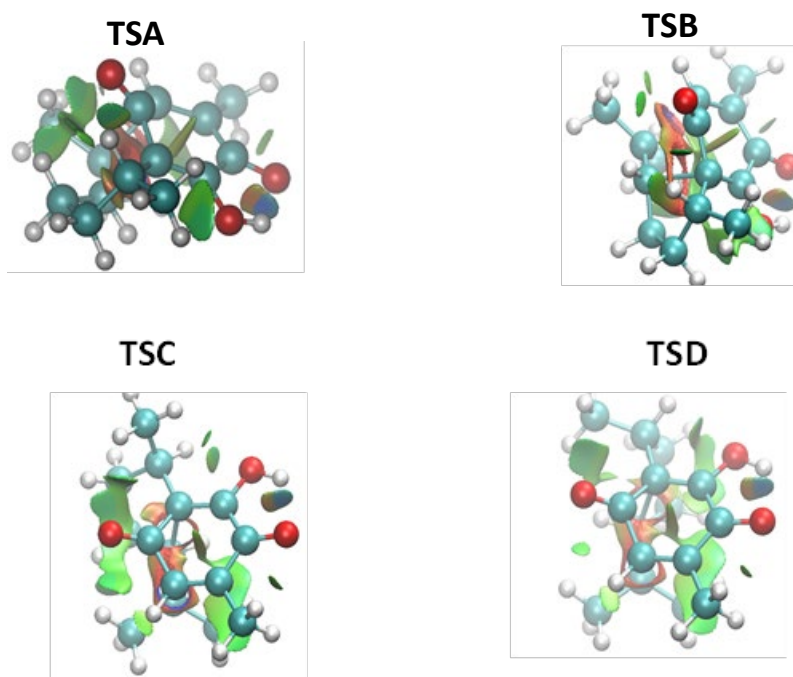


Fig. 5. Low gradient isosurfaces ($s=0.5$ u.a.) for the TS's in the thermal reaction.

Firstly, we considered the *endo-exo* selectivity in the thermal reaction to prove if the steric compression of the lateral chain is decisive for the stereoselectivity of the *exo* isomers over the *endo*, as is suggested by the atomic properties calculated using QTAIM.

Fig. 5 collects NCI surfaces of TSA, TSB, TSC, and TSD. We can observe a complicated group of NCI surfaces, where bicolored isosurfaces appear reflecting stabilizing features counter-balanced by destabilizing interactions due to steric crowding. Due to this complexity, it is not possible to point out that NCI is the cause of the observed selectivity. Therefore, we have performed an integration of the electronic density in NCI. The integration of the electronic density in volume elements, defined by $\text{sign}(\lambda_2)\rho$ ranges, has been proved to be a useful tool for the estimation of the strength of the NCI. [29] We performed the

integration of ρ in two ranges, corresponding to attractive ($-0.05 \leq \text{sign}(\lambda^2)\rho \leq 0.00$) and the repulsive ones ($0.00 \leq \text{sign}(\lambda^2)\rho \leq 0.05$). The results are depicted in Table 4.

Table 4. Repulsive and attractive electronic density integrals and their difference for TSs in the thermal reaction.

	$\iiint_{NCI} \rho(r) d\mathbf{v}$	
	Attractive	Repulsive
TSA	0.39	4.66
TSB	0.35	4.68
TSC	0.37	4.66
TSD	0.37	4.72

Analyzing the integral values for TSA and TSB in **Table 4**, it is clear that the attractive and repulsive NCI seems to govern the *endo-exo* selectivity. TSA presents the higher value of attractive NCI where the difference relative to TSB is equal to 0.04 u.a. On the other hand, the repulsive NCI integrals in the TSB are slightly higher than in the TSA case by 0.02 u.a. Therefore, we can conclude that both sorts of interaction lead the *exo* approximation as the preferred one. That is, in the *exo* TS the attractive NCI are maximized whereas the repulsive ones are slightly alleviated.

In the β -piperizol case, the density integral values show that TSC present less steric repulsion than TSD with a difference of 0.06 u.a., whereas the value of the attractive density integral are the same. Therefore, these results allowed us to conclude that the *exo* preference in this instance is explained by the less steric hindrance in the *exo* approximation.

Methodology

All electronic structure calculations were performed under the Density Functional Theory (DFT) methodology, implemented in Gaussian09 software. [29] The stationary state geometries (reactants, transition states and products) were optimized using the meta-GGA M06-2X hybrid functional with the 6-311++G(2d,2p) Pople basis set; containing divided triple zeta valence and polarization functions on light and heavy atoms. M06-2x functional was employed since it has been recommended to study kinetics and thermochemical properties.[31] The geometry optimizations were carried out considering implicit solvent effects calculated with the SMD model along with the UAHF molecular cavity; tetraline solvent was employed for the thermal mechanism, while dichloromethane for the catalyzed mechanisms. Normal modes of vibration analysis allowed us to determine the nature of the stationary transition states (TS and energy minima displayed one and zero frequencies, respectively). Zero-point vibrational energy (ZPVE) and thermal corrections at 480 K (experimental conditions reported by J. Romo and coworkers[2] for the thermal mechanism). The intrinsic reaction coordinate (IRC) mapping was conducted in order to corroborate that transition structures were connecting the proposed minima. Changes in potential energy related to the different fragments of perezone were obtained through the topological analysis of the electron density of perezone using AIMAll software.[32] The NCI calculations were performed by means of a NCIPLLOT4 program,[29] and the resulting isosurfaces were visualized with the Visual Molecular Dynamics (VMD) software[34] following the next colour code: blue for attractive interactions, green for dispersive interactions (attractive or repulsive) and red for repulsive interactions.

Conclusions

Studying the concerted mechanism of perezzone transformation in to pipitzols, it is feasible to explain why only products originated from the *exo* approximation of the lateral chain have been described in the literature. The employed computational methodology at the M06-2X/6-311++G(2d,2p) level of theory allows establishing the selectivity of the reaction and the origin of the isotopic labelling distribution observed in the thermic process. The formation of *exo*-isomers with respect to the *endo* has its origin in the conformational arrangement of the side chain, which undergoes severe steric compression in the second case.

Acknowledgements

The authors are grateful to Gladys Cortés Romero and María Magdalena Aguilar Araiza, for technical assistance, we also thank the Dirección de Cómputo y de Tecnologías de Información y Comunicación of the Universidad Nacional Autónoma de México, via the grant LANCAD-UNAM-DGTIC-094, and to the Dirección General de Asuntos del Personal Académico (DGAPA) via grants No. IN-205620 and IN-208623. E R-L and FMSS. We are grateful to the Mexican Consejo Nacional de Ciencia y Tecnología (CONACYT) for the scholarship granted and also MM is grateful to the Sistema Nacional de Investigadores for sponsorship.

References

1. Walls, F.; Padilla, J.; Joseph-Nathan, P.; Giral, F.; Romo, J. *Tetrahedron Lett.* **1965**, 1577-1582. DOI: [https://doi.org/10.1016/S0040-4039\(01\)84094-6](https://doi.org/10.1016/S0040-4039(01)84094-6).
2. Walls, F.; Padilla, J.; Joseph-Nathan, P.; Giral, F.; Escobar, M.; Romo, J. *Tetrahedron.* **1966**, 22, 2387-2399. DOI: [https://doi.org/10.1016/S0040-4020\(01\)82159-1](https://doi.org/10.1016/S0040-4020(01)82159-1).
3. Evans, S.V.; Yee, V.C.; García-Garibay, M.A.; Trotter, J. *Acta Cryst.* **1994**, C50, 278-281. DOI: <https://doi.org/10.1107/S0108270193009060>.
4. Ylijoki, K.E.O.; Stryker, J.M. *Chem Rev.* **2013**, 113, 2244-2266. DOI: <https://doi.org/10.1021/cr300087g>.
5. Weld, M.C. *Ann. Ueber die Pipitzahöinsäure, eineneigenthümlichen Pflanzenstoff*, **1855**, 95, 188-192. DOI: <https://doi.org/10.1002/jlac.18550950205>.
6. Ortiz-Reynoso, M.; Cuevas González-Bravo G. E. *History of Pharmacy and Pharmaceuticals.* **2022**, 64, 154-186. DOI: <https://doi.org/10.3368/hopp.64.2.154>.
7. Rio de la Loza, L.; *Discurso pronunciado por el catedrático de Química Médica de la Escuela de Medicina el Noviembre 23, 1852. Periódico de la Escuela de Medicina.* **1853**, 1, 131-137.
8. a) Pérez, S. *Remitido. La Unión Médica.* **1857**, 2, 44-46. b) Jonás, A. *La Farmacia. En la Exposición Internacional de Filadelfia. Semanario Farmacéutico.* **1877**, 6, 5764.
9. Pérez, S. *La Farmacia.* **1890**, 1, No. 7. 101-107.
10. Remfry, F.G.P. *CXVI-Perezzone. J. Chem. Soc.* **1913**, 103, 1076-1088. DOI: <https://doi.org/10.1039/CT9130301076>.
11. Kögl, F.; Boer, A. G. *Rec. Trav. Chim.* **1935**, 54, 779-794. DOI:10.1002/recl.19350541005
12. Walls, F.; Salmón, M.; Padilla, J.; Joseph-Nathan, P.; Romo, J. *Bol. Inst. Quím. Univ. Nac. Auton. Mex.* **1965**, 17, 3-15.
13. Archer, D.A.; Thomson, R.H. *J. Chem. Soc. Chem. Commun.* **1965**, 354-355. DOI: <https://doi.org/10.1039/C19650000354>.
14. Bates, R.B.; Paknikar, S.K.; Thalacker, V.P. *Chem & Ind.* **1965**, 1793.
15. Wagner, E.R.; Moss, R.D.; Brooker, R.M. *Tet. Lett.* **1965**, 47, 4233-4239. DOI: [https://doi.org/10.1016/S0040-4039\(01\)89113-9](https://doi.org/10.1016/S0040-4039(01)89113-9).

16. a) Cortés, E.; Salmón, M.; Walls, F. *Bol. Inst. Quim. Univ. Nal. Autón. Méx.* **1965**, *17*, 19-33. b) Sánchez, I. H.; Larraza, M. I.; Basurto, F.; Yañez, R.; Avila, S.; Tovar, R.; Joseph-Nathan, P. *Tetrahedron*. **1985**, *41*, 2355-2359. DOI: [https://doi.org/10.1016/S0040-4020\(01\)96630-X](https://doi.org/10.1016/S0040-4020(01)96630-X).
17. Joseph-Nathan, P.; Mendoza, V.; García, E. *Tetrahedron*. **1977**, *33*, 1573-1576. DOI: [https://doi.org/10.1016/0040-4020\(77\)80163-4](https://doi.org/10.1016/0040-4020(77)80163-4).
18. Woodward, R.B.; Hoffman, R. in: *The Conservation of Orbital Symmetry*, Academic Press, New York, **1970**, 87. DOI: <https://doi.org/10.1002/anie.196907811>.
19. Barquera-Lozada, J.E.; Cuevas, G. *J. Org. Chem.* **2009**, *74*, 874-883. DOI: <https://doi.org/10.1021/jo802445n>.
20. Barquera-Lozada, J.E.; Quiroz-García B.; Quijano, L.; Cuevas, G. *J. Org. Chem.* **2010**, *75*, 2139-2146. DOI: <https://doi.org/10.1021/jo902170w>.
21. Aguilar-Martínez, M.; Bautista-Martínez, J. A.; Macías-Ruvalcaba, N.; González, I.; Tovar, E.; Marín del Alizal, T.; Collera, O.; Cuevas, G. *J. Org. Chem.* **2001**, *66*, 8349-8363. DOI: <https://doi.org/10.1021/jo010302z>.
22. Joseph-Nathan, P. in: *El deuterio, mi pequeño y valioso ayudante para estudiar productos naturales*, en Paredes-López, O.; Estrada-Orihuela, S (eds.) *Aportaciones científicas y humanísticas mexicanas en el siglo XX*. Fondo de Cultura Económica. **2008**, 435.
23. Lowry, T.H.; Richardson, K.S. in: *Mechanism and Theory in Organic Chemistry*, 2a. Ed., Harper & Row: New York. **1976**.
24. Zepeda, L.G.; Burgueño-Tapia, E.; Pérez-Hernández, N.; Cuevas, G.; Joseph-Nathan, P. *Reson. Chem.* **2013**, *51*, 245-250. DOI: <https://doi.org/10.1002/mrc.3940>.
25. Liu, F.; Paton, R.S.; Kim, S.; Liang, Y.; Houk, K.N. *J. Am. Chem. Soc.* **2013**, *135*, 15642–15649. DOI: <https://doi.org/10.1021/ja408437u>.
26. Bader, R. F. W. in: *Atoms in Molecules. A Quantum Theory*; Clarendon Press. Oxford, **1990**.
27. Keith, T.A., Version (13.11.04), TK Gristmill Software, Overlan, Oveland Park KS, USA **2013**.(aim.tkgristmill.com).
28. Joseph R. Lane, J. C.-G.; Piquemal, J.-P.; Miller, B. J.; Kjaergaard, H. G. *J. Chem. Theory Comput.* **2013**, *9*, 3263-3266. DOI: <https://doi.org/10.1021/ct400420r>.
29. Boto, R.A.; Peccati, F.; Laplaza, R.; Quan, C.; Carbone, A.; Piquemal, J.-P.; Maday, Y.; Contreras-García, J. *J. Chem. Theory Comput.* **2020**, *7*, 4150-4158. DOI: <https://doi.org/10.1021/acs.jctc.0c00063>.
30. Frisch, M.J.; Trucks, G. W.; Schlegel, H. B.; Scuseria, G. E.; Robb, M. A.; Cheeseman, J. R.; Scalmani G.; Barone, V.; Mennucci, B.; Petersson, G. A.; Nakatsuji, H.; Caricato, M. ; Li, X.; Hratchian, H. P.; Izmaylov, A. F.; Bloino, J.; Zheng, G.; Sonnenberg, J. L.; Hada, M.; Ehara, M.; Toyota, K.; Fukuda, R.; Hasegawa, J.; Ishida, M.; Nakajima, T.; Honda, Y.; Kitao, O.; Nakai, H.; Vreven, T.; Montgomery, J. A.; Peralta, J. E.; Ogliaro, F.; Bearpark M.; Heyd, J. J.; Brothers, E.; Kudin, K. N.; Staroverov, V. N.; Keith, T.; Kobayashi, R.; Normand, J.; Raghavachari, K.; Rendell, A.; Burant, J. C.; Iyengar, S. S.; Tomasi, J.; Cossi, M.; Rega, N.; Millam, J. M.; Klene, M.; Knox, J. E.; Cross, J. B.; Bakken, V.; Adamo, C.; Jaramillo, J.; Gomperts, R.; Stratmann, R. E.; Yazyev, O.; Austin, A. J.; Cammi, R.; Pomelli, C.; Ochterski, J. W.; Martin, R. L.; Morokuma, K.; Zakrzewski, V. G.; Voth, G. A.; Salvador, P.; Dannenberg, J. J.; Dapprich, S.; Daniels, A. D.; Farkas, O.; Foresman, J. B.; Ortiz, J. V.; Cioslowski, J.; Fox, D. J. *Gaussian 09*, Revision D.01, Gaussian, Inc., Wallingford CT, **2013**.
31. Zhao, Y.; Truhlar, D.G. *Acc. Chem. Res.* **2008**, *41* 157–167; DOI: <https://doi.org/10.1021/ar700111a>
32. Sánchez, I. H.; Yañez, R.; Enríquez, R. *J. Org. Chem.* **1981**, *46*, 2818-2819. DOI: <https://doi.org/10.1021/jo00326a052>.
33. Sánchez, I.H.; Basurto, F.; Joseph-Nathan, P. *J. Nat Prod.* **1984**, *47*, 382-383. DOI: <https://doi.org/10.1021/np50032a027>.
34. Humphrey, W.; Dalke, A.; Schulten, K. *J. Mol. Graphics.* **1996**, *14*, 33–38. DOI: [https://doi.org/10.1016/0263-7855\(96\)00018-5](https://doi.org/10.1016/0263-7855(96)00018-5).

DFT and Molecular Docking Studies of Melatonin and Some Analogues Interaction with Xanthine Oxidase as a Possible Antiradical Mechanism

Brenda Manzanilla, Minerva Martinez-Alfaro, Juvencio Robles *

Departamento de Farmacia, DCNE, Universidad de Guanajuato, Noria Alta S/N. Col. Noria Alta, C. P. 36050, Guanajuato, Gto., México.

*Corresponding author: Juvencio Robles, email: roblesj@ugto.mx

Received May 28th, 2023; Accepted July 14th, 2023.

DOI: <http://dx.doi.org/10.29356/jmcs.v68i1.2072>

This article is fondly and respectfully dedicated to Prof. Joaquín Tamariz, a great Companion in the Road, celebrating his retirement after a very enriching career.

Abstract. Melatonin (Mel) and some of its active metabolites such as N1-acetyl-5-methoxykynuramine (AMK), N1-acetyl-N2-formyl-5-methoxykynuramine (AFMK), 6-hydroxymelatonin (6OHM), and the analogues **Ir** and **It** recently designed by Galano's group, have been studied within density functional theory (DFT). The purpose is to evaluate some plausible mechanisms of action of melatonin's metabolites and analogues with the free radicals (FR): OH^{\bullet} , NO_2^{\bullet} , HOO^{\bullet} , and CH_3O^{\bullet} . We calculated global chemical reactivity descriptors from conceptual DFT to evaluate their antiradical properties. We used water and pentyl ethanoate as solvents to simulate the physiological conditions, modeled via the continuum solvation model based on density (SMD). We assess the following plausible mechanisms: single electrons transfer (SET), hydrogen atom transfer (HAT) and xanthine oxidase (XO) inhibition. We performed our calculations at the M06-2X/6-31+G* level of theory. The results indicate that Mel, AMK, AFMK, 6OHM, It, and Ir are good antiradicals towards the FRs: NO_2^{\bullet} and CH_3O^{\bullet} , while It and Ir could be suitable XO inhibitors.

Keywords: Antiradical properties; Density Functional Theory; melatonin; xanthine oxidase; molecular docking.

Resumen. La melatonina (Mel) y algunos de sus metabolitos activos como N1-acetil-5-metoxiquinuramina (AMK), N1-acetil-N2-formil-5-metoxiquinuramina (AFMK), 6-hidroximelatonina (6OHM) y los análogos **Ir** e **It**, diseñados recientemente por el grupo de Galano, han sido estudiados con la teoría de funcionales de la densidad (DFT). El propósito es evaluar algunos mecanismos de acción plausibles de los metabolitos y análogos de la melatonina con los radicales libres (FR): OH^{\bullet} , NO_2^{\bullet} , HOO^{\bullet} , y CH_3O^{\bullet} . Calculamos los descriptores de reactividad química global a partir de DFT conceptual para evaluar sus propiedades antirradicales. Usamos agua y etanoato de pentilo como solventes para simular las condiciones fisiológicas, modeladas a través del modelo continuo de solvatación basado en la densidad (SMD). Evaluamos los siguientes mecanismos plausibles: transferencia de electrones individuales (SET), transferencia de átomos de hidrógeno (HAT) e inhibición de la xantina oxidasa (XO). Realizamos nuestros cálculos al nivel de teoría M06-2X/6-31+G*. Los resultados indican que Mel, AMK, AFMK, 6OHM, It e Ir son buenos antirradicales frente a los FRs: NO_2^{\bullet} y CH_3O^{\bullet} , mientras que It e Ir podrían ser inhibidores adecuados de XO.

Palabras clave: Propiedades antirradicales; teoría de funcionales de la densidad; melatonina; xantina oxidasa; acoplamiento molecular.

Introduction

Reactive oxygen species (ROS) and reactive nitrogen species (RNS), namely free radicals (FRs), are continuously generated in typical biological systems by enzymes like xanthine oxidase (XO) [1, 2]. However, high levels of FRs are associated with increased oxidative stress (OS) [3]. Then, the inappropriate scavenging or inhibition of FRs has been linked with aging, inflammatory disorders, and chronic diseases [4, 5]. Nevertheless, antiradicals (ARs) molecules can interact with FRs and terminate their chain reaction by different mechanisms to prevent OS [5–7]. There is evidence that melatonin and related compounds are efficient as ARs [8–11]. The literature has extensively studied the role of melatonin (Mel) and its metabolites against OS. The different mechanisms of melatonin and its metabolites have been reported, finding that melatonin metabolites are better antioxidants than melatonin itself [11–16]. In this sense, melatonin derivatives have been sought with better antiradical properties that regenerate, are non-toxic, and do not have pro-oxidant behavior.

Melatonin and metabolites have been studied against ROS by evaluating different mechanisms of action [8, 14]. However, there is no previous research on melatonin's metabolites and analogues to their mode of interaction with FR-producing enzymes, like XO. Mel has been reported as an inhibitor of these types of enzymes by theoretical [17, 18] and experimental works [19–23]. Hence, we propose inhibiting this enzyme by melatonin's metabolites and analogues could considerably reduce oxidative stress in the cell. With this aim, we decided to study Mel, its three active metabolites N1-acetyl-5-methoxy kynuramine (AMK), N1-acetyl-N2-formyl-5-methoxykynuramine (AFMK), 6-hydroxymelatonin (6OHM), and two analogues developed by Galano's group Ir ((E)-1-methyl-3-((2-phenylhydrazine)methyl)-1H-indol-7-ol) and It ((E)-3-((2-(2-fluorophenyl)hydrazine)methyl)-1-methyl-1H-indol-7-ol)) [24,25], (Fig. 1). Moreover, some ARs may exhibit more than one mechanism; they are classified as multifunctional antiradicals [26]. Then, we studied some possible mechanisms such as XO inhibition, single electron transfer (SET), and hydrogen transfer (HAT) with FRs: OH^\bullet , NO_2^\bullet , HOO^\bullet , and CH_3O^\bullet . Previous works studied Mel, 6OHM, AMK, and AFMK interacting with HOO^\bullet , and OH^\bullet through the mechanisms of action SET, HAT, and radical adduct formation [12,14,15,27,28]. Henceforth, we use these results and evaluate the interaction with NO_2^\bullet and CH_3O^\bullet that, as far as we are aware, have not been reported in computational studies for Mel, 6OHM, AMK, AFMK, It, and Ir.

Consequently, we examine the antiradical properties by global chemical reactivity descriptors of Conceptual Density Functional Theory (CDFT) [29] and mechanisms (SET, HAT, and XO inhibition) of Mel, 6OHM, AMK, AFMK, It, and Ir (Fig. 1) using computer-assisted protocols that significantly reduce costs and expedite the process. The search mainly consisted of computing CDFT reactivity descriptors to assess the reactivity properties, log P, solvation free energy, and mechanisms of action of the selected species.

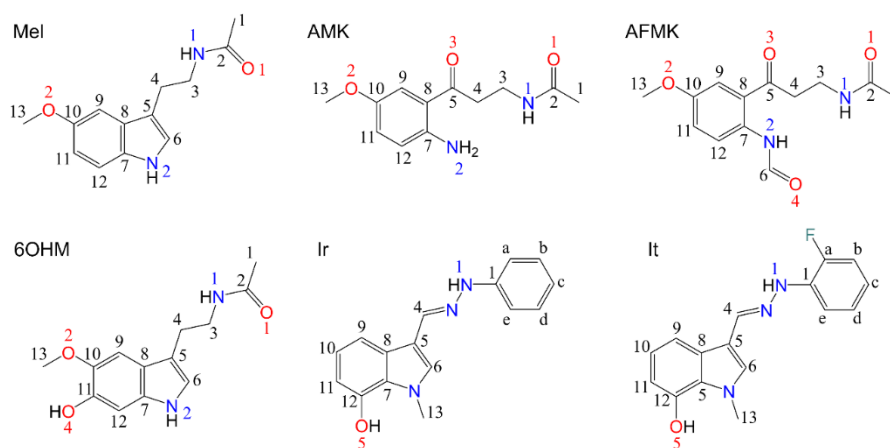


Fig. 1. Chemical structures of Mel and its analogues studied in this work and atom-numbers labels.

Computational methodology

We used Gaussian 09 [30] for the molecular DFT calculations. We performed for each geometry optimization a frequency analysis to properly identify local minima in the potential energy surface (PES). The final M06-2X/6-31+G* level of theory was chosen through calibration and comparison with eight levels of theory. Since the details of the methods used are similar as in our previous work, we refer the reader to it [31]. The calculated ionization potential (I) value was used as a control and compared with the experimental I value of melatonin, 7.70 eV [32]. To simulate aqueous and lipid environments, we use the continuum solvation model based on density (SMD) [33], used to simulate solvent effects (water, $\epsilon = 78.36$ and pentyl ethanoate as a model for lipidic ones, $\epsilon = 4.73$).

Conformers

Initially, a conformational search is done [31,34] with the MMFF force field [35-38]. Although 10,000 conformers are inspected in the search, we select only the lowest-energy ten conformers, with a methodology detailed in our previous work [31], finally reoptimized to the level M06-2X/6-31+G* DFT.

pK_a determination

It is necessary to know the pK_a value to assess the dominant acid/base species at physiological conditions (aqueous phase and average pH=7.4). Therefore, we determine the pK_a values of all computed AR molecules. Since the details of the method used is similar as in our previous work, we refer the reader to it [31,39].

DFT global descriptors

Global CDFT reactivity descriptors [29] were computed to assess the reactivity of the studied molecules towards the FRs. In this work, since the details of the computational methods used are similar as in our previous work, we refer the reader to it [31]. Among them, we computed the vertical ionization energy (I) and the electron affinity (A) [40,41]. Also computed are the electronegativity (χ) [42], chemical hardness (η) [43,44]. Both χ and η were computed with the well-known finite difference approximations. Other calculated descriptors are the electrophilicity index (ω) [45], the electrodonating power index (ω^-), and the electroaccepting power index (ω^+) [46].

Solvation free energy and log P

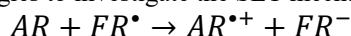
To assess the relative stability of a chemical species in solution respect to the gas phase, we computed the solvation-free Gibbs energy (ΔG_{solv}°) [47]. Thus, we have computed the optimized Gibbs free energies in gas phase (G_{gas}) and in the two solvents: water and pentyl ethanoate ($G_{solvent}$),

$$\Delta G_{solv}^\circ = G_{solvent} - G_{gas}$$

We also used the log P value (octanol/water partition coefficient) to assess the hydrophobicity of compounds and their membrane permeability [48]. The log P value was computed using Spartan 18 [49] with the quantitative structure-activity relationships (QSAR) method of Ghose, Pritchett, and Crippen [50].

Single electron transfer

We used two graphical strategies to investigate the SET mechanism,



One strategy is to calculate the full-electron donor-acceptor map (FEDAM), and the second is the donator-acceptor map (DAM). FEDAM provides information about electron-donor and electron-acceptor behaviors of a given AR molecule [51]. In FEDAM one graphs I versus A to evaluate and characterize the electron-transfer process between AR and FR. The FRs evaluated were: OH^\bullet , NO_2^\bullet , HOO^\bullet , and CH_3O^\bullet . On the

other hand, in DAM one compares different molecules and classifies them according to their electron donating-accepting capacity relative to the F and Na atomic values.

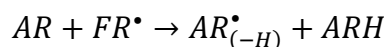
Thus, one graphs the electron acceptance (Rd) versus the electron donation index (Ra), defined as

$$Ra = \frac{\omega_L^+}{\omega_F^+}$$

$$Rd = \frac{\omega_L^-}{\omega_{Na}^-}$$

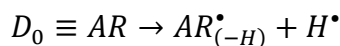
Hydrogen atom transfer

The HAT mechanism, is represented in general by



We studied the HAT mechanism of our selected molecules for the FRs: OH^{\bullet} , NO_2^{\bullet} , HOO^{\bullet} , and CH_3O^{\bullet} . Then, we computed the adiabatic Gibbs free energy for all reactions.

Also, we studied the dissociation energy of one hydrogen atom within the molecule (D_0),



Molecular docking studies

To estimate the XO enzyme inhibition, we performed a flexible Docking study. We used the X-ray structure of Bos Taurus with PDB code: 1FIQ [52], (90 % homology with human XO) at 2.5 Å resolution, cocrystallized with its competitive inhibitor salicylic acid (SAL). We employed the AutoDock Tools package version 1.5.6 and AutoDock 4.2.6 [53]. The protocol we followed was to merge nonpolar hydrogens, add Kollman charges, and use a Lamarckian Genetic Algorithm [54]. The A and B chains of the protein and small molecules were removed except for the molybdopterin cofactor (MTE) and Mo cofactor (MOS) in the C subunit of the XO protein. Since the details of the methods used are similar as in our previous work, we refer the reader to it [31]. All molecular graphics material was processed using the software Discovery Studio [55].

Results and discussion

To perform the calculations of Mel and its active metabolites, we selected the M06-2X/6-31+G* level of theory after assessing the cost/performance in several levels of theory. Since the details of the methods used are similar as in our previous work, we refer the reader to it [31]. We compare the absolute error between calculated I and experimental I , Table 1, where we see that M06-2X/6-31+G* has the second smallest absolute error. As a result, M06-2X/6-31+G* was selected for its low computational cost and similarity to the experimental data. Afterwards, we performed a conformational analysis at the M06-2X/6-31+G* level of theory.

Table 1. Mel vertical ionization energy (eV), at different levels of theory and % absolute error (calculated I vs experimental I).

Level of theory	I	[% Error]
<i>Melatonin</i>		
B3LYP/6-31+G*	7.37	4.3
B3LYP/6-311G**	7.32	5.0
B3LYP/6-311+G*	7.41	3.7
M06-L/6-31G*	6.90	10.3
M06-L/6-31+G*	7.04	8.5
M06/6-31+G*	7.37	4.3
LC- ω PBE/6-31+G*	7.63	0.9
M06-2X/6-31+G*	7.60	1.3
Exp.	7.70	

Conformational search

The conformational analysis shows the most stable and thermodynamically more favorable conformers. Some of them have intra-molecular hydrogen bonds, Fig. 2; this may cause the highest value of D_0 and ΔG in HAT mechanism and, consequently, the lowest antioxidant potential. Then, Mel does not show any hydrogen bond in water and pentyl ethanoate, but noteworthy, the alkyl chain interacts with the benzene ring. AMK has one strong hydrogen bond between the amine and the ketone groups in both solvents. AFMK has one strong hydrogen bond and one weak hydrogen bond, where the hydrogens of the amine groups require more energy to be removed. Similarly, 6OHM has one strong hydrogen bond between the alcohol and ether groups.

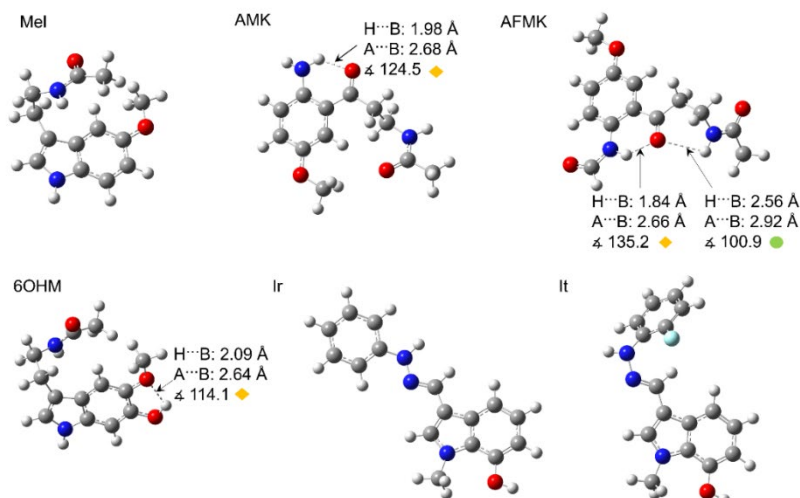


Fig. 2. Optimized geometries of Mel and its analogues in the water phase (same in pentyl ethanoate). Arrows indicate the hydrogen bonds with geometric parameter values. The colored circles and rhombuses indicate the types of hydrogen bonds formed, where yellow rhombuses show strong hydrogen bonds, and green circles show weak hydrogen bonds. Distances are reported in Å.

pK_a calculation

The pK_a values of Mel and its derivatives are displayed in Table 2, together with the corresponding molar fractions at physiological pH (7.4). Table 2 shows that the dominant species at physiological pH are neutral molecules. Consequently, all the molecules were computed in their neutral forms. Previous works report the pK_a value of Mel, AMK, AFMK, and 6OHM; see Table 2. However, in this work, the pK_a values of It and Ir were obtained using the direct method of the proton exchange scheme, cycle A [39] in this work. It is well known that cycle A is not very accurate for proton exchange schemes, but our results agree with experimental results, which is sufficient for the scope of this work.

Table 2. First pK_a values and molar fraction calculated of the neutral (mf_{neutral}) and anionic (mf_{anion}) species at pH=7.4 for Mel and its derivatives at 1 M standard state.

Molecule	pK _a	mf_{neutral}	mf_{anion}	Ref.
Mel	12.3	~1.00	0.00	[56]
AMK	16.8	~1.00	0.00	[14]
AFMK	8.7	0.95	0.05	[14]
6OHM	9.4	0.99	0.01	[12]
It	19.2	~1.00	0.00	This work
Ir	22.5	~1.00	0.00	This work

Global descriptors

Our study of the reactivity of Mel and analogues has been performed by determining the global DFT reactivity descriptors, Table 3. We find that the analogues Ir and It have good antiradical activity. Furthermore, we found that Mel and analogues are more reactive in water than in pentyl ethanoate. We can see the order of molecules with the lower values of I is as follows: Ir<It<6OHM<AFMK<Mel<AMK. A lower I means a higher probability of losing an electron, thus Ir and It have higher capability for donating an electron to FRs. These results agree with the previous work of Galano [57]. In addition, we compared the molecules with lower values of A which may be ordered accordingly as: 6OHM<Mel<It<Ir<AFMK<AMK. A higher value of A means a higher capability for gaining an electron, so AFMK and AMK can accept an electron more easily from FRs.

Furthermore, a lower value of η means low resistance to change in electron number or towards deformation of the electron cloud (higher values of η for more stable molecules). Thus, molecules with lower values of η have the following order: AFMK<Ir<AMK<It<6OHM<Mel. Additionally, lower values mean they are more proficient in giving away electrons than capturing them. The less electronegative molecules follow the order Ir<6OHM<It<Mel<AFMK<AMK. Hence, Ir and 6OHM can donate one electron more easily.

Meanwhile, the value of ω shows that all the molecules in water except 6OHM are strong electrophiles, according to Domingo et al. [58]. These authors established an electrophilicity scale for the classification of organic molecules, defining as strong electrophiles those with $\omega > 1.5$ eV, moderate electrophiles with $0.8 < \omega < 1.5$ eV, and marginal electrophiles with $\omega < 0.8$ eV. Our molecules with the lower values of ω have the following order 6OHM<Mel<It<Ir<AFMK<AMK, where molecules with a lower value of ω are expected to be efficient for scavenging free radicals via electron transfer. Also, we see molecules with the highest value of ω^+ display the following order AMK>AFMK>Ir>It>Mel>6OHM. A higher value of ω^+ means a higher probability to accept charge; thus, AFMK and AMK can accept charge more easily. Molecules with lower values of ω^- display this trend: 6OHM<Mel<It<Ir<AFMK<AMK. Where, the lower value of ω^- means a higher probability to donate charge to FRs, i. e. 6OHM and Mel can donate charge more easily. This trend was also observed in the pentyl ethanoate phase.

Table 3. Global DFT descriptors values in eV for Mel and analogues at M06-2X/6-31+G*/SMD level of theory, in water and pentyl ethanoate phases.

	Mel	AMK	AFMK	6OHM	It	Ir
<i>I</i>	5.68 ^a 6.04 ^b	6.11 ^a 6.50 ^b	5.55 ^a 5.80 ^b	5.48 ^a 5.83 ^b	5.35 ^a 5.78 ^b	5.08 ^a 5.5 ^b
<i>A</i>	0.88 ^a 0.36 ^b	2.34 ^a 1.81 ^b	2.10 ^a 1.35 ^b	0.74 ^a 0.19 ^b	1.21 ^a 0.72 ^b	1.33 ^a 0.89 ^b
χ	3.28 ^a 3.20 ^b	4.23 ^a 4.16 ^b	3.82 ^a 3.58 ^b	3.11 ^a 3.01 ^b	3.28 ^a 3.25 ^b	3.21 ^a 3.20 ^b
η	4.80 ^a 5.67 ^b	3.76 ^a 4.68 ^b	3.45 ^a 4.45 ^b	4.74 ^a 5.64 ^b	4.14 ^a 5.06 ^b	3.75 ^a 4.62 ^b
ω	1.12 ^a 0.90 ^b	2.37 ^a 1.84 ^b	2.12 ^a 1.44 ^b	1.02 ^a 0.80 ^b	1.30 ^a 1.05 ^b	1.37 ^a 1.10 ^b
ω^+	0.90 ^a 0.56 ^b	2.87 ^a 1.90 ^b	2.54 ^a 1.37 ^b	0.78 ^a 0.46 ^b	1.22 ^a 0.78 ^b	1.37 ^a 0.90 ^b
ω^-	4.18 ^a 3.76 ^b	7.09 ^a 6.06 ^b	6.36 ^a 4.94 ^b	3.89 ^a 3.47 ^b	4.50 ^a 4.03 ^b	4.58 ^a 4.10 ^b

^awater^bpentyl ethanoate

Solvation free energy and log P

We found that melatonin and its metabolites can be classified as amphiphilic, while It and Ir are lipophilic molecules according to their log *P* values; see Table 4. Compounds can be classified as highly lipophilic with a value of log *P* > 6 (i. e. vitamin E and vitamin A); very hydrophilic with log *P* < -3 (i. e. vitamin C); and amphiphilic with a log *P* between -1 and 2 (i. e. melatonin) [59]. Although the value of ΔG_{sol}° indicates greater solubility in water, this may be due to the difference in solvents used to represent the lipid layer. The hydrophobicity of antiradicals helps passive transport through cell membranes. As a result, these molecules will cross the cell membrane more easily; because they are not very lipophilic, they do not tend to bioaccumulate.

Table 4. log *P* value and solvation free energy (ΔG_{sol}) values in water ($\Delta G_{sol,w}$) and pentyl ethanoate ($\Delta G_{sol,p}$) of each studied molecule at the M06-2X/6-31+G*/SMD level of theory.

Molecule	log <i>P</i> ^a	log P Ref	$\Delta G_{sol,w}$ (kcal/mol)	$\Delta G_{sol,p}$ (kcal/mol)
Mel	1.45	0.96±0.44 ^b	-15.65	-14.65
AMK	0.34	0.82±0.50 ^b	-16.43	-13.87
AFMK	-0.03	0.65±0.40 ^b	-16.36	-14.96
6OHM	0.73	0.02±0.80 ^b	-16.98	-14.7
It	4.88	4.88 ^c	-13.68	-7.50
Ir	4.71	4.71 ^c	-14.35	-7.30

^aCalculated by using Molinspiration online tool www.molinspiration.com.^bADC/Chemsketch log P plugin <http://www.acdlabs.com> in ref. [59].^cCalculated by using online Molinspiration www.molinspiration.com in ref. [14].

In addition, melatonin and its metabolites have good bioavailability and low toxicity [57]. Ir and It have 1749 and 1795 mg/kg LD₅₀ values, respectively. Also, the Ames mutagenicity value (M) is 0.41(-) and 0.43(-), respectively [57]. Then, It and Ir are estimated as not toxic. Moreover, according to Galano's work, these molecules are estimated to be easily synthesized. Considering that they have good bioavailability and low toxicity, different mechanisms of action have been evaluated in this work. Nevertheless, it is important to note that previous works mention that 6OHM acts against FRs as a good antiradical with primary mechanisms of action. In contrast, AMK, AFMK, and Mel act by secondary action mechanisms such as metal chelation [12,15].

Single electron transfer (SET)

We used two strategies to evaluate the SET mechanism: DAM and FEDAM maps. In the DAM map, Fig. 3, we found that all the molecules are bad acceptors and donors because they need a lot of energy to donate electron charge and have low electron affinity. As one can see, SET and SET-PT mechanisms are not favorable for all the molecules evaluated. This behavior was seen in both solvents. On the other hand, in Fig. 4, in the FEDAM, we found that AMK and AFMK can be expected to accept an electron from HOO^* , especially in water. Galano et al. evaluated Mel, It, and Ir with DPPH using the FEDAM map, where they found that It and Ir are better electron acceptors than Mel [57]. In this map, the molecules down and left will transfer electrons more easily to the FR molecules located up and right, and molecules near FR can accept electrons from FRs.

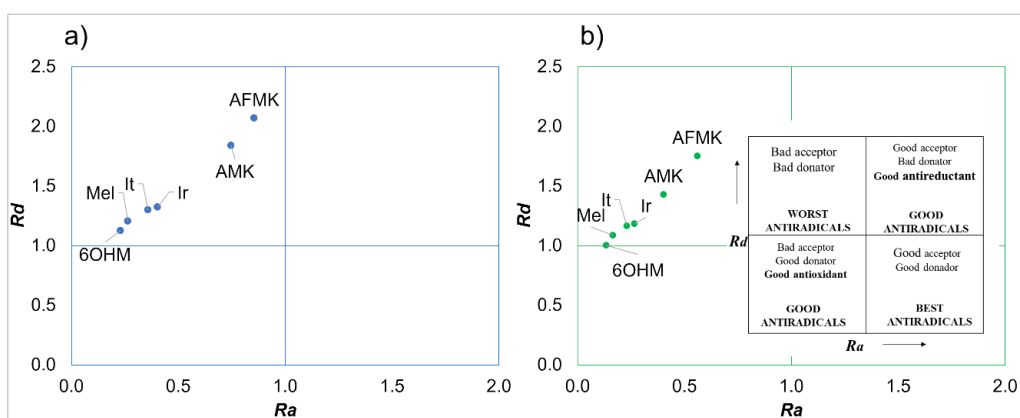


Fig. 3. DAM map of the molecules studied here where (a) molecules in water and (b) molecules in pentyl ethanoate.

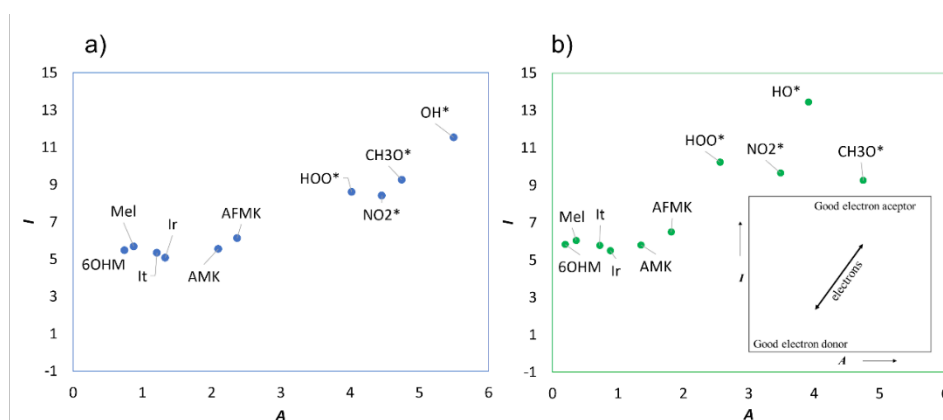


Fig. 4. FEDAM map of the molecules studied here where (a) molecules in water and (b) molecules in pentyl ethanoate.

Hydrogen atom transfer

The mechanism of hydrogen atom transfer was evaluated for all the molecules, where all of them may neutralize OH^\bullet and CH_3O^\bullet . The active hydrogens for Mel and the selected metabolites are reported in previous works; in order not to repeat results, only the active hydrogen atoms already reported were considered [9,15,28,60]. On the other hand, since this was never done before, all available hydrogen atoms were studied for Ir and It.

Previous work on Mel and its metabolites [9,15,28,60] evaluated OH^\bullet and HOO^\bullet radicals, whereas in this work, CH_3O^\bullet and NO_2^\bullet were included. The results indicate that these molecules can neutralize FRs such as CH_3O^\bullet and NO_2^\bullet . The best antiradical is represented by the number of reactive hydrogen atoms and the values of ΔG . Negative values of ΔG indicate that the reaction is exergonic, hence thermodynamically possible. Dissociated hydrogen atoms that produce exergonic reactions are considered active hydrogens. Consequently, those molecules with several active hydrogen atoms are more reactive; therefore, they may be better antiradicals, at least by this mechanism of action.

The number of atoms studied, and the most reactive ones are displayed in Table 5. In all cases, the hydrogen atom most easily removed is the acid hydrogen shown in Fig. 2 with the lowest D_0 value, see Tables S1-S6.

Table 5. Atoms selected for hydrogen atom transfer mechanism for each molecule. This table shows the number of reactive atoms within each FR; in bold, the more exergonic reactions are depicted.

Molecule	# atoms	Water				Pentyl ethanoate			
		OH^\bullet	CH_3O^\bullet	HOO^\bullet	NO_2^\bullet	OH^\bullet	CH_3O^\bullet	HOO^\bullet	NO_2^\bullet
Mel	5	5 (1°)	3 (2°)	--	--	5 (1°)	3 (2°)	--	--
AMK	4	4 (1°)	3 (2°)	--	--	4 (1°)	3 (2°)	--	--
AFMK	5	5 (1°)	4 (2°)	--	--	5 (1°)	4 (2°)	--	--
6OHM	7	7 (1°)	4 (2°)	1 (3°)	1 (4°)	7 (1°)	4 (2°)	1 (3°)	1 (4°)
It	12	12 (1°)	3 (2°)	2 (3°)	2 (4°)	7 (1°)	2 (2°)	1 (3°)	1 (4°)
Ir	13	10 (1°)	3 (2°)	2 (3°)	2 (4°)	13 (1°)	4 (2°)	2 (3°)	2 (4°)

(°) order of exergonicity

-- not exergonic reaction

Therefore, hydrogen bonds are important in hydrogen atom transfer since they can increase the energetic cost of removing them [61]. A strong hydrogen bond is thermodynamically more favorable; this causes a high value of D_0 and ΔG ; consequently, one has a low antiradical potential. In this case, the metabolites are those with hydrogen bonds between the acidic hydrogens, increasing their energy cost to be transferred. In Table 6, It and Ir present more exergonic reactions than Mel and its metabolites; as a result, It and Ir are assessed as good candidates as antiradicals, see more values in Tables S1-S6.

Inhibition of xanthine oxidase

XO is a pro-oxidative enzyme because it increases the production of ROS [2,62]. The mechanism of XO starts with the hydroxylation of hypoxanthine; then, it is converted to uric acid, releasing ROS during this catalytic process. XO contains a molybdopterin (Mo) cofactor that is responsible for oxidation. We performed a molecular docking study of XO compounds to evaluate the XO inhibition, where It and Ir could be XO inhibitors. Then, the docking study was carried out on the C subunit with the Mo cofactor [2]. For the analysis

of the molecules, we included allopurinol, a molecule known to be a suitable XO inhibitor and commonly employed in the treatment of excessive uric acid and gout [63].

The docking methodology was validated by the RMSD value of the known species. The method is considered adequate if the RMSD value is smaller than 3.5 Å [64]. Therefore, docking method validation was done by redocking the natural ligand (salicylic acid (SAL)), receptor on the active site. As a result, the docked inhibitor has a 1.33 Å RMSD value. For all molecules we found that the most significant interactions are hydrogen bond, π - π stacking, and π -alkyl, see Fig. 5.

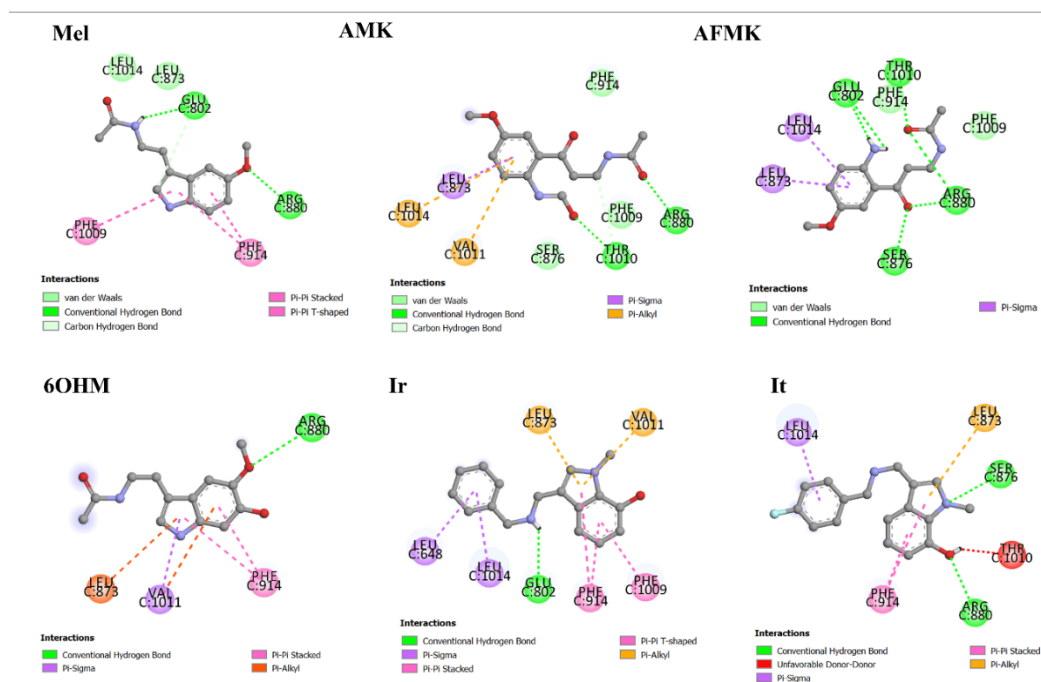


Fig. 5. 2D representation of molecular interactions of Mel, metabolites, and analogues with residues of the active site of XO.

The allopurinol inhibitor and SAL were studied previously with same protocol in our previous work [31]. It is found that SAL and allopurinol exhibit strong molecular interactions with XO [31]. The binding energy and ligand efficiency reflect this, in Table 6. SAL has strong interactions with catalytic residues by a hydrogen bond with THR1010, a salt bridge with ARG880, and π - π stacking with PHE1009 and PHE914. At the same time, allopurinol has interactions with catalytic residues by π - π stacking with PHE1009 and PHE914. It is found that Mel has four significant interactions with the catalytic residues GLU802, ARG880, PHE1009, and PHE914. In the other hand, AMK has four interactions with the catalytic residues THR1010, ARG880, LEU873, and VAL1011; AFMK has five interactions with the catalytic residues GLU802, THR1010, ARG880, LEU873, and PHE914; 6OHM has four interactions with ARG880, PHE914, VAL1011, and LEU873. Whereas Ir has six significant interactions with catalytic residues GLU802, PHE1009, LEU873, VAL1011, PHE914, and LEU648; and it has three with ARG880, LEU873, and PHE914. All observed interactions are in agreement with the results reported in other works with curcumin, tetrazoles, flavonoids, febuxostat, and analogues [65-68]. As we can see, the docking results indicated interactions with residues ARG880 and GLU802 by hydrogen bonds. The aromatic residues PHE914 and PHE1009 could interact by π -stacking, and the hydrophobic residues LEU648, LEU873, VAL1011, and LEU1014 could interact by π -sigma.

Furthermore, we found that It and Ir have the highest interaction energy and binding efficiency values and the lowest K_i value, Table 6. A high binding energy and ligand efficiency value means a stronger interaction

with the target. Ligand efficiency is used to compare the activity of different molecules regardless of their sizes. On the other hand, the inhibition constant, K_i , indicates how potent an inhibitor is. Then, K_i is the concentration required to produce half-maximum inhibition. In consequence, Ir and It are the most promising compounds for inhibiting XO of the compounds evaluated.

Table 6. Binding energy, ligand efficiency, and K_i values for each molecule.

Molecule	Binding energy (kcal/mol)	Ligand efficiency (kcal/mol)	Inhibition constant, K_i (uM)
Mel	-8.67	-0.51	440.64
AMK	-6.84	-0.36	9.68
AFMK	-8.66	-0.51	440.64
6OHM	-8.48	-0.47	606.77
It	-10.52	-0.50	19.54
Ir	-10.77	-0.54	12.83
SAL	-7.54*	-0.75*	2.96*
Allopurinol	-8.13*	-0.81*	1.10*

*Values taken from the ref. [31].

Conclusions

Antiradical properties of Mel, its metabolites, and analogues proposed by Galano's group [24,25] were evaluated at the M06-2X/6-31+G(d) level of theory. This level of theory was selected considering the best compromise time/performance, after calibration of several levels of theory and using the experimental value of the vertical ionization potential of Mel as a reference. Furthermore, we evaluated some possible mechanisms of action such as SET, HAT, and XO inhibition.

The SET possible mechanisms of Mel, metabolites, and analogues were evaluated, and we computed the CDFT chemical descriptors. 6OHM, Mel, It, and Ir are the best donating electronic charges to FRs. Subsequently, the SET mechanism was evaluated using DAM and FEDAM tools, where the molecules showed resistance to transfer or accept electronic charge. On the other hand, we computed the HAT mechanism finding that the molecules show favorable results to inhibit FRs: OH^\bullet , NO_2^\bullet , HOO^\bullet , and CH_3O^\bullet . In this work, we suggest that Mel, metabolites, and their analogues Ir and It, may neutralize the FRs CH_3O^\bullet and NO_2^\bullet . Finally, It and Ir appear to be suitable inhibitors of XO since they have relatively good value of ligand efficiency, compared to that of the inhibitors: allopurinol and SAL, and a low value of the K_i . Some of the conclusions that are drawn from our extensive docking studies are in good agreement with what would intuitively be expected. Nevertheless, we believe that the amount of quantitative data and results presented, fully support the conclusions.

Noteworthy, other mechanisms of action, such as electron-proton sequence transfer (SET-PT), can be anticipated with the help of the global reactivity descriptors. The high I values, indicate that the studied molecules are unlikely to exhibit the SET-PT mechanism in physiological and lipophilic media. The same applies to the sequential proton-losing hydrogen atom transfer (SPLHAT) mechanism. Still, other mechanisms of primary, secondary, and tertiary action need to be evaluated to complete our study of these molecules as antiradicals and their possible active metabolites. Therefore, due to the very favorable values obtained of low toxicity, good solubility, and accessible synthesis, Ir and It may be recommended as good synthetic antiradicals against oxidative stress.

Data availability

All data generated or analyzed during this study are included in this article and in the **Supporting Information (SI)** submitted to this journal.

Declaration and Competing Interest

The authors declare that they have no known competing financial interests or personal relationships that could have appeared to influence the work reported in this paper.

Acknowledgements

Guanajuato National Laboratory (CONACYT 1237332) is acknowledged for supercomputing resources. BM acknowledges support from CONACYT for a Ph.D. scholarship (580068/296892). JR gratefully acknowledges funding from University of Guanajuato (DAIP-Convocatoria Institucional de Investigación Científica 2022, Project No. 268.)

References

1. Dharmaraja, A. T. *J. Med. Chem.* **2017**, *60*, 3221–3240. DOI: <https://doi.org/10.1021/acs.jmedchem.6b01243>.
2. Kostić, D. A.; Dimitrijević, D. S.; Stojanović, G. S.; Palić, I. R.; Đorđević, A. S.; Ickovski, J. D. *J. Chem.* **2015**, *2015*, 294858. DOI: <https://doi.org/10.1155/2015/294858>.
3. Giorgi, C.; Marchi, S.; Simoes, I. C. M.; Ren, Z.; Morciano, G.; Perrone, M.; Patalas-Krawczyk, P.; Borchard, S.; Jędrak, P.; Pierzynowska, K.; et al. Chapter Six. in: *Mitochondria and Longevity*; López-Otín, C., Galluzzi, L. B. T.-I. R. of C. and M. B., Eds.; Academic Press, **2018**; *340*, 209–344 DOI: <https://doi.org/https://doi.org/10.1016/bs.ircmb.2018.05.006>.
4. Phaniendra, A.; Jestadi, D. B.; Periyasamy, L. *Indian J. Clin. Biochem.* **2015**, *30*, 11–26. DOI: <https://doi.org/10.1007/s12291-014-0446-0>.
5. Alkadi, H. *Infect. Disord. Drug. Targets.* **2020**, *20*, 16–26. DOI: <https://doi.org/10.2174/1871526518666180628124323>.
6. Oroian, M.; Escriche, I. *Int. Food Res. J.* **2015**, *74*, 10–36. DOI: <https://doi.org/10.1016/j.foodres.2015.04.018>.
7. Jamshidi-kia, F.; Wibowo, J. P.; Elachouri, M.; Masumi, R.; Salehifard-Jouneghani, A.; Abolhasanzadeh, Z.; Lorigooini, Z. *J. Herbmed. Pharmacol.* **2020**, *9*, 191–199. DOI: <https://doi.org/10.34172/jhp.2020.25>.
8. Galano, A.; Tan, D. X.; Reiter, R. J. *J. Pineal Res.* **2011**, *51*, 1–16. DOI: <https://doi.org/10.1111/j.1600-079X.2011.00916.x>.
9. Galano, A. *RSC Adv.* **2016**, *6*, 22951–22963. DOI: <https://doi.org/10.1039/c6ra00549g>.
10. Poeggeler, B.; Saarela, S.; Reiter, R. J.; Tan, D. X.; Chen, L. D.; Manchester, L. C.; Barlow-Walden, L. R. *Ann. N. Y. Acad. Sci.* **1994**, *738*, 419–420. DOI: <https://doi.org/10.1111/j.1749-6632.1994.tb21831.x>.
11. Galano, A.; Reiter, R. J. *J. Pineal Res.* **2018**, *65*, e12514. DOI: <https://doi.org/https://doi.org/10.1111/jpi.12514>.
12. Álvarez-Diduk, R.; Galano, A.; Tan, D. X.; Reiter, R. J. *Theor. Chem. Acc.* **2016**, *135*, 38. DOI: <https://doi.org/10.1007/s00214-015-1785-5>.
13. Ramis, M. R.; Esteban, S.; Miralles, A.; Tan, D.-X.; Reiter, R. J. *Curr. Med. Chem.* **2015**, *22*, 2690–2711. DOI: <https://doi.org/10.2174/0929867322666150619104143>.

14. Galano, A.; Tan, D. X.; Reiter, R. J. *J. Pineal Res.* **2013**, *54*, 245–257. DOI: <https://doi.org/10.1111/jpi.12010>.
15. Álvarez-Diduk, R.; Galano, A.; Tan, D. X.; Reiter, R. J. *J. Phys. Chem. B.* **2015**, *119*, 8535–8543. DOI: <https://doi.org/10.1021/acs.jpcc.5b04920>.
16. Hardeland, R. *Endocrine.* **2005**, *27*, 119–130. DOI: <https://doi.org/10.1385/endo.27.2:119>.
17. Costa, J. D.; Ramos, R. D.; Costa, K. D.; Brasil, D. D.; Silva, C. H.; Ferreira, E. F.; Borges, R. D.; Campos, J. M.; Macêdo, W. J.; Santos, C. B. *Mol.* **2018**. DOI: <https://doi.org/10.3390/molecules23112801>.
18. Guerra-Vargas, M. A.; Rosales-Hernández, M. C.; Martínez-Fonseca, N.; Padilla-Martínez, I.; Fonseca-Sabater, Y.; Martínez-Ramos, F. *Med. Chem. Res.* **2018**, *27*, 1186–1197. DOI: <https://doi.org/10.1007/s00044-018-2139-3>.
19. Kaçmaz, A.; User, E. Y.; Şehirli, A. Ö.; Tilki, M.; Ozkan, S.; Şener, G. *Surg. Today.* **2005**, *35*, 744–750. DOI: <https://doi.org/10.1007/s00595-005-3027-2>.
20. Okutan, H.; Savas, C.; Delibas, N. *Interact. Cardiovasc. Thorac. Surg.* **2004**, *3*, 519–522. DOI: <https://doi.org/10.1016/j.icvts.2004.05.005>.
21. Juan, C. A.; Pérez de la Lastra, J. M.; Plou, F. J.; Pérez-Lebeña, E. *Int. J. Mol. Sci.* **2021**. DOI: <https://doi.org/10.3390/ijms22094642>.
22. Teixeira, A.; Morfim, M. P.; de Cordova, C. A. S.; Charão, C. C. T.; de Lima, V. R.; Creczynski-Pasa, T. B. *J. Pineal Res.* **2003**, *35*, 262–268. DOI: <https://doi.org/https://doi.org/10.1034/j.1600-079X.2003.00085.x>.
23. Zhou, J.; Zhang, S.; Zhao, X.; Wei, T. *J. Pineal Res.* **2008**, *45*, 157–165. DOI: <https://doi.org/https://doi.org/10.1111/j.1600-079X.2008.00570.x>.
24. Castañeda-Arriaga, R.; Pérez-González, A.; Reina, M.; Galano, A. *Theor. Chem. Acc.* **2020**, *139*, 1–12. DOI: <https://doi.org/10.1007/s00214-020-02641-9>.
25. Reina, M.; Castañeda-Arriaga, R.; Perez-Gonzalez, A.; Guzman-Lopez, E. G.; Tan, D.-X.; Reiter, R. J.; Galano, A. *Melatonin Res.* **2018**, *1*, 27–58. DOI: <https://doi.org/10.32794/mr11250003>.
26. Galano, A.; Raúl Alvarez-Idaboy, J. *Int. J. Quantum. Chem.* **2019**, *119*, e25665. DOI: <https://doi.org/10.1002/qua.25665>.
27. Reina, M.; Martínez, A. *Comput. Theor. Chem.* **2018**, *1123*, 111–118. DOI: <https://doi.org/https://doi.org/10.1016/j.comptc.2017.11.017>.
28. Galano, A. *Phys. Chem. Chem. Phys.* **2011**, *13*, 7178–7188. DOI: <https://doi.org/10.1039/c0cp02801k>.
29. Geerlings, P.; De Proft, F.; Langenaeker, W. *Chem. Rev.* **2003**, *103*, 1793–1874. DOI: <https://doi.org/10.1021/cr990029p>.
30. Frisch, M. J.; Trucks, G. W.; Schlegel, H. B.; Scuseria, G. E.; Robb, M. A.; Cheeseman, J. R.; Scalmani, G.; Barone, V.; Mennucci, B.; Petersson, G. A.; et al. Gaussian 09. Revision C.01. *Gaussian 09. Revision C.01, Gaussian, Inc, Wallingford CT.* Gaussian, Inc.: Wallingford CT **2010**.
31. Manzanilla, B.; Robles, J. *J. Mol. Model.* **2022**, *28*, 68. DOI: <https://doi.org/10.1007/s00894-022-05056-4>.
32. Cannington, P. H.; Ham, N. S. *J. Electron. Spectrosc. Relat. Phenom.* **1983**, *32*, 139–151. DOI: [https://doi.org/10.1016/0368-2048\(83\)85092-0](https://doi.org/10.1016/0368-2048(83)85092-0).
33. Marenich, A. V.; Cramer, C. J.; Truhlar, D. G. *J. Phys. Chem. B.* **2009**, *113*, 6378–6396. DOI: <https://doi.org/10.1021/jp810292n>.
34. Spartan, W. I. Spartan 08. Irvine, CA. **2008**.
35. Halgren, T. A. *J. Comput. Chem.* **1996**, *17*, 490–519. DOI: [https://doi.org/10.1002/\(SICI\)1096-987X\(199604\)17:5/6<490::AID-JCC1>3.0.CO;2-P](https://doi.org/10.1002/(SICI)1096-987X(199604)17:5/6<490::AID-JCC1>3.0.CO;2-P).
36. Halgren, T. A. *J. Comput. Chem.* **1996**, *17*, 520–552. DOI: [https://doi.org/10.1002/\(SICI\)1096-987X\(199604\)17:5/6<520::AID-JCC2>3.0.CO;2-W](https://doi.org/10.1002/(SICI)1096-987X(199604)17:5/6<520::AID-JCC2>3.0.CO;2-W).
37. Halgren, T. A. *J. Comput. Chem.* **1996**, *17*, 553–586. DOI: [https://doi.org/10.1002/\(SICI\)1096-987X\(199604\)17:5/6<553::AID-JCC3>3.0.CO;2-T](https://doi.org/10.1002/(SICI)1096-987X(199604)17:5/6<553::AID-JCC3>3.0.CO;2-T).
38. Halgren, T. A.; Nachbar, R. B. *J. Comput. Chem.* **1996**, *17*, 587–615. DOI: [https://doi.org/10.1002/\(SICI\)1096-987X\(199604\)17:5/6<587::AID-JCC4>3.0.CO;2-Q](https://doi.org/10.1002/(SICI)1096-987X(199604)17:5/6<587::AID-JCC4>3.0.CO;2-Q).
39. Ho, J.; Coote, M. L. *Theor. Chem. Acc.* **2009**, *125*, 3–21. DOI: <https://doi.org/10.1007/s00214-009-0667-0>.
40. Janak, J. F. *Phys. Rev. B.* **1978**, *18*, 7165–7168. DOI: <https://doi.org/10.1103/PhysRevB.18.7165>.

41. Casida, M. E. *Phys. Rev. B.* **1999**, *59*, 4694–4698. DOI: <https://doi.org/10.1103/PhysRevB.59.4694>.
42. Saha, B.; Bhattacharyya, P. K. *RSC Adv.* **2016**, *6*, 79768–79780. DOI: <https://doi.org/10.1039/C6RA15016K>.
43. Parr, R. G.; Pearson, R. G. *J. Am. Chem. Soc.* **1983**, *105*, 7512–7516. DOI: <https://doi.org/10.1021/ja00364a005>.
44. Yang, W.; Parr, R. G. *PNAS.* **1985**, *82*, 6723–6726 DOI: <https://doi.org/10.1073/pnas.82.20.6723>.
45. Parr, R. G.; Yang, W. *J. Am. Chem. Soc.* **1984**, *106*, 4049–4050. DOI: <https://doi.org/10.1021/ja00326a036>.
46. Gázquez, J. L.; Cedillo, A.; Vela, A. *J. Phys. Chem. A.* **2007**, *111*, 1966–1970. DOI: <https://doi.org/10.1021/jp065459f>.
47. Duarte Ramos Matos, G.; Kyu, D. Y.; Loeffler, H. H.; Chodera, J. D.; Shirts, M. R.; Mobley, D. L. *J. Chem. Eng. Data.* **2017**, *62*, 1559–1569. DOI: <https://doi.org/10.1021/acs.jced.7b00104>.
48. Leo, A. *J. Chem. Rev.* **1993**, *93*, 1281–1306. DOI: <https://doi.org/10.1021/cr00020a001>.
49. Spartan, W. I. Spartan 18. Irvine, CA. **2018**.
50. Ghose, A. K.; Pritchett, A.; Crippen, G. M. *J. Comput. Chem.* **1988**, *9*, 80–90. DOI: <https://doi.org/10.1002/jcc.540090111>.
51. Martínez, A.; Vargas, R.; Galano, A. *J. Phys. Chem. B.* **2009**, *113*, 12113–12120. DOI: <https://doi.org/10.1021/jp903958h>.
52. Enroth, C.; Eger, B. T.; Okamoto, K.; Nishino, T.; Nishino, T.; Pai, E. F. *Proc. Natl. Acad. Sci. U. S. A.* **2000**, *97*, 10723–10728. DOI: <https://doi.org/10.1073/pnas.97.20.10723>.
53. Morris, G. M.; Huey, R.; Lindstrom, W.; Sanner, M. F.; Belew, R. K.; Goodsell, D. S.; Olson, A. J. *J. Comput. Chem.* **2009**, *30*, 2785–2791. DOI: <https://doi.org/10.1002/jcc.21256>.
54. Morris, G. M.; Goodsell, D. S.; Halliday, R. S.; Huey, R.; Hart, W. E.; Belew, R. K.; Olson, A. J. *J. Comput. Chem.* **1998**, *19*, 1639–1662. DOI: [https://doi.org/10.1002/\(SICI\)1096-987X\(19981115\)19:14<1639::AID-JCC10>3.0.CO;2-B](https://doi.org/10.1002/(SICI)1096-987X(19981115)19:14<1639::AID-JCC10>3.0.CO;2-B).
55. BIOVIA. Discovery Studio Visualizer. Dassault Systèmes: San Diego 2020.
56. Mahal, H. S.; Sharma, H. S.; Mukherjee, T. *Free Radic. Biol. Med.* **1999**, *26*, 557–565. DOI: [https://doi.org/10.1016/s0891-5849\(98\)00226-3](https://doi.org/10.1016/s0891-5849(98)00226-3).
57. Galano, A. A. *Theor. Chem. Acc.* **2016**, *135*, 157. DOI: <https://doi.org/10.1007/s00214-016-1917-6>.
58. Domingo, L. R.; Aurell, M. J.; Pérez, P.; Contreras, R. *Tetrahedron.* **2002**, *58*, 4417–4423. DOI: [https://doi.org/https://doi.org/10.1016/S0040-4020\(02\)00410-6](https://doi.org/https://doi.org/10.1016/S0040-4020(02)00410-6).
59. Johns, J. R.; Platts, J. A. *Org. Biomol. Chem.* **2014**, *12*, 7820–7827. DOI: <https://doi.org/10.1039/c4ob01396d>.
60. Galano, A.; Tan, D. X.; Reiter, R. J. *RSC Adv.* **2014**, *4*, 5220–5227. DOI: <https://doi.org/10.1039/c3ra44604b>.
61. Romero, Y.; Martínez, A. *J. Mol. Model.* **2015**, *21*, 220. DOI: <https://doi.org/10.1007/s00894-015-2773-3>.
62. Chung, H. Y.; Baek, B. S.; Song, S. H.; Kim, M. S.; Huh, J. I.; Shim, K. H.; Kim, K. W.; Lee, K. H. *Age (Omaha)*. **1997**, *20*, 127–140. DOI: <https://doi.org/10.1007/s11357-997-0012-2>.
63. Lin, H.-C.; Tsai, S.-H.; Chen, C.-S.; Chang, Y.-C.; Lee, C.-M.; Lai, Z.-Y.; Lin, C.-M. *Biochem. Pharmacol.* **2008**, *75*, 1416–1425. DOI: <https://doi.org/10.1016/j.bcp.2007.11.023>.
64. Kontoyianni, M.; McClellan, L. M.; Sokol, G. S. *J. Med. Chem.* **2004**, *47*, 558–565. DOI: <https://doi.org/10.1021/jm0302997>.
65. Chen, Y.; Gao, Y.; Wu, F.; Luo, X.; Ju, X.; Liu, G. *New J. Chem.* **2020**, *44*, 19276–19287. DOI: <https://doi.org/10.1039/D0NJ03221B>.
66. Shen, L.; Ji, H.-F. *Bioorg. Med. Chem. Lett.* **2009**, *19*, 5990–5993. DOI: <https://doi.org/10.1016/j.bmcl.2009.09.076>.
67. Fatima, I.; Zafar, H.; Khan, K. M.; Saad, S. M.; Javaid, S.; Perveen, S.; Choudhary, M. I. *Bioorg. Chem.* **2018**, *79*, 201–211. DOI: <https://doi.org/10.1016/j.bioorg.2018.04.021>.
68. Santi, M. D.; Paulino Zunini, M.; Vera, B.; Bouzidi, C.; Dumontet, V.; Abin-Carriquiry, A.; Grougnet, R.; Ortega, M. G. *Eur. J. Org. Chem.* **2018**, *143*, 577–582. DOI: <https://doi.org/10.1016/j.ejmech.2017.11.071>.

Synthesis and Evaluation of the Antifungal Sensibility of Novel Thienopyridine 1,2,3-Triazole Derivatives

Ramírez-Villalva Alejandra¹, Cervantes-Rebolledo Claudia², González-González Carlos A.³, Mastachi-Loza Salvador^{3*}

¹Escuela Profesional en Química Farmacéutica Biológica-INIES, Universidad de Ixtlahuaca, CUI. Carretera Ixtlahuaca-Jiquipilco KM 1, Estado de México, 50740, México.

²Escuela Profesional de Médico Cirujano-INIES, Universidad de Ixtlahuaca, CUI. Carretera Ixtlahuaca-Jiquipilco KM 1, Estado de México, 50740, Mexico.

³Departamento de Química Orgánica, Facultad de Química, Universidad Autónoma del Estado de México, Paseo Colón/Paseo Tollocan s/n, Toluca, Estado de México, 50120, México.

*Corresponding author: Mastachi-Loza Salvador, email: mastas20@hotmail.com

Received November 29th, 2022; Accepted August 11th, 2023.

DOI: <http://dx.doi.org/10.29356/jmcs.v68i1.1917>

In honor of Professor Joaquín Tamariz on the occasion of his retirement from the ENCB of the IPN.

Abstract. The family of compounds known as azoles are part of most of the antimicrobial drugs used for the treatment of infections. Within this family triazoles have been extensively studied as pharmacophores with very promising results. In this work, four novel trisubstituted 1,2,3-triazole compounds with a thienopyridine moiety (**1a,b**; **2a,b**) were synthesized through an azide-enolate 1,3-dipolar cycloaddition. Their cheminformatic properties were calculated using simulation software available online such as Molinspiration, Molsoft, Osiris Property Explorer, pkCSM, SwissADME, and GUSA. The results provided important information which allowed us to consider the evaluation of the antifungal activity of these novel compounds. Therefore, the antifungal activity of these compounds was evaluated *in vitro* against four filamentous fungi, including *Aspergillus fumigatus* ATCC 16907, *Trichosporon cutaneum* ATCC 28592, *Rhizopus oryzae* ATCC 10329, and *Mucor hiemalis* ATCC 8690; as well as six species of yeast from the *Candida* genus; *C. albicans* ATCC 10231, *C. utilis* ATCC 9226, *C. tropicalis* ATCC 13803, *C. parapsilosis* ATCC 22019, *C. glabrata* ATCC 34138 and *C. krusei* ATCC 14243. The sensibility studies suggest that compounds **1b**, **2a** and **2b** can be considered candidates for complementary biological studies due to the exhibited antifungal activity.

Keywords: Triazoles; antifungal; cycloaddition; azide-enolate; thienopyridine.

Resumen. La familia de compuestos conocidos como azoles forman parte de la mayoría de los medicamentos utilizados para el tratamiento de infecciones. Dentro de este grupo, los triazoles han sido extensamente estudiados como farmacóforos con resultados muy prometedores. En este trabajo, se sintetizaron cuatro nuevos 1,2,3-triazoles trisustituidos, que incluyen un anillo de tienopiridina en su estructura (**1a,b**; **2a,b**) a través de una cicloadición 1,3-dipolar del tipo azida-enolato. Sus propiedades químicas informáticas fueron calculadas utilizando programas de simulación encontrados en línea como Molinspiration, Molsoft, Osiris Property Explorer, pkCSM, SwissADME y GUSAR. Los resultados obtenidos presentaron información importante que permitió considerar la evaluación de la actividad antifúngica de estos nuevos compuestos. Por lo tanto, esta actividad fue evaluada *in vitro* en cuatro cepas de hongos filamentosos, incluyendo *Aspergillus fumigatus* ATCC 16907, *Trichosporon cutaneum* ATCC

28592, *Rhizopus oryzae* ATCC 10329, and *Mucor hiemalis* ATCC 8690, así como también seis especies de levaduras del género *Candida*; *C. albicans* ATCC 10231, *C. utilis* ATCC 9226, *C. tropicalis* ATCC 13803, *C. parapsilosis* ATCC 22019, *C. glabrata* ATCC 34138 and *C. krusei* ATCC 14243. En estos estudios se observó que los compuestos **1a**, **2a**, y **2b** pueden ser considerados para estudios posteriores de la evaluación biológica debido a la inhibición observada.

Palabras clave: Triazoles; antifúngica; cicloadición; azida-enolato; tienopiridina.

Introduction

The most used class of antifungals are compounds that include an azole moiety [1]. Hence, many triazole and imidazole derivatives have been shown to have a broad spectrum of antibiotic activity which makes them target pharmacophores to counteract mycosis caused by yeast and filamentous fungi [2]. Antifungals such as fluconazole, voriconazole and itraconazole are commonly prescribed drugs for treating invasive fungal infections (IFIs) [3], which continue to be an important cause of morbidity and mortality in immunocompromised patients. These drugs share the presence of a triazole moiety in their structure, which is responsible for the interaction between the molecule and the 14- α -demethylase (the cytochrome P-450 dependent enzyme). Inhibition of this enzyme causes the formation of toxic esters in the fungal membrane; therefore, its permeability is modified and reduces the fungus ability to reproduce [4]. Other nitrogen heterocyclic moieties such as pyridine and thienopyridine have been found in natural compounds and exert significant biological activity in several studies. Some of these compounds have shown important anticancer [5], antibacterial [6], antimalarial, and antifungal biological activity [7]. (Fig. 1).

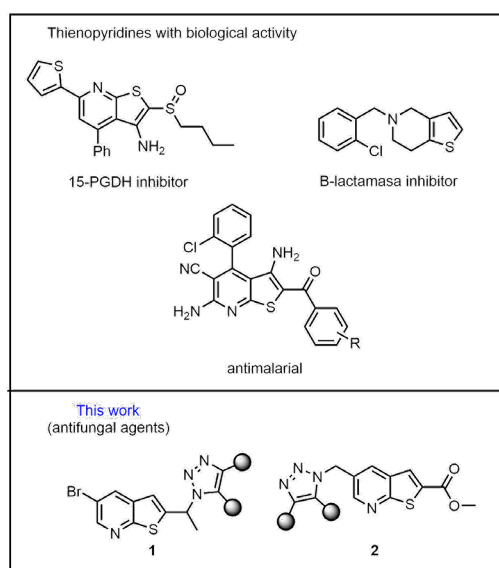


Fig. 1. The novel compounds involve the extremely important 1,2,3-triazole pharmacophoric cores and thienopyridines, a similar feature found in other compounds reported.

The continuous increase of antimicrobial resistance that some fungi are developing makes the design and development of compounds effective for treating these infectious species of clinical importance a constant

necessity (e.g. *Candida albicans*, *C. glabrata* [8], *Aspergillus fumigatus*, *A. niger* [9,10], and *Mucor sp.* and *Cryptococcus neoformans* [10]).

Currently, fungal diseases are of great importance due to the increase of medical conditions that cause immunosuppression in the host and enable the establishment of infections that can range from mild and common superficial infections to potentially fatal invasive infections. Most common pathogens include *Candida* species, which are mainly responsible for invasive candidiasis and candidemia, especially *C. albicans*, *C. glabrata* and *C. krusei* species. The infection usually affects patients admitted to the intensive care unit (ICU) who receive treatments for malignant tumors or stem cell, and organ transplantation [11]. Attention has been focused on these species because of the worldwide increase in resistance they have been displaying against azoles-based drugs and echinocandins [12].

Another important example is *Aspergillus fumigatus* fungus which is the main cause of *Aspergillus* pulmonary disease. An invasive pulmonary aspergillosis (IPA) causes 30-60 % mortality in patients with a compromised immune system [13]. IPA became highly relevant in the COVID-19 pandemic in patients with acute respiratory distress syndrome associated with a high mortality rate that in some reports reached 64.7 % [14].

Mucormycosis is an infection caused by fungi of the Mucorales order which includes several genera. Of this group, *Rhizopus* is associated with around 48 % of cases, followed by *Mucor* which is associated with 14 %. This mycosis affects more patients with HIV, but during the SARS-CoV-2 virus pandemic, cases of co-infection with black fungus, a name given to the lesions caused by mucormycosis, were reported in India with a mortality rate of 30.7 % [15,16].

Similarly, *Trichosporum* species has been reported as the second cause invasive yeast infections in the central nervous system in patients with hematological cancer [17], although it normally causes superficial infections forming nodules along the hair follicle [17]. In the case of *Trichosporum cutaneum* it has been implicated as the causative agent of the summer-type hypersensitivity pneumonitis in Japan [18].

The use of computer software to calculate molecular properties and predict bioactivity is often required in the design of alternative treatments for the above-mentioned infections. Cheminformatic properties have the advantage of predicting the site of action, likely route of administration, pharmacokinetic and pharmacodynamic behavior and potential toxic effects.

Simulation techniques and online servers such as Molinspiration, Molsoft, and the Osiris Property Explorer server, allow the cheminformatic and biological properties of the molecules to be known. These include the partition coefficient, the polar surface area, the number of rotating bonds, hydrogen bond acceptors (HBA), hydrogen bond donors (HBD) and Lipinski rules (Molinspiration and Molsoft). Then the best route of administration can be predicted with the gathered data [19]. Similarly, the pharmacokinetic properties of absorption, distribution, metabolism, excretion, and toxicity (ADMET) can be predicted from the online tool pkCSM and SwissADME. Another important aspect is to know the possible toxicological effects that the compounds may have, for which the Osiris Property Explorer compares molecular properties of the designed compounds with properties of known drug molecules to assess their possible tumorigenic or mutagenic risks [20].

Experimental

Flash column chromatography

SiO₂ 60 (230–400 mesh). TLC: Silica-gel plates (SiO₂; 0.20-mm thickness); visualization with UV light at 254 nm. *m.p.*: Fischer-Johns Scientific melting point apparatus. ¹H- and ¹³C-NMR spectra: Bruker Avance 300 MHz and Varian 500 MHz; δ in ppm rel. to Me₄Si as an internal standard, *J* in Hz. MS: The results were collected using a direct insertion probe and the electron impact ionization method on a Shimadzu GCMS-QP2010 Plus instrument; results are reported in *m/z* (rel. %).

General procedure for the synthesis of the triazole derivatives

The corresponding azide **4** or **6** (0.15 mmol) and the ketone **7 a-c** (0.15 mmol) were dissolved in anhydrous DMF (3 mL) under a nitrogen atmosphere. Then, DBU (0.3 mmol) was added, and the resulting

mixture was stirred at 50–60 °C until reaction completion (monitored through TLC ~24h). Afterwards the solution was cooled to room temperature under continuous stirring. Then, DMF was removed with extractions using a brine solution and EtOAc. The combined organic extracts were filtered and dried over anhydrous Na₂SO₄. Finally, the extracts were concentrated under reduced pressure and the crude reaction mixture was purified by flash chromatography with EtOAc/hexane 7:3.

5-bromo-2-(1-(5-(p-tolyl)-4-tosyl-1H-1,2,3-triazol-1-yl) ethyl)thieno[2,3-b]pyridine (1a).

Following the general procedure, azide **4** (0.042 g, 0.15 mmol) and ketone **7a** (0.043 g, 0.15 mmol) were dissolved in anhydrous DMF (3 mL). DBU (0.044 mL, 0.3 mmol) was added, and the solution was stirred for 24 h at 50–60°C. The mixture was extracted with EtOAc (3x10 mL) and the crude extract was purified by flash column chromatography to afford a white solid **1a** (0.043 g, 52 %), m.p. 152–154 °C. ¹H NMR: (30 MHz, CDCl₃) δ = 8.68 (d, *J* = 2.4 Hz, 1H), 8.29 (d, *J* = 8.0 Hz, 2H), 8.28 (s, 1H), 8.12 (d, *J* = 8.8 Hz, 2H), 7.99 (s, 1H), 7.78 (s, 1H), 7.72 (d, *J* = 8.8, 2H), 7.33 (d, *J* = 8.0 Hz, 2H), 4.75 (d, *J* = 4.5 Hz, 1H), 2.93 (s, 3H), 2.86 (s, 3H), 2.68 – 2.61 (m, 3H) ppm. ¹³C NMR (75 MHz, CDCl₃) δ = 162.6, 161.4, 150.5, 145.5, 135.3, 134.1, 130.5, 130.1, 128.5, 125.7, 124, 117.2, 64.2, 26.7, 21.8 ppm. MS [EI⁺] *m/z* (%) calculated for C₂₅H₂₁BrN₃O₂S₂: 552 [M]⁺ (15), 149 (28), 71 (28), 57 (65), 41 (59).

(1-(1-(5-bromothieno[2,3-b]pyridin-2-yl)ethyl)-5-phenyl-1H-1,2,3-triazol-4-yl)(phenyl)methanone (1b).

Following the general procedure, azide **4** (0.042 g, 0.15 mmol) and ketone **7b** (0.043 g, 0.15 mmol) were dissolved in anhydrous DMF (3 mL). DBU (0.044 mL, 0.3 mmol) was added, and the solution was stirred for 24 h at 50–60°C. The mixture was extracted with EtOAc (3x10 mL) and the crude extract was purified by flash column chromatography to afford a yellow solid **1b** (0.034 g, 47 %), m.p. 138–140 °C. ¹H NMR (300 MHz, CDCl₃) δ = 8.58 (d, *J* = 2.3 Hz, 1H), 8.13 (s, 1H), 7.88 (s, 2H), 7.80 (s, 1H), 7.51 – 7.40 (m, 2H), 7.39 – 7.25 (m, 6H), 5.53 (s, 1H), 2.27 (s, 3H) ppm. ¹³C NMR (75 MHz, CDCl₃) δ = 191.4, 147.8, 145.5, 145.1, 139.7, 134.9, 133.7, 133.1, 130.1, 129.6, 129.3, 128.1, 125.8, 125.3, 123.6, 119.1, 116.8, 63.7, 21.3 ppm. MS [EI⁺] *m/z* (%) calculated for C₂₄H₁₇BrN₄O₂S: 488 [M]⁺ (7), 121 (31), 84 (100), 57 (31), 47 (52), 35 (47).

methyl-5-((4-benzoyl-5-phenyl-1H-1,2,3-triazol-1-yl)methyl)thieno[2,3-b]pyridine-2-carboxylate (2a).

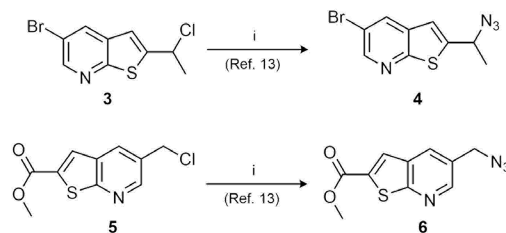
Following the general procedure, azide **6** (0.042 g, 0.15 mmol) and ketone **7b** (0.043 g, 0.15 mmol) were dissolved in anhydrous DMF (3 mL). DBU (0.044 mL, 0.3 mmol) was added, and the solution was stirred for 24 h at 50–60°C. The mixture was extracted with EtOAc (3x10 mL) and the crude extract was purified by flash column chromatography to afford a yellow solid **2a** (0.036 g, 53 %), m.p. 219–221 °C. ¹H NMR (300 MHz, CDCl₃) δ = 8.30 – 8.20 (m, 5H), 7.90 (d, *J* = 3.7 Hz, 2H), 7.74 (s, 1H), 7.59 – 7.51 (m, 1H), 7.52 – 7.37 (m, 4H), 5.59 (s, 2H), 2.87 (s, 3H) ppm. ¹³C NMR (75 MHz, CDCl₃) δ = 177.7, 162.6, 137.0, 133.1, 132.1, 130.7, 130.5, 129.8, 129.8, 129.7, 129.1, 128.3, 128.3, 127.7, 126.8, 126.2, 126.1, 52.9, 49.7 ppm. MS [EI⁺] *m/z* (%) calculated for C₂₅H₁₈N₄O₃S: 454 [M]⁺ (9), 235 (35), 161 (80), 57 (35), 41 (38)

methyl 5-((4-cyano-5-phenyl-1H-1,2,3-triazol-1-yl) methyl)thieno[2,3-b]pyridine-2-carboxylate (2b).

Following the general procedure, azide **6** (0.042 g, 0.15 mmol) and ketone **7c** (0.043 g, 0.15 mmol) were dissolved in anhydrous DMF (3 mL). DBU (0.044 mL, 0.3 mmol) was added, and the solution was stirred for 24 h at 50–60°C. The mixture was extracted with EtOAc (3x10 mL) and the crude extract was purified by flash column chromatography to afford a yellow solid **2b** (0.025 g, 45 %), m.p. 205–207 °C. ¹H NMR (300 MHz, CDCl₃) δ = 8.32 (d, *J* = 2.2 Hz, 1H), 7.89 (d, *J* = 2.2 Hz, 1H), 7.65 – 7.48 (m, 3H), 7.42 – 7.30 (m, 3H), 5.67 (s, 2H), 2.86 (s, 3H) ppm. ¹³C NMR (75 MHz, CDCl₃) δ = 162.6, 147.1, 143.9, 142.2, 133.0, 131.9, 131.7, 129.9, 129, 128.9, 126.8, 126.1, 123.1, 121.3, 50.3, 49.7 ppm. MS [EI⁺] *m/z* [M]⁺ calculated for C₁₉H₁₃N₅O₂S: found 375.0793 [M]⁺ (23.6), 366.9792 (17.8), 354.9792 (20.1).

Results and discussion

In the initial part of this study, the synthesis of azides **4** and **6** was key for introducing the thienopyridine core (Scheme 1). Thus, the synthesis of the derivatives was achieved through nucleophilic substitution of the halogenated thienopyridine analogs **3** and **5** with sodium azide. The reaction proceeded with moderate yields and the compounds were easily purified by chromatography. The introduction of the azide moiety was confirmed by the IR spectra where the characteristic signal for the $-N=N=N$ stretch was identified as a strong sharp signal between $2100\text{--}2200\text{ cm}^{-1}$.



Scheme 1. Reagents and conditions: (i) NaN_3 (1.1 eq), DMF anh., $60\text{ }^\circ\text{C}$, 12 h, N_2

Once the desired azides were synthesized, the next step was their transformation into the corresponding triazoles **1a,b** and **2a,b**. One of the most important methodologies for obtaining a 1,2,3-triazole core, is the Copper-catalyzed azide-alkyne cycloaddition (CuAAC) [21]. However, other strategies have emerged with the objective of providing new alternatives with a greener approach. We previously reported a novel synthetic protocol to afford the efficient assembly of 1,4,5-trisubstituted 1,2,3-triazoles through an azide-enolate cycloaddition [22]. Thus, thienopyridine triazoles **1a,b** and **2a,b** were synthesized by the efficient 1,3-dipolar cycloaddition between azide **4** and **6** and different enolates prepared *in situ* from ketones **7** under basic catalysis using 1,8-Diazabicyclo[5.4.0]undec-7-ene (DBU). Table 1 summarizes the results from the cycloaddition. The structure of this novel compounds was confirmed by spectroscopical, and spectrometric methods. All compounds were afforded in moderate yields.

Table 1. Synthesis of thienopyridines and imidazole linked-1,2,3-triazoles from azide **4** and **6** by coupling with active ketones **7**.

Entry ^a	Ketone	Triazole ^b (Yield%) ^c
1	6a : $\text{R}_1 = 4\text{-CH}_3\text{Ph}$; $\text{R}_2 = \text{SO}_2\text{-4-Tolyl}$	1a : 52
2	6b : $\text{R}_1 = \text{Ph}$; $\text{R}_2 = \text{COPh}$	1b : 47
Entry ^a	Ketone	Triazole ^b (Yield%) ^c
1	6b : $\text{R}_1 = \text{Ph}$; $\text{R}_2 = \text{COPh}$	2a : 53
2	6c : $\text{R}_1 = \text{Ph}$; $\text{R}_2 = \text{CN}$	2b : 45

^aReaction conditions: To a solution of azide compound (1.0 eq) and ketone **7** (1.0 eq) in DMF anh. was added (2.0 eq) of DBU. The reaction mixture was stirred at $50\text{--}60\text{ }^\circ\text{C}$ for 12–24 h.

^bConfirmed by $^1\text{H-NMR}$, $^{13}\text{C-NMR}$ and MS.

^cYields refer to chromatographically pure isolated compounds.

Computational studies

Molecular and chemoinformatic properties were obtained using the Molinspiration, Molsoft and Osiris Property Explorer simulators. The predicted property values of compounds **1a,b** and **2a,b** are summarized in Table 2. Based on the Lipinski rules, all compounds have good therapeutic potential. Only compounds **1a** and **1b** showed violations for the rule of five. However, all compounds displayed HBA and HBD values less than 10 and 5, respectively which indicates good drug permeation [23]. Moreover, triazole derivatives having a molecular weight of less than 500 g/mol and a logP value of less than 5, indicate that the permeability of the compounds through oral administration is favored. In the case of compound **1a** with molecular weight more than 500 and with a logP that exceeds 5, shows a pair of violation to the Lipinski rules but still the compound can be considered for oral administration, or it could be administered by another route, for example parenteral, intravenous or intraperitoneal.

Table 2. Molecular and chemoinformatic properties of compounds **1** and **2**.

Properties	1a	1b	2a	2b
MF	C ₂₅ H ₂₁ BrN ₄ O ₂ S ₂	C ₂₄ H ₁₇ BrN ₄ OS	C ₂₅ H ₁₈ N ₄ O ₃ S	C ₁₉ H ₁₃ N ₅ O ₂ S
MW	553.51	489.39	454.50	375.40
No. HBA	6	5	7	7
No. HBD	0	0	0	0
PSA	77.75	60.68	86.99	93.71
LogP	6.37	6.15	4.62	3.26
δ	1.34 ±0.1	1.29 ±0.1	1.37 ±0.1	1.42 ±0.1
ST	51.9 ±0.1	52.1 ±0.1	57.0 ±0.1	60.9 ±0.1
Polarizability	55.32	50.12	51.08	41.55
MR	139.57	126.42	128.85	104.81
MV	364.3	327.1	331.6	263.4
nrotb	5	5	7	5
Drug likeness	-10.89	-1.88	-2.33	-7.09
Lipinski's rules Violations	2	1	0	0

MF= Molecular formula, MW= Molecular weight (g/mol), HBA= Hydrogen bond acceptors, HBD: Hydrogen bond donors, PSA= Polar Surface Area (Å²), LogP= Partition coefficient, δ= density (g/cm³), ST= Surface tension, MR= Molar refractivity (cm³), nrotb= No. of rotatable bonds, MV= Molar volume (cm³).

Molinspiration and Osiris Property Explorer simulators were used to predict the bioactivity of compounds against important drug target sites and predict their potential tumorigenic or mutagenic risks, these results are found in Table 3. The chemoinformatic and bioactivity properties together indicate that these structures are of pharmacological interest, mainly at the kinase inhibitor target site in compounds **2a** and **2b**. The major failure in the drug discovery process is the toxicity and according to the predictions, none of the synthesized triazoles should exhibit mutagenic or tumorigenic impacts, as well as negative reproductive effects. Based on the joint results of the chemoinformatic properties, the most promising compounds to have the desired biological activity are compounds **2a** and **2b** (Table 2), since they do not present violations of the Lipinski's rules and are the ones that present a lower partition coefficient (4.62 and 3.26 respectively). The latter prediction translates in a better availability and distribution of the compound in the organism, and this is supported by the absorption and metabolism data in Table 4.

Table 3. Prediction of bioactivity and toxicity of compounds **1** and **2**.

Compound	NCL	IE	GPCR	KI	RE	T	M
1a	-0.99	-0.17	-0.21	-0.30	No	No	No
1b	-0.81	-0.07	-0.17	-0.04	No	No	No
2a	-0.61	0.04	-0.07	0.06	No	No	No
2b	-0.69	0.00	-0.12	0.13	No	No	No

*NCL= Nuclear receptor ligand, IE= Enzyme inhibitor, GPCR= GPCR ligand,
KI= Kinase inhibitor, RE= Reproductive effective, T= Tumorigenic, M= Mutagenic.

Cheminformatic properties related to ADMET processes were predicted using the online predictors pkCSM and SwissADME (Table 4). In ADMET, the absorption properties indicate that the compounds can be administered orally according to the Lipinsky rules. Other predicted properties such as LogP data, intestinal absorption (% absorbed), P-glycoprotein substrate, and skin permeability (logKp) suggest that these compounds have a high degree of therapeutic bioavailability. In addition, neither compound appears to permeate the blood-brain barrier due to its hydrophilicity, making it difficult to treat pathologies that affect the SNC, although they could have effects on other systems.

Table 4. Data of cheminformatic properties of ADMET processes.

ADMET		1a	1b	2a	2b
Absorption	WS	-4.182	-3.541	-3.158	-3.927
	IA (%)	94.433	98.168	100	97.494
	SP	-2.735	-2.735	-2.735	-2.735
	SGP	No	No	No	No
Distribution	BBBP	No	No	No	No
	CNSP	-1.719	-1.705	-3.422	-2.453
Metabolism	CYP3A4 inhibitor	Yes	No	Yes	Yes
Excretion	TC	-0.078	0.088	0.339	0.295

*WS water solubility (log mol/L), IA intestinal absorption, SP skin permeability (logKp), SGP P-glycoprotein substrate, BBBP blood brain barrier permeability (logBB), CNSP CNS permeability (logPS), TC total clearance (log mL/min/kg), OCT2-s transporters organic cation transporter 2 substrates.

Microbiology

The antifungal *in vitro* sensibility study was carried out for compounds **1a,b** and **2a,b** against four filamentous fungi (*Trichosporon cutaneum* ATCC-28592, *Aspergillus fumigatus* ATCC-16907, *Mucor hiemalis* ATCC-8690, and *Rhizopus oryzae* ATCC-10329), as well as in six yeast specimens of *Candida sp.* (*C. albicans* ATCC-10231, *C. krusei* ATCC-14243, *C. utilis* ATCC-9226, *C. tropicalis* ATCC-13803, *C. parapsilopsis* ATCC-22019, *C. glabrata* ATCC-34138) following the Clinical Laboratory Standards Institute (CLSI) guidelines for standardized microbiological methods. The antifungal study for yeasts was determined by the microdilution method M27-A3 [24], whereas method M38-A [25] was used for filamentous microorganisms. Both studies were performed against itraconazole as a reference standard. The minimum inhibitory concentration (MIC) values of the standard and compounds **1a,b** and **2a,b** are expressed in

micrograms per milliliter and were determined in 96-well plates using MOPS (3- [N-morpholino] propanesulfonic acid buffered RPMI-1640 medium, Sigma- Aldrich).

The antifungal activities of the evaluated compounds are summarized in Table 5.

Compound **2a** showed good inhibitory activity against *C. albicans* (MIC= 0.5 µg/mL) although it was at a considerable higher concentration than the standard (MIC= 0.03 µg/mL). On the other hand, **1b** had important activity against *C. glabrata* (MIC= 0.12 µg/mL). Remarkably, MIC of **1b** was better than the MIC of itraconazole (1 µg/mL). Another important observation was the activity of compound **2b** (MIC= 1 µg/mL) which was comparable to the observed MIC for the standard antifungal drug against *Rhizopus oryzae*. Compound **1a**, however, had no important activity against any of the tested microorganisms.

Table 5. *In vitro* antifungal activities of the synthesized compounds (MIC, µg/mL).

Compound	<i>C. alb</i>	<i>C. uti</i>	<i>C. kru</i>	<i>C. gla</i>	<i>C. par</i>	<i>M. hie</i>	<i>A. fum</i>	<i>T. cut</i>	<i>R. ory</i>
1a	16	16	16	16	16	16	8	16	16
1b	8	16	16	0.12	8	16	8	16	16
2a	0.5	16	2	16	8	16	16	16	2
2b	8	16	8	16	8	16	8	8	1
Standard^a	0.03	0.25	0.25	1	0.06	4	1	8	1

Abbreviations: *C. alb.*, *Candida albicans*; *C. uti.*, *Candida utilis*; *C. kru.*, *Candida krusei*; *C. gla.*, *Candida glabrata*; *C. par.*, *Candida parapsilosis*; *M. hie.*, *Mucor hiemalis*; *A. fum.*, *Aspergillus fumigatus*; *T. cut.*, *Trichosporon cutaneum*; *R. ory.*, *Rhizopus oryzae*.

According to these results, the presence of the COPh group in position 4, as well as the Ph group in position 5 of the triazole heterocycle resulted in an increase of the biological activity against strains of yeasts of *C. albicans* and *C. glabrata*. The results of compound **2b** showed good activity in the *Rhizopus oryzae* strain since it has the same MIC as the reference drug (MIC= 1 µg/mL). These results indicate that the exchange of the group -COPh at position 4 by a group -CN favors the antifungal activity of **2b** against the filamentous fungus.

These outcomes can also be described by susceptibility parameters of yeast according to the document M27-A3 (Table 6). Generally, *C. glabrata* and *C. albicans* showed some susceptibility to the evaluated compounds, meanwhile *C. krusei*, *C. parapsilosis* and *C. utilis* were resistant to all the evaluated compounds according to the breakpoints described in such document.

Table 6. The determination of the sensibility of yeast (according to document M27-A3): Susceptible (S), dose-dependent sensitive (SDD) and resistant (R).

Compound	<i>C. alb</i>	<i>C. uti</i>	<i>C. kru</i>	<i>C. gla</i>	<i>C. par</i>
1a	R	R	R	R	R
1b	R	R	R	S	R
2a	SDD	R	R	R	R
2b	R	R	R	R	R
Standard^a	S	SDD	SDD	R	S

Abbreviations: *C. alb.*, *Candida albicans*; *C. uti.*, *Candida utilis*; *C. kru.*, *Candida krusei*; *C. gla.*, *Candida glabrata*; *C. par.*, *Candida parapsilosis*.

^aItraconazole. Interpretive criteria: Breakpoints (MIC, µg/mL) = 0.12 [S], 0.25–0.5 [SDD], 1[R].

To better relate the antifungal activity of compounds **1a-b** and **2a-b**, table 7 shows the MIC ratio in $\mu\text{mol/mL}$ concentrations, noting that compound **1b** has a lower MIC ($2.55 \times 10^{-7} \mu\text{mol/mL}$) than the reference substance (itraconazole = $1.41 \times 10^{-6} \mu\text{mol/mL}$) in the *C. glabrata* strain, this is the best result due to the clinical manifestations of this strain and the low amount of antifungal (**1b**) required to inhibit its growth. Compound **2b** presents the lowest MIC in the strains of *Trichosporon cutaneum* and *Rhizopus oryzae*, where the concentration required to inhibit the growth of the strains is slightly higher than that of itraconazole (standard), being $2.13 \times 10^{-5} \mu\text{mol/mL}$ for *Trichosporon cutaneum* and $2.66 \times 10^{-6} \mu\text{mol/mL}$ for *Rhizopus oryzae*. On the other hand, compound **2a** shows better activity inhibiting yeast growth, highlighting the MIC in *C. albicans* ($1.1 \times 10^{-6} \mu\text{mol/mL}$) and in *C. krusei* ($4.4 \times 10^{-6} \mu\text{mol/mL}$), although according to the established sensitivity criteria. by CLSI, both strains are resistant to compound **2a**. Therefore, we could consider the structures of **1b** and **2b** as a leading compounds for the synthesis of new analogues and to continue with *in vivo* and *in vitro* biological tests.

Table 7. *In vitro* antifungal activities of the synthesized compounds (MIC, $\mu\text{mol/mL}$).

Compound	<i>C. alb</i>	<i>C. uti</i>	<i>C. kru</i>	<i>C. gla</i>	<i>C. par</i>	<i>M. hie</i>	<i>A. fum</i>	<i>T. cut</i>	<i>R. ory</i>
1a	2.89×10^{-5}	1.44×10^{-5}	2.89×10^{-5}	2.89×10^{-5}					
1b	3.26×10^{-5}	3.26×10^{-5}	3.26×10^{-5}	2.55×10^{-7}	1.63×10^{-5}	3.26×10^{-5}	1.63×10^{-5}	3.26×10^{-5}	3.26×10^{-5}
2a	1.1×10^{-6}	3.5×10^{-5}	4.4×10^{-6}	3.5×10^{-5}	1.76×10^{-5}	3.5×10^{-5}	3.5×10^{-5}	3.5×10^{-5}	4.4×10^{-6}
2b	2.13×10^{-5}	4.26×10^{-5}	2.13×10^{-5}	4.26×10^{-5}	2.13×10^{-5}	4.26×10^{-5}	2.13×10^{-5}	2.13×10^{-5}	2.66×10^{-6}
Standard ^a	4.4×10^{-8}	3.54×10^{-7}	3.54×10^{-7}	1.41×10^{-6}	8.8×10^{-8}	5.66×10^{-6}	1.41×10^{-6}	1.13×10^{-5}	1.41×10^{-6}

Conclusions

In summary, the azide-enolate 1,3-dipolar cycloaddition afforded the synthesis of four 1,2,3-triazole derivatives (**1a,b** and **2a,b**) in good yields. *In vitro* studies showed that compound **1b** is the most efficient antimicrobial agent in yeasts followed by compounds **2a**, **2b**, and **1a**, since the first (**1b**) was better than itraconazole against *C. glabrata*. The compound **2b** had better activity against filamentous fungi, showing a MIC $1 \mu\text{g/mL}$ in *R. oryzae*. Compounds **2b** and **2a** had better activity against filamentous fungi, being very close to the MIC values of itraconazole. Consequently, these can be considered candidate drugs for future complementary biological studies.

Acknowledgements

Financial support from Secretaría de Investigación y Estudios Avanzados/UAEMéx (grant 5011/2020CIB and grant 4512/2018C) and CONACyT is gratefully acknowledged. The authors want to thank the referees for valuable comments and suggestions. The authors would also like to thank the referees for their valuable comments and suggestions, and M.N. Zavala-Segovia and L. Triana-Cruz (CCIQS UAEMéx–UNAM) for technical support.

References

1. Benhamou, R. I.; Bibi, M.; Steinbuch, K. B.; Engel, H.; Levin, M.; Roichman, Y.; Berman, J.; Fridman, M. *ACS Chem. Biol.* **2017**, *12*, 1769–1777. DOI: <https://doi.org/10.1021/acscchembio.7b00339>.

- 2.(a) Zhang, Y.-Y.; Zhou, C.-H. *Bioorg. Med. Chem. Lett.* **2011**, *21*, 4349–4352. DOI: <https://doi.org/10.1016/j.bmcl.2011.05.042>. (b) Zhang, H.-Z.; Damu, G. L. V.; Cai, G.-X.; Zhou, C.-H. *Eur. J. Med. Chem.* **2013**, *64*, 329–344. DOI: <https://doi.org/10.1016/j.ejmech.2013.03.049>.
- 3.(a) Guillon, R.; Pagniez, F.; Picot, C.; Hédou, D.; Tonnerre, A.; Chosson, E.; Duflos, M.; Besson, T.; Logé, C.; Le Pape, P. *ACS Med. Chem. Lett.* **2013**, *4*, 288–292. DOI: <https://doi.org/10.1021/ml300429p>. (b) Wang, S.; Zhang, L.; Jin, Y.; Tang, J. H.; Su, H.; Yu, S.; Ren, H. *Asian J. Chem.* **2014**, *26*, 2362–2364. DOI: <https://doi.org/10.14233/ajchem.2014.15956>.
4. Yao, B.; Ji, H.; Cao, Y.; Zhou, Y.; Zhu, J.; Lü, J.; Li, Y.; Chen, J.; Zheng, C.; Jiang, Y.; Liang, R.; Tang, H. *J. Med. Chem.* **2007**, *50*, 5293–5300. DOI: <https://doi.org/10.1021/jm0701167>.
- 5.(a) Lucas, S. C. C.; Moore, J. E.; Donald, C. S.; Hawkins, J. L. *J. Org. Chem.* **2015**, *80*, 12594–12598. DOI: <https://doi.org/10.1021/acs.joc.5b01735>. (b) Elansary, A. K.; Moneer, A. A.; Kadry, H. H.; Gedawy, E. M. *Arch. Pharm. Res.* **2012**, *35*, 1909–1917. DOI: <https://doi.org/10.1007/s12272-012-1107-6>.
6. Leal, B.; Afonso, I. F.; Rodrigues, C. R.; Abreu, P. A.; Garrett, R.; Pinheiro, L. C. S.; Azevedo, A. R.; Borges, J. C.; Vegi, P. F.; Santos, C. C. C.; da Silveira, F. C. A.; Cabral, L. M.; Frugulhetti, I. C. P. P.; Bernardino, A. M. R.; Santos, D. O.; Castro, H. C. *Bioorg. Med. Chem.* **2008**, *16*, 8196–8204. DOI: <https://doi.org/10.1016/j.bmc.2008.07.035>.
- 7.(a) Fugel, W.; Oberholzer, A. E.; Gschloessl, B.; Dzikowski, R.; Pressburger, N.; Preu, L.; Pearl, L. H.; Baratte, B.; Ratin, M.; Okun, I.; Doerig, C.; Kruggel, S.; Lemcke, T.; Meijer, L.; Kunick, C. *J. Med. Chem.* **2013**, *56*, 264–275. DOI: <https://doi.org/10.1021/jm301575n>. (b) Verma, A. K.; Kotla, S. K. R.; Choudhary, D.; Patel, M.; Tiwari, R. K. *J. Org. Chem.* **2013**, *78*, 4386–4401. DOI: <https://doi.org/10.1021/jo400400c>.
8. Dayanandan, N.; Paulsen, J. L.; Viswanathan, K.; Keshipeddy, S.; Lombardo, M. N.; Zhou, W.; Lamb, K. M.; Sochia, A. E.; Alverson, J. B.; Priestley, N. D.; Wright, D. L.; Anderson, A. C. *J. Med. Chem.* **2014**, *57*, 2643–2656. DOI: <https://doi.org/10.1021/jm401916j>.
9. Jain, K. S.; Khedkar, V. M.; Arya, N.; Rane, P. V.; Chaskar, P. K.; Coutinho, E. C. *Eur. J. Med. Chem.* **2014**, *77*, 166–175. DOI: <https://doi.org/10.1016/j.ejmech.2014.02.066>.
10. Serpi, M.; Ferrari, V.; Pertusati, F. *J. Med. Chem.* **2016**, *59*, 10343–10382. DOI: <https://doi.org/10.1021/acs.jmedchem.6b00325>.
11. McCarty, T. P.; White, C. M.; Pappas, P. G. *Infect. Dis. Clin. North Am.* **2021**, *35*, 389–413. DOI: <https://doi.org/10.1016/j.idc.2021.03.007>.
12. Pristov, K. E.; Ghannoum, M. A. *Clin. Microbiol. Infect.* **2019**, *25*, 792–798. DOI: <https://doi.org/10.1016/j.cmi.2019.03.028>.
13. Earle, K.; Valero, C.; Conn, D. P.; Vere, G.; Cook, P. C.; Bromley, M. J.; Bowyer, P.; Gago, S. *Virulence* **2023**, *14*, 2172264. DOI: <https://doi.org/10.1080/21505594.2023.2172264>.
14. Khan, A. A.; Farooq, F.; Jain, S. K.; Golinska, P.; Rai, M. *Microb. Ecol.* **2022**, *84*, 1236–1244. DOI: <https://doi.org/10.1007/s00248-021-01913-6>.
15. Prakash, S.; Kumar, A. *J. Basic Microbiol.* **2023**, *63*, 119–127. DOI: <https://doi.org/10.1002/jobm.202200334>.
16. Dam, P.; Cardoso, M. H.; Mandal, S.; Franco, O. L.; Sağıroğlu, P.; Polat, O. A.; Kokoglu, K.; Mondal, R.; Mandal, A. K.; Ocsoy, I. *Travel Med. Infect. Dis.* **2023**, *52*, 102557. DOI: <https://doi.org/10.1016/j.tmaid.2023.102557>.
17. Góralaska, K.; Blaszkowska, J.; Dzikowicz, M. *Infection* **2018**, *46*, 443–459. DOI: <https://doi.org/10.1007/s15010-018-1152-2>.
18. Ando, M.; Arima, K.; Yoneda, R.; Tamura, M. *Am. Rev. Respir. Dis.* **1991**, *144*, 765–769. DOI: <https://doi.org/10.1164/ajrccm/144.4.765>.
19. Hemalatha, K.; Selvin, J.; Girija, K. *Asian J. Pharm. Res.* **2018**, *8*, 125–132. DOI: <https://doi.org/10.5958/2231-5691.2018.00022.9>.
20. Hassan, M.; Ashraf, Z.; Abbas, Q.; Raza, H.; Seo, S.-Y. *Interdiscip. Sci. Comput. Life Sci.* **2018**, *10*, 68–80. DOI: <https://doi.org/10.1007/s12539-016-0171-x>.

21. Ramírez-Villalva, A.; González-Calderón, D.; Rojas-García, R. I.; González-Romero, C.; Tamariz-Mascarúa, J.; Morales-Rodríguez, M.; Zavala-Segovia, N.; Fuentes-Benites, A. *Med. Chem. Comm.* **2017**, 8, 2258–2262. DOI: <https://doi.org/10.1039/C7MD00442G>.
22. Chandrasekaran, S. *Click Reactions in Organic Synthesis*, Ed., Wiley-VCH, **2016**.
23. Vanjare, B. D.; Seok Eom, Y.; Raza, H.; Hassan, M.; Hwan Lee, K.; Ja Kim, S. *Bioorg. Med. Chem.* **2022**, 63, 116745. DOI: <https://doi.org/10.1016/j.bmc.2022.116745>.
24. Rex, J. H. *Reference Method for Broth Dilution Antifungal Susceptibility Testing of Yeasts: Approved Standard*, 3. ed., Ed., Clinical and Laboratory Standards Institute, **2008**.
25. Rex, J. H. *Reference Method for Broth Dilution Antifungal Susceptibility Testing of Filamentous Fungi: Approved Standard*, 2. ed., Ed., Clinical and Laboratory Standards Institute, **2008**.

Synthesis, *in vitro* Antitrichomonal Activity, and Docking Study of *N*-[(4-substituted phenyl)-1,3-thiazol-2-yl]-4-substituted Benzenesulfonamides

Rubén M. Carballo¹, Héctor A. Peniche-Pavía¹, Ramiro Quijano-Quiñones¹, David Cáceres-Castillo¹, Gumersindo Mirón-López¹, Manlio Graniel-Sabido¹, Andrea Reyes-Cuapio¹, Rosa E. Moo-Puc², Lía Valencia-Chan², Gonzalo J. Mena-Rejón^{1*}

¹Facultad de Química, Universidad Autónoma de Yucatán, C. 43 No. 613, Col. Inalámbrica, Mérida, 97069, Yucatán, México.

²Unidad de Investigación Médica Yucatán, Unidad Médica de Alta Especialidad, Centro Médico “Ignacio García Téllez”, IMSS, C. 41, No. 439, Col. Industrial, C.P., Mérida, 97150, Yucatán, México.

*Corresponding author: Gonzalo J. Mena-Rejón, email: mrejon@correo.uady.mx

Received February 15th, 2023; Accepted August 24th, 2023.

DOI: <http://dx.doi.org/10.29356/jmcs.v68i1.1975>

Abstract. Infection by *Trichomonas vaginalis* has a high incidence/prevalence worldwide. It has been associated with a predisposition to cervical neoplasia or prostate cancer and an increased risk of acquisition of human papillomavirus (HPV) and human immunodeficiency virus (HIV). Besides, resistance to the drugs used for trichomoniasis treatment has increased in the last 30 years. Herein, thirteen phenylthiazolylbenzene sulfonamides were synthesized and evaluated for their *in vitro* activity against *Trichomonas vaginalis*. Among them, four derivatives showed higher anti-trichomonal activity than metronidazole ($IC_{50} = 0.93 \mu M$), while their cytotoxicity levels were not significant. These compounds were subject to molecular docking studies using *Trichomonas vaginalis* ferredoxin as target. The results revealed that the orientation of the nitro group of the active derivatives is toward [2Fe-2S], the cluster responsible for high reactive oxygen species generation. Finally, it was evident that the presence of a nitro group in the structure of the synthesized phenylthiazolylbenzene sulfonamides is essential for their trichomonocidal activity.

Keywords: Phenylthiazolyl benzenesulfonamide; phenylthiazole; benzenesulfonamide; *Trichomonas vaginalis*; trichomoniasis; docking studies; *Trichomonas vaginalis* ferredoxin.

Resumen. A nivel mundial la infección por *Trichomonas vaginalis* tiene una alta incidencia/prevalencia y se ha asociado con una predisposición a padecer neoplasia cervical o cáncer de próstata, así como a generar un mayor riesgo de adquirir el virus del papiloma humano (VPH) y el virus de la inmunodeficiencia humana (VIH). Además, en los últimos 30 años, la resistencia a los fármacos utilizados para el tratamiento de la tricomoniasis ha aumentado. En el presente trabajo, trece sulfonamidas de feniltiazolilbenceno fueron sintetizadas y evaluadas *in vitro* contra *Trichomonas vaginalis*. Cuatro de ellas exhibieron una actividad anti-tricomonas mayor que el metronidazol ($CI_{50} = 0.93 \mu M$), a la vez que citotoxicidad no significativa. Por tal motivo, estos compuestos fueron sometidos a estudios de acoplamiento molecular utilizando como diana a la ferredoxina de *T. vaginalis*. Los resultados revelaron que la orientación del grupo nitro de los derivados activos está dirigida hacia el grupo [2Fe-2S], responsable de la generación de especies de oxígeno altamente reactivas. Finalmente, se evidenció que la presencia de al menos un grupo nitro en la estructura de las sulfonamidas de feniltiazolilbenceno sintetizadas es esencial para su actividad tricomonocida.

Palabras clave: Feniltiazolil bencensulfonamida; feniltiazol; bencensulfonamida; *Trichomonas vaginalis*; trichomoniasis; acoplamiento molecular; ferredoxina de *Trichomonas vaginalis*.

Introduction

Parasite diseases have enormous health, social, and economic impact worldwide [1] because of their high prevalence rates and morbidity. Indeed, it has been reported estimations regard 20 % of the world's population is infected by at least one parasite [2]. In this sense, trichomoniasis, a sexually transmitted protozoal infection caused by *Trichomonas vaginalis*, affects both women and men with a high incidence/prevalence worldwide. The WHO estimated that in 2016, the global prevalence and incidence estimates of trichomoniasis were 5.9% and 156 million cases, respectively [3].

Trichomoniasis has been catalogued as a mild and curable disease that, in most cases, courses without symptoms. However, it can cause pelvic inflammatory disease, infertility, and adverse pregnancy outcomes such as premature rupture of membranes, preterm birth, and low birth weight [4]. Importantly, an aspect of concern of this disease is its association with a predisposition to cervical intraepithelial neoplasia or prostate cancer, as well as with an increased risk of acquisition of human papillomavirus (HPV) and human immunodeficiency virus (HIV) [4,5].

Metronidazole and tinidazole, 5-nitroimidazoles developed decades ago [6], are the current drugs approved by the Food and Drug Administration for the systemic treatment of trichomoniasis. Unfortunately, since 1990, the appearance of resistance to these drugs has been described [7,8]. Thus, these facts show the obvious necessity to search for new trichomonocidal compounds.

It is well known that thiazole derivatives exhibit a wide range of biological activities, including anti-protozoal properties; consequently, this heterocycle system is considered a privileged structural motif [9]. As part of our search for anti-protozoal heterocyclic compounds and accordingly to those data, few years ago, in our laboratory were synthesized a series of 2-amino-4-phenylthiazole derivatives which showed to have interesting activity against trophozoites of *Giardia lamblia* [10]. More recently, we found that two acetamide derivatives also have potent activity against *Trichomonas vaginalis* ($IC_{50} = 0.60 \mu M$) [11].

On the other hand, one strategy used in the search for new bioactive compounds is fusing a privileged structure with relevant biological active scaffolds. In this context, sulfonamide is considered relevant scaffold because its derivatives have, besides their well-known antibacterial properties, important biological activities. Also, it is remarkable that hybrids obtained by adding a sulfonamide group to biologically active scaffolds showed new activities or an enhancement of the previous showed activities [12]. An excellent example of those hybrids is sulphimidazole, which presents sulfonamide and 5-nitroimidazole moieties in its structure and exhibits a remarkable activity against *T. vaginalis* strains [13,14].

Thereby, based on our previous findings and the antitrichomonal activity exhibited by sulphimidazoles, we decided to synthesize several benzenesulfonamide derivatives of 2-amino-4-phenyl thiazole, to evaluate their antitrichomoniasis capability their activity against trophozoites of *T. vaginalis*, and to perform a docking study on *Trichomonas vaginalis* ferredoxin (TvFn).

Experimental

Materials and methods

All commercial reagents were obtained from Sigma-Aldrich (Saint Louis, MO, USA) and used as received. Microwave reactions were conducted in 25 mL open glass vessels using a CEM Discover microwave reactor. Analytical thin-layer chromatography (TLC) was performed on 25 μm particle size silica gel GF-254 aluminum plates. Column chromatography was undertaken with 0.063–0.037 mm particle size silica gel. FT-IR spectra were recorded on a Nicolet iS5 FTIR spectrometer, using an accessory for attenuated total reflectance

(ATR). $^1\text{H-NMR}$ and $^{13}\text{C-NMR}$ spectra were recorded in DMSO-d_6 on Bruker Avance 400 spectrometer at 400 and 100 MHz, respectively, and the residual solvent peak was used as an internal reference. The δ values are given in ppm. Mass spectra (MS) were obtained on a Jeol GC-Mate II under electron impact (EI) at 70 eV.

General procedure for the synthesis of thiazole derivatives

Thiazole derivatives were synthesized following the methodology previously reported by us [13]. Briefly, a mixture of thiourea (17.2 mmol, 1.3 g), *p*-substituted acetophenone (8.6 mmol), and iodine (8.6 mmol, 2.2 g) were placed in an open vessel and subjected to MW irradiation (50 W) at indicated temperature for 10 min. After, the crude mixture was cooled to 70 °C and then it was triturated, filtered, and washed with Et_2O . The crude product was dissolved in hot water at pH 11–12. The precipitated was filtered and crystallized from $\text{EtOH-H}_2\text{O}$ (1:4) to obtain the 2-amino-4-aryl-1,3-thiazole derivative.

General procedure for the synthesis of compounds 5, 6a, 6c-f, 7a, 7c-f

A thiazole derivative (1.7 mmol), DMAP (0.17 mmol), and triethylamine (3.4 mmol) were added to a solution of a 2.5 mmol of the suitable sulphonyl chloride in 9 mL of anhydrous dichloromethane. The mixture was stirred at room temperature. The reaction was monitored by TLC until completion, then the formed precipitated was washed with acetone, dried at room temperature, and purified by column chromatography on silica gel using a gradient elution with *n*-hexane–ethyl acetate (10–100 % of ethyl acetate) to yield the desired compound.

General procedure for the synthesis of compounds 6b, 7b

A thiazole derivative (1.7 mmol), DMAP (0.34 mmol), and triethylamine (5.1 mmol) were added to a solution of a 4.25 mmol of the suitable sulphonyl chloride in 9 mL of anhydrous dichloromethane. The mixture was stirred at room temperature for 48 h, then were added, for 10 minutes, 10 mL of a 2.5 M NaOH solution, and the mixture were extracted with dichloromethane. The organic layer was dried under vacuum and subject column chromatography on silica gel using a gradient elution with *n*-hexane–ethyl acetate (10–100% of ethyl acetate) to yield the desired compound.

***N*-(4-phenyl-1,3-thiazol-2-yl) benzenesulfonamide (5)**: Yield 20 %. ATR-FTIR: ν_{max} , 1598 ($\text{Csp}^2\text{-Csp}^2$), 1499 ($\text{Csp}^2\text{-Csp}^2$), 1291 (SO_2), 1139 (SO_2) cm^{-1} . $^1\text{H NMR}$ (400 MHz, DMSO-d_6) δ : 13.27 (s, 1H, H-1), 7.87 (d, $J = 8$ Hz, 2H, H-2'', H-6''), 7.70 (d, $J = 7.6$ Hz, 2H, H-2', H-6'), 7.62-7.54 (m, 3H, H-3', H-4', H-5'), 7.44-7.39 (m, 3H, H-3'', H-4'', H-5''), 7.21 (s, 1H, H-5') ppm. $^{13}\text{C NMR}$ (100 MHz, DMSO-d_6) δ 168.8 (C-2'), 142.2 (C-4''), 136.7 (C-1'), 132.2 (C-4'), 129.2 (C-4''), 129.1 (C-3', C-5'), 129.0 (C-3'', C-5''), 128.7 (C-1''), 125.9 (C-2', C-6'), 125.6 (C-2'', C-6''), 103.5 (C-5'). MS (EI, 70 eV): 316 [M^+] (100), 285 (2), 251 (4), 175 (30), 134 (22), 77 (16), 18 (5) *m/z*.

***N*-(4-phenyl-1,3-thiazol-2-yl)-4-methyl benzenesulfonamide (6a)** [25]: Yield 30 %. ATR-FTIR: ν_{max} 3024 ($\text{Csp}^2\text{-H}$), 2919 ($\text{Csp}^3\text{-H}$), 1594 ($\text{Csp}^2\text{-Csp}^2$), 1486 ($\text{Csp}^2\text{-Csp}^2$), 1384 (SO_2), 1167 (SO_2) cm^{-1} . $^1\text{H NMR}$ (400 MHz, DMSO-d_6) δ : 7.72 (d, $J = 8$ Hz, 2H, H-2'', H-6''), 7.50-7.40 (m, 5H, H-2', H-3', H-5', H-6', H-4''), 7.21 (s, 1H, H''-5), 7.12 (d, $J = 8$ Hz, 2H, H-3'', H-5''), 2.29 (s, 3H, C-4'- CH_3); $^{13}\text{C NMR}$ (100 MHz, DMSO-d_6) δ 170.5 (C-2'), 144.7 (C-4''), 139.3 (C-1'), 138.4 (C-4'), 129.5 (C-4''), 129.1 (C-3', C-5'), 128.8 (C-3'', C-5''), 128.4 (C-1''), 125.8 (C-2'', C-6''), 125.5 (C-2', C-6'), 102.9 (C-5'), 20.9 (C-4'- CH_3). MS (EI, 70 eV): 331 [$\text{M}^+ + 1$] (2), 177 (100), 134 (8), 93 (2), 68 (20), 51 (44), 32 (32) *m/z*.

***N*-[4-(*p*-tolyl)-1,3-thiazol-2-yl]-4-methyl benzenesulfonamide (6b)** [25]: Yield 40 %. ATR-FTIR: ν_{max} 1601 ($\text{Csp}^2\text{-Csp}^2$), 1448 ($\text{Csp}^2\text{-Csp}^2$), 1318 (SO_2), 1131 (SO_2) cm^{-1} . $^1\text{H NMR}$ (400 MHz, DMSO-d_6) δ : 13.17 (1H, H-1), 7.73 (d, $J = 7.68$ Hz, 2H, H-2'', H-6''), 7.58 (d, $J = 7.44$ Hz, 2H, H-2', H-6'), 7.34 (d, $J = 7.68$ Hz, 2H, H-3', H-5'), 7.23 (d, $J = 7.72$ Hz, 2H, H-3'', H-5''), 7.12 (s, 1H, H-5'), 2.34 (s, 3H, C-4'- CH_3), 2.30 (s, 3H, C-4''- CH_3). $^{13}\text{C NMR}$ (100 MHz, DMSO-d_6) δ 169.1 (C-2'), 142.4 (C-4''), 139.4 (C-1'), 138.8 (C-4'), 136.7 (C-4''), 129.5 (C-3'', C-5''), 129.4 (2CH, C-3', C-5'), 129.9 (C-1''), 126.0 (C-2', C-6'), 125.5 (C-2'', C-

6'''), 102.3 (CH-5''), 21.0 (C-4'-CH₃), 20.8 (C-4'''-CH₃). MS (EI, 70 eV): 344 [M⁺] (75), 279 (30), 189 (100), 148 (85), 91 (60), 39 (8) m/z.

N-[4-(4-methoxyphenyl)-1,3-thiazol-2-yl] 4-methyl benzenesulfonamide (6c) [25]: Yield 60 %. ATR-FTIR: ν_{\max} 3099 (Csp²-H), 2980 (Csp³-H), 1621 (Csp²-Csp²), 1448 (Csp²-Csp²), 1300 (SO₂), 1172 (SO₂) cm⁻¹. ¹H NMR (400 MHz, DMSO-d₆) δ : 8.91 (brs, 1H, H-1), 7.65 (d, J = 8.8 Hz, 2H, H-2', H-6'), 7.51 (d, J = 8 Hz, 2H, H-2'', H-6''), 7.14 (d, J = 7.9 Hz, 2H, H-3', H-5'), 7.08 (s, 1H, H-5''), 7.04 (d, J = 8.8 Hz, 2H, H-3'', H-5''), 3.80 (s, 3H, C-4'''-OCH₃), 2.29 (s, 3H, C-4'-CH₃). ¹³C NMR (100 MHz, DMSO-d₆) δ : 170.6 (C-2''), 160.3 (C-4''), 144.6 (C-4'), 139.0 (C-1'), 138.7 (C-4'), 128.5 (C-3', C-5'), 127.5 (C-2'', C-6''), 125.7 (C-2', C-6'), 121.3 (C-1'''), 114.6 (C-3'', C-5''), 100.8 (C-5'), 55.5 (C-4'''-OCH₃), 21.0 (C-4'-CH₃). MS (EI, 70 eV): 246 [M⁺-114] (66), 205 (100), 175 (8), 149 (35), 121 (20), 77 (11), 39 (5) m/z.

N-[4-(4-fluorophenyl)thiazol-2-yl]-4-methyl benzenesulfonamide (6d): Yield 50 %. ATR-FTIR: ν_{\max} 3094 (Csp²-H), 1615 (Csp²-Csp²), 1443 (Csp²-Csp²), 1311 (SO₂), 1135 (SO₂) cm⁻¹. ¹H NMR (400 MHz, DMSO-d₆) δ : 8.79 (s, 1H, H-1), 7.77 (t, J = 8 Hz, 2H, H-2'', H-6''), 7.54 (d, J = 8 Hz, 2H, H-2', H-6'), 7.33-7.29 (t, J = 8.8, 2H, H-3'', H-5''), 7.20 (s, 1H, H-5'), 7.15 (d, J = 7.88, 2H, H-3', H-5'), 2.28 (s, 3H, C-4'-CH₃); ¹³C NMR (100 MHz, DMSO-d₆) δ 170.2 (C-2''), 162.4 (d, J = 245.42 Hz, C-4''), 144.8 (C-4'), 140.0 (C-1'), 138.4 (C-4'), 128.4 (C-3', C-5'), 128.1 (d, J = 8 Hz, C-2'', C-6''), 126.4 (C-1'''), 125.6 (C-2', C-6'), 116.0 (d, J = 22 Hz, C-3'', C-5''), 102.6 (CH-5''), 20.9 (C-4'-CH₃). MS (EI, 70 eV): 348 [M⁺] (75), 283 (40), 193 (100), 152 (100), 122 (6), 91 (36), 65 (10), 39 (4) m/z.

N-[4-(4-chlorophenyl)thiazol-2-yl]-4-methyl benzenesulfonamide (6e) [25]: Yield 70 %. ATR-FTIR: ν_{\max} 3089 (Csp²-H), 1616 (Csp²-Csp²), 1448 (Csp²-Csp²), 1308 (SO₂), 1167 (SO₂) cm⁻¹. ¹H NMR (400 MHz, DMSO-d₆) δ : 8.92 (s, 1H, H-1), 7.73 (d, J = 8.4 Hz, 2H, H-2'', H-6''), 7.55 (d, J = 8.6 Hz, 2H, H-2', H-6'), 7.52 (d, J = 7.9 Hz, 2H, H-3'', H-5''), 7.31 (s, 1H, H-5'), 7.14 (d, J = 8 Hz, 2H, H-3', H-5'), 2.29 (s, 3H, C-4'-CH₃). ¹³C NMR (100 MHz, DMSO-d₆) δ : 170.5 (C-2''), 144.8 (C-4'), 138.3 (C-1'), 138.3 (C-4'), 134.0 (C-4'), 129.1 (C-3'', C-5''), 128.3 (C-3', C-5'), 127.8 (C-1'), 127.6 (C-2'', C-6''), 125.5 (C-2', C-6'), 103.8 (C-5'), 20.9 (C-4'-CH₃). MS (EI, 70 eV): 250 [M⁺-114] (42), 209 (100), 168 (50), 133 (30), 89 (36), 41(15) m/z.

N-[4-(4-nitrophenyl)-1,3-thiazol-2-yl]-4-methyl benzenesulfonamide (6f) [25]: Yield 65 %. ATR-FTIR: ν_{\max} 3077 (Csp²-H), 1598 (Csp²-Csp²), 1537 (-NO₂), 1348 (-NO₂), 1499 (Csp²-Csp²), 1349 (SO₂), 1139 (SO₂) cm⁻¹. ¹H NMR (400 MHz, DMSO-d₆) δ : 8.28 (d, J = 8.9 Hz, 2H, H-3'', H-5''), 8.02 (d, J = 8.9 Hz, 2H, H-2'', H-6''), 7.49 (d, J = 7.9 Hz, 2H, H-2', H-6'), 7.49 (s, 1H, H-5'), 7.12 (d, J = 7.9 Hz, 2H, H-3', H-5'), 2.29 (s, 3H, C-4'-CH₃). ¹³C NMR (100 MHz, DMSO-d₆) δ : 170.3 (C-2''), 147.1 (C-4''), 144.6 (C-4'), 139.3 (C-1'), 138.5 (C-4'), 135.8 (C-1'''), 128.4 (C-3', C-5'), 126.7 (C-3'', C-5''), 125.6 (C-2', C-6'), 124.3 (C-2'', C-6''), 107.4 (C-5'), 20.90 (C-4-CH₃). MS (EI, 70 eV): 278 [M⁺-97] (8), 253 (2), 221 (6), 172 (4), 157 (100), 139 (28), 121 (73), 89 (74), 77 (20), 51 (8), 28 (8), 18 (22) m/z.

N-(4-phenylthiazol-2-yl)-4-nitro benzenesulfonamide (7a): Yield 40 %. ATR-FTIR: ν_{\max} 2985 (Csp²-H), 1640 (Csp²-Csp²), 1561 (-NO₂), 1501 (Csp²-Csp²), 1167 (SO₂) cm⁻¹. ¹H NMR (400 MHz, DMSO-d₆) δ : 13.52 (brs, 1H, H-1), 8.38 (d, J = 8.8 Hz, 2H, H-3', H-5'), 8.10 (d, J = 8.8 Hz, 2H, H-2', H-6'), 7.71 (d, J = 6.8 Hz, 2H, H-2'', H-6''), 7.44-7.41 (m, 3H, H-3'', H-4'', H-5''), 7.28 (s, 1H, H-5'). ¹³C NMR (100 MHz, DMSO-d₆) δ : 169.7 (C-2'), 149.4 (C-4'), 147.6 (C-4''), 137.1 (C-1'), 129.3 (C-1'''), 129.1 (C-2', C-6'), 128.5 (C-4''), 127.4 (C-3'', C-5''), 125.7 (C-2'', C-6''), 124.6 (C-3', C-5'), 104.1 (C-5'). MS (EI, 70 eV): 296 [M⁺-65] (100), 250 (30), 179 (37), 134 (13), 105(7), 76(40), 45(7) m/z.

N-[4-(*p*-tolyl)-1,3-thiazol-2-yl]-4-nitro benzenesulfonamide (7b): Yield 45 %. ATR-FTIR: ν_{\max} 2918 (Csp³-H), 1598 (Csp²-Csp²), 1538.01 (-NO₂), 1322 (SO₂), 1142 (SO₂) cm⁻¹. ¹H NMR (400 MHz, DMSO-d₆) δ : 13.48 (s, 1H, H-1), 8.36 (d, J = 8.5 Hz, 2H, H-3', H-5'), 8.08 (d, J = 8.6 Hz, 2H, H-2', H-6'), 7.58 (d, J = 7.8 Hz, 2H, H-2'', H-6''), 7.22 (d, J = 7.8 Hz, 2H, H-3'', H-5''), 7.18 (s, 1H, H-5'), 2.29 (s, 3H, C-4''', -CH₃). ¹³C NMR (100 MHz, DMSO-d₆) δ : 169.7 (C-2''), 149.4 (C-4'), 147.7 (C-4''), 139.0 (C-1'), 132.3 (C-4'''), 129.6

(C-2', C-6'), 127.4 (C-3'', C-5''), 125.9 (C-1''), 125.6 (C-2'', C-6''), 124.6 (C-3', C-5'), 103.1 (C-5''), 20.9 (C-4''-CH₃). MS (EI, 70 eV): 310 [M⁺-65] (100), 264(30), 223 (3), 193 (29), 147 (13), 115(9), 76(23), 45(3) m/z.

N-[4-(4-methoxyphenyl)-1,3-thiazol-2-yl]-4-nitro benzenesulfonamide (7c) [25]: Yield 47 %. ATR-FTIR: ν_{\max} , 2962 (Csp²-H), 2840 (Csp³-H), 1617 (Csp²-Csp²), 1526 (-NO₂), 1460 (Csp²-Csp²), 1351 (-NO₂), 1296 (SO₂), 1182 (SO₂) cm⁻¹. ¹H NMR (400 MHz, DMSO-d₆) δ : 8.96 (s, 1H, H-1), 8.21 (d, *J* = 8.84 Hz, 2H, H-3', H-5'), 7.87 (d, *J* = 8.88 Hz, 2H, H-2', H-6'), 7.63 (d, *J* = 8.8 Hz, 2H, H-2'', H-6''), 7.09 (s, 1H, H-5''), 7.04 (d, *J* = 8.8 Hz, 2H, H-3'', H-5''), 3.79 (s, 3H, C-4''-OCH₃). ¹³C NMR (100 MHz, DMSO-d₆) δ : 170.4 (C-2''), 160.2 (C-4''), 153.8 (C-4'), 147.4 (C-4''), 138.8 (C-1'), 127.4 (C-2', C-6'), 127.0 (C-2'', C-6''), 123.5 (C-3', C-5'), 121.1 (C-1''), 114.5 (C-3'', C-5''), 100.8 (C-5''), 55.4 (C-4''-OCH₃). MS (EI, 70 eV): 346 [M⁺-46] (100), 283 (3), 205 (94), 164 (90), 121 (11), 77 (35), 45 (5) m/z.

N-[4-(4-fluorophenyl)-1,3-thiazol-2-yl]-4-nitro benzenesulfonamide (7d): Yield 15 %. ATR-FTIR: ν_{\max} , 2985 (Csp²-H), 1643 (Csp²-Csp²), 1565 (-NO₂), 1166 (SO₂) cm⁻¹. ¹H NMR (400 MHz, DMSO-d₆) δ : 8.23 (d, *J* = 8.6 Hz, 2H, H-3', H-5'), 7.83 (d, *J* = 8.64 Hz, 2H, H-2', H-6'), 7.66 (dd, *J* = 8.36 & 5.36 Hz, 2H, H-2'', H-6''), 7.18 (t, *J* = 8.64 Hz, 2H, H-3'', H-5''), 6.92 (s, H-5''). ¹³C NMR (100 MHz, DMSO-d₆) δ : 170.4 (C-2''), 162.5 (d, *J* = 245.93 Hz, C-4''), 154.0 (C-4'), 147.4 (C-4''), 138.5 (C-1'), 128.4 (d, *J* = 8.59 Hz, C-2'', C-6''), 127.0 (C-2', C-6'), 125.2 (C-1''), 123.5 (C-3', C-5'), 116.1 (d, *J* = 21.84, C-3'', C-5''), 102.9 (C-5''). MS (EI, 70 eV): 356 [M⁺-65] (5), 314 (100), 281 (9), 243 (37), 197 (46), 152 (17), 122 (16), 76 (23), 30 (10) m/z.

N-[4-(4-chlorophenyl)-1,3-thiazol-2-yl]-4-nitro benzenesulfonamide (7e) [26]: Yield 35 %. ATR-FTIR: ν_{\max} , 1605 (Csp²-Csp²), 1539 (-NO₂), 1387 (-NO₂), 1296 (SO₂), 1138 (SO₂) cm⁻¹. ¹H NMR (400 MHz, DMSO-d₆) δ : 8.20 (d, *J* = 8.6 Hz, 2H, H-3', H-5'), 7.86 (d, *J* = 8.6 Hz, 2H, H-2', H-6'), 7.73 (d, *J* = 8.6 Hz, 2H, H-2'', H-6''), 7.55 (d, *J* = 8.6 Hz, 2H, H-3'', H-5''), 7.29 (s, 1H, H-5''). ¹³C NMR (100 MHz, DMSO-d₆) δ : 170.4 (C-2''), 154.0 (C-4'), 147.4 (C-4''), 138.7 (C-1'), 133.9 (C-4''), 129.1 (C-3'', C-5''), 128.0 (C-1''), 127.7 (C-2'', C-6''), 127.0 (C-2'', C-6''), 123.5 (C-3', C-5'), 103.6 (C-5''). MS (EI, 70 eV): 361 [M⁺-33] (100), 322 (4), 298 (40), 251 (4), 223 (4), 175 (44), 134 (48), 76 (17), 51 (14) m/z.

N-[4-(4-nitrophenyl)-1,3-thiazol-2-yl]-4-nitro benzenesulfonamide (7f): Yield 70 %. ATR-FTIR: ν_{\max} , 1592 (Csp²-Csp²), 1522 (-NO₂), 1344 (-NO₂), 1158.53 (SO₂) cm⁻¹. ¹H NMR (400 MHz, DMSO-d₆) δ : 8.27 (d, *J* = 9 Hz, 2H, H-3'', H-5''), 8.20 (d, *J* = 8.8 Hz, 2H, H-3', H-5'), 8.03 (d, *J* = 8.98 Hz, 2H, H-2'', H-6''), 7.83 (d, *J* = 8.8 Hz, 2H, H-2', H-6'), 7.46 (s, 1H, H-5''). ¹³C NMR (100 MHz, DMSO-d₆) δ : 170.5 (C-2''), 154.4 (C-4'), 147.8 (C-4''), 147.4 (C-4''), 139.5 (C-1''), 136.8 (C-1'), 127.4 (C-2'', C-6''), 127.2 (C-2', C-6'), 124.6 (C-3'', C-5''), 123.9 (C-3', C-5'), 107.6 (C-5''). MS (EI, 70 eV): 405 [M⁺-1] (4), 221 (100), 202 (88), 191 (50), 175 (99), 156 (48), 133 (50), 109 (50), 89 (99), 75 (48), 50 (8), 18 (23) m/z.

Trichomonocidal assay

In vitro susceptibility assays used *Trichomonas vaginalis* strain GT3 and the sub-culture method of Cedillo-Rivera *et al* [15]. The compounds were dissolved in 1 mL of dimethylsulfoxide (DMSO) and added to microtubes containing 1.5 mL of medium in order to reach concentrations of 1, 2, 10, and 20 μ g/mL. The solutions were inoculated with *T. vaginalis* trophozoites to achieve an inoculum of 4×10^4 trophozoites/mL and then were incubated for 48 h at 37 °C. Each test included metronidazole as positive control, a control (culture medium plus trophozoites and DMSO), and a blank (culture medium). After incubation, the trophozoites were detached by chilling and samples of each tube were sub-cultured in fresh medium for another 48 h, without anti-protozoal drugs or compounds. The final number of parasites was determined with a haemocytometer and the 50 % inhibitory concentration (IC₅₀) was calculated by probit analysis (GraphPad Prim 4 software). The experiments were performed in duplicate and replicated.

Cytotoxicity assay

Cytotoxic activities were determined by the sulforhodamine B technique [16] using African green monkey kidney (VERO, ATCC-CCL-81) cells, from the American Type Culture Collection (ATCC). Cells undergoing exponential growth were seeded in a 96-well cell culture plate; 100 μL of cell suspension at a concentration of 5×10^4 cells/mL were added to each well and it was incubated at 37 °C for 24 h in a CO₂ incubator. Cytotoxicity (CC₅₀) was measured until cells reached 90 % confluency without FBS. Each compound was tested at increasing concentrations in serial dilution (50-1.625 $\mu\text{g/mL}$) mL and incubated for 48 h. At the end of the exposure time, the medium was removed, and the cells were fixed by adding 50 μL of 10 % trichloroacetic acid solution to each well and incubated at 4 °C for 30 min. After incubation, the trichloroacetic acid was eliminated and 50 μL of sulforhodamine B (0.1 % sulforhodamine B in 1 % acetic acid) were added to each well and left in contact with the cells for 30 min, after which they were washed with 150 μL of 1 % acetic acid, and rinsed three times until only dye adhering to the cells was left. The plates were dried and 100 μL of 10 mM Tris base were added to each well to solubilize the dye. The plates were shaken gently for 10 min and the cellular proliferation was determined by measuring the optical density (OD) at 540 nm using a bioassay reader (BioRad, USA). Docetaxel (Taxotere[®], Sigma- Aldrich Co.) was used as positive control, whereas untreated cells were used as a negative control. Each concentration was evaluated by triplicate in an assay by three independent experiments. The concentration of each compound that killed 50 % of the cells (CC₅₀), was calculated by GraphPad Prism 4 software. The selectivity index (SI) of the compounds is defined as the ratio of cytotoxic activity on normal cells to antitrichomonal activity (SI = CC₅₀ Vero cells/IC₅₀ *T. vaginalis*).

Molecular docking

The molecular geometries of all compounds were fully optimized using density functional theory with a 6-31G (d, p) basis set. The exchange-correlation potential was evaluated using the hybrid functional B3LYP [17]. After optimization, a frequencies calculation was performed to characterize all the stationary points at the same computational level and no imaginary frequency was observed. All the calculations, including polar surface areas, were carried out using the SPARTAN 20 program [18].

The crystal structure of the *Trichomonas vaginalis* Ferredoxin (PDB-ID: 1L5P) at 2.2 Å resolution was obtained from the Protein Data Bank (<http://www.rcsb.org/pdb>) [19]. The molecular docking studies were performed using the software Autodock v 4.2 and the Autodock tools v 4.2 (ADT) [20] graphical user interface was used to calculate the Gasteiger–Marsili charges for the protein and to add polar hydrogens. The polar hydrogen charges of Gasteiger-type were assigned, and the nonpolar hydrogens were merged with the carbon atoms. The partial charges of the ligands were computed using PM6 semiempirical calculation employing the SPARTAN20 code. All the protein was considered as a rigid body and the ligands being flexible. All the torsion and rotatable bonds in the ligand were defined. The grid box for chalcones derivatives were centered at the residue Thr37, with a dimension of $52 \times 52 \times 52$ with a spacing grid of 0.375 Å. The search was performed with the Lamarckian Genetic Algorithm as is implemented in Autodock v 4.2 code. The population of 150 individuals was mutated with a mutation rate of 0.02 and evolved for 10 generations. The number of the docking runs was 50. A cluster analysis was performed based on a rms deviation values lower than 2.0 Å referenced to the starting geometry. The best binding mode was selected based on the lowest energy binding and the more populated cluster. The visualization of the complex was done using Maestro [21].

Results and discussion

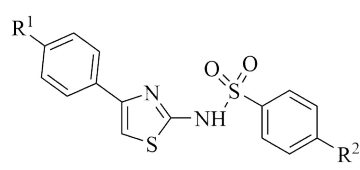
Chemistry

Firstly, the 2-amino-4-phenyl thiazoles were obtained by condensation of *p*-substituted acetophenones and thiourea according to our previously reported method [22]. As a second step, equimolar reactions between 2-amino-4-phenyl thiazol derivatives and arylsulfonyl chlorides (4) were performed in the presence of Et₃N (2 eq.) and 4-dimethylaminopyridine (DMAP) (0.1 eq) [23]. Thus, eleven sulfonamides were obtained (**5**, **6a**, **6c-f**, **7a**, **7c-f**) (Fig. 1).

Another two sulfonamides (**6b** and **7b**) were synthesized, increasing the concentration of promoters (Et₃N at 3 eq. and DMAP at 0.2 eq) and, according to Greenfield *et al.* [24], the equivalents of arylsulfonyl chloride were increased up to 2.5, and basic hydrolysis was included (NaOH at 2.5 M).

Synthesized sulfonamides yields range from 15 to 70 %. Thirty percent of the sulfonamides were synthesized with yields over 50 %, being the yields of compounds **6e** and **7f** the highest; moreover, compound **6e** exhibited a yielding 2.5-fold than when pyridine was used as catalyst but, contrastingly, compounds **5**, **6b**, and **7e** exhibited the lowest yields. Interestingly, only the compound **7e** yield was significant lesser than that reported in the literature. Therefore, the use of DMAP instead pyridine moderately improved the yielding.

The synthesized sulfonamides were split into two small series, one formed by the sulfonamides *para*-substituted at phenylthiazolyl moiety and the other one grouped those sulfonamides showing *para*-substitution at phenylsulfonyl moiety. All synthesized compounds were characterized by IR, ¹H, ¹³C NMR, and mass spectra.



Comp.	R ¹	R ²
5	H	H
6a	H	Me
6b	Me	Me
6c	MeO	Me
6d	F	Me
6e	Cl	Me
6f	NO ₂	Me
7a	H	NO ₂
7b	Me	NO ₂
7c	MeO	NO ₂
7d	F	NO ₂
7e	Cl	NO ₂
7f	NO ₂	NO ₂

Fig. 1. *N*-[4-(4-substituted phenyl)-1,3-thiazol-2-yl]-4-substituted benzenesulfonamides synthesized

Antitrichomonal activity

The synthesized thiazole sulfonamides were tested *in vitro* against *Trichomonas vaginalis* trophozoites, as well as against Green monkey kidney cells (Vero cells). The results of the bioassay tests are summarized in Table 1.

Usually, small molecules are tested in *in vitro* cellular assays at concentrations of 1 - 50 μM [27], and any compound exhibiting activity at a concentration lower than 25 μM can be considered as having significant activity [28]. Therefore, in the present study, a compound with an IC₅₀ < 25 μM was considered active. Thus, *T. vaginalis* were sensitive to six of 13 synthesized thiazole sulfonamides derivatives (**6f**, **7a-c**, **e**, **f**). Noteworthy, the IC₅₀'s showed by active thiazole sulfonamides ranged from 0.27 to 2.53 μM. Remarkably, four of those compounds (**7a**, **7b**, **7c**, and **7f**) exhibited more potent anti-trichomonal activity than the used positive control, metronidazole (IC₅₀ = 0.93 μM) (Table 1).

The synthesized trichomonocidal sulfonamides can be distinguished according to the position of their nitro group, then a set of four compounds bear a nitro group at phenylsulfonyl moiety (**7a-c,e**); while only one presents the nitro group located at phenylthiazolyl moiety (**6f**). The potency values of those two sets of sulfonamides showed marked differences, being three compounds belonging to the first set were 3-fold more potent than compound **6f**. Curiously, sulfonamide **7c** was almost equipotent to sulfonamide **6f**.

Table 1. Antitrichomonal activity, selectivity index and lipophilic parameters of phenylthiazolyl benzenesulfonamides.

C	R ¹	R ²	<i>T. vaginalis</i> IC ₅₀ μM ± SD ¹	Vero cells CC ₅₀ μM ± SD	SI ²
6f	NO ₂	Me	2.05 ± 0.09	33.24 (±0.98)	16.22
7a	H	NO ₂	0.58 ± 0.08	1136.97 (±7.22)	1960.00
7b	Me	NO ₂	0.64 ± 0.01	37.59 (±0.76)	58.73
7c	MeO	NO ₂	2.53 ± 0.02	1174.50(±3.45)	464.23
7e	Cl	NO ₂	0.58 ± 0.04	238.96 (±2.35)	412.00
7f	NO ₂	NO ₂	0.27 ± 0.02	>1230.31	>4556.70
MTZ ³			0.93 ± 0.02	367 (±2.87)	394

¹Standard deviation²Selectivity index³Metronidazole

Interestingly, compound **7f** (*N*-[4-(4-nitrophenyl)-1,3-thiazol-2-yl]-4-nitrobenzenesulfonamide) exhibited the highest trichomonocidal activity (0.27 μM), evidencing that the simultaneous presence of two nitro groups at the sulfonamide structure probably improves the anti-trichomonas activity. Furthermore, this compound was remarkably even 3.4-fold more potent than metronidazole.

Considering these findings and the fact that compound **5** was not active (IC₅₀ > 25 μM); then, it is plausible to think that trichomonocidal activity is related to the presence of a nitro group in sulfomanide structure.

Cytotoxic activity

The non-specific cytotoxicity (CC₅₀'s) of the synthesized trichomonocidal sulfonamides, evaluated against Green monkey kidney cells (Vero cells), ranged from 33.24 to >1230.31 μM. From those data, the harmfulness level for each compound was determined by calculating the selectivity index (SI = CC₅₀/IC₅₀). All sulfonamides exhibited notably low harmfulness levels (SI's > 10), being four of them even less harmful than metronidazole (SI = 394) and, surprisingly, the most active compound (**7f**) also resulted in the most selective one with a prominent SI >4556.70.

It is important to note that all assayed sulfonamides exhibited remarkable trichomonocidal activities *in vitro* (IC₅₀ ≤ 1 μg/mL), as well as prominent selectivity indexes (SI ≥ 10), therefore, they can be classified as antiparasitic hit compounds [29].

Molecular docking

Currently, 5-nitroimidazoles, mainly metronidazole, are the drugs of choice to treat trichomoniasis. Like all nitroaromatic drugs, these drugs owe their activity to high reactive oxygen species generated by the single-electron transfer reduction of their nitro group [30]. In *T. vaginalis*, TvFd (*Trichomonas vaginalis* ferredoxin) is a hydrogenosomal protein involved in the bioreduction of metronidazole. TvFd is a 9.8 kD protein constituted by 93 residues containing a [2Fe-2S] cluster responsible for electron transfer reactions [31, 32].

Since the anti-trichomonal activity of the synthesized sulfonamides depends on the presence of a nitro group in their structures, it is plausible to theorise that it is the result of the bioreduction of the nitro group [30].

Notably, the first electron transfer to form the ArNO₂/ArNO₂^{•-} couple is a factor involved in the nitroreduction control, hence in the order of bioreduction of the most important groups of ArNO₂, which is: nitropyridines > nitrofurans ≥ nitrothiophenes > nitrobenzenes > nitroimidazoles. Thus, this fact can explain the higher trichomonocidal activity exhibited by four of the synthesized sulfonamides.

To explore the putative mechanism of action of the compounds with higher antitrichomonal activity than metronidazole, a molecular docking study was performed with *Trichomonas vaginalis* ferredoxin (PDB-ID: 1L5P) as target. Thus, the affinity of those compounds, including metronidazole, for the amphipathic binding site of the iron-sulfur cluster was studied.

Metronidazole showed a binding affinity of -2.50 Kcal/mol (Table 2); besides that, its nitro group is oriented toward Lys46 and Thr37, which together Asp36, Gln39, Asn41, and Lys42 are the hydrophilic residues forming the front, top, and bottom of the binding site [31].

The binding affinity of all docked sulfonamides (**7a**, **7b**, **7e**, **7f**) ranged from -2.91 to -2.57 kcal/mol, being better than the one exhibited by metronidazole, and as was expected, their nitro group pointed toward the cluster binding loop of the [2Fe-2S] core. Interestingly, molecular docking showed these sulfonamides interact with the binding site in the same fashion as metronidazole (Table 2). Curiously, each sulfonamide interacts through interactions with residues Met32 and Ile48. These interactions are remarkable because are quite close to the residues 33–47, which form the loop covering the [2Fe-2S] cluster (Fig. 2) [31].

Table 2. Docking scores of the most active phenylthiazolyl benzenesulfonamides and metronidazole in the binding site for *Trichomonas vaginalis* ferredoxin.

Comp	Binding affinity (Kcal/mol)	Interactions with residues
7a	-2.57	Ser33, Met32, Cys47, Ile48
7b	-2.77	Lys7, Ser33, Thr37, Met32, Cys47, Ile48, Leu93
7e	-2.72	Ser33, Thr37, Phe23, Met32, Ile48
7f	-2.91	Ser33, Thr37, Gln70, Leu31, Met32, Ile48, Leu93
Metronidazole	-2.50	Ser33, Met32, Met32, Cys47, Ile48, Lys46

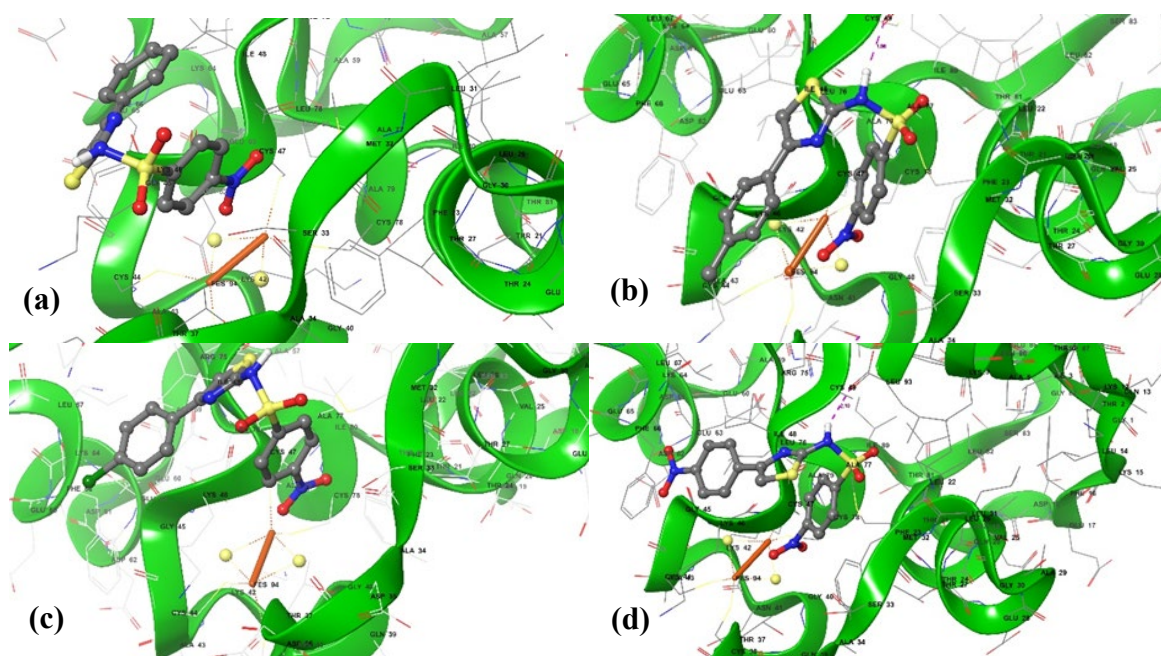


Fig. 2. 3D representations of the binding model of compound (a)**7a**, (b)**7b**, (c)**7e**, and (d)**7f** in the binding site of the [2Fe-2S] cluster of *Trichomonas vaginalis* ferredoxin.

Conclusions

Two sets of 13 *N*-[(4-substituted phenyl)-1,3-thiazol-2-yl]-4-substituted benzenesulfonamides were synthesized with modest yields, which not correlated to the chemical nature of the *para*-substituents in the starting sulfonyl chlorides. Four synthesized sulfonamides were more active against *Trichomonas vaginalis* than metronidazole, and remarkably, two of them were significantly more selective. Although antitrichomonal activity did not correlate with the chemical nature of the *para*-substituents at phenylthiazolyl moiety, it is clear that presence of a nitro group in the skeleton of the compound is essential for this activity. The docking study of the four more active sulfonamides revealed their interaction with the binding site of the *Trichomonas vaginalis* ferredoxin iron-sulfur cluster. Finally, it is necessary to expand the number of sulfonamides to improve the SAR analysis and perform a QSAR study.

Acknowledgements

This work was funded by grant FQUI-2011-0001 provided by Facultad de Química, Universidad Autónoma de Yucatán. Rosa E. Moo-Puc is grateful with Fundación IMSS A.C. for allowing access to the infrastructure of the Centro de Investigación en Salud “Dr. Jesús Kumate Rodríguez”.

References

1. Capela, R.; Moreira, R.; Lopes, F. *Int. J. Mol. Sci.* **2019**, *20*, 5748. DOI: <https://doi.org/10.3390/ijms20225748>.
2. Garrido-Cardenas, J.A.; Mesa-Valle, C.; Manzano-Agugliaro F. *Parasitology*. **2018**, *145*, 699-712. DOI: <https://doi.org/10.1017/S0031182017001718>.
3. Rowley J.; Vander Hoorn, S.; Korenromp, E.; Low, N.; Unemo, M.; Abu-Raddad, L.J.; Chico, R.M.; Smolak, A.; Newman, L.; Gottlieb, S.; Thwin, S.S.; Broutet, N.; Taylor, M.M. *Bull. World Health Organ.* **2019**, *97*, 548-562. DOI: <https://doi.org/10.2471/BLT.18.228486>.
4. Margarita, V.; Fiori, P.L.; Rappelli, P. *Front. Cell. Infect. Microbiol.* **2020**, *10*, 179. DOI: <https://doi.org/10.3389/fcimb.2020.00179>.
5. Stark, J.R.; Judson, G.; Alderete, J.F.; Mundodi, V.; Kucknoor, A.S.; Giovannucci, E.L.; Platz, E.A.; Sutcliffe, S.; Fall, K.; Kurth, T.; Ma, J.; Stampfer, M.J.; Mucci, L.A. *J. Natl. Cancer Inst.* **2009**, *101*, 1406-1411. DOI: <https://doi.org/10.1093/jnci/djp306>.
6. Pasupuleti, V.; Escobedo, A.A.; Deshpande, A.; Thota, P.; Roman, Y.; Hernandez, A.V. *PLoS Negl. Trop. Dis.* **2014**, *8*, e2733. DOI: <https://doi.org/10.1371/journal.pntd.0002733>.
7. Grossman III, J.H.; Galask, R.P. *Obstet. Gynecol.* **1990**, *76*, 521-522. PMID: 2381638.
8. Bala, V.; Chhonker, Y.S. *Eur. J. Med. Chem.* **2018**, *143*, 232-243. DOI: <https://doi.org/10.1016/j.ejmech.2017.11.029>.
9. Borcea, A.M.; Ionut, I.; Crisan, O.; Oniga, O. *Molecules*. **2021**, *26*, 624. DOI: <https://doi.org/10.3390/molecules26030624>.
10. Mocoelo-Castell, R.; Villanueva-Novelo, C.; Caceres-Castillo, D.; Carballo, R.M.; Quijano-Quinones, R.F.; Quesadas-Rojas, M.; Cantillo-Ciau, Z.; Cedillo-Rivera, R.; Moo-Puc, R.E.; Moujir, L.M.; Mena-Rejon, G. *J. Open Chem.* **2015**, *13*, 1127-1136. DOI: <https://doi.org/10.1515/chem-2015-0127>.
11. Mena-Rejón, G.; Pérez-Navarro, Y.; Torres-Romero, J.C.; Vázquez-Carrillo, L.; Carballo, R.M.; Arreola, R.; Herrera-España, A.; Arana-Argáez, V.; Quijano-Quinones, R.; Fernández-Sánchez, J.M.; Alvarez-Sánchez, M.E. *Parasitol. Res.* **2021**, *120*, 233-241. DOI: <https://doi.org/10.1007/s00436-020-06931-w>.

12. Apaydın, S.; Török, M. *Bioorg. Med. Chem. Lett.* **2019**, *29*, 2042-2050. DOI: <https://doi.org/10.1016/j.bmcl.2019.06.041>.
13. Malagoli, M.; Rossi, T.; Baggio, A.; Zandomeneghi, G.; Zanca, A.; Casolari, C.; Castelli, M. *Pharmacol. Res.* **2002**, *46*, 469-472. DOI: <https://doi.org/10.1080/14756366.2020.1863958>.
14. Hernández-Núñez, E.; Tlahuext, H.; Moo-Puc, R.; Torres-Gómez, H.; Reyes-Martínez, R.; Cedillo-Rivera, R.; Nava-Zuazo, C.; Navarrete-Vazquez, G. *Eur. J. Med. Chem.* **2009**, *44*, 2975-2984. DOI: <https://doi.org/10.1016/j.ejmech.2009.01.005>.
15. Cedillo-Rivera, R.; Chávez, B.; González-Robles, A.; Tapia-Contreras, A.; Yépez-Mulia, L. *J. Euk. Microbiol.* **2002**, *49*, 201-208. DOI: <https://doi.org/10.1111/j.1550-7408.2002.tb00523.x>.
16. Rahman, A.; Choudhary, M.I.; Thomsen, W.J. Bioassay techniques for drug development. In: *Manual of bioassay techniques for natural products research*. Harwood Academic Publishers Netherlands, **2001**. ISBN: 0-203-34349-2.
17. Lee, C.; Yang, W.; Parr, R.G. *Phys. Rev. B.* **1988**, *37*, 785-789. DOI: <https://doi.org/10.1103/physrevb.37.785>.
18. Spartan '20 Wavefunction, Inc., Irvine, CA.
19. Berman, H.M.; Westbrook, J.; Feng, Z.; Gilliland, G.; Bhat, T.N.; Weissig, H.; Shindyalov, I.N.; Bourne, P.E. *Nucleic Acids Res.* **2000**, *28*, 235-242. DOI: <https://doi.org/10.1093/nar/28.1.235>.
20. Morris, G. M.; Huey, R.; Lindstrom, W.; Sanner, M.F.; Belew, R.K.; Goodsell, D.S.; Olson, A.J. *J. Comput. Chem.* **2009**, *30*, 2785-2791. DOI: <https://doi.org/10.1002/jcc.21256>.
21. Maestro, Schrödinger, LLC, New York, NY, **2019**.
22. Caceres-Castillo, D.; Carballo, R.M.; Tzecz-Interian, J.A.; Mena-Rejon, G. *J. Tetrahedron Lett.* **2012**, *53*, 3934-3936. DOI: <https://doi.org/10.1016/j.tetlet.2012.05.093>.
23. Carballo, R.M.; Padilla-Montano, N.; Reyes-Martínez, R.; Miron-Lopez G.; Hernandez-Ortega, S. *Acta Crystallogr., Sect. E: Struct. Rep. Online.* **2014**, *70*, o6-7. DOI: <https://doi.org/10.1107/S1600536814002086>.
24. Greenfield, A.; Grosanu, C. *Tetrahedron Lett.* **2008**, *43*, 6300-6303. DOI: <https://doi.org/10.1016/j.tetlet.2008.08.054>.
25. Röver, S.; Cesura, A.M.; Huguenin, P.; Kettler, R.; Szente, A. *J. Med. Chem.* **1997**, *40*, 4378-4385. DOI: <https://doi.org/10.1021/jm970467t>.
26. Hitchin, J.R.; Blagg, J.; Burke, R.; Burns, S.; Cockerill, M.J.; Fairweather, E.E.; Hutton, C.; Jordan, A.M.; McAndrew, C.; Mirza, A.; Mould, D.; Thomson, G.J.; Waddella, I.; Ogilvie, D.J. *MedChemComm.* **2013**, *4*, 1513-1522. DOI: <https://doi.org/10.1039/C3MD00226H>.
27. Keseru, G.M.; Makara, G.M. *Drug Discov. Today.* **2006**, *11*, 741-748. DOI: <https://doi.org/10.1016/j.drudis.2006.06.016>.
28. Cos, P.; Vlietinck, A.J.; Berghe, D.V.; Maes, L. *J. Ethnopharmacol.* **2006**, *106*, 290-302. DOI: <https://doi.org/10.1016/j.jep.2006.04.003>.
29. Pink, R.; Hudson, A.; Mouries, M.-A.; Bendig, M. *Nat. Rev. Drug Discov.* **2005**, *4*, 727-740. DOI: <https://doi.org/10.1038/nrd1824>.
30. Čenas, N.; Nemeikaitė-Čėnienė, A.; Kosychova, L. *Int. J. Mol. Sci.* **2021**, *22*, 8534. DOI: <https://doi.org/10.3390/ijms22168534>.
31. Crossnoe, C.R.; Germanas, J.P.; LeMagueres, P.; Mustata, G.; Krause, K.L. *J. Mol. Biol.* **2002**, *318*, 503-18. DOI: [https://doi.org/10.1016/S0022-2836\(02\)00051-7](https://doi.org/10.1016/S0022-2836(02)00051-7).
32. Weksberg, T.E.; Lynch, G.C.; Krause, K.L.; Pettitt, B.M. *Biophys. J.* **2007**, *92*, 3337-3345. DOI: <https://doi.org/10.1529/biophysj.106.088096>.

Fabrication of a Reactive Functionalized Microfilm with Aromatic Amines Applied to the Growth of Langerhans Cells

Martha Ávila-Cossío¹, Ignacio A. Rivero^{1*}, Victor García-González²

¹Tecnológico Nacional de México/Instituto Tecnológico de Tijuana, Centro de Graduados e Investigación en Química, Blvd. Alberto Limón Padilla S/N 22510 Tijuana, B. C., México.

²Departamento de Bioquímica, Facultad de Medicina Mexicali, Universidad Autónoma de Baja California, B. C., México.

*Corresponding author: Ignacio A. Rivero, email: irivero@tectijuana.mx; Phone: (664) 6233772.

Received June 7th, 2023; Accepted August 24th, 2023.

DOI: <http://dx.doi.org/10.29356/jmcs.v68i1.2081>

Abstract. This study reports the synthesis of ultrathin polymeric films through layer-by-layer deposition and covalent cross-linking of poly(2-vinyl-4,4'-dimethylazlactone) and branched poly(ethylene imine) (PEI) which were functionalized with aromatic amines that encompass anilines. To assess the effect of these aromatic molecules on the adhesion and proliferation of Langerhans β -cells, we prepared 35 bilayers of unfunctionalized and functionalized films with aromatic amines, which were characterized in terms of their physical, chemical, and biological properties by a battery of experimental techniques including ¹H and ¹³C, NMR, mass spectrometry, attenuated total reflectance Fourier transform infrared spectroscopy, field emission scanning electron microscopy and cell adhesion and staining. The films were nanometric, transparent, resistant to manipulation, chemically reactive, and highly cytocompatible. We demonstrated that films functionalized with aromatic molecules support the attachment and growth of *in vitro* Langerhans β -cells. This study provides the basis for a general approach to designing and functionalizing ultrathin films that promote cell growth on surfaces of interest for investigation in cell biology studies and a broad range of other biomedical applications. **Keywords:** Ultrathin films; azlactone; β -cells; aromatic amine.

Resumen. En este estudio se describe la síntesis de películas poliméricas ultrafinas mediante la técnica de capa por capa y la reticulación covalente de poli(2-vinil-4,4'-dimetilazlactona) y poli etilenimina (PEI) ramificado y, se funcionalizaron con aminas aromáticas que engloba las anilinas. Para evaluar el efecto de estas moléculas aromáticas en la adhesión y proliferación de las células β de Langerhans, se prepararon películas de 35 bicapas y se funcionalizaron con aminas aromáticas; se caracterizaron en términos de sus propiedades físicas, químicas y biológicas mediante una serie de técnicas experimentales que incluyeron ¹H y ¹³C, RMN, espectrometría de masas, espectroscopia de infrarrojo por transformada de Fourier, microscopía electrónica de barrido por emisión de campo y tinción celular. En general, las películas fueron nanométricas, transparentes, resistentes a la manipulación, químicamente reactivas y altamente citocompatibles. Se demostró, además, que las películas funcionalizadas con moléculas aromáticas favorecen la adhesión y el crecimiento de células β *in vitro*. Este estudio establece las bases de un enfoque general para diseñar y funcionalizar películas ultrafinas, que promuevan el crecimiento celular en superficies de interés, para la investigación en estudios de biología celular y una gama amplia de aplicaciones biomédicas potenciales. **Palabras clave:** Películas ultrafinas; azlactona; células β ; aminas aromáticas.

Palabras clave: Películas ultrafinas; azlactona; células β ; aminas aromáticas.

Introduction

With much of our lives spent sedentarily and with food being so readily available, metabolic diseases are becoming a real problem.[1] Metabolic syndrome (MetS) is a collection of issues such as obesity, high blood pressure, high cholesterol, and difficulty in metabolizing carbohydrates, increasing the risk of type 2 diabetes.[2] Insulin resistance and hyperinsulinemia in the body are linked to MetS, but it's still unclear which of these comes first.[3-5] Both of these issues affect the pancreas, which produces, stores, and releases insulin to keep blood sugar levels in check. This connection between MetS and how the pancreas works shows the importance of understanding the problem with the pancreas in MetS. [6]

A serious global health issue, diabetes mellitus is a non-communicable, multifactorial, complex metabolic condition.[7] It is characterized by abnormalities in the metabolism of carbohydrates, proteins, and lipids brought on by defects in insulin secretion, insulin synthesis, or both.[8,9] Obesity is a significant risk factor for the onset of type 2 diabetes (T2D), as is well known. Since 1975 to the present, the incidence of obesity has increased thrice globally, which has contributed to the sharp increase in T2D prevalence in recent years.[10,11] Due to increased adipose tissue bulk and decreased FFA clearance, obesity is linked to raised amounts of circulating free fatty acids (FFAs).[12] Higher amounts of free fatty acids being released from the esterification of fat in the body have been linked to this.[13] Rising evidence suggests that higher FFA levels may play a role in the etiology of T2D and hence serve as a mechanistic link between obesity and diabetes. According to a large body of evidence, the two main abnormalities that underlie the pathophysiology of T2D are insulin resistance and pancreatic β -cell dysfunction.[14,15] Lipotoxicity is a frequent term for these harmful effects of FFAs on glucose homeostasis.[16] The ability of islet cells to make, store, and insulin release in response to nutrients like glucose, lipids[17], and a subset of amino acids distinguishes them from other types of cells. The β -cells are incredibly sensitive to the nutrient's environment and can change significantly the amount of insulin produced within minutes due to a complex process called stimulus-secretion coupling in response to changes in blood glucose levels (between 4.5 and 8 mM).[18-21]

Surface-microfabrication techniques have been widely used to control cells in cultures. Different surface properties like charge, hydrophilicity, and topology have been used to influence how cells attach. Also, recently, different types of molecules have been attached to regulate growth, differentiation, and apoptosis.[22]

This research builds on other studies that have discussed creating materials that can either help or prevent mammalian cells and bacterial cells from sticking on a surface.[23-25] In this study, we report a step toward these broad goals through the creation of covalently crosslinked and chemically reactive ultrathin films that are easily modifiable to encourage cell adhesion. Our method is based on techniques for the reactive layer-by-layer fabrication of thin polymer films to create surface coatings that can be functionalized and patterned post-fabrication to present a wide range of chemical or biological functionality.[26] These films will allow us to seed β -cells to analyze their adhesion and growth behaviour with aromatic amines; their study is vital because of the important role β -cells play in glucose homeostasis.[27]

The method described here is based on techniques for fabricating thin polymer films on surfaces one layer at a time.[28] Given that layer-by-layer assembly allows for precise control over the thicknesses and compositions of multicomponent polymer films and can be used to deposit conformal coatings on the surfaces of topographically or topologically complex substrates, it is a particularly useful technique for fabricating surface coatings.[29] Our prior research has shown that the chemically reactive polymer poly(2-vinyl-4,4'-dimethylazlactone) (PVDMA) can be used to produce crosslinked thin films via reactive layer-by-layer assembly. The PVDMA azlactone activity quickly forms a 'click'-type reaction with primary amines, laying the groundwork for reactive layer-by-layer assembly with polymers containing primary amine groups.[30,31] The structure of this strategy is shown schematically in Fig. 1.



Fig. 1. (A) Schematic drawing of the prepared LBL assembly, (B) LBL film with PVDMA at the uppermost layer (35 bilayers).

The synthesis of PVDMA was carried out by condensing acryloyl chloride (1) with 2-methylalanine (2) to produce the amide (3), which was reacted with ethyl chloroformate to obtain the vinyl-azlactone (VDMA) (4). This monomer was polymerized with the activation of AIBN to obtain PVDMA (5) (see Fig.2(A)). In particular, PVDMA reacts rapidly at room temperatures with primary amines, and aromatics amines in this study, making these materials attractive for the synthesis of a functionalized reactive thin film that can be easily modified post-fabrication with any chemical and/or biological motif that permits the interactions with cells. Due to its swiftness and precision, this ring-opening reaction has become a handy resource for many organic synthesis projects (Fig. 2(B)).

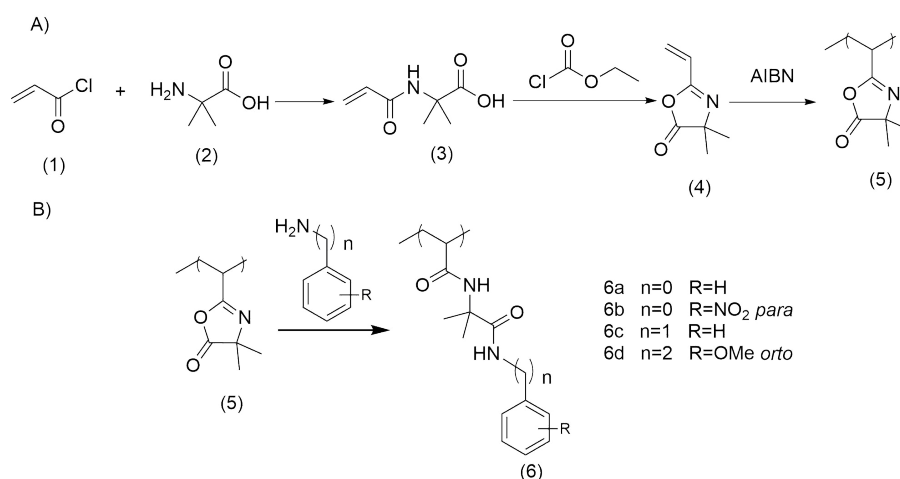


Fig. 2. (A) Steps to obtain the PVDMA, (B) The ring-opening reaction of PVDMA with aromatics amines.

In this report, we describe the fabrication of a PVDMA/PEI ultrathin thin film functionalized with aromatic amines (aniline (6a), 4-nitroaniline (6b), benzylamine (6c), and 2-methoxyphenethylamine (6d)), to

demonstrate that these films functionalized with HAAs can promote adhesion and growth of β -cells.[32] During food cooking, heterocyclic aromatic amines (HAAs) are produced. HAAs have been tested in mice, proving to be carcinogenic, inducing liver, gastrointestinal tract, pancreas, mammary gland, and prostate cancers. These results with HAAs in solution. In this report, the aromatic amines covalently bound to the films were studied, and the capacity of this modified surface on β -cell adhesion and proliferation was evaluated. Therefore, it is important to study the biocompatibility of films functionalized with aromatic amines. Inspection of the optical images reveals that β -cells have adhered and grown normally on these surfaces.

Experimental

Materials and methods

Acryloyl chloride (97 % containing 400 ppm phenothiazine stabilizer), 2-methylalanine (98 %), ethyl chloroformate (97 %), triethylamine (99 %), NaOH (reagent grade), HCl (reagent grade, 37 %), 1, 4-dioxane (99.8 %), 2,2'-azobis (2-methylpropionitrile) (98 %), Branched poly (ethylene imine) (PEI, MW = 25000) reagent grade, DMSO, hexane, acetone, glass microscope slides, aniline, 4-nitroaniline, benzylamine and 2-methoxyphenethylamine were purchased from a commercial source (Aldrich) and use without further purification. Anhydrous solvents for organics synthesis were prepared by passing through a solvent purification tower. Compressed air used to dry films and coated substrates was purchased from Aldrich.

General procedures

Glass substrates (76 × 25 mm) used as a surface for the films, were cleaned with acetone, ethanol, methanol, and deionized water and dried with compressed air. The optical thicknesses of films deposited on glass substrates were determined using Field Emission Scanning Electron Microscopy (FESEM), thicknesses were determined at least five different standardized locations on each substrate. Laser scanning confocal microscopy images were acquired on a Leica TCS SP8 laser scanning confocal microscope (Mannheim, Germany). Thin-layer chromatography (TLC) was performed on silica gel F₂₅₄ plates (Merck). All compounds were detected using UV light. Melting points were obtained on an Electrothermal 88629 apparatus and are not corrected. Infrared spectra (IR) were recorded on a Perkin Elmer FT-IR 1600 spectrometer. ¹H and ¹³C NMR spectra at 400 MHz and 100 MHz, respectively, were recorded on a Bruker Avance III spectrometer in CDCl₃, DMSO-d₆ with TMS as the internal standard. Mass spectra were obtained on an Agilent Technologies 5975C MS Spectrometer at 70 eV by direct insertion and an Agilent HPLC (Mod 1100) coupled to MSD version SL₂. UV/Vis absorption spectra were obtained using Cary 50 spectrophotometer. Fluorescence spectra were recorded on a Photon Technology International Fluorescence System (USA) with a 1 cm standard quartz cell. Single crystal X-Ray diffraction Smart Apex. Gel permeation chromatography (GPC) was performed on a Variant 9002 chromatograph equipped with a series of three columns (Phenogel: OH-646-K0, OH-645-K0, and OH-643-K0) and two detectors: a refractive index detector (Varian RI-4 and a triangle light scattering detector (LS detector MINI-DAWN, Wyatt). The measurements were performed in THF at 35 °C. Polystyrene standards were used for the calibration of the LS detector. THF was used for the mobile phase at a 0.7 mL/min flow rate. Sample solutions were prepared using 20 mg/mL concentration and filtered through a 0.45 μ m PTFE membrane filter before analysis.

Synthesis of 4,4-dimethyl-2-vinyloxazol-5(4H)-one (4). VDMA (4) monomer was synthesized using procedures reported by Rivero et al. [26]

2-acrylamide-2-methylpropanoic acid (3). 2-Methylalanine (2) (2.0 g, 0.0194 mol) in NaOH (1.8 g, 0.0442 mol), 2,3-di-tert-butyl-4-methoxyphenol (2.0 mg, 0.009 mmol) was weighed into a 100-mL round-bottomed flask equipped with a magnetic stir bar and dissolved in distilled water (4.8 mL). The solution was stirred in an ice bath until the temperature was ~ 4 °C. Acryloyl chloride (1) (2.0 g, 0.0221 mol) was added slowly using an addition funnel for approximately 5 min. The reaction was stirred for 3 hours. After that,

concentrated HCl (~ 2.5 mL) was added slowly to the reaction solution until the solution reached pH 2, and a white precipitate formed. The solution was stirred for an additional 30 min on ice. The product was filtered in a Buchner funnel and rinsed with cold acetone. White solid. Yield: 2.25 g, 74%. Rf = 0.66 (ethyl acetate 100 %). mp 187-189 °C. FT-IR (ATR) ν / cm^{-1} 3340(N-H), 3073(C-H), 2991(C-H, CH₃), 1705(C=O), 1649(C=O), 1599(C=C). ¹H NMR (400 MHz, DMSO d₆) δ 8.35 (s, 1H, NH), 6.26 (dd, Htrans, *J*=17.0 Hz, *J*Htrans-Hcis=10.0 Hz, 1H, Vin), 6.02 (dd, Htrans, *J*=17.2 Hz, *J*Htrans-Hgem=2.4 Hz, 1H, Vin), 5.55 (dd, Hcis, *J*=10.0 Hz, *J*Hcis-Hgem=2.4 Hz, 1H, Vin), 1.34 (s, 6H, C(CH₃)₂). ¹³C NMR (100 MHz, CDCl₃) δ 176.0, 132.0, 126.0, 125.9, 55.67, 25.60. MS m/z: 157.2⁺ (4 %), 112.2⁺(100 %) amu.

4,4-dimethyl-2-vinyloxazol-5(4H)-one (4). *N*-Acryloyl-2-methylalanine (3) (1.9 g, 0.0122 mol), triethylamine (2.5 mL, 0.0183 mol), and acetone (44.0 mL) were combined in a two-neck flask round-bottomed flask. The reaction mixture was purged with argon while cooling in an ice bath until the temperature was about 5 °C. Ethyl chloroformate (1.7 mL, 0.0183 mol) was added very slowly using a pressure-equalizing addition funnel. Once the addition was complete the reaction was stirred on ice under an inert atmosphere for 3 hours. The solution was filtered using a Buchner funnel, and the precipitate was washed with cold acetone. The filtrate was concentrated via rotary evaporation and purified by vacuum distillation (bp ~ 70 °C, 60 mbar). Clear liquid. Yield: 0.86 g, 45%. Rf = 0.83 (ethyl acetate 100%). FT-IR (ATR) ν / cm^{-1} 2984(C-H), 2938(C-H, CH₃), 2868(C-H, CH₃), 1818(C=O, ester), 1666(C=N imine), 1596(C=C). ¹H NMR (400MHz DMSO d₆) δ 6.30 (dd, Htrans, *J*=17.6 Hz; *J*Htrans-Hcis= 9.60 Hz, 1H, Vin), 6.23 (dd, Htrans, *J*=17.6 Hz; *J*Htrans-Hgem=2.0 Hz, 1H, Vin), 5.92 (dd, Hcis, *J*=9.60 Hz, *J*Hcis-Hgem=2.0 Hz, 1H, Vin), 1.47(s, CH₃, 6H). ¹³C NMR (100 MHz, CDCl₃) δ 180.6, 159.1, 129.0, 124.1, 65.5, 24.4. MS m/z: 139.2⁺(5%), 111.2⁺ (45%), 95.2⁺ (43%) amu.

Synthesis of Poly(2-vinyl-4,4'-dimethylazlactone) (PVDMA) (5). AIBN, 2,2'-azobisisobutyronitrile (2.6 mg, 0.02 mmol) was added into a 10-mL Schlenk flask equipped with a stir bar, anhydrous 1,4-dioxane (0.7 mL) was added. The mixture was stirred until the AIBN was dissolved completely. Later, VDMA (4) (0.2 g, 1.6 mmol) was added to the flask, and the flask was capped with a septum and purged with argon for 25 min. The reaction mixture was stirred at 70 °C for 16 hours. At the end of the reaction, the flask was cooled in an ice bath, acetone (~1 mL) was added, and hexane was added to precipitate the product. The polymer was precipitated twice in hexanes. White solid. Yield 0.2 g, 95%. GPC: Mn=67,300 g/mol; PDI=1.03. FT-IR (ATR) ν / cm^{-1} 2981, 2933 (C-H), 1818 (C=O), 1666 (C=N). ¹H NMR (400 MHz, CD₃COCD₃) δ 2.84(m, 2H, CH, -CH₂CH-), 2.01(m, 1H, -CH₂CH-), 1.37(s, 6 H, -CH₃).

Layer-by-Layer fabrication of films

Solutions of PEI and PVDMA were prepared in acetone (20 mM regarding the molecular weight of the polymer repeat segment). All the ultrathin films were fabricated layer-by-layer on glass substrates automatically based on the following: (1) the glass was introduced into the solution of PEI for 20 s, (2) the glass was removed and submerged in an acetone bath for 20 s followed by a second acetone bath for another 20 s, (3) glass was introduced in a solution of PVDMA for 20 s, and (4) glass was rinsed in the form described above. This sequence was repeated in 35 cycles. Films were dry under a stream of compressed air and stored in a vacuum desiccator. All films were fabricated at room temperature.

Post-fabrication functionalization of thin films

PEI / PVDMA films 35 bilayers were functionalized post-fabrication by immersing film-coated substrates in solutions of either aniline, 4-nitroaniline, benzylamine, and 2-methoxyphenethylamine 20 mM in DMSO at room temperature for ~24 hours. Films were soaked in DMSO for ~1 hour after functionalization and the DMSO was changed at least once during the soak, washed with ETOH, and dried with compressed air before being analyzed or being used to grow β -cell cultures.

Characterization of adhesion and growth of β cells on PEI/PVDMA films

β -cell line RIN-m5F cells (American Type Culture Collection, ATCC, USA) were grown in RPMI-1640 medium supplemented with 10 % fetal bovine serum, 10 U/mL penicillin, 10 μ g/mL streptomycin, and

25 µg/mL amphotericin B. The culture medium was changed every 3 to 4 days and also passaged once per week, according to previous work.[33] Cultures were maintained at 37 °C in a humidified atmosphere of 95 % air and 5 % CO₂. Cells were seeded onto 100 mm plates at 230,000 cells/mL density and allowed to grow at 90 % of confluence. Next, cell cultures were recovered and grown on coverslips composed of PEI/PVDMA films 35 bilayers at a density of 2.3 X10⁶ cells in a 10 mL RMPI culture medium. Furthermore, at 72 of incubation, cells were rinsed twice with cold PBS 1X, fixed with paraformaldehyde (2 %), and crystal violet stained. In previous work, this cell line was a cellular model to characterize physiopathological conditions such as metabolic overload.[34]

Results and discussion

The LBL technique enables the assembly of reactive polymer thin films in a wide variety of substrates. This film was created in acetone and is driven by an interfacial reaction between poly (2-alkenyl azlactone) and branched poly (ethylene imine). We created ultrathin films that are crosslinked and chemically reactive, making them easy to modify with aromatic amines. The films can promote β-cell attachment by presenting a broad range of chemical or biological functionality. The approach uses azlactone-functionalized polymers, which are highly versatile and reactive, to create surface coatings. This innovative technique could lead to significant advancements in the field of cell adhesion and communication, then represent an adequate model to characterize the physiology of Langerhans β-cells.

Surface reactivity is essential for creating materials that can be chemically modified with molecules like aromatic amines to be used for seeding cells.[35]

As mentioned, the ultrathin film was made in an automated way, which has 4 stations as shown in Fig. 3; this cycle is repeated until the desired number of layers is obtained, for this study, it was 70 layers or 35 bilayers.

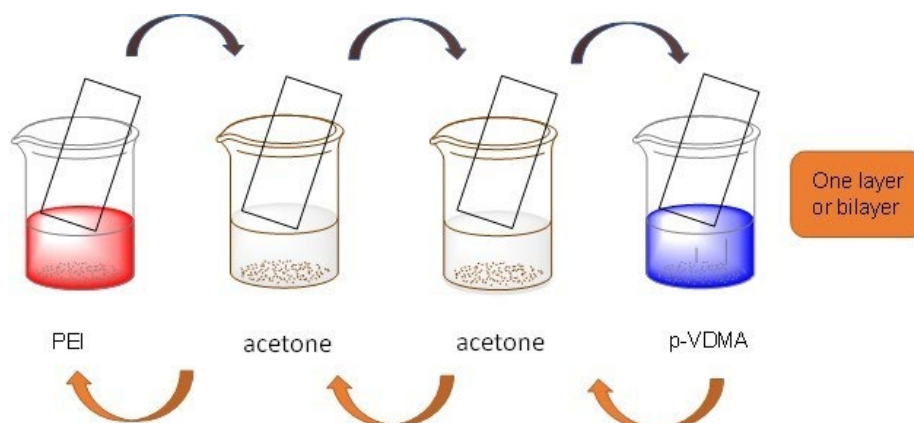


Fig. 3. Schematic illustration of the fabrication of the layer-by-layer ultra-thin films.

All films used in these initial studies were deposited on a glass slide substrate to allow the characterization of film thicknesses and growth profiles using FESEM. Fig. 4 shows the appearance, thickness, and topography of the ultrathin films.

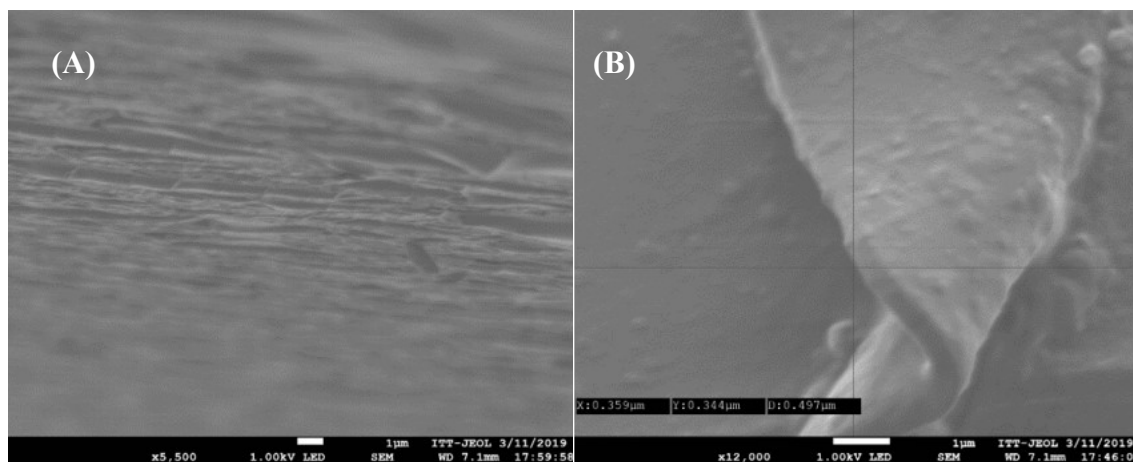


Fig. 4. Representative FESEM images of the film: (A) image of a 35-bilayer thin film, (B) and its measure.

The thickness of the film was determined by FESEM by measuring in at least five different points, giving an average value of 524 nm. It should be mentioned that the transparent films were obtained in an automated system so that each layer of the film was built up uniformly. The fabrication of ultrathin films on glass substrates allowed the characterization of the chemical structure of these materials using reflective infrared (IR) spectroscopy. Inspection of these data reveals an absorbance peak at 1820 cm^{-1} corresponding to the carbonyl in the azlactone group of PVDMA. Closer inspection reveals the presence of a second absorbance peak at 1647 cm^{-1} , which corresponds to C-N functionality on the azlactone ring. Functionalized PVDMA-PEI ultrathin films have been used in other studies to enhance cell performance and manage cell growth, and they are reliable and sturdy even in biological settings. [36,37]

To move our research ahead, we looked into how well β -cells adhere and grow on PVDMA-PEI films with aromatic amines (**2a-d**).

Fig. 5 shows optical images of the ultrathin films functionalized with aromatic amines. In this sense, we performed the growth of the β -cell cultures on the PVDMA-PEI films, representative images are shown, which correspond to **2a** (Fig. 5(A)), **2b** (Fig. 5(B)), **2d** (Fig. 5(C)), and **2c** (Fig. 5(D)). The results suggest an adhesion process and, therefore, a differential growth between the different samples, particularly a higher capacity for **2b** (Fig. 5(B)). The images show normal growth in 2D and less growth in 2A and 2C. It is the nitro group (electron withdrawing group) that influences the greater growth of beta cells. The mechanisms are complex, but they could be associated with the adsorption and sequestration of signaling molecules such as growth factors and membrane receptors.

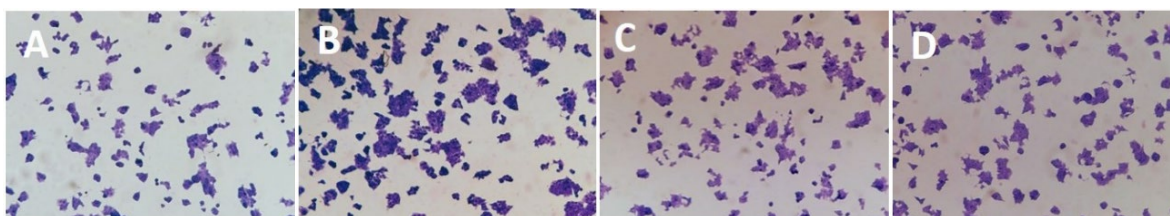


Fig. 5. Schematic representation of the ultrathin films functionalized with: (A) aniline, (B) 4-nitroaniline. (C) benzylamine and (D). 2-methoxyphenethylamine.

Conclusions

The layer-by-layer technique has recently been validated as a practical and versatile approach to constructing functional films. The process of Lbl assembly is straightforward, and its interest has grown due to its flexibility and ability to control the thickness of the film growth.[26,38] Based on that, ultrathin polymeric films of 35 bilayers of PVDMA/PEI were constructed. The ultrathin films were robust, transparent, and resistant against mechanical manipulation and pressure, with smooth and uniform surfaces. The films were functionalized with aromatic amines like aniline, 4-nitroaniline, benzylamine, and 2-methoxyphenethylamine and β cells were seeded. The results of this work suggest that the PVDMA/PEI ultrathin films can be used to modify surfaces with chemical or biological functionality, like proteins, peptides, or small molecules like aromatic amines, to design ultrathin films to investigate β -cells or other broad areas of medicine or biotechnology. It is worth mentioning that the nitro group interacts with the membrane proteins of the β -cells, resulting in cytocompatibility for the cells.

Acknowledgements

We gratefully acknowledge the support for this project of the Consejo Nacional de Humanidades, Ciencias y Tecnologías (CONAHCYT, GRANT No. CF-2023-I-327) and postdoctorate scholarship (No. 559644), we also acknowledge Tecnológico Nacional de México for the support of this project (No. 7814-20P).

References

1. Hudish, L. I.; Reusch, J. E. B.; Sussel, L. *J. Clin. Invest.* **2019**, *129*, 4001–4008. DOI: <https://doi.org/10.1172/JCI129188>.
2. Smith, G. I.; Mittendorfer, B.; Klein, S. *J. Clin. Invest.* **2019**, *129*, 3978–3989. DOI: <https://doi.org/10.1172/JCI129186>.
3. Reaven, G. M. *Annu. Rev.* **2003**, *44*, 121–131. DOI: <https://doi.org/10.1146/ANNUREV.ME.44.020193.001005>.
4. Reaven, G. M. *Diabetes* **1988**, *37*, 1595–1607. DOI: <https://doi.org/10.2337/DIAB.37.12.1595>.
5. O'Neill, S.; O'Driscoll, L. *Obes. Rev.* **2015**, *16*, 1–12. DOI: <https://doi.org/10.1111/OBR.12229>.
6. Lorenzo, C.; Okoloise, M.; Williams, K.; Stern, M. P.; Haffner, S. M. *Diabetes Care* **2003**, *26*, 3153–3159. DOI: <https://doi.org/10.2337/DIACARE.26.11.3153>.
7. Anuradha, R.; Saraswati, M.; Kumar, K. G.; Rani, S. H. *DNA Cell Biol.* **2014**, *33*, 743–748. DOI: <https://doi.org/10.1089/DNA.2014.2352>.
8. Dotta, F.; Fondelli, C.; Di Mario, U. *Acta Biomed.* **2005**, *76 Suppl 3*, 14–18.
9. Wild, S.; Roglic, G.; Green, A.; Sicree, R.; King, H. *Diabetes Care* **2004**, *27*, 1047–1053. DOI: <https://doi.org/10.2337/DIACARE.27.5.1047>.
10. Pérez-Bravo, F.; Carrasco, E.; Gutierrez-López, M. D.; Martínez, M. T.; Lopez, G.; García De Los Rios, M. *J. Mol. Med. (Berl)*. **1996**, *74*, 105–109. DOI: <https://doi.org/10.1007/BF00196786>.
11. Krijnen, P. A. J.; Simsek, S.; Niessen, H. W. M. *Apoptosis*. **2009**, *14*, 1387. DOI: <https://doi.org/10.1007/S10495-009-0419-6>.
12. Martinez, S. C.; Tanabe, K.; Cras-Méneur, C.; Abumrad, N. A.; Bernal-Mizrachi, E.; Permutt, M. A. *Diabetes*. **2008**, *57*, 846–859. DOI: <https://doi.org/10.2337/DB07-0595>.
13. Randle, P. J.; Garland, P. B.; Hales, C. N.; Newsholme, E. A. *Lancet*. **1963**, *1*, 785–789. DOI: [https://doi.org/10.1016/S0140-6736\(63\)91500-9](https://doi.org/10.1016/S0140-6736(63)91500-9).
14. Newsholme, P.; Keane, D.; Welters, H. J.; Morgan, N. G. *Clin. Sci. (Lond)*. **2007**, *112*, 27–42. DOI: <https://doi.org/10.1042/CS20060115>.

15. Acosta-Montaño, P.; Rodríguez-Velázquez, E.; Ibarra-López, E.; Frayde-Gómez, H.; Mas-Oliva, J.; Delgado-Coello, B.; Rivero, I. A.; Alatorre-Meda, M.; Aguilera, J.; Guevara-Olaya, L.; García-González, V. *Cells*. **2019**, *8*. DOI: <https://doi.org/10.3390/CELLS8080884>.
16. Lewis, G. F.; Carpentier, A.; Adeli, K.; Giacca, A. *Endocr. Rev.* **2002**, *23*, 201–229. DOI: <https://doi.org/10.1210/EDRV.23.2.0461>.
17. Acosta-Montaño, P.; García-González, V. *Nutrients*. **2018**, *10*. DOI: <https://doi.org/10.3390/NU10040393>.
18. Heimberg, H.; De Vos, A.; Vandercammen, A.; Van Schaftingen, E.; Pipeleers, D.; Schuit, F. *EMBO J.* **1993**, *12*, 2873–2879. DOI: <https://doi.org/10.1002/J.1460-2075.1993.TB05949.X>.
19. Gupta, D.; Jetton, T. L.; LaRock, K.; Monga, N.; Satish, B.; Lausier, J.; Peshavaria, M.; Leahy, J. L. *J. Biol. Chem.* **2017**, *292*, 12449–12459. DOI: <https://doi.org/10.1074/JBC.M117.781047>.
20. Poitout, V.; Amyot, J.; Semache, M.; Zarrouki, B.; Hagman, D.; Fontés, G. *Biochim. Biophys. Acta*. **2010**, *1801*, 289–298. DOI: <https://doi.org/10.1016/J.BBALIP.2009.08.006>.
21. Donath, M. Y.; Shoelson, S. E. *Nat. Rev. Immunol.* **2011**, *11*, 98–107. DOI: <https://doi.org/10.1038/NRI2925>.
22. Ito, Y. *Biomaterials*. **1999**, *20*, 2333–2342. DOI: [https://doi.org/10.1016/S0142-9612\(99\)00162-3](https://doi.org/10.1016/S0142-9612(99)00162-3).
23. Wancura, M. M.; Anex-Ries, Q.; Carroll, A. L.; Paola Garcia, A.; Hindocha, P.; Buck, M. E. *J. Polym. Sci. A Polym. Chem.* **2017**, *55*, 3185–3194. DOI: <https://doi.org/10.1002/POLA.28664>.
24. Buck, M. E.; Breitbach, A. S.; Belgrade, S. K.; Blackwell, H. E.; Lynn, D. M. *Biomacromolecules*. **2009**, *10*, 1564. DOI: <https://doi.org/10.1021/BM9001552>.
25. Singhvi, R.; Kumar, A.; Lopez, G. P.; Stephanopoulos, G. N.; Wang, D. I. C.; Whitesides, G. M.; Ingber, D. E. *Science*. **1994**, *264*, 696–698. DOI: <https://doi.org/10.1126/SCIENCE.8171320>.
26. Ávila-Cossío, M. E.; Rivero, I. A.; García-González, V.; Alatorre-Meda, M.; Rodríguez-Velázquez, E.; Calva-Yáñez, J. C.; Espinoza, K. A.; Pulido-Capiz, A. *ACS Omega*. **2020**, *5*, 5249–5257. DOI: <https://doi.org/10.1021/ACSOMEGA.9B04313>.
27. Nadal, A.; Alonso-Magdalena, P.; Soriano, S.; Quesada, I.; Ropero, A. B. *Mol. Cell Endocrinol.* **2009**, *304*, 63–68. DOI: <https://doi.org/10.1016/J.MCE.2009.02.016>.
28. Decher, G. *Science (1979)*. **1997**, *277*, 1232–1237. DOI: <https://doi.org/10.1126/SCIENCE.277.5330.1232>.
29. Tang, Z.; Wang, Y.; Podsiadlo, P.; Kotov, N. A. *Adv. Mater.* **2006**, *18*, 3203–3224. DOI: <https://doi.org/10.1002/ADMA.200600113>.
30. Buck, M. E.; Zhang, J.; Lynn, D. M. *Adv. Mater.* **2007**, *19*, 3951–3955. DOI: <https://doi.org/10.1002/ADMA.200700822>.
31. Kolb, H. C.; Sharpless, K. B. *Drug Discov. Today*. **2003**, *8*, 1128–1137. DOI: [https://doi.org/10.1016/S1359-6446\(03\)02933-7](https://doi.org/10.1016/S1359-6446(03)02933-7).
32. Mrksich, M. *Chem. Soc. Rev.* **2000**, *29*, 267–273. DOI: <https://doi.org/10.1039/A705397E>.
33. Guevara-Olaya, L.; Chimal-Vega, B.; Castañeda-Sánchez, C. Y.; López-Cossío, L. Y.; Pulido-Capiz, A.; Galindo-Hernández, O.; Díaz-Molina, R.; Ruiz Esparza-Cisneros, J.; García-González, V. *Metabolites*. **2022**, *12*. DOI: <https://doi.org/10.3390/METABO12080754>.
34. Martínez-Navarro, I.; Díaz-Molina, R.; Pulido-Capiz, A.; Mas-Oliva, J.; Luna-Reyes, I.; Rodríguez-Velázquez, E.; Rivero, I. A.; Ramos-Ibarra, M. A.; Alatorre-Meda, M.; García-González, V. *Biomolecules*. **2020**, *10*, 1–21. DOI: <https://doi.org/10.3390/BIOM10091201>.
35. Manna, U.; Raman, N.; Welsh, M. A.; Zayas-Gonzalez, Y. M.; Blackwell, H. E.; Palecek, S. P.; Lynn, D. M. *Adv. Funct. Mater.* **2016**, *26*, 3599–3611. DOI: <https://doi.org/10.1002/ADFM.201505522>.
36. Broderick, A. H.; Azarin, S. M.; Buck, M. E.; Palecek, S. P.; Lynn, D. M. in: *Fabrication of Amine-Reactive Polymer Multilayers on Microwell Cell Culture Arrays: Combining Methods for the Topographic Patterning of Cell Substrates with Approaches to Facile Surface Functionalization*. AIChE January 1, 2011, 72–73. <https://experts.umn.edu/en/publications/fabrication-of-amine-reactive-polymer-multilayers-on-microwell-ce>, accessed June 2023.
37. Weeks, C. A.; Aden, B.; Zhang, J.; Singh, A.; Hickey, R. D.; Kilbey, S. M.; Nyberg, S. L.; Janorkar, A. V. *J. Biomed. Mater. Res. A*. **2017**, *105*, 377–388. DOI: <https://doi.org/10.1002/JBMA.35910>.
38. Li, Y.; Wang, X.; Sun, J. *Chem. Soc. Rev.* **2012**, *41*, 5998–6009. DOI: <https://doi.org/10.1039/C2CS35107B>.

4(S)-Benzyl-1,3-thiazolidin-2-one a Novel Chiral Auxiliary for Asymmetric Aldol Coupling through Titanium Enolates

Dulce M. Mejía-Nuñez¹, Salvador Mastachi-Loza¹, Diego Martínez-Otero², Moisés Romero-Ortega^{1*}

¹Departamento de Química Orgánica, Facultad de Química, Universidad Autónoma del Estado de México. Toluca, México.

²Centro Conjunto de Investigación en Química Sustentable UAEMéx-UNAM Toluca, México.

*Corresponding author: Moisés Romero-Ortega, email: mromero@uaemex.mx; Phone +52 7222175109.

Received May 17th, 2023; Accepted September 9th, 2023.

DOI: <http://dx.doi.org/10.29356/jmcs.v68i1.2067>

In honour of Professor Joaquín Tamariz on the occasion of his retirement from the ENCB of the IPN.

Abstract. The chlorotitanium enolate of *N*-propionyl-4(*S*)-benzyl-1,3-thiazolidin-2-one, was condensed with aryl aldehydes, in good diastereoselectivity to give the ‘Evans *syn*’ aldol (73:27 - 97:3), using equimolar amounts of titanium tetrachloride (1.5 equiv), and *N,N*-diisopropylethylamine (DIPEA). The facial selectivity in the aldol additions probably involves a *non*-chelated transition state. In all aldol reactions, the presence of a minor product, the ‘*non*-Evans *syn*’ aldol, was obtained and confirmed by X-ray diffraction analysis of a single-crystal compound containing the mixture of diastereoisomers. The chiral auxiliary in these 1,3-thiazolidin-2-one aldol derivatives can be easily removed by nucleophilic species through acyl substitution.

Keywords: Chiral auxiliaries; coupling reaction; stereoselective synthesis; aldol adducts; thiazolidinone.

Resumen. El enolato de clorotitanio de *N*-propionil-4(*S*)-bencil-1,3-tiazolidin-2-ona, fue condensado con arilaldehídos, con buena diastereoselectividad produciendo el aldol “*syn* Evans” (73:27 - 97:3), utilizando cantidades equimolares de tetracloruro de titanio (1.5 equiv) y *N,N*-diisopropiletilamina (DIPEA). La selectividad facial en las adiciones aldólicas probablemente implica un estado de transición no-quelatao. En todas las reacciones aldólicas, la presencia de un producto minoritario, el aldol “*non*-Evans”, fue obtenido y confirmado por el análisis de difracción de rayos-X de monocristal de una mezcla de los diastereoisómeros. El auxiliar quiral en estos derivados de 1,3-tiazolidin-2-onas puede ser removido fácilmente por especies nucleofílicas a través de la sustitución del grupo acilo.

Palabras clave: Auxiliar quiral; reacción de acoplamiento; síntesis estereoselectiva; aductos aldolicos; tiazolidinona.

Introduction

The Asymmetric synthesis is an important topic in organic chemistry with many applications in the pharmaceutical field. The creation of asymmetric centers by stereoselective synthesis is one of the most important methodologies in asymmetric chemistry. In this context, the asymmetric versions of the aldol addition reaction continue to attract the attention of organic chemists and have been subject of intense synthetic and mechanistic study, because of their importance in the asymmetric construction of carbon-carbon bonds.

It is well known that 1,3-oxazolidin-2-ones **1**,[1] 1,3-thiazolidine-2-thiones **2**,[2] and 1,3-oxazolidine-2-thiones **3**,[3] have been extensively applied as chiral auxiliaries in numerous asymmetric syntheses (Fig. 1).[4]

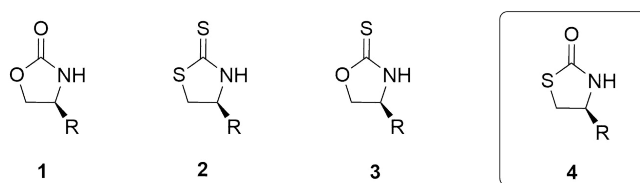


Fig. 1. Aminoacid-derived chiral auxiliaries.

These heterocyclic α -aminoacid-derived chiral auxiliaries have become an integral tool for the preparation of enantiomerically pure intermediates in the synthesis of natural products and specially in the stereoselective preparation of aldol-acetate fragments. Additionally, this class of chiral auxiliaries is popular because of the ease in preparation, their reliable efficiency providing excellent chemical yield and predictable diastereoselectivity.[5]

Evans and co-workers pioneered the use of 1,3-oxazolidinones **1** in asymmetric aldol additions in the early 1980s.[6] These induction-asymmetric reactions resulted in high levels of diastereoselectivity. It was reported that the boron enolates (or their synthetic equivalents) of *N*-propionyloxazolidinones, undergo aldol addition to aldehydes and ketones in a highly stereo regulated fashion to form the ‘Evans *syn*’ aldol adduct.[7]

The ‘Evans *syn*’ aldol adducts, can also be obtained using titanium tetrachloride instead dibutyl boron triflate.[8] In this context, titanium tetrachloride is more economical, and does not require the extra step of oxidation needed to allow hydrolysis of the dibutyl borylaldolates. Titanium enolates, as well as other enolates (e.g. lithium, zinc, or tin derivatives), give rise to ‘*non*-Evans *syn*’ aldol adducts when an additional Lewis acid is added to coordinate the aldehyde.[9]

The *N*-acyl-1,3-oxazolidinethiones **3** were first used as chiral auxiliaries in aldol-type reactions by Nagao and Fujita.[10] More recently, chlorotitanium enolates of *N*-propionyl 1,3-oxazolidine-2-thiones and *N*-propionyl-1,3-thiazolidine-2-thione, have been used to access both ‘Evans *syn*’ and ‘*non*-Evans *syn*’ aldol adducts from the same enantiomer of the chiral auxiliary; simply by altering the reaction conditions.[11] Specifically, one equivalent of titanium tetrachloride, (-)-sparteine as the base, and in the presence of *N*-methyl-2-pyrrolidinone (NMP), gives ‘Evans *syn*’ aldol adducts with selectivities in ratio of 97:3 to >99:1. The ‘*non*-Evans *syn*’ aldol adducts can also be obtained using 1,3-oxazolidine-2-thiones **3** and 1,3-thiazolidinethiones **2** by altering the stoichiometry of titanium tetrachloride, without NMP present.

On the other hand, the 1,4-addition of nucleophiles to α,β -unsaturated carbonyl systems is one of the most useful methods for asymmetric carbon-carbon or carbon-heteroatom bond formation.[12] The conjugate addition of organometallic reagents to *N*-enoyloxazolidinone derivatives, has been employed in the synthesis of natural products.[13] Chiral auxiliary-mediated asymmetric Michael addition reactions have been studied extensively and are now an important and general method for asymmetric carbon-carbon bond formation.[14] The addition of organo-copper reagents to chiral alkenoate derivatives (Michael addition) with oxazolidinone, has provided high diastereoselectivity.[15] Alternatively, enoyl-thiazolidinethiones are advantageous as they are more easily cleavable auxiliaries when compared to oxazolidinones **1** or oxazolidinethiones **3**. [16]

Moreover, there are reports about the transfer of the exocyclic sulfur atom into *N*-enoylthiazolidinethiones and *N*-enoyloxazolidinethiones.[17]

Thiazolidin-2-ones **4** are important compounds in both pharmaceutical and synthetic organic chemistry. They are widely encountered as building blocks in natural products with important pharmacological properties,[18] pesticides,[19] and other compounds with anti-HIV3 and anticancer activity.[20] Some synthetic methods for thiazolidin-2-one **4** and substituted thiazolidin-2-ones have been developed. Desulfurization (the S/O-exchange) of thiazolidine-2-thiones **2** is an alternative method for synthesizing the corresponding thiazolidin-2-ones **4** via reactions with oxiranes [21] or hydrogen peroxide.[22] Additionally, 4-substituted thiazolidinones also can be generated (45 % - 85 % yields, from thiazolidinethiones using bromoethanol in ethanol with sodium ethoxide as a base.[23])

Experimental

All chemicals were purchased from Sigma-Aldrich and used without any further purification. Thin-layer chromatography (TLC) was visualized using UV light (254 nm). Products were purified by flash chromatography using silica gel (MN Kieselgel 80; Silica gel 60 A; 0,04-0,063 mm / 230 – 400 mesh ASTM). Nuclear Magnetic Resonance (NMR) spectra were measured on Bruker 300 or Varian 500 MHz instruments. ¹H NMR chemical shifts (δ) are reported in parts per million (ppm) relative to tetramethylsilane ($\delta = 0.0$ ppm) with coupling constants (J) reported in hertz (Hz). ¹³C NMR signals are reported using 77.0 ppm (CDCl₃) as the internal reference. Melting points were measured in (Mel-Temp II) instrument without corrections. The optical rotations were measured on a PerkinElmer polarimeter model 343 and the diastereomeric ratios were determined comparing the crude ¹H NMR spectra.

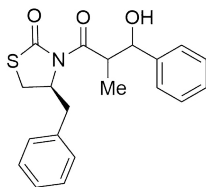
(4S)-Benzyl-1,3-thiazolidin-2-one (4a). Hydrogen peroxide (36 %, 46 μ L, 5.47 mmol) was added dropwise to a mixture of (4S)-benzy-1,3-lthiazolidine-2-thione (1.0 g, 4.77 mmol), sodium hydroxide (1.53 g, 38.25 mmol) and water (8.0 mL). The mixture was stirred for 2.0 h at room temperature. Then, aqueous sodium hydrogen sulfite was added, and the desired product was extracted with DCM (3 x 125 mL). The organic extracts were dried over Na₂SO₄ and concentrated under reduced pressure. Purification was accomplished by flash chromatography using silica gel (8:2 hexanes :EtOAc) to afford, after recrystallization from (DCM–hexanes), the (4S)-benzy-1,3-thiazolidine-2-one as a white crystalline solid in 67% yield, mp: 69–71°C, ¹H NMR (300 MHz, CDCl₃) δ (ppm): 7.39 – 7.20 (m, 3H), 7.23 – 7.13 (m, 2H), 6.07 (s, 1H), 4.07 (p, *J* = 6.7 Hz, 1H), 3.42 (ddd, *J* = 11.0, 7.1, 1.7 Hz, 1H), 3.16 (dd, *J* = 11.0, 6.3 Hz, 1H), 3.01 – 2.83 (m, 2H). ¹³C NMR (75 MHz, CDCl₃) δ (ppm): 174.9 (C=O), 136.5, 129.0, 128.9, 127.2, 56.5 (CH), 40.9 (CH), 34.3 (CH₂). EIMS *m/z* (%): *m/z* 355 (6, M⁺), 117 (100). [α]_D²⁵ +32.64 (*c* = 0.01, CHCl₃). CCDC 1839074

(4S)-Benzyl-3-propionyl-1,3-thiazolidin-2-one (5). Compound **4a** (1.0 g, 5.18 mmol) was dissolved in DCM (10 mL) and cooled to 0 °C. Then Et₃N (2.46 g, 24.38 mmol) was added dropwise and stirred for 20 min. Then, propionyl chloride (0.67mL, 0.630 g, 6.85 mmol) was added dropwise and stirred at 0 °C for 1.0 h. The reaction mixture was allowed to reach room temperature and stirred for 2.0 h. The reaction was quenched by the addition of a saturated solution of NH₄Cl (15 mL). After further extraction with DCM (3 x 30 mL), the combined organic layers were dried over anhydrous Na₂SO₄, filtered, and concentrated under reduced pressure. Purification was accomplished by flash chromatography using silica gel (95:5 hexanes:EtOAc) to afford, after crystallization from (DCM– hexanes), (4S)-benzyl-3-propionyl-1,3-thiazolidin-2-one as a white crystalline solid in 61 % yield, mp: 68–70°C, ¹H RMN (CDCl₃, 300 MHz.) δ (ppm): 7.40 – 7.22 (m, 5H), 4.97 – 4.84 (m, 1H), 3.33 (dd, *J* = -11.4, 7.4 Hz, 1H), 3.15 (dd, *J* = -13.2, 3.6 Hz, 1H), 3.08 – 2.74 (m, 4H), 1.17 (td, *J* = 7.3, 1.8 Hz, 3H). ¹³C RMN (CDCl₃, 300 MHz.) δ (ppm): 173.4 (C=O), 172.3 (C=O), 136.7, 129.4, 128.9, 128.8, 127.1, 77.4, 59.4 (CH), 37.3 (CH₂), 30.4 (CH₂), 28.6 (CH₂), 8.3 (CH₃). EIMS *m/z* 249 (48, M⁺), 91 (100). [α]_D²⁵ +63.7 (*c* = 0.1, CHCl₃).

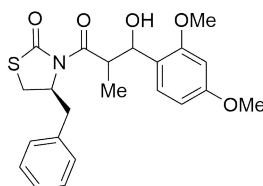
General aldol condensation procedure

A solution of **5** (100 mg, 0.401 mmol, 1 eq) in DCM (3.0 mL) was cooled at -10 °C, and TiCl₄ (60 μL, 1.0 M/ DCM, 1.5 eq) was added dropwise to give an orange solution. After stirring for 20 min at -10 °C, DIPEA (11 μL, 0.805 mmol, 1.5 eq.) was added dropwise. When the reaction turned red stirring continued for 30 min at 10 °C. Then, a solution of the corresponding aldehyde (1.5 eq.) dissolved in DCM (1.0 mmol/mL) was added dropwise. The resulting mixture was stirred for 12 h at -15 °C and then allowed to reach room temperature. The reaction mixture was quenched by the addition of saturated solution of NH₄Cl (15 mL) and the desired product was extracted with DCM (3 x 10 mL). The combined organic layers were dried over anhydrous Na₂SO₄, filtered, and concentrated under reduced pressure. The diastereoisomeric mixture was purified by silica gel flash chromatography to afford the corresponding aldols **6** and **7** as mixture.

(4S)-Benzyl-3-(3-hydroxy-2-methyl-3-phenylpropanoyl) thiazolidin-2-one (6,7a). Following the general procedure, this compound was prepared by reacting **5** with benzaldehyde. The diastereoisomeric mixture was purified by column chromatography using hexanes:EtOAc (95:5) as eluents, affording a mixture of **6a** and **7a** (97:3) as a solid in 86 % yield. After crystallization (DCM–hexanes) mp: 87–89 °C; ¹H NMR (300 MHz, CDCl₃) δ (ppm): 7.43 (d, *J* = 7.1 Hz, 2H), 7.39 – 7.22 (m, 8H), 5.16 (s, 1H), 4.96 (ddd, *J* = 10.6, 7.2, 3.9 Hz, 1H), 4.06 (qd, *J* = 7.0, 3.4 Hz, 1H), 3.40 – 3.30 (m, 1H), 3.04 (dd, *J* = -13.2, 4.0 Hz, 1H), 2.94 (s, 1H), 2.93 – 2.83 (m, 2H), 1.19 (d, *J* = 6.8 Hz, 3H), 1.11 (d, *J* = 7.0 Hz, 3H). ¹³C NMR (75 MHz, CDCl₃) δ (ppm): 175.9 (C=O), 172.4 (C=O), 141.3, 136.4, 130.0, 129.2, 128.9, 128.7, 128.4, 128.3, 128.3, 128.1, 128.0, 127.2, 127.0, 126.1, 126.0, 73.1 (CH), 59.5 (CH), 45.2 (CH), 37.4 (CH₂), 28.6 (CH₂), 10.5 (CH₃). EIMS *m/z* (%): *m/z* 355 (6, M⁺), 117 (100). [α]_D²⁵ +32.64 (*c* = 0.01 g/100 mL, CHCl₃). CCDC: 1839075.

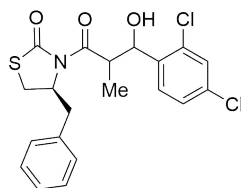


(4S)-Benzyl-3-(3-(2,4-dimethoxyphenyl)-3-hydroxy-2-methyl propanoyl) thiazolidin-2-one (6,7b). Following the general procedure, this compound was prepared by reacting **5** with 2,4-dimethoxybenzaldehyde. The diastereoisomeric mixture was purified by column chromatography using hexanes:EtOAc (95:5) as eluents, affording a mixture of **6b** and **7b** (68:32) as a solid in 86 % yield. After crystallization (DCM–hexanes) mp: 131–133 °C; ¹H NMR (500 MHz, CDCl₃) δ (ppm): 7.38 – 7.30 (m, 4H), 7.30 – 7.21 (m, 6H), 7.07 (d, *J* = 2.9 Hz, 1H), 6.96 (dd, *J* = 9.2, 2.7 Hz, 1H), 6.85 – 6.74 (m, 4H), 5.26 (d, *J* = 4.0 Hz, 1H), 5.07 – 5.01 (m, 1H), 4.97–4.94 (m, 1H), 4.90 (ddd, *J* = 10.7, 7.4, 3.5 Hz, 1H), 4.45 (p, *J* = 7.0 Hz, 1H), 4.25 (qd, *J* = 7.0, 3.2 Hz, 1H), 3.83 (s, 3H), 3.82 (s, 3H), 3.75 (s, 3H), 3.74 (s, 3H), 3.28 (dd, *J* = 11.5, 7.6 Hz, 1H), 3.16 – 3.06 (m, 1H), 3.05 – 2.97 (m, 1H), 2.97 – 2.77 (m, 4H), 1.18 (d, *J* = 7.3, 3H), 1.06 (d, *J* = 7.0, 3H). ¹³C NMR (75 MHz, CDCl₃) δ (ppm): 176.7(C=O), 176.3(C=O), 176.1(C=O), 172.8(C=O), 153.5, 153.4, 153.3, 151.0, 150.4, 150.3, 136.7, 136.5, 136.4, 130.7, 130.1, 129.9, 129.3, 129.3, 129.2, 128.7, 128.7, 127.0, 126.9, 114.5, 114.2, 114.0, 113.9, 113.2, 113.0, 112.9, 112.8, 111.7, 111.3, 111.3, 111.0, (CH), 72.4(CH), 70.4(CH), 59.8(CH), 59.4(CH), 55.7(OMe), 55.6(OMe), 55.6(OMe), 55.6(OMe), 43.8(CH), 43.0(CH), 37.3(CH₂), 37.2(CH₂), 28.5(CH₂), 28.2(CH₂), 15.0(Me), 11.7(Me). EIMS *m/z* (%): 415 (74, M⁺), 166 (100). [α]_D²⁵ +38.23 (*c* = 0.01 g/100 mL, CHCl₃). CCDC: 1839076.

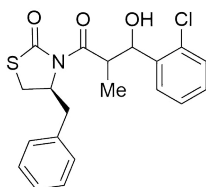


(4S)-Benzyl-3-(3-(2,4-dichlorophenyl)-3-hydroxy-2-methyl propanoyl) thiazolidin-2-one (6,7c).

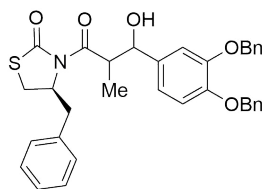
Following the general procedure, this compound was prepared by reacting **5** with 2,4-dichlorobenzaldehyde. The diastereoisomeric mixture was purified by column chromatography using hexanes:EtOAc (95:5) as eluents, affording a mixture of **6c** and **7c** (85:15) as a solid in 75 % yield. After crystallization (DCM– hexanes) mp: 151–153°C; ¹H NMR (500 MHz, CDCl₃) δ (ppm): 7.57 (d, *J* = 8.4 Hz, 1H), 7.51 (d, *J* = 8.4 Hz, 1H), 7.41 – 7.22 (m, 9H), 5.41 (t, *J* = 2.2 Hz, 1H), 5.30 (t, *J* = 7.7 Hz, 1H), 4.94 (ddd, *J* = 10.6, 7.1, 4.0 Hz, 1H), 4.27 (p, *J* = 7.0 Hz, 1H), 4.13 (qd, *J* = 7.2, 2.3 Hz, 1H), 3.84 (d, *J* = 2.1 Hz, 1H, OH), 3.59 (d, *J* = 7.6 Hz, 1H, OH), 3.36 (ddd, *J* = 11.5, 7.3, 1.0 Hz, 1H), 3.18 (dd, *J* = -13.3, 4.0 Hz, 1H), 3.10 (dd, *J* = -13.4, 3.5 Hz, 1H), 3.05 – 2.85 (m, 3H), 1.14 (d, *J* = 7.0 Hz, 3H), 1.06 (d, *J* = 7.2 Hz, 3H). ¹³C NMR (75 MHz, CDCl₃) δ (ppm): EIMS *m/z* (%): 428 (1, M + 4), 426(2, M + 2), 424 (3, M⁺), 117 (100). [α]_D²⁵ +11.26 (*c* = 0.01 g/100 mL, CHCl₃). CCDC: 1839077.

**(4S)-Benzyl-3-(3-(2-chlorophenyl)-3-hydroxy-2-methylpropanoyl) thiazolidin-2-one: (6,7d).**

Following the general procedure, this compound was prepared by reacting **5** with 2-chlorobenzaldehyde. The diastereoisomeric mixture was purified by column chromatography using hexanes:EtOAc (95:5) as eluents, affording a mixture of **6d** and **7d** (73:17) as a solid in 77% yield. After crystallization from (DCM– hexanes) it had mp: 176–178°C; ¹H NMR (500 MHz, CDCl₃) δ (ppm): 7.63 (dd, *J* = 7.6, 1.9 Hz, 1H), 7.57 (dd, *J* = 7.6, 1.8 Hz, 1H), 7.40 – 7.17 (m, 12H), 5.48 (t, *J* = 2.4 Hz, 1H), 5.35 (t, *J* = 7.6 Hz, 1H), 4.94 (ddd, *J* = 10.7, 7.2, 3.9 Hz, 2H), 4.33 (p, *J* = 7.1 Hz, 1H), 4.17 (qd, *J* = 7.1, 2.4 Hz, 1H), 3.74 (d, *J* = 2.4 Hz, 1H), 3.51 (d, *J* = 7.6 Hz, 1H), 3.41 – 3.29 (m, 2H), 3.21 – 3.05 (m, 2H), 3.04 – 2.82 (m, 3H), 1.15 (d, *J* = 6.9 Hz, 3H), 1.09 (d, *J* = 7.1 Hz, 3H). ¹³C NMR (126 MHz, CDCl₃) δ (ppm): 177.3 (C=O), 175.7 (C=O), 173.0 (C=O), 171.9 (C=O), 139.5, 138.2, 136.5, 136.4, 136.3, 133.0, 131.6, 130.8, 129.4, 129.4, 129.4, 129.3, 129.3, 128.9, 128.9, 128.9, 128.8, 128.7, 128.5, 128.5, 128.0, 127.2, 127.2, 127.2, 127.1, 126.6, 126.5, 73.3 (CH), 69.8 (CH), 59.8 (CH), 59.5 (CH), 44.7 (CH), 42.1 (CH), 37.5 (CH₂), 37.3 (CH₂), 28.5 (CH₂), 28.3 (CH₂), 14.7 (Me), 10.5 (Me). EIMS *m/z* (%): 392 (1, M + 2), 390 (2, M⁺), 57 (100). [α]_D²⁵ +78.78 (*c* = 0.01 g/100 mL, CHCl₃). CCDC: 1839078.

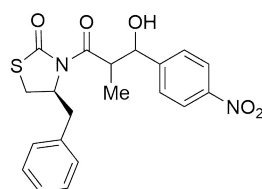
**(4S)-Benzyl-3-(3-(3,4-bis (benzyloxy)phenyl)-3-hydroxy-2-methylpropanoyl) thiazolidin-2-one (6,7e).**

Following the general procedure, this compound was prepared by reacting **5** with piperonal. The diastereoisomeric mixture was purified by column chromatography using hexanes:EtOAc (97:3) as eluents, affording a mixture of **6e** and **7e** (94:6) as an oil in 76 % yield. ¹H NMR (300 MHz, CDCl₃) δ (ppm): 7.50 – 7.20 (m, 17H), 7.12 – 7.07 (m, 1H), 6.89 (t, *J* = 1.7 Hz, 2H), 5.20 – 5.14 (m, 2H), 5.11 (d, *J* = 2.4 Hz, 2H), 5.03 (dd, *J* = 3.8, 2.2 Hz, 1H), 4.92 (ddd, *J* = 10.6, 7.3, 3.8 Hz, 1H), 4.05 – 3.95 (m, 1H), 3.38 – 3.23 (m, 1H), 2.98 (dd, *J* = -13.3, 3.7 Hz, 1H), 2.94 – 2.71 (m, 4H), 1.16 (d, *J* = 6.9 Hz, 3H), 1.05 (d, *J* = 7.1 Hz, 3H). ¹³C NMR (126 MHz, CDCl₃) δ (ppm): 175.8 (C=O), 172.3 (C=O), 148.7, 148.2, 137.3, 137.2, 136.5, 134.8, 129.4, 128.8, 128.4, 128.4, 127.7, 127.7, 127.5, 127.2, 127.2, 119.2, 114.8, 113.1, 73.0 (CH), 71.4 (OCH₂Bn), 71.1 (OCH₂Bn), 59.4 (CH), 45.2 (CH), 37.4 (CH₂), 28.5 (CH₂), 10.7 (Me). EIMS *m/z* (%): 549 (1, M⁺), 43 (100). [α]_D²⁵ +10.16 (*c* = 0.01 g/100 mL, CHCl₃).



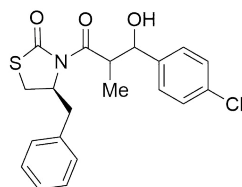
(4S)-Benzyl-3-(3-hydroxy-2-methyl-3-(4-nitrophenyl) propanoyl) thiazolidin-2-one (6,7f).

Following the general procedure, this compound was prepared by reacting **5** with 4-nitrobenzaldehyde. The diastereoisomeric mixture was purified by column chromatography using hexanes:EtOAc (92:8) as eluents, affording a mixture of **6f** and **7f** (97:3) as a solid in 92 % yield. After crystallization (DCM– hexanes) mp: 150-152°C; ¹H NMR (300 MHz, CDCl₃) δ (ppm): 8.26 – 8.15 (m, 2H), 7.67 – 7.58 (m, 2H), 7.41 – 7.22 (m, 6H), 5.25 (d, *J* = 2.7 Hz, 1H), 4.99 (ddd, *J* = 10.3, 7.1, 4.1 Hz, 1H), 4.02 (qd, *J* = 7.1, 2.7 Hz, 1H), 3.46 – 3.32 (m, 1H), 3.25 (t, *J* = 2.7 Hz, 1H), 3.17 (dd, *J* = -13.2, 4.1 Hz, 1H), 3.06 – 2.92 (m, 2H), 1.13 (d, *J* = 6.9 Hz, 3H), 1.01 (d, *J* = 7.1 Hz, 3H). ¹³C NMR (75 MHz, CDCl₃) δ (ppm): 175.5 (C=O), 172.8 (C=O), 148.6, 147.2, 136.3, 129.4, 128.9, 127.3, 126.9, 123.4, 72.0 (CH), 59.6 (CH), 44.8 (CH), 37.5 (CH₂), 28.9 (CH₂), 9.7 (Me). EIMS *m/z* (%): *m/z* 401 (3, M⁺), 102 (100). [α]_D²⁵ +14.90 (*c* = 0.01 g/100 mL, CHCl₃). CCDC: 1839079.



(4S)-Benzyl-3-(3-(4-chlorophenyl)-3-hydroxy-2-methylpropanoyl) thiazolidin-2-one (6,7g).

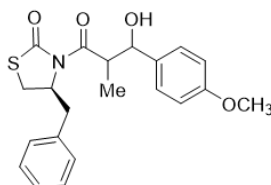
Following the general procedure, this compound was prepared by reacting **5** with 4-chlorobenzaldehyde. The diastereoisomeric mixture was purified by column chromatography using hexanes:EtOAc (95:5) as eluents, affording a mixture of **6g** and **7g** (93:7) as a solid in 70 % yield. After crystallization from (DCM– hexanes) it had mp: 124-126°C; ¹H NMR (300 MHz, CDCl₃) δ (ppm): 7.39 – 7.22 (m, 13H), 5.12 (d, *J* = 3.1 Hz, 1H), 5.02 (d, *J* = 3.9 Hz, 1H), 4.95 (ddd, *J* = 10.7, 7.1, 4.0 Hz, 1H), 4.63 (s, 1H), 3.98 (qd, *J* = 7.0, 3.1 Hz, 1H), 3.34 (dd, *J* = -11.5, 7.3 Hz, 1H), 3.08 (dd, *J* = -13.2, 4.0 Hz, 1H), 2.98 – 2.83 (m, 4H), 1.13 (d, *J* = 6.9 Hz, 3H), 1.05 (d, *J* = 7.0 Hz, 3H). ¹³C NMR (75 MHz, CDCl₃) δ (ppm): 175.6 (C=O), 172.6 (C=O), 139.8, 136.3, 133.0, 129.3, 128.8, 128.5, 128.2, 128.2, 127.5, 127.2, 72.3 (CH), 59.5 (CH), 45.0 (CH), 37.4 (CH₂), 28.6 (CH₂), 10.1 (Me). EIMS *m/z* (%): 391(10, M + 2), 389 (12, M⁺), 117 (100). [α]_D²⁵ +20.89 (*c* = 0.01 g/100 mL, CHCl₃). CCDC: 1839080.



(4S)-Benzyl-3-(3-hydroxy-3-(4-methoxyphenyl)-2-methylpropanoyl) thiazolidin-2-one (6,7h)

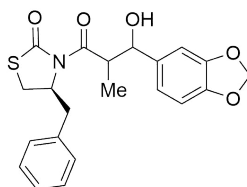
(Fig. x). Following the general procedure, this compound was prepared by reacting **5** with 4-methoxybenzaldehyde. The diastereoisomeric mixture was purified by column chromatography using hexanes:EtOAc (92:8) as eluents, affording a mixture of **6h** and **7h** (86:14) as an oil in 74 % yield. ¹H NMR (300 MHz, CDCl₃) δ (ppm): 7.38 – 7.21 (m, 9H), 6.89 – 6.83 (m, 2H), 5.08 (d, *J* = 3.8 Hz, 1H), 4.99 – 4.88 (m, 1H), 4.72 (d, *J* = 8.7 Hz, 1H), 4.28 – 4.14 (m, 1H), 4.04 (qd, *J* = 7.0, 3.8 Hz, 1H), 3.78 (s, 3H), 3.77 (s,

3H), 3.32 (ddd, $J = -11.4, 7.3, 1.0$ Hz, 1H), 2.99 (dd, $J = -13.3, 3.9$ Hz, 1H), 2.94 – 2.78 (m, 3H), 1.11 (d, $J = 7.0$ Hz, 3H), 1.02 (d, $J = 6.9$ Hz, 3H). ^{13}C NMR (126 MHz, CDCl_3) δ (ppm): 175.7 (C=O), 172.4 (C=O), 158.8, 136.5, 136.5, 133.5, 132.2, 129.3, 128.8, 127.9, 127.3, 127.3, 127.1, 113.5, 73.0 (CH), 59.4 (CH), 55.2 (OMe), 45.3 (CH), 37.3 (CH_2), 28.4 (CH_2), 10.7 (Me). EIMS m/z (%): 385 (M^+), 367 (5, M - 18) 117 (100). $[\alpha]_{\text{D}} +24.48$ ($c = 0.01$ g/100 mL, CHCl_3). CCDC: 1839081.



(S)-3-(3-(Benzo[d][1,3]dioxol-5-yl)-3-hydroxy-2-methylpropanoyl)-4-benzylthiazolidin-2-one

(6,7i). Following the general procedure, this compound was prepared by reacting **5** with piperonal. The diastereoisomeric mixture was purified by column chromatography using hexanes:EtOAc (95:5) as eluents, affording a mixture of **6i** and **7i** (97:3) as a solid in 84 % yield. After crystallization from (DCM – hexanes) it had m.p.: 103–105°C; ^1H NMR (500 MHz, CDCl_3) δ (ppm): 7.38 – 7.32 (m, 2H), 7.27 (t, $J = 6.3$ Hz, 3H), 6.95 (d, $J = 1.9$ Hz, 1H), 6.89 (dd, $J = 8.1, 1.9$ Hz, 1H), 6.77 (dd, $J = 8.1, 1.9$ Hz, 1H), 5.97 – 5.88 (m, 2H), 5.06 (t, $J = 2.7$ Hz, 1H), 5.01 – 4.90 (m, 1H), 4.03 – 3.95 (m, 1H), 3.39 – 3.28 (m, 1H), 3.13 – 2.96 (m, 1H), 2.97 – 2.76 (m, 4H), 1.19 (d, $J = 6.7$ Hz, 3H), 1.11 (d, $J = 7.0$ Hz, 3H). ^{13}C NMR (126 MHz, CDCl_3) δ (ppm): 175.7 (C=O), 172.4 (C=O), 147.4, 146.6, 136.4, 135.4, 129.3, 128.8, 127.1, 119.3, 107.9, 106.8, 100.8 (CH_2), 72.8 (CH), 59.4 (CH), 45.3 (CH), 37.4 (CH_2), 28.5 (CH_2), 10.5 (Me). EIMS m/z (%): 399 (3, M^+), 117 (100). $[\alpha]_{\text{D}}^{25} +23.36^\circ$ ($c = 0.01$ g/100 mL, CHCl_3).



Chiral auxiliary removal

Mixture of compounds **6c** and **7c** (100 mg, 0.234 mmol) was dissolved in DCM (3.0 mL), *p*-nitrobenzyl alcohol (40 mg, 0.280 mmol) and 5 mg of DMAP were then added. The reaction mixture was stirred at room temperature for 60 min and quenched by the addition of saturated solution of NH_4Cl (15 mL). The crude product was extracted with DCM (3 x 30 mL) and the organic fraction was dried over anhydrous Na_2SO_4 , filtered, and concentrated under reduced pressure. Purification was accomplished by flash chromatography (9:1 hexanes:EtOAc) to give the stereoisomeric mixture 4-nitrobenzyl-3-(2,4-dichlorophenyl)-3-hydroxy-2-methylpropanoate (**8**) as a yellow oil in a 93 % of yield. ^1H NMR (300 MHz, CDCl_3) δ (ppm): 8.33 – 8.13 (m, 2H), 7.60 – 7.45 (m, 3H), 7.42 – 7.25 (m, 2H), 5.51 (s, 1H), 5.28 (s, 2H), 3.16 – 2.93 (m, 2H), 1.11 (d, $J = 7.2$ Hz, 3H). ^{13}C NMR (75 MHz, CDCl_3) δ (ppm): 175.2 (C=O), 147.8, 142.8, 136.9, 133.9, 131.9, 129.3, 129.2, 128.3, 127.1, 123.9, 69.7 (CH), 65.1 (CH_2), 42.8 (CH), 29.7 (CH), 9.8 (Me).

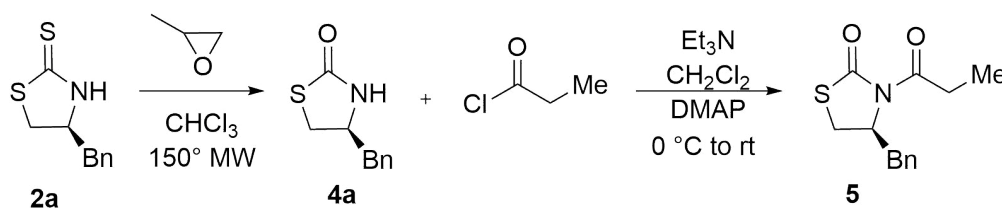
Results and discussion

In 2012, we reported the synthesis of some derivatives of 1,3-thiazolin-2-ones **4**, through desulfurization-oxygenation reaction of 1,3-thiazolidine-2-thiones **2**.^[24] To our knowledge, no reports dealing with the use of 1,3-thiazolidin-2-ones **4** in asymmetric synthesis have been published so far. In order to explore

the synthetic potential and the influence of endocyclic sulfur atom on the chiral 1,3-thiazolidine-2-ones **4**, in relation to the application in asymmetric synthesis, we report our preliminary results about the use of these chiral auxiliaries in asymmetric aldol coupling with aldehydes.

Due to the similarity in structure with their congeners **1**, **2** and **3**, we reasoned that thiazolidine-2-one **4** derivatives, might have applications in the field as well. Therefore, we decided to investigate whether these entities **4** could function as chiral auxiliaries in processes of asymmetric aldol coupling.

We started with the synthesis of (4*S*)-benzyl-1,3-thiazolidin-2-one **4a**[20] from **2a** which was prepared according to published procedure from *L*-phenylalanine.[25] The *N*-acylation reaction of **4a** was achieved using Et₃N as base and propionyl chloride as acylating agent, which under these conditions the *N*-propionyl derivative was obtained in 67 % yield (Scheme 1).

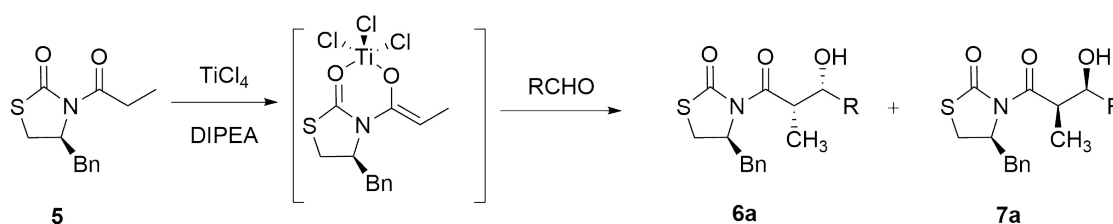


Scheme 1. *N*-acylation of (4*S*)-benzyl-1,3-thiazolidin-2-one **4a**.

To confirm the absolute structure and absolute configuration of **4a** and **5** a single crystal X-ray diffraction was carried out, the compounds **4a** and **5** crystallize in the orthorhombic system in the P2(1)2(1)2(1) space group, and the method used for checking the enantiopurity was the Flack parameter,[27] For valid absolute structure assignments, the absolute value of Flack parameter should be close to zero and for enantiopure compounds s.u. should be less than 0.1. In the case of **4a** and **5**, the Flack parameters were 0.053(17), 0.02(9) respectively confirming the optical structure of the analyzed samples.

We decided to study the coupling reaction of *N*-propionyl-(4*S*)-benzylthiazolidin-2-one **5** with benzaldehyde as a model reaction. Initially, thiazolidin-2-one **5** was treated with LDA (1.0 equiv) in anhydrous THF solution at -78 °C, followed by the addition of benzaldehyde; under these conditions only the cleavage of the chiral auxiliary was observed by TLC. Therefore, we decided try the enolate generation of **5** with TiCl₄ (1.0 equiv) in the presence of a base more selective to form aldol adducts as DIPEA (1.0 equiv) at -10 °C (Scheme 2).[26] The analysis by TLC shows a clean reaction with the formation of aldol derivatives **6a**:**7a** in 55 % (chemical yield) as mixture of diastereoisomers with a diastereoselectivity ratio **6a**:**7a** of 82:18. Increasing the amount of Lewis acid, DIPEA and benzaldehyde (1.5 equiv, each/1.0 equiv **5**), an improved chemical yield was obtained (86 %), and the diastereoselectivity was observed whit a ratio **6a**:**7a** of 97:3. (Table 1, entry 1). The kinetic diastereomeric ratios were directly determined by comparing the crude ¹H NMR spectra.

With the optimized reaction conditions in hand, this methodology of asymmetric aldol coupling was extended. We decided probe these reaction conditions with a variety of aldehydes including aliphatic and aromatic derivatives with electron-withdrawing and electron-releasing groups (Table 1).



Scheme 2. Asymmetric aldol coupling of *N*-propionyl-(4*S*)-thiazolidinone **5** with aldehydes.

Table 1. Aldol coupling of thiazolidinone **5** with arylaldehydes.

Entry ^a	Aldehyde (RCHO)	6:7 ^b	Yield % ^c
1	a R = C ₆ H ₅	97:3	86
2	b R = 2,4-(CH ₃ O) ₂ C ₆ H ₃	97:3	84
3	c R = R = 2,4-Cl ₂ C ₆ H ₃	85:15	75
4	d R = 2-ClC ₆ H ₄	73:27	77
5	e R = 3,4-(BnO) ₂ C ₆ H ₃	94:6	76
6	f R = 4-NO ₂ C ₆ H ₄	97:3	92
7	g R = 4-ClC ₆ H ₄	97:3	70
8	h R = 4-CH ₃ OC ₆ H ₄	86:14	74
9	i R = 3,4-(OCH ₂ O)C ₆ H ₃	97:3	84

^aFor a representative procedure, see Supporting Information.

^bDiastereomeric ratios were determined by ¹HNMR from mix of diastereomers.

^cYield of the mix of diastereoisomers after purification.

Important aspects of this asymmetric aldol coupling deserve comment. Firstly, the chemical yield was acceptable in all cases (70 – 92 %), we observed high diastereoselectivity ratio, when a variety of aromatic aldehydes were used independently of the electron nature of the substituent group (electron-releasing or with electron-withdrawing substituent). (See supporting information).

After carrying out the asymmetric aldol condensation to obtain **6** and **7** derivatives, the absolute configuration and the stereochemistry of the new chiral centers created must be verified. This was possible by growing suitable crystals of the major diastereomers (for the compounds **6a**, **6c**, **6d**, **6f**, and **6g**) and suitable crystals for the diastereoisomeric mixture of **6b** and **7b**. To these crystals, a single crystal X-ray diffraction study was developed (see support information). The compounds **6a**, **6c**, and **6d**, crystallized in the monoclinic system, in the P2(1) chiral space group. The Flack parameters obtained for the compounds **6a**, **6c** and **6d** were 0.026(9), 0.009(17), 0.039(15) and 0.065(5) respectively. The compounds **6f** and **6g** crystallized in the orthorhombic system, in the P2(1)2(1)2(1) chiral space group. The Flack parameters obtained for the compound **6g** was -0.03(2). The mixture of **6b** and **7b** crystallized in the monoclinic system, in the P2(1) chiral space group with a Flack parameter of 0.005(4). The configuration was found for the chiral carbons: for the carbon bonded to the benzyl group (C4), for carbon in the alkyl chain bonded to the methyl group (C14), and for carbon in the alkyl chain bonded to the hydroxyl group (C16), in compounds **6a**, **6c**, **6d**, **6f**, and **6g**, were *S*, *R*, *R* for all cases. In the case of the analyzed crystal of the mixture **6b** and **7b**, in the asymmetric unit the compounds interact through hydrogen-bonds forming a ring described in graph set terms as C₂²(12) with configuration for molecule of **7b** as *S*, *S*, *S* (non-Evans *syn* aldol) and configuration for molecule of **6b** as *S*, *R*, *R* (Evans *syn* aldol) (Fig. 2).[28]

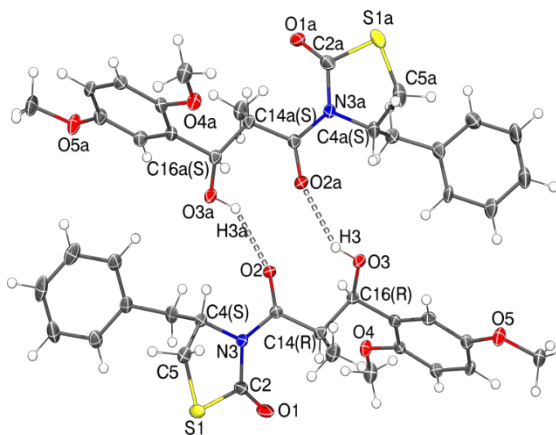


Fig. 2. ORTEP plot at 50 % of probability for asymmetric unit in the mixture of compound **7b** at the top and compound **6b** at the bottom.

Unfortunately, single crystals for **6e**, and **6i** suitable for X-ray diffraction analysis could not be obtained and the exact stereochemistry for these compounds was not determined. However, their ^1H NMR respective show signals with the same characteristics in chemical shift and coupling constants that the others diastereoisomers **6** and **7**. (See supporting information)

According to the results of the single-crystal X-ray structural analysis, the enolization of *N*-propanoylthiazolidinone with titanium tetrachloride followed by the coupling reaction with the respective aldehydes at $-10\text{ }^\circ\text{C}$, produced the ‘Evans *syn*’ adduct **6**. Probably this can be attributed to a proposed highly *non*-chelated transition state pre-reacting (TSs) **complex A** is envisaged first, where the $\text{C}=\text{O}$ group of the incoming electrophile (benzaldehyde) coordinates with the titanium atom. Coordination from the carbonyl oxygen of the enolate and the electrophile results in a hexacoordinate titanium **complex B** (Fig. 3). The number of possible conformers for such complexes is therefore restricted. A schematic diagram representing important *non*-chelated TSs for C-C bond formation between titanium *Z*-enolate, and benzaldehyde is provided in Fig. 3. The *non*-chelated TSs, minimizes the dipole interactions between the carbonyl group of the chiral auxiliary and the carbonyl group of the aldehyde along with the developing carbonyl of the aldol group in the thiazolidinone, like oxazolidinones due to presence of the carbonyl group, and dipole minimization considerations could be more important under these reaction conditions.[29] In the *non*-chelated TS model, attack by the less hindered *re* face of the enolate on the *si* face of benzaldehyde is found to be energetically the most favored approach, led to formation of Evans-*syn* aldol adduct.

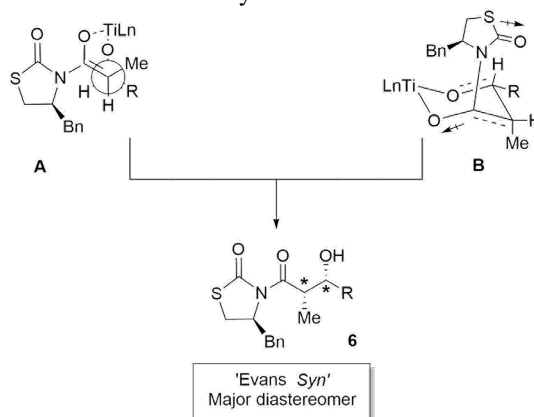
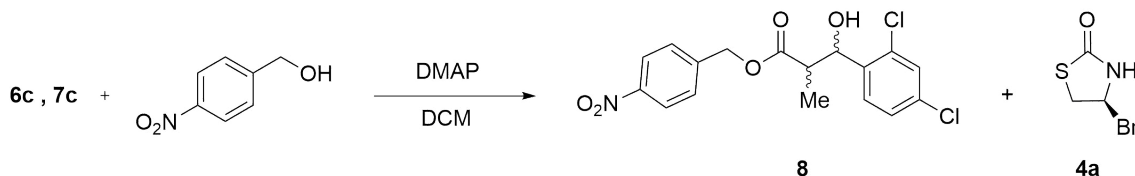


Fig. 3. Possible models to account for the observed stereoselectivity.

Finally, according with the literature this kind of aldol products formed can be converted to a variety of derivatives.[15a] One example was carried out for demonstrate the easy remotion of chiral auxiliary under mild conditions, using the diastereoisomers mixture of **6c**:**7c**, trough the acyl substitution reaction (Scheme 3) with *p*-nitrobenzyl alcohol in DCM and DMAP 5% mol at room temperature, obtaining the corresponding mixture of stereoisomers **8** in 93 %, yield.



Scheme 3. Removal of the chiral auxiliary.

Conclusions

In summary, we have developed a reaction using (4*S*)-benzyl-1,3-thiazolidin-2-one as a new type of α -aminoacid-derived chiral auxiliary, which provides high levels of diastereoselective in aldol reactions with a variety of aromatic aldehydes in good yields.

A considerable selectivity was obtained for the ‘Evans *syn*’ aldol product through a *non*-chelated transition state.

Removal of the chiral auxiliary was carried out under mild reaction conditions to obtain the expected product in a good yield. This kind of derivatives can be easily deprotected due to the presence of the endocyclic sulfur atom in the chiral auxiliary structure.

Acknowledgements

The financial support from SIEA (Secretaría de Investigación y Estudios Avanzados (SIEA – UAEMex) (Grant 6162/2020CIB) is gratefully acknowledged. The authors wish also to thank M. Sc. Maria de las Nieves Zavala Segovia (CCIQS UNAM-UAEM) for obtaining NMR spectra, M. Sc. Lizbeth Triana Cruz for obtaining Mass spectra and to Prof. Horacio F. Olivo for helpful discussions and interest in our work.

References

1. (a) Anger D.J.; Prakash, I.; Schaad, D.R. *Aldrichim. Acta* **1997**, 30, 3-12. (a) Anger D. J.; Prakash, I.; Schaad, D. R. *Aldrichim. Acta* 1997, 30, 3-12, (b) Evans, D. A.; Bartoli, J.; Shih, T. L. *J. Am. Chem. Soc.* **1981**, 103, 2127–2129. (c) Evans, D. A.; Ennis, M. D.; Mathre, D. J. *J. Am. Chem. Soc.* **1982**, 104, 1737–1739. (d) Evans, D. A.; Chapman, K. T.; Bisaha, J. *J. Am. Chem. Soc.* **1984**, 106, 4261–4263. (e) Evans D.A.; J.S. Clark, R. Mettemich, V.J. Novack, G.S. Sheppard, *J. Am. Chem. Soc.* **1990**, 112, 866.
2. (a) Oppolzer, W.; Blagg, J.; Rodriguez, I.; Walther, E. *J. Am. Chem. Soc.* **1990**, 112, 2767-2772. (b) Ortiz, A.; Sansinenea, E. *J. Sulf. Chem.* **2007**, 28, 109-147. (c) Crimmins, M. T. King, B.W.; Tabet, E. A. *J. Am. Chem. Soc.* **1997**, 119, 7883-7884. (d) Ortiz, A.; Sansinenea, E. *J. Sulf. Chem.* **2007**, 28, 109-147.
3. (a) Velázquez, F.; Olivo, H.F. *Curr. Org. Chem.* **2002**, 6, 1-38, (b) Yan, T.-H.; Tan, C.-W.; Lee, H.-C.; Lo, H.-C.; Huang, T.-Y. *J. Am. Chem. Soc.* **1993**, 115, 2613-2621, (c) T.-H.; Hung, A.-W.; Lee,

- H.-C.; Chang, C.-S.; Liu, W.-H. *J. Org. Chem.* **1995**, 60, 3301-3306. (d) Crimmins, M. T.; King, B. W.; Tabet, E. A. *J. Am. Chem. Soc.*, **1997**, 119, 7883-7884.
- Farina, V.; Reeves, J.T.; Senanayake, C.H.; Song, J. *J. Chem. Rev.* **2006**, 106, 2734-2793.
 - Crimmins, M.T.; King, B.W.; Tabet, E.A.; Chaudhary, K. *J. Org. Chem.* **2001**, 66, 894-902.
 - Evans, D.A.; Bartroli, J.; Shih, T.L. *J. Am. Chem. Soc.* **1981**, 103, 2127-2129.
 - Evans, D.A.; Nelson, J.V.; Vogel, E.; Taber, T.R. *J. Am. Chem. Soc.* **1981**, 103, 3099-3111.
 - Evans, D.A.; Rieger, D.L.; Bilodeau, M.T.; Urpi, F. *J. Am. Chem. Soc.* **1991**, 113, 1047-1049.
 - Walker, M.A.; Heathcock, C. H. *J. Org. Chem.* **1991**, 56, 5747-5755.
 - Crimmins, M.T.; King, B. W.; Tabet, E. A.; Chaudhary, K. *J. Org. Chem.* **2001**, 66, 894-902.
 - Nagao, Y.; Yamada, S.; Kumagai, T.; Ochiai, M.; Fujita, E. *J. Chem. Soc. Chem. Commun.* **1985**, 1418-1419.
 - Alexakis, A.; Bäckwall, J.E.; Krause, N.; Pamies, O.; Dieguez, M. *Chem. Rev.* **2008**, 108, 2796-2823.
 - (a) Williams, D.R.; Nold, A.L.; Mullins, R.J. *J. Org. Chem.* **2004**, 69, 5374-5382. (b) Esumi, T.; Shimizu, H.; Kashiyama, A.; Sasak C.; Toyota, M. *Tetrahedron Lett.* **2008**, 49, 6846-6849.
 - (a) Kitajima, H.; Ito, K.; Katsuki, T. *Tetrahedron.* **1997**, 53, 17015-17028; (b) Krause, N.; Hoffmann-Roeder, A. *Synthesis.* **2001**, 171-196
 - (a) Crimmins, M. T.; Chaudhary, K. *Org. Lett.* **2000**, 2, 775-777; (b) Crimmins, M. T.; Caussanel, F. *J. Am. Chem. Soc.* **2006**, 128, 3128-3129; (c) Crimmins, M. T.; Slade, D. *J. Org. Lett.* **2006**, 8, 2192-2194.
 - (a) Palomo, C.; Oiarbide, M.; Dias, F.; Ortiz, A.; Linden, A. *J. Am. Chem. Soc.* **2001**, 123, 5602. (b) Ortiz, A.; Quintero, L.; Hernandez, H.; Maldonado, S.; Mendoza, G.; Bernes, S. *Tetrahedron Lett.* **2003**, 44, 1129. (c) Palomo, C.; Oiarbide, M.; Lopez, R.; Gonzalez, P. B.; Gomez-Bengoa, E.; Sa, J. M.; Linden, A. *J. Am. Chem. Soc.* **2006**, 128, 15236.
 - Amagata, T.; Johnson, T. A.; Cichewicz, R. H.; Tenney, K.; Mooberry, S. L.; Media, J.; Edelstein, M.; Valeriote, F. A.; Crews, P. *J. Med. Chem.* **2008**, 51, 7234-7242.
 - Sonnenschein, R. N.; Johnson, T. A.; Tenney, K.; Valeriote, F. A.; Crews, P. *J. Nat. Prod.* **2006**, 69, 145-147.
 - (a) Shibahara, F.; Suenami, A.; Yoshida, A.; Murai, T. *Chem. Commun.* **2007**, 2354. (b) Mohammadpoor-Baltork, I.; Khodaei, M. M.; Nikoofar, K. *Tetrahedron Lett.* **2003**, 44, 591. (c) Kim, Y. H.; Chung, B. C.; Chang, S. *Tetrahedron Lett.* **1985**, 26, 1079. (d) Jorgensen, K. A.; El-Wassimy, M. T. M.; Lawesson, S. O. *Tetrahedron.* **1983**, 39, 469. (e) Kochhar, K. S.; Cottrell, D. A.; Pinnick, H. W. *Tetrahedron Lett.* **1983**, 24, 1323.
 - (a) Liu, Z. G.; Dai, C. S. *Acta Chim. Sinica* **1965**, 31, 258-259; (b) Zheng, B.; Yang, Q. C.; Li, L. Chinese patent, CN 1403447, **2003**.
 - (a) Moreno-Manas, M.; Padros, I. *J. Heterocycl. Chem.* **1993**, 30, 1235-1239; (b) Kitoha, S.; Kubotab, A.; Kunimotoa, K.; Kuwaec, A.; Hanaic, K. *J. Mol. Struct.* **2005**, 737, 277-282
 - Deng, X.; Chen, N.; Wang, Z.; Li, X.; Hu, H.; Xu, J. *Phosphorus, Sulfur Silicon* **2011**, 186, 1563.
 - Romero, O.; Minor-Villar, L.; Olivo, H.; *Synlett*, **2012**, 23, 2835-2839.
 - Evans, D. A.; Bartroli, J.; Shih, T. L. *J. Am. Chem. Soc.* **1981**, 103, 2127-2129.
 - D. Delaunay, L. Toupet, M.L. Corre, *J. Org. Chem.* **1995**, 60, 6604.
 - Crimmins, M. T. Chaudhary, K. *Org. Lett.* **2000**, 2, 775-777.
 - (a) Flack, H. D.; Bemardinelli, G. *Acta Cryst. A* **1999**, 55, 908-915. (b) Flack H. D.; Bemardinelli G. *J. Appl Cryst.* **2000**, 33, 1143-1148.
 - CCDC 1839074 (**4a**), 1839075 (**6a**), 1839076 (**6b**), 1839077 (**6c**), 1839078 (**6d**), 1839079 (**6f**), 1839080 (**6g**), 1839081 (**6h**). <https://www.ccdc.cam.ac.uk/structures/>, Accessed December 14, 2023.
 - Evans, D. A. In *Proceedings of The Robert A. Welch Foundation Conferences on Chemical Research. XXXVII. Stereospecificity in Chemistry and Biochemistry*; Ed. Welch Foundation, **1984**.

Alpha-glucosidase and Alpha-amylase Inhibitors Derived from Naturally Occurring Prenylated Isoflavones

Brandon Hernández-Gutiérrez¹, María C. Cruz-López¹, Omar Gómez-García², Elvia Becerra-Martínez³, Fabiola E. Jiménez-Montejo¹, Aarón Mendieta-Moctezuma^{1*}

¹Centro de Investigación en Biotecnología Aplicada, Instituto Politécnico Nacional, Carretera Estatal Santa Inés Tecuexcomax-Tepetitla, Km 1.5, Tepetitla de Lardizábal, 90700 Tlaxcala, Mexico.

²Departamento de Química Orgánica, Escuela Nacional de Ciencias Biológicas, Instituto Politécnico Nacional, Prol. Carpio y Plan de Ayala S/N, 11340 Ciudad de México, Mexico.

³Centro de Nanociencias y Micro y Nanotecnologías, Instituto Politécnico Nacional, Av. Luis Enrique Erro S/N, Ciudad de México, 07738, Mexico.

*Corresponding author: Aarón Mendieta-Moctezuma, email: amendietam@ipn.mx

Received September 3rd, 2023; Accepted September 19th, 2023.

DOI: <http://dx.doi.org/10.29356/jmcs.v68i1.2129>

Abstract. A series of prenylated isoflavones were synthesized to evaluate their inhibitory effect against α -glucosidase and α -amylase enzymes, analyzing the bioisosteric effect of the linear or cyclized prenyl moiety in these benzopyran derivatives. Compound **5a** exhibited higher α -glucosidase inhibition ($IC_{50} = 60.5 \mu M$) and lower α -amylase inhibition ($IC_{50} = 85.0 \mu M$) compared to acarbose ($IC_{50} = 527.5 \mu M$ for α -glucosidase and $20.1 \mu M$ for α -amylase). In contrast, prenylated isoflavone **5c** showed higher inhibition in both enzymes ($IC_{50} = 17.6 \mu M$ for α -glucosidase and $21.2 \mu M$ for α -amylase). This suggests that the attachment of a prenyl moiety to the 7-hydroxy group of isoflavone provides higher inhibition in the enzymes α -glucosidase and α -amylase. Docking studies of compounds **5a** and **5c** displayed key interactions towards both enzymes. The type of inhibition for **5c** was analyzed, where the results indicate a competitive inhibition of both α -glucosidase and α -amylase. Finally, ADMET studies support that compounds **5a** and **5c** are candidates for the design of novel isoflavones derivatives with antidiabetic potential.

Keywords: Diabetes mellitus; α -glucosidase; α -amylase; prenylated isoflavones; pyranisoflavones.

Resumen. Una serie de isoflavonas preniladas se sintetizaron para evaluar su efecto inhibitorio sobre las enzimas α -glucosidasa y α -amilasa, analizando el efecto bioisotérico del fragmento prenilo tipo lineal o ciclado en estos benzopiranos derivados. El compuesto **5a** exhibió una inhibición alta de α -glucosidasa ($CI_{50} = 60.5 \mu M$) y una inhibición más baja de α -amilasa ($CI_{50} = 85.0 \mu M$, respectivamente) en comparación con acarbosa ($CI_{50} = 527.5$ y $20.1 \mu M$). La isoflavona prenilada **5c** mostró mayor inhibición en ambas enzimas ($CI_{50} = 17.7 \mu M$ para α -glucosidasa y $21.2 \mu M$ para α -amilasa). Esto sugiere que la unión del fragmento prenilo al hidroxilo de la posición 7 de la isoflavona ocasiona una mayor inhibición en las enzimas α -glucosidasa y α -amilasa. Los compuestos **5a** y **5c** mostraron interacciones clave hacia el sitio activo de ambas enzimas, de acuerdo con los cálculos de acoplamiento. Se analizó el tipo de inhibición para **5c**, donde los resultados indican una inhibición competitiva tanto de α -glucosidasa como de α -amilasa. Finalmente, los estudios ADMET respaldan que los compuestos **5a** and **5c** son candidatos para el diseño de nuevos derivados de isoflavonas con potencial antidiabético.

Palabras clave: Diabetes mellitus; α -glucosidasa; α -amilasa; isoflavonas preniladas; piranoisoflavonas.

Introduction

Type 2 diabetes is characterized by a postprandial increase in blood glucose due to the lack of insulin action or secretion, leading to an increased risk of cardiovascular and cerebrovascular diseases, retinopathy, and cancer. According to the World Health Organization (WHO), about 422 million people have diabetes [1]. A therapeutic treatment of diabetes is to reduce blood glucose levels through enzyme inhibitors. The α -amylase and α -glucosidase enzymes are involved in the breakdown of dietary starch and sugars into glucose, where α -amylase catalyzes the hydrolysis of starch and other carbohydrate polymers through the cleavage of 1-4- α -D-glycosidic links generating smaller oligosaccharides while α -glucosidase catalyzes the cleavage of the 1-4- α -D-glycosidic bonds of these oligosaccharides into glucose units [2]. Acarbose is a pseudo-tetrasaccharide that inhibits both enzymes, thus delaying glucose absorption and reducing postprandial glucose levels [3]. However, its gastrointestinal side effects have led to the search for new glucosidase inhibitors from diverse sources, such as natural products and synthetic compounds.

Isoflavones are secondary metabolites of plants, these heterocycles are based on a 3-phenylchroman skeleton, biogenetically derived from a 2-phenylchroman skeleton of flavonoid. They are well-known for their beneficial properties mainly exerting antioxidant [4], antidiabetic [5], anticancer [6], anti-inflammatory [7], anti-ulcer [8], and anti-obesity effects [9]. The main isoflavones sources are soybeans and red clover, with daidzein, genistein, and formononetin as the main compounds. These have attracted attention due to their antidiabetic properties, as they reduce blood glucose levels by acting as α -glucosidase inhibitors [5,10]. Moreover, these natural inhibitors have been employed as lead compounds to obtain new molecules with a higher inhibitory effect on α -glucosidase as well as low adverse effects [7,9,11,12].

Prenylated isoflavones along with pyranisoflavones are a subclass of natural isoflavones that own at least one prenylated side chain on the flavonoid backbone, exhibiting antimicrobial [13], antidiabetic [14,15], anti-inflammatory [7,16], anticancer [17,18], and neuroprotective properties [12]. Their antidiabetic features are attributed to inhibition of α -glucosidase enzyme [4,14,19,20]. Structure-activity relationship studies of natural isoflavones as α -glucosidase and α -amylase inhibitors suggest that at the C-7 position in the isoflavone core, the presence of a linear or cyclized prenyl moiety seems to favor this effect biological [2,14,20].

The α -glucosidase and α -amylase inhibitory activities shown by the isoflavones daidzein, genistein, and their prenylated derivatives have been reported, but no data are available for prenylated formononetin derivatives (calopogonium isoflavone A, 6-methoxycalopogonium isoflavone and maxima isoflavone J), which is important for the development of dual inhibitors on those carbohydrate-hydrolyzing enzymes (Fig. 1) [11,21]. Considering these facts, the aim of the current study was to synthesize prenylated isoflavones derived-formononetin and test their potential as α -amylase and α -glucosidase inhibitors. Enzymatic and *in silico* studies were performed to better understand the interaction of the compounds with the active site of both enzymes.

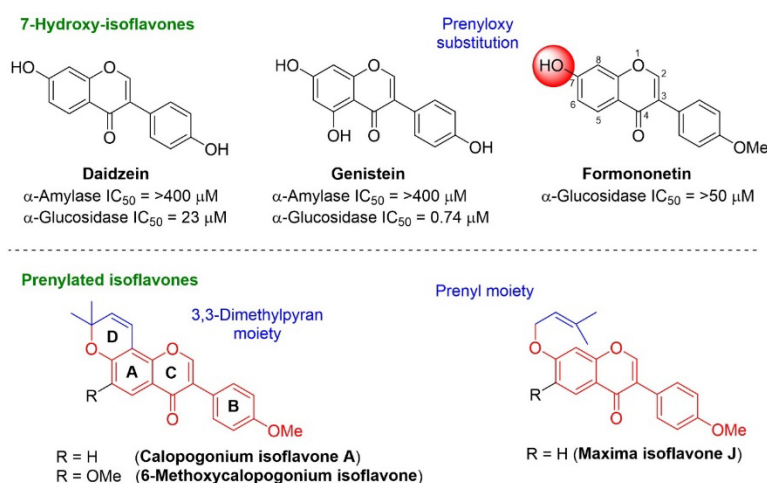


Fig. 1. Prenylated isoflavones as potential α -glucosidase and α -amylase inhibitors.

Experimental

Chemistry

All Raw data measurements of melting points were determined by an Electrothermal apparatus and are uncorrected. Nuclear Magnetic Resonance (^1H -, ^{13}C -NMR) spectra were recorded on Bruker Avance (600 or 750 MHz) spectrometers. The chemical shifts (δ) are expressed in ppm relative to the TMS as internal standard and multiplicities are indicated by the following symbols: s (singlet), d (doublet), t (triplet), dd (double of doublets), brs (broad singlet), brd (broad doublet), and m (multiplet). A UPLC (Waters) coupled to a quadrupole time-of-flight mass spectrometer (Waters Xevo G2-XS QTOF; electrospray ionization mode ESI-tandem quadrupole) was used for UPLC and mass spectrometer analyses (LC-MS/MS). All the reagents used were acquired from Sigma-Aldrich, and anhydrous solvents were obtained by a distillation process. Analytical TLC was carried out on precoated silica gel plates (Merck 60F₂₅₄). Silica gel (230-400 mesh) was used for flash chromatography. The synthesis of compounds **1a-c** and **2a-c** have been previously described [22].

Method (A) for the preparation of pyranoisoflavones (3a-c)

Procedure for the synthesis of 7-hydroxy-isoflavones (2a-c)

A mixture of the corresponding substituted 2,4-dihydroxyacetophenones **1a-c** (1.0 mol equiv.) and DMFDMA (2.0 mol equiv.) was poured into at room temperature in a threaded ACE glass pressure tube with a sealed Teflon screw cap. The mixture was heated at 120 °C for 3 h, diluted with CH_2Cl_2 (30 mL) and the solvent was removed under vacuum. The residue was purified by flash chromatography over silica gel (hexane/EtOAc, 80:20).

7-Hydroxy-3-(4-methoxyphenyl)-4H-chromen-4-one (2a). A crystalline beige solid (1.25 g, 92 %). *R_f* 0.57 (hexane/EtOAc, 7:3); mp 257-258 °C. Characterization of **2a** has been previously reported in the literature [22].

7-Hydroxy-6-methoxy-3-(4-methoxyphenyl)-4H-chromen-4-one (2b). A beige solid (1.25 g, 80 %). *R_f* 0.15 (hexane/EtOAc, 7:3); mp 222-224 °C. Characterization of **2b** has been previously reported in the literature [22].

6-Chloro-7-hydroxy-3-(4-methoxyphenyl)-4H-chromen-4-one (2c). A beige solid (2.01 g, 82%). *R_f* 0.27 (hexane/EtOAc, 7:3); mp 232-233 °C. Characterization of **2c** has been previously reported in the literature [22].

Procedure for the synthesis of pyranoisoflavones (3a-c)

A solution of the corresponding 7-hydroxy-isoflavones (**2a-c**) (1.0 mol equiv.), 1,1-diethoxy-3-methylbut-2-ene (1.2 mol equiv.), and 3-methylpyridine (0.6 mol equiv.) in xylene (5 mL) was poured into at room temperature in a threaded ACE glass pressure tube with a sealed Teflon screw cap. The mixture was heated at 120 °C for 36 h, diluted with CH_2Cl_2 (20 mL) and the solvent was removed under vacuum. The residue was purified by flash chromatography over silica gel (hexane/EtOAc, 90:10)

3-(4-Methoxyphenyl)-8,8-dimethyl-4H,8H-pyrano[2,3-f]chromen-4-one (3a) [12]. A white solid (0.10 g, 43 %). *R_f* 0.55 (hexane/EtOAc, 7:3); m.p. 135-137 °C. ^1H -NMR (750 MHz, CDCl_3) δ : 1.50 (s, 6H, $(\text{CH}_3)_2$), 3.84 (s, 3H, OCH₃), 5.72 (d, *J* = 9.75 Hz, 1H, H-9), 6.81 (d, *J* = 9.75 Hz, 1H, H-10), 6.86 (d, *J* = 9.0 Hz, 1H, H-6), 6.95-6.99 (m, 2H, H-3'), 7.48-7.51 (m, 2H, H-2'), 7.93 (s, 1H, H-2), 8.06 (d, *J* = 8.2 Hz, 1H, H-5). ^{13}C -NMR (187.5 MHz, CDCl_3) δ : 28.1 ($(\text{CH}_3)_2$), 55.3 (OCH₃), 77.6 (C-8), 109.1 (C-10a), 113.9 (C-3'), 114.9 (C-10), 115.1 (C-6), 118.3 (C-4a), 124.2 (C-1'), 124.6 (C-3), 126.7 (C-5), 130.1 (C-2'), 130.2 (C-9), 151.7 (C-2), 152.3 (C-1a), 157.2 (C-6a), 159.5 (C-4'), 175.8 (C=O). HRMS (ESI) $[\text{M}-\text{H}]^-$ Calculated for: $\text{C}_{21}\text{H}_{17}\text{O}_4$. 333.1127. Found: 333.1120 $[\text{M}-\text{H}]^-$.

6-Methoxy-3-(4-methoxyphenyl)-8,8-dimethyl-4H,8H-pyrano[2,3-f]chromen-4-one (3b) [23]. A white solid (0.074 g, 61 %). *Rf* 0.33 (hexane/EtOAc, 7:3); m.p. 164-165 °C. ¹H-NMR (750 MHz, CDCl₃) δ: 1.56 (s, 6H, (CH₃)₂), 3.84 (s, 3H, OCH₃-C-4'), 3.96 (s, 3H, OCH₃-C-6), 5.74 (d, *J* = 9.75 Hz, 1H, H-9), 6.81 (d, *J* = 9.75 Hz, 1H, H-10), 6.96-6.99 (m, 2H, H-3'), 7.49-7.52 (m, 2H, H-2'), 7.56 (s, 1H, H-5), 7.95 (s, 1H, H-2). ¹³C-NMR (187.5 MHz, CDCl₃) δ: 27.9 ((CH₃)₂), 55.3 (OCH₃-C-4'), 56.3 (OCH₃-C-6), 78.1 (C-8), 105.1 (C-5), 110.1 (C-10a), 113.9 (C-3'), 115.1 (C-10), 117.6 (C-4a), 124.1 (C-3), 124.4 (C-1'), 130.1 (C-2'), 130.3 (C-9), 147.10 (C-6), 147.16 (C-1a), 147.35 (C-6a), 151.5 (C-2), 159.4 (C-4'), 175.5 (C=O). HRMS (ESI) [M-H]⁻ Calculated for: C₂₂H₁₉O₅. 363.1232. Found: 363.1225 [M-H]⁻.

6-Chloro-3-(4-methoxyphenyl)-8,8-dimethyl-4H,8H-pyrano[2,3-f]chromen-4-one (3c). A white solid (0.09 g, 53 %). *Rf* 0.50 (hexane/EtOAc, 7:3); m.p. 150-151 °C. ¹H-NMR (750 MHz, CDCl₃) δ: 1.55 (s, 6H, (CH₃)₂), 3.83 (s, 3H, OCH₃), 5.78 (d, *J* = 9.75 Hz, 1H, H-9), 6.80 (d, *J* = 9.75 Hz, 1H, H-10), 6.95-6.99 (m, 2H, H-3'), 7.45-7.50 (m, 2H, H-2'), 7.93 (s, 1H, H-2), 8.12 (s, 1H, H-5). ¹³C-NMR (187.5 MHz, CDCl₃) δ: 28.0 ((CH₃)₂), 55.3 (OCH₃), 79.0 (C-8), 110.7 (C-10a), 113.9 (C-3'), 114.7 (C-10), 118.4 (C-6), 120.4 (C-4a), 123.8 (C-1'), 124.6 (C-3), 126.0 (C-5), 130.0 (C-2'), 130.8 (C-9), 150.5 (C-1a), 151.8 (C-2), 152.6 (C-6a), 159.6 (C-4'), 174.9 (C=O). HRMS (ESI) [M-H]⁻ Calculated for: C₂₁H₁₆ClO₄. 367.0737. Found: 367.1691.

Method (B) for the preparation of pyranoisoflavones (3a-c)

Procedure for the synthesis of chromenes (4a-c)

Following the method of preparation for **3a**, a mixture of the corresponding 2,4-dihydroxyacetophenone (**1a-c**) (1.0 mol equiv.), 1,1-diethoxy-3-methylbut-2-ene (1.2 mol equiv.), and 3-methylpyridine (0.6 mol equiv.) in xylene (3 mL) was heated at 120 °C for 12 h. The residue was purified by flash chromatography over silica gel (hexane/EtOAc, 98:2).

1-(5-hydroxy-2,2-dimethyl-2H-chromen-6-yl)-2-(4-methoxyphenyl)ethan-1-one (4a) [24]. Yellow crystals (0.178 g, 71 %). *Rf* 0.63 (hexane/EtOAc, 8:2); m.p. 115-116 °C. ¹H-NMR (750 MHz, CDCl₃) δ: 1.37 (s, 6H, (CH₃)₂), 3.71 (s, 3H, OCH₃), 4.06 (s, 2H, CH₂-H-2'), 5.49 (d, *J* = 10.2 Hz, 1H, H-3), 6.26 (d, *J* = 9.0 Hz, 1H, H-8), 6.62 (d, *J* = 10.2 Hz, 1H, H-4), 6.77-6.83 (m, 2H, H-3''), 7.07-7.13 (m, 2H, H-2''), 7.56 (d, *J* = 9.0 Hz, 1H, H-7), 12.88 (s, 1H, OH). ¹³C-NMR (187.5 MHz, CDCl₃) δ: 28.3 ((CH₃)₂), 43.8 (CH₂-C-2'), 55.2 (OCH₃), 77.7 (C-2'), 108.3 (C-8), 109.3 (C-4a), 112.9 (C-6), 114.1 (C-3''), 115.6 (C-4), 126.3 (C-1''), 128.1 (C-3), 130.3 (C-2''), 131.3 (C-7), 158.5 (C-4''), 159.7 (C-8a), 160.0 (C-5), 202.4 (C=O). HRMS (ESI) [M-H]⁻ Calculated for: C₂₀H₁₉O₄. 323.1289. Found: 323.1295.

1-(5-hydroxy-8-methoxy-2,2-dimethyl-2H-chromen-6-yl)-2-(4-methoxyphenyl)ethan-1-one (4b) [25]. Yellow crystals (0.15 g, 65 %). *Rf* 0.44 (hexane/EtOAc, 8:2); m.p. 177-178 °C. ¹H-NMR (750 MHz, CDCl₃) δ: 1.50 (s, 6H, (CH₃)₂), 3.79 (s, 3H, OCH₃-C-4'), 3.81 (s, 3H, OCH₃-C-8), 4.13 (s, 2H, CH₂-H-2'), 5.59 (d, *J* = 9.75 Hz, 1H, H-3), 6.70 (d, *J* = 9.75 Hz, 1H, H-4), 6.86-6.90 (m, 2H, H-3''), 7.15 (s, 1H, H-7), 7.17-7.20 (m, 2H, H-2''), 12.76 (s, 1H, OH). ¹³C-NMR (187.5 MHz, CDCl₃) δ: 28.2 ((CH₃)₂), 44.3 (CH₂-C-2'), 55.2 (OCH₃-C-4'), 57.0 (OCH₃-C-8), 78.2 (C-2), 110.4 (C-4a), 111.0 (C-6), 112.9 (C-7), 114.2 (C-3''), 115.9 (C-4), 126.4 (C-1''), 128.3 (C-3), 130.2 (C-2''), 141.1 (C-8), 150.3 (C-8a), 155.5 (C-5), 158.6 (C-4''), 201.9 (C=O). HRMS (ESI) [M-H]⁻ Calculated for: C₂₁H₂₁O₅. 353.1394. Found: 353.1378.

1-(8-chloro-5-hydroxy-2,2-dimethyl-2H-chromen-6-yl)-2-(4-methoxyphenyl)ethan-1-one (4c). A yellow solid (0.143 g, 58 %). *Rf* 0.66 (hexane/EtOAc, 8:2); m.p. 140-142 °C. ¹H-NMR (750 MHz, CDCl₃) δ: 1.49 (s, 6H, (CH₃)₂), 3.79 (s, 3H, OCH₃-C-4'), 4.12 (s, 2H, CH₂-H-2'), 5.61 (d, *J* = 9.75 Hz, 1H, H-3), 6.68 (d, *J* = 9.75 Hz, 1H, H-4), 6.86-6.90 (m, 2H, H-3''), 7.14-7.19 (m, 2H, H-2''), 7.70 (s, 1H, H-7), 12.75 (s, 1H, OH). ¹³C-NMR (187.5 MHz, CDCl₃) δ: 28.3 ((CH₃)₂), 43.8 (CH₂-C-2'), 55.2 (OCH₃-C-4'), 79.1 (C-2), 110.8 (C-4a), 112.3 (C-8), 113.1 (C-6), 114.2 (C-3''), 115.5 (C-4), 125.7 (C-1''), 128.6 (C-3), 130.3 (C-2''), 130.5 (C-7), 155.0 (C-8a), 158.3 (C-5), 158.7 (C-4''), 202.0 (C=O). HRMS (ESI) [M-H]⁻ Calculated for: C₂₀H₁₈ClO₄. 357.0899. Found: 357.0861.

Procedure for the synthesis of pyranoisoflavones (3a-c). Following the method for preparation for **2a**, a mixture of the corresponding chromene (**4a-c**) (1.0 mol equiv.) and DMFDMA (2.0 mol equiv.) was heated at 120 °C for 12 h. The residue was purified by flash chromatography over silica gel (hexane/EtOAc, 90:10).

3-(4-Methoxyphenyl)-8,8-dimethyl-4H,8H-pyrano[2,3-f]chromen-4-one (3a). A white solid (0.05 g, 50 %), *Rf* 0.55 (hexane/EtOAc, 7:3); m.p. 135-137 °C.

6-Methoxy-3-(4-methoxyphenyl)-8,8-dimethyl-4H,8H-pyrano[2,3-f]chromen-4-one (3b). A white solid (0.046 g, 47 %), *Rf* 0.33 (hexane/EtOAc, 7:3); m.p. 164-165 °C.

6-Chloro-3-(4-methoxyphenyl)-8,8-dimethyl-4H,8H-pyrano[2,3-f]chromen-4-one (3c). A white solid (0.055 g, 55 %), *Rf* 0.50 (hexane/EtOAc, 7:3); m.p. 150-151 °C.

General Method for the preparation of 7-O-prenyl-isoflavones (5a-c)

At room temperature (rt), 3,3-dimethylallyl bromide (1.5 mol equiv.) was added dropwise to a solution of 7-hydroxy-isoflavone **2a-c** (1.0 mol equiv.), and K₂CO₃ (2.0 mol equiv.) in dried acetone (20 mL), then stirred for 15 minutes. The reaction mixture was refluxed at 60 °C for 3 h, filtered, and the solvent removed under vacuum. The crude residue was purified by flash chromatography over silica gel (hexane/EtOAc, 80:20)

3-(4-Methoxyphenyl)-7-((3-methylbut-2-en-1-yl)oxy)-4H-chromen-4-one (5a) [7]. A white solid (0.434 g, 87 %). *Rf* 0.57 (hexane/EtOAc, 7:3), mp 131-132 °C. ¹H NMR (750 MHz, DMSO-*d*₆): δ 1.74 (s, 3H, H-4''), 1.76 (s, 3H, H-5''), 3.79 (s, 3H, CH₃O), 4.68 (sbr, 2H, CH₂-H-1''), 5.47 (tbr, 1H, CH-H2''), 6.90-7.10 (m, 3H, H-3', H-6), 7.06 (dbr, *J* = 6.7 Hz, 1H, H-8), 7.43-7.60 (m, 2H, H-2'), 8.01 (dbr, *J* = 6.7 Hz 1H, H-5), 8.41 (sbr, 1H, H-2). ¹³C NMR (187.5 MHz, DMSO-*d*₆): δ 18.5 (C-5''), 25.4 (C-4''), 55.1 (OCH₃), 65.3 (OCH₂-C1''), 101.2 (C-8), 113.6 (C-3'), 115.2 (C-6), 117.4 (C-4a), 118.9 (C-2''), 123.3 (C-3), 124.0 (C-1'), 126.8 (C-5), 130.0 (C-2'), 138.3 (C-3''), 153.4 (C-2), 157.3 (C-8a), 159.0 (C-4'), 162.8 (C-7), 174.6 (CO-4). HRMS (ESI) [M-H]⁻ Calculated for: C₂₁H₁₉O₄: 335.1283. Found: 335.1302 [M-H]⁻.

6-Methoxy-3-(4-methoxyphenyl)-7-((3-methylbut-2-en-1-yl)oxy)-4H-chromen-4-one (5b). A white solid (0.177 g, 72 %). *Rf* 0.36 (hexane/EtOAc, 7:3), mp 156-157 °C. ¹H NMR (600 MHz, CDCl₃): δ 1.71 (s, 3H, H-4''), 1.74 (s, 3H, H-5''), 3.76 (s, 3H, CH₃O-H-4'), 3.89 (s, 3H, CH₃O-H-6), 4.61 (d, *J* = 6.6 Hz, 2H, CH₂-H-1''), 5.47 (t, *J* = 6.6 Hz, 1H, CH-H2''), 6.79 (s, 1H, H-8), 6.86-6.92 (m, 2H, H-3'), 7.39-7.46 (m, 2H, H-2'), 7.54 (s, 1H, H-5), 7.85 (s, 1H, H-2). ¹³C NMR (150 MHz, CDCl₃): δ 18.3 (C-5''), 25.8 (C-4''), 55.2 (OCH₃-C4'), 56.2 (OCH₃-C6), 66.2 (OCH₂-C1''), 100.5 (C-8), 104.9 (C-5), 113.9 (C-3'), 117.7 (C-4a), 118.5 (C-2''), 124.3 (C-1'), 124.5 (C-3), 130.1 (C-2'), 139.0 (C-3''), 148.0 (C-6), 151.7 (C-2), 152.1 (C-8a), 153.6 (C-4'), 159.5 (C-7), 175.5 (CO-4). HRMS (ESI) [M-H]⁻ Calculated for: C₂₂H₂₁O₅: 365.1389. Found: 365.1386.

6-Chloro-3-(4-methoxyphenyl)-7-((3-methylbut-2-en-1-yl)oxy)-4H-chromen-4-one (5c). A white solid (0.206 g, 84 %). *Rf* 0.52 (hexane/EtOAc, 7:3), mp 166-167 °C. ¹H NMR (600 MHz, DMSO-*d*₆): δ 1.76 (s, 3H, H-4''), 1.79 (s, 3H, H-5''), 3.79 (s, 3H, CH₃O), 4.78 (d, *J* = 6.6 Hz, 2H, CH₂-H-1''), 5.50 (t, *J* = 6.6 Hz, 1H, CH-H2''), 6.97-7.03 (m, 2H, H-3'), 7.43 (s, 1H, H-8), 7.50-7.57 (m, 2H, H-2'), 8.05 (s, 1H, H-5), 8.49 (s, 1H, H-2). ¹³C NMR (150 MHz, DMSO-*d*₆): δ 18.2 (C-5''), 25.5 (C-4''), 55.1 (OCH₃), 66.6 (OCH₂-C1''), 102.4 (C-8), 113.6 (C-3'), 117.6 (C-4a), 118.4 (C-2''), 120.3 (C-3), 123.3 (C-1'), 123.7 (C-6), 125.7 (C-5), 130.0 (C-2'), 139.1 (C-3''), 153.8 (C-2), 155.8 (C-8a), 157.7 (C-7), 159.1 (C-4'), 173.7 (CO-4). HRMS (ESI) [M-H]⁻ Calculated for: C₂₁H₁₈ClO₄: 369.0894. Found: 369.0909.

Biological activity

Inhibition of α-glucosidase

A reaction was prepared by mixing 20 μL α-glucosidase solution (0.5 unit/mL), 120 μL of 0.1 M phosphate buffer (pH 6.9), and 10 μL of the samples at concentrations from 400 μM to 4.0 μM. The solution

was incubated in a 96-well microplate at 37 °C for 15 min. Then the enzymatic reaction was initiated by adding 20 μL of 5 mM *p*-NPG solution in 0.1 M phosphate buffer (pH 6.9), followed by incubation at 37 °C for 15 min. The reaction was stopped by adding 80 μL of 0.2 M Na_2CO_3 and absorbance was read at 405 nm [22]. Acarbose was used as reference control. IC_{50} is the concentration that gives 50 % α -glucosidase inhibition.

Inhibition of α -amylase

The reaction mixture consisting of 50 μL of 0.1 M phosphate buffer (pH 6.8), 10 μL of α -amylase solution (5.0 unit/mL), and 20 μL of the sample at various concentrations (from 100 μM to 5.0 μM) was placed in a 96-well plate and pre-incubated at 37 °C for 15 min, and 20 μL of 1 % soluble starch (0.1 M phosphate buffer, pH 6.8) was then added as a substrate and incubated at 37 °C for 45 min. Finally, 100 μL of 3,5-dinitrosalicylic acid (DNS) was added and heated at 100 °C for 20 min, and absorbance was then read at 540 nm [26]. Acarbose was used as reference control. IC_{50} is the concentration that gives 50 % α -glucosidase inhibition.

Kinetic study

Kinetic studies were carried out with α -glucosidase and α -amylase using a methodology such as that describe in the inhibitory activity assays. The prenylated isoflavone was evaluated at two concentrations according to their IC_{50} . Various concentrations of substrates were used for each of the enzymes in the range of 0.5–5.0 mM for *p*-NPG in α -glucosidase and 0.1–1.0 % for α -amylase. The type of inhibition for this compound was determined by utilizing double reciprocal plots. Inhibition constants (K_i) were calculated from substrate versus reaction rate curves using nonlinear regression of the enzyme inhibition kinetic function [22].

Docking studies

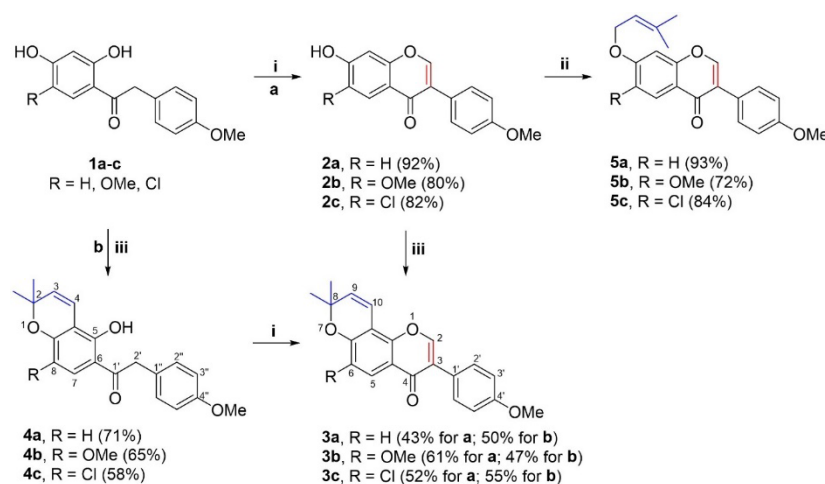
The molecular docking studies were carried out in the AutoDock 4 program [27] using the crystallized proteins of isomaltase from *Saccharomyces cerevisiae* (PDB: 3A4A) and human pancreatic α -amylase (PDB: 1B2Y) in complex with the inhibitor acarbose. In these proteins, water molecules were removed, hydrogen atoms were added to the polar atoms (considering pH at 7.4), and Kollman charges were assigned with AutoDock Tools 1.5.6. The 3D structures of acarbose (**5**) and isoflavone derivative **5c** were sketched in two dimensions (2D) with ChemSketch and then converted to 3D in a mol2 format using the Open Babel GUI program [28]. The ligands were optimized with PM6 on Gaussian 98 software to obtain the lowest energy conformation. All the possible rotatable bonds, torsion angles, atomic partial charges, and non-polar hydrogens were determined for each ligand. In AutoDockTools, the grid dimensions for α -glucosidase were $78 \times 60 \times 78 \text{ \AA}^3$ with points separated by 0.375 \AA and centered at $X = 26.313$, $Y = -3.544$, and $Z = 26.146$. The grid dimensions for α -amylase were $90 \times 70 \times 66 \text{ \AA}^3$ with points separated by 0.375 \AA and centered at $X = 16.758$, $Y = 8.692$, and $Z = 49.959$. The hybrid Lamarckian genetic algorithm was applied for minimization and utilized default parameters. A total of one hundred docking runs were conducted to determine the conformation with the lowest binding energy (kcal/mol), which was adopted for all further simulations. AutoDockTools was used to prepare the script and files as well as to visualize the docking results, and these were edited with Discovery Studio Visualizer [29].

Results and discussion

Chemistry

Pyranisoflavones are generally obtained using hydroxyketones as building blocks through two approaches: i) synthesis of hydroxylated isoflavones and formation of the 3,3-dimethyl pyran ring; and ii) synthesis of benzopyran moiety followed by the assembling of the isoflavone core [7]. In order to evaluate the pyran moieties within the isoflavone core, both strategies were applied and the synthesis of prenylated isoflavones is described in scheme 1.

In the first case, 7-hydroxyisoflavones derivatives **2a-c** were prepared in good yields by treatment of 2,4-dihydroxyacetophenones **1a-c** with DMFDMA under thermal conditions [22]. Then, the cyclization of 7-hydroxyisoflavones **2a-c** with 1,1-diethoxy-3-methylbut-2-ene in presence of 3-methylpicoline provided the pyranoisoflavones calopogonium isoflavone A (**3a**), 6-methoxycalopogonium isoflavone (**3b**), and 6-chloropyranoisoflavone (**3c**) in moderate to good yields. On the other hand, the chromene derivatives **4a-c** were obtained by cyclization of 2,4-dihydroxyketones **1a-c** with 1,1-diethoxy-3-methylbut-2-ene in presence of 3-methylpicoline, which were cyclized with DMFDMA giving the corresponding pyranoisoflavones **3a-c**. Finally, the *O*-alkylation reaction of isoflavones **2a-c** with 3,3-dimethylallyl bromide generated the series of 7-prenyloxy-isoflavones **5a-c** in good yields [7].



Scheme 1. Synthesis of prenylated isoflavone derivatives. Reagents and conditions: (i) DMFDMA, 120 °C, 3-12 h; (ii) 3,3-dimethylallyl bromide, acetone, K₂CO₃, 60 °C, 3 h; (iii) 1,1-diethoxybut-2-ene, 3-methylpicoline, xylene, 120 °C, 24-36 h.

Pyranoisoflavones calopogonium isoflavone A (**3a**), 6-methoxycalopogonium isoflavone (**3b**), and 7-prenyloxyisoflavone maxima isoflavone J (**5a**) have been isolated from plants of the genus *Millettia* and *Placolum* (Fabaceae) [23,30-33]. Recently, compound **4b** has been isolated from *P. vietnamense* and has been given the name Placovinone D [25]. The elucidation of the natural and synthetic prenylated isoflavones was confirmed by NMR and HRMS techniques, and the spectroscopic data of **3a-b**, **4b**, and **5a** were in accordance with the published literature [7,12].

In vitro α -glucosidase inhibition

The inhibitory activity of α -glucosidase was assessed for all the synthesized compounds. The obtained IC₅₀ values were compared to the corresponding value of acarbose (**6**), a well-known drug that inhibits α -glucosidase and α -amylase enzymes. As summarized in Table 1, most of the compounds display significant α -glucosidase inhibition with IC₅₀ values in the range of 17.69 to 391.46 μ M in comparison to **6** with IC₅₀ of 527.5 μ M. An exception was compound **3b**, which showed IC₅₀ >400 μ M. 7-hydroxyisoflavones **2a-c** showed good inhibitory activity whereas compound **2c** (IC₅₀ = 91.99 \pm 0.21 μ M) produced a better effect of almost 6-fold higher than **6**. The addition of a cyclized prenyl moiety at C-7 - C-8 (E-ring) of the 7-hydroxyisoflavone backbone led to a significant loss of inhibitory effect with IC₅₀ values of 208.0 \pm 0.45 and 260.1 \pm 0.52 μ M (compounds **3a** and **3c**). Interestingly, chromene benzyl derivatives **4a-c** (without C-ring) displayed greater inhibition than **3a-c**, where **4c** exhibited 9-fold higher than **6**. In order to explore that linear prenyl moiety favors inhibition, derivatives **5a-c** were evaluated. These latter compounds exhibited better inhibitory effect than

pyranoisoflavones (**3a-c**), being **5c** as the most potent derivative ($IC_{50} = 17.7 \pm 0.02 \mu\text{M}$), with almost 30-fold greater inhibition of α -glucosidase than **6**.

Regarding the inhibitory effect of the cyclized prenyl moiety (D-ring) on the 7-hydroxyisoflavone core, the analysis of the structure-activity relationship revealed that the dimethylpyran group in the pyranoisoflavone (**3a-c**) presented a weak inhibitory behavior. In contrast, chromene benzyl derivatives **4a-c**, compounds without the pyran ring (C-ring) exhibited greater inhibition, which indicates that the hydroxy group contributed to a higher inhibitory effect. These data suggest that the incorporation of a cyclized prenyl moiety to the isoflavone core significantly decreased the α -glucosidase inhibition, while a prenyloxy moiety at C-7 enhanced inhibitory activity. Furthermore, the presence of the chlorine atom at C-6 increased the inhibitory effects, while that the methoxy group decreased the activity. These results are in accordance with Jo *et al.* who reported that the α -glucosidase inhibitory activity was stronger in isoflavones with a linear prenyl group than cyclized ones [2,14].

Table 1. α -Glucosidase and α -amylase inhibition by the test compounds.

Compound	α -Glucosidase inhibition		α -Amylase inhibition	
	% (400 μM)	IC_{50} (μM)	% (100 μM)	IC_{50} (μM)
2a	94.21 \pm 0.91	95.78 \pm 0.04 ^F	63.53 \pm 2.55	70.68 \pm 1.2 ^D
2b	92.0 \pm 0.15	111.4 \pm 0.23 ^F	30.69 \pm 2.65	>100
2c	99.65 \pm 0.26	91.99 \pm 0.21 ^{FG}	81.93 \pm 1.37	56.87 \pm 0.7 ^E
3a	59.34 \pm 1.01	208.0 \pm 0.45 ^D	92.56 \pm 3.70	42.23 \pm 0.9 ^F
3b	32.59 \pm 0.52	>400	6.45 \pm 1.25	- ^a
3c	93.30 \pm 0.61	260.1 \pm 0.52 ^C	99.05 \pm 0.51	34.96 \pm 1.18 ^F
4a	99.38 \pm 0.05	78.01 \pm 0.21 ^H	99.44 \pm 0.17	123.20 \pm 0.03 ^C
4b	94.83 \pm 0.15	147.65 \pm 0.15 ^B	8.69 \pm 0.04	-
4c	99.64 \pm 0.03	57.30 \pm 0.05 ^I	70.61 \pm 0.22	143.10 \pm 0.07 ^G
5a	97.00 \pm 1.65	60.56 \pm 0.14 ^{GH}	99.33 \pm 0.93	85.09 \pm 1.7 ^B
5b	51.74 \pm 1.67	391.46 \pm 0.18 ^E	6.81 \pm 2.43	-
5c	99.15 \pm 0.30	17.69 \pm 0.02 ^H	98.33 \pm 0.07	21.2 \pm 0.1 ^A
Acarbose	45.65 \pm 1.0	527.5 \pm 0.6 ^A	98.01 \pm 0.25	20.18 \pm 1.48 ^G

Data represent the mean + standard deviation ($n = 4$). Means in a column not sharing the same letter are significantly different at $p < 0.5$ probability according to Tukey tests; ^a Not active (less than 30% inhibition at 400 μM).

In vitro α -amylase inhibition

All the synthesized compounds were assessed for their inhibition of α -amylase. The IC_{50} values obtained were compared to the corresponding value of acarbose (**6**) (Table 1). In general, almost all compounds showed good to weak α -amylase activity with IC_{50} values in the range of 21.2 to 143.1 μM compared to **6** ($IC_{50} = 20.18 \pm 1.48 \mu\text{M}$). Derivatives **2b**, **3b**, **4b**, and **5b** did not show activity at 100 μM . Initially, 7-hydroxyisoflavones **2a** and **2c** showed moderate to weak inhibitory effects. The incorporation of the 3,3-dimethylpyrano group (D-ring) to the isoflavone core displayed almost two-fold greater effect than their parent compounds **2a** and **2c**. Contrarily, derivatives **4a** and **4c** were the less effective compounds, presenting IC_{50} values of 123.2 \pm 0.03 and 143.1 \pm 0.07 μM , respectively. In addition, the presence of the prenyloxy group at C-7 (compound **5a**) resulted in a lower inhibitory effect compared to **2a**. Interestingly, compound **5c** ($IC_{50} = 21.2 \pm 0.1 \mu\text{M}$)

significantly increased the inhibitory effect concerning **2c**. Therefore, the presence of a chlorine atom at C-6 of the isoflavone core significantly enhanced the inhibition, while with the methoxy group did not show any inhibitory activity. These observations suggest that by introducing a linear or cyclized prenyl moiety into the isoflavone core, the inhibitory effect of α -amylase was enhanced.

In summary, the incorporation of a cyclized prenyl moiety (**3a** and **3c**) at the isoflavone scaffold exhibited moderate inhibition of α -glucosidase and α -amylase, while that compounds **4a** and **4c** (without C-ring) displayed higher inhibition of α -glucosidase and lowest inhibition of α -amylase. On the other hand, a greater inhibition of α -glucosidase with a moderate inhibition of α -amylase were found by addition of a prenyloxy moiety (**5a** and **5c**).

Enzymatic kinetic study

In order to explore the mechanism of interaction of **5c** with α -glucosidase and α -amylase, the type of inhibition was evaluated by analyzing Lineweaver-Burk (double reciprocal) plots. The X-axis values represent the reciprocal for the α -glucosidase substrate, *p*-nitrophenyl- α -D-glucopyranoside (*p*-NPG), thus being $1/(p\text{-NPG})$, while for the α -amylase substrate, starch. Thus being $1/(\text{starch})$. The Y-axis value are the reciprocal of the reaction velocity (V_o), thus being $1/V_o$. Given that the plots intersect the Y-axis, the inhibition for α -glucosidase exerted by this compound is carried out in competitive mode (Fig. 2(a) and 2(b)). The K_i value of **5c** is 28.5 μM . The K_i value for this compound is less than K_m , indicating that it has a higher affinity for the enzyme than the substrate used in the assay.

The α -amylase plot made it possible to determine that **5c** is a competitive type of inhibitor. Its K_i value (15.2 μM) indicates that has greater affinity for the enzyme.

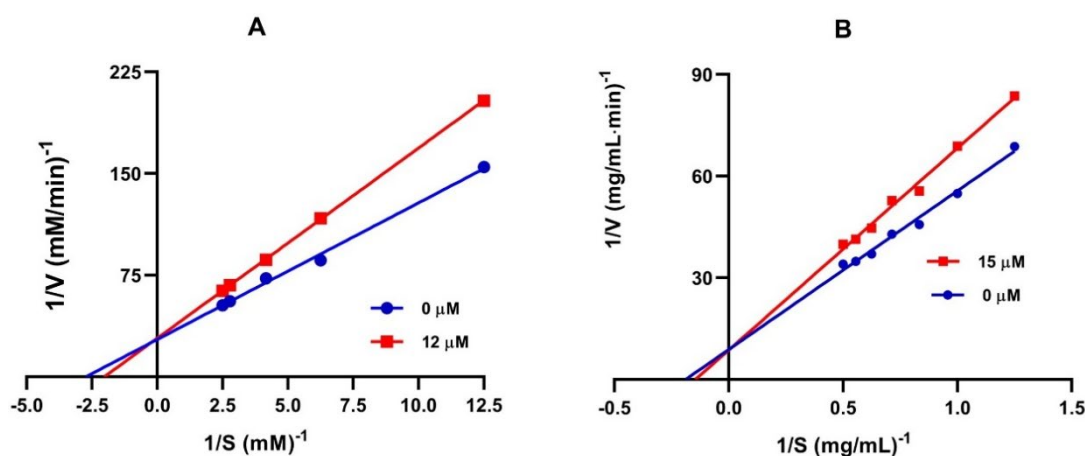


Fig. 2. Lineweaver-Burk plots of **5c** against α -glucosidase (a) and α -amylase (b).

Molecular docking analysis

To explore the binding interactions of the most active compound, molecular docking studies of the isoflavone derivative **5c** and the enzymes isomaltase (α -glucosidase from *S. cerevisiae*) and the human α -amylase were carried out. The results are illustrated in 2D and 3D (Fig. 3(a) and 3(b)), revealing that **5c** recognized some of the key amino acid residues in the catalytic pocket, such as Arg213, Asp215, Glu277, His351, Asp352, and Arg442 [22,34]. Regarding the binding energy of the compound **5c** with the enzymes, has better binding energy values (ΔG) than the reference drug (**6**) (Table 2). The docking studies with α -glucosidase reveal that isoflavone system is involved in hydrophobic interactions of various types: π - π -T-shaped (Tyr158), π -anion (Asp352), π -cation (Arg442), and π -sigma (Tyr172), as well as hydrogen bond interactions with Asp215 and Asp352. The prenyloxy moiety at C-7 of the isoflavone core shows a hydrophobic interaction with Phe314 and

a hydrophilic interaction with Arg315. According to these results, **5c**, interacts with at least two of the acid residues of the catalytic triad, confirming the competitive inhibition of this compound.

Table 2. Docking results of **5c** and acarbose (**6**) at the active site of isomaltase and α -amylase.

Compound	Binding energy ΔG (kcal/mol)	Interacting residues	Polar interactions	Hydrophobic interactions
Isomaltase				
6	-7.78	Asp69, Tyr72, His112, Tyr158, Phe159, Phe178, Arg213, Asp215, Val216, Glu277, Gln279, His280, Phe303, Asp307, Arg315, Tyr316, His351, Asp352, Gln353, Glu411, Arg442, Arg446	C-H \cdots O (Asp69) O-H \cdots O (Asp215) O \cdots H-N (Gln279) O-H \cdots O (Asp307) O \cdots H-N (His351) O-H \cdots O (Glu411) O \cdots H-N (Arg446)	-
5c	8.62	Tyr72, Lys156, Ser157, Tyr158, Phe159, Phe178, Arg213, Asp215, Val216, Glu277, Gln279, His280, Phe303, Leu313, Phe314, Arg315, Tyr316, His351, Asp352, Gln353, Glu411, Asn415, Arg442	C-H \cdots O (Asp215) O \cdots H-N (Arg315) C-H \cdots N (His351) C-H \cdots O (Asp352)	π -sigma-Tyr172 Alkyl-Lys156 π - π T-shaped-Tyr158 π -alkyl-Phe314, Arg315, Tyr316 π -anion-Asp352 π -cation-Arg442
α-Amylase				
6	-2.92	Asp197, Glu233, Asp300, His305	O-H \cdots O (Asp197) O-H \cdots O (Glu233) C-H \cdots O (Glu233) O-H \cdots O (Asp300) C-H \cdots O (Asp300) O \cdots H-N (His305)	-
5c	-8.25	Trp58, Trp59, Tyr62, Gln63, Gly104, Val107, Thr163, Leu165, Arg195, Asp197, Glu233, His299, Asp300, His305	-	π -alkyl-Trp59 π - π stacked-Trp59, Tyr62 π -sigma-Tyr62 Alkyl-Val107, Leu165

For α -amylase, compound **5c** exhibiting interactions with some amino acid residues at the site binding pocket of the enzyme, including Trp58, Trp59, Tyr62, Leu165, Asp197, Glu233, and Asp300 [33]. Analysis of

Table 3. Prediction of the lead-likeness and ADMET of compounds **3a**, **4a**, **5a**, **5c**, and acarbose.

Druglikeness/ ADMET ^a	Compound				
	3a	4a	5a	5c	Acarbose
Rule of five ^b	Suitable	Suitable	Suitable	Suitable	Violated
Caco2	39.0976	29.4715	41.3766	53.5303	9.44448
HIA	97.520337	95.737762	97.520337	97.658677	0.000000
BBB	0.0385324	0.342734	0.0776034	0.17198	0.0271005
Skin permeability	-2.5087	-2.03321	-2.62531	-2.6785	-5.17615
Ames test	Mutagen	Non-mutagen	Mutagen	Mutagen	Non-mutagen
Carcino mouse	Negative	Negative	Negative	Negative	Positive
Carcino rat	Positive	Negative	Positive	Negative	Negative
hERG inhibition	Medium risk	Medium risk	Medium risk	Medium risk	Ambiguous

^aThe recommended ranges for Caco2: <25 poor, >500 greater, HIA: >80% is high <25% is poor, BBB = -3.0 to 1.2, and Skin Permeability = -8.0 to -1.

^bMW molecular weight (<500 g/mol), Log P octanol/water partition coefficient (<5), Log S aqueous solubility, PSA topological polar surface area, HA hydrogen bond acceptor (<10), HD hydrogen bond donor (<5).

Conclusions

Prenylated isoflavones **3a-c** and **5a-c** were synthesized and their α -glucosidase and α -amylase inhibitory activities were evaluated. Compounds **5a** and **5c** showed higher α -glucosidase activities and moderate α -amylase activities than standard drug acarbose (**6**). This suggests that bearing a prenyloxy moiety favors the inhibitory effect against α -glucosidase in comparison to α -amylase. Enzymatic kinetics showed that **5c** is a competitive inhibitor for both α -glucosidase and α -amylase enzymes. Docking studies showed that the hydrophobic effect of the prenyloxy moiety at the C-7 position of the isoflavone backbone favors the interaction with both α -glucosidase and α -amylase active sites. Finally, prediction of the lead-likeness and ADMET studies suggest that compounds **5a** and **5c** are candidate for development of dual inhibitors on carbohydrate-hydrolyzing enzymes.

Acknowledgements

This study was supported by SIP/IPN (SIP20221403, 20231326) and CONACyT (Grants CF-20232-I-2072). BHG gratefully to CONACyT and SIP/IPN (BEIFI) for awarding scholarships. This paper is dedicated to Dr. Joaquín Tamariz Mascarúa with admiration for his academic career in the field of chemistry of natural products.

References

1. World Health Organization. [Diabetes \(who.int\)](https://www.who.int), accessed in February 2023.
2. Proenca, C.; Ribeiro, D.; Freitas, M.; Fernandes, E. *Crit. Rev. Food Sci. Nut.* **2022**, *62*, 3137-3207. DOI: <https://doi.org/10.1080/10408398.2020.1862755>.

3. Upadhyay, J.; Polyzos, S. A.; Perakakis, N.; Thakkar, B.; Paschou, S. A.; Katsiki, N.; Underwood, P.; Park, K.-H.; Seufert, J.; Kang, E. S.; Sternthal, E.; karagiannis, A.; Mantzoros, C. S. *Metabolism*. **2018**, *78*, 13-42. DOI: <https://doi.org/10.1016/j.metabol.2017.08.10>
4. Jo, Y. H.; Lee, S.; Yeon, S. W.; Ryu, S. H.; Turk, A.; Hwang, B. Y.; Han, Y. K.; Lee, K. Y.; Lee, M. K. *Phytochemistry*. **2022**, *194*, 113016. DOI: <https://doi.org/10.1016/j.phytochem.2021.113016>.
5. Ahmed, Q. U.; Ali, A. H. M.; Mukhtar, S.; Alsharif, M. A.; Parveen, H.; Sabere, A. S. M.; Nawi, M. S. M.; Khatib, A.; Siddiqui, M. J.; Umar, A.; Alhassan, A. M. *Molecules*. **2020**, *25*, 5491. DOI: <https://doi.org/10.3390/molecules25235491>.
6. Hu, W.; Wu, X.; Tang, J.; Zhao, G.; Xiao, N.; Zhang, L.; Li, S. *J. Cell Mol. Med*. **2019**, *23*, 3505-3511. DOI: <https://doi.org/10.1111/jcmm.14248>.
7. Wei, Z.; Yang, Y.; Xie, C.; Li, C.; Wang, G.; Ma, L.; Xiang, M.; Sun, J.; Wei, Y.; Chen, L. *Fitoterapia*. **2014**, *97*, 172-183. DOI: <https://doi.org/10.1016/j.fitote.2014.06.002>.
8. Ndemangou, B.; Sielinou, V. T.; Vardamides, J. C.; Ali, M. S.; Lateef, M.; Iqbal, L.; Afza, N.; Nkengfack, E. *J. Enzyme Inhib. Med. Chem.* **2013**, *28*, 1156-1161. DOI: <https://doi.org/10.3109/14756366.2012.719025>.
9. Cardullo, N.; Muccilli, V.; Pulvirenti, L.; Tringali, C. *J. Nat. Prod.* **2021**, *84*, 654-665. DOI: <https://dx.doi.org/10.1021/acs.jnatprod.0c01387>.
10. Demir, Y.; Durmaz, L.; Taslimi, P.; Gulçin, I. *Biotechnol. Appl. Biochem.* **2019**, 781-786. DOI: <https://doi.org/10.1002/bab.1781>.
11. Sun, H.; Li, Y.; Zhang, X.; Lei, Y.; Ding, W.; Zhao, X.; Wang, H.; Song, X.; Yao, Q.; Zhang, Y.; Ma, Y.; Wang, R.; Zhu, T.; Yu, P. *Bioorg. Med. Chem. Lett.* **2015**, *25*, 4567-4571. DOI: <https://doi.org/10.1016/j.bmcl.2015.08.059>.
12. Wu, C.; Tu, Y.-B.; Li, Z.; Li, Y.-F. *Bioorg. Chem.* **2019**, *88*, 102949. DOI: <https://doi.org/10.1016/j.bioorg.2019.102949>.
13. Polbuppha, I.; Suthiphasilp, V.; Maneerat, T.; Charoensup, R.; Limtharakul, T.; Cheenpracha, S.; Pyne, S. G.; Laphookhieo, S. *Phytochemistry*. **2021**, *187*, 112773. DOI: <https://doi.org/10.1016/j.phytochem.2021.112773>.
14. Jo, Y. H.; Lee, S.; Yeon, S. W.; Turk, A.; Lee, J. H.; Hong, S. M.; Han, Y. K.; Lee, K. Y.; Hwang, B. Y.; Kim, S. Y.; Lee, M. K. *Bioorg. Chem.* **2021**, *114*, 105098. DOI: <https://doi.org/10.1016/j.bioorg.2021.105098>.
15. Lv, H.-W.; Wang, Q.-L.; Luo, M.; Zhu, M.-D.; Lian, H.-M.; Li, W.-J.; Cai, H.; Zhou, Z.-B.; Wang, H.; Tong, S.-Q.; Li, X.-N. *Arch. Pharm. Res.* **2023**, *46*, 207-272. DOI: <http://doi.org/10.1007/s12272-023-01443-4>.
16. Wen, R.; Lv, H.; Jiang, Y.; Tu, P. *Bioorg. Med. Chem. Lett.* **2018**, *28*, 1050-1055. DOI: <https://doi.org/10.1016/j.bmcl.2018.02.026>.
17. Hikita, K.; Salgusa, S.; Takeuchi, Y.; Matsuyama, H.; Nagai, R.; Kato, K.; Murata, T.; Tanaka, H.; Wagh, Y. S.; Asao, N.; Kaneda, N. *Bioorg. Med. Chem.* **2020**, *28*, 115490. DOI: <https://doi.org/10.1016/j.bmc.2020.115490>.
18. Buyinza, D.; Yang, L. J.; Derese, S.; Ndakala, A.; Coghi, P.; Heydenreich, M.; Wong, V. K. W.; Moller, H. M.; Yenesew, A. *Nat. Prod. Res.* **2021**, *35*, 2744-2747. DOI: <https://doi.org/10.1080/14786419.2019.1660335>.
19. Chang, S. K.; Jiang, Y.; Yang, B. *Trends Food Sci. Technol.* **2021**, *108*, 197-213. DOI: <https://doi.org/10.1016/j.tifs.2020.12.022>.
20. Dirir, A.M.; Daou, M.; Yousef, A.; Yousef, L. F. *Phytochem Rev.* **2022**, *21*, 1049-1079. DOI: <https://doi.org/10.1007/s11101-021-09773-1>.
21. Park, M.-H.; Ju, J.-W.; Park, M.-J.; Han, J.-S. *Eur. J. Pharmacol.* **2013**, *712*, 48-52. DOI: <https://doi.org/10.1016/j.ejphar.2013.04.047>.
22. Aguila-Muñoz, D. G.; Cervantes-Espinoza, E.; Escalante, C. H.; Gutiérrez, R. U.; Cruz-López, M. C.; Jiménez-Montejo, F. E.; Villa-Ruano, N.; Gómez-García, O.; Tamariz, J.; Mendieta-Moctezuma, A. *Med. Chem. Res.* **2022**, *31*, 1298-1312. DOI: <https://doi.org/10.1007/s00044-022-02910-1>.

23. Yenesew, A.; Midiwo, J. O.; Waterman, P. G. *J. Nat. Prod.* **1997**, 60, 806-807. DOI: <https://doi.org/10.1021/np9605955>.
24. Yao, H.; Xu, F.; Wang, G.; Xie, S.; Li, W.; Yao, H.; Ma, C.; Zhu, Z.; Xu, J.; Xu, S. *Eur. J. Med. Chem.* **2019**, 167, 485-498. DOI: <https://doi.org/10.1016/j.ejmech.2019.02.014>.
25. Do, L. T. M.; Huynh, T. T. N.; Sichaem, J. *Molecules.* **2022**, 27, 4624. DOI: <https://doi.org/10.3390/molecules27144624>.
26. Chokki, M.; Cudalbeanu, M.; Zongo, C.; Dah-Nouvlessounon, D.; Ghinea, I. O.; Furdui, B.; Raclea, A.; Savadogo, A.; Baba-Moussa, L.; Avamescu, S. M.; Dinica, F. M.; Baba-Moussa, F. *Foods.* **2020**, 9, 434. DOI: <https://doi.org/10.3390/foods9040434>.
27. Morris, G. M.; Huey, R.; Lindstrom, W.; Sanner, M. F.; Belew, R. K.; Goodsell, D. S.; Olson, A. J. *J. Comput. Chem.* **2009**, 30, 2785-2791. DOI: <https://doi.org/10.1002/jcc.21256>.
28. Bioinformatics and Molecular Design Research Center. Seoul, South Korea, 2004. PreADMET Program. Available from: <https://preadmet.webservice.bmdrc.org>, accessed in June 2023.
29. BIOVIA, Dassault Systèmes, Discovery Studio Visualizer v20.1.0.19295, San Diego: Dassault Systèmes (2020).
30. Choudhury, M. K.; Shiferaw, Y.; Sur, K. R.; Dey, D.; Debnathan, S.; Ghosh, S.; Ray, R.; Hazra, B. *J. Coast. Life Med.* **2016**, 4, 556-563. DOI: <https://doi.org/10.12980/jclm.4.2016J6-84>.
31. Deyou, T.; Marco, M.; Heydenreich, M.; Pan, F.; Gruhonjic, A.; Fitzpatrick, P. A.; Koch, A.; Derese, S.; Pelletier, J.; Rissanen, K.; Yenesew, A.; Erdélyi, M. *J. Nat. Prod.* **2017**, 2060-2066. DOI: <https://doi.org/10.1021/acs.jnatprod.7b00255>.
32. Na, Z.; Fan, Q-F.; Song, Q-S.; Hu, H-B. *Phytochem. Lett.* **2017**, 19, 215-219. DOI: <https://doi.org/10.1016/j.phytol.2017.02.002>.
33. Do, L. T. M.; Huynh, T. T. N.; Tran, Q. H. N.; Nguyen, H. T. M.; Nguyen, T. T. A.; Nguyen, T. T. N.; Nguyen, P. H. H.; Sichaem, J. *Nat. Prod. Res.* **2022**, 1-7. DOI: <https://doi.org/10.1080/14786419.2022.2110092>.
34. Aguila-Muñoz, D. G.; Vázquez-Lira, G.; Sarmiento-Tlale, E.; Cruz-López, M. C.; Jiménez-Montejo, F. E.; López y López, V. E.; Escalante, C. H.; Andrade-Pavón, D.; Gómez-García, O.; Tamariz, J.; Mendieta-Moctezuma, A. *Molecules.* **2023**, 28, 4180. DOI: <https://doi.org/10.3390/molecules28104180>.

***In Vitro* and *In Silico* Studies of *Bis-furyl-pyrrolo*[3,4-*b*]pyridin-5-ones on Dengue Virus**

Ivette Morales-Salazar¹, Carlos E. Garduño-Albino¹, Flora P. Montes-Enríquez¹, Atilano Gutiérrez-Carrillo¹, Yareli Rojas-Aguirre², Nancy Viridiana Estrada-Toledo³, Jorge Sandoval-Basilio⁴, Sofia Lizeth Alcaraz-Estrada^{5*}, Erik Díaz-Cervantes^{6*}, Eduardo González-Zamora^{1*}, Alejandro Islas-Jácome^{1*}

¹Departamento de Química, Universidad Autónoma Metropolitana-Iztapalapa, Av. Ferrocarril San Rafael Atlixco 186, Col. Leyes de Reforma 1A Sección, Iztapalapa, Ciudad de México, C.P. 09310, México.

²Departamento de Polímeros, Instituto de Investigaciones en Materiales, Universidad Nacional Autónoma de México, Circuito Exterior S/N, Ciudad Universitaria, Coyoacán, Ciudad de México, C.P. 04510, México.

³Coordinación de Comités de Evaluación en Salud, Centro de Investigación Clínica, Health Pharma Professional Research S.A. de C.V., Ciudad de México, C.P. 03100, México.

⁴Laboratorio de Biología Molecular, Universidad Hipócrates, Andrés de Urdaneta 360, Hornos, Acapulco de Juárez, Guerrero, C.P. 39355, México.

⁵División de Medicina Genómica, Centro Médico Nacional 20 de Noviembre, ISSSTE, Félix Cuevas 540, Col. Del Valle Sur, Benito Juárez, Ciudad de México, C.P. 03100, México.

⁶Departamento de Alimentos, Centro Interdisciplinario del Noreste, Universidad de Guanajuato, Tierra Blanca, Guanajuato, C.P. 37975, México.

***Corresponding author:** Sofia Lizeth Alcaraz-Estrada, email: sofializeth@gmail.com; Erik Díaz-Cervantes, email: e.diaz@ugto.mx; Eduardo González-Zamora, email: egz@xanum.uam.mx; Alejandro Islas-Jácome, email: aij@xanum.uam.mx

Received July 13th, 2023; Accepted November 17th, 2023.

DOI: <http://dx.doi.org/10.29356/jmcs.v68i1.2103>

Abstract. A series of six *bis-furyl-pyrrolo*[3,4-*b*]pyridin-5-ones synthesized *via* an Ugi-Zhu reaction coupled to a cascade process [*aza* Diels-Alder cycloaddition/*N*-acylation/aromatization] were evaluated *in vitro* against Dengue virus serotype 4 infection, and the Dengue virus replicon system encoding a *Renilla* luciferase gene reporter. Also, *in silico* studies on the non-structural protein 3 (NS3), a flavivirus protease comprising an attractive target for development of therapeutic antivirals bound to non-structural protein 2B (NS3-NS2B) were performed. The *in vitro* results showed that compounds **1a** and **1b** reduced the expression of *Renilla* luciferase in 44.2 and 31.6%, respectively. Additionally, the same compounds decreased viral load, thus revealing their potential activity against Dengue virus serotype 4. From *in silico* simulations, it was developed a NS3-NS2B model, which was used as a target for the studied molecules. Computational results agree with experimental data, showing that **1a** is the best ligand. Finally, a pharmacophoric model was computed for NS3-NS2B, which shows that the ligands need two hydrophobic and one hydrophilic fragment. Such results suggest that two out of the six synthesized *bis-furyl-pyrrolo*[3,4-*b*]pyridin-5-ones derivatives presents potential antiviral activity against Dengue virus *in vitro*.

Keywords: Dengue virus replicon; dengue virus serotype 4; *in vitro* assays; *in silico* simulations; docking; pyrrolo[3,4-*b*]pyridin-5-ones; Ugi-Zhu reaction.

Resumen. Una serie de seis *bis-furil-pirrol*[3,4-*b*]piridin-5-onas sintetizadas *via* una reacción Ugi-Zhu acoplada a un proceso en cascada [cicloaddición *aza* Diels-Alder/*N*-acilación/aromatización] fueron evaluadas *in vitro* contra

infección por el serotipo 4 del virus del dengue y el sistema de replicón del virus del Dengue que codifica un gen reportero de la luciferasa de la *Renilla*. Además, se realizaron estudios *in silico* sobre la proteína no estructural 3 (NS3), una proteasa de flavivirus que comprende un blanco atractivo para el desarrollo de antivirales terapéuticos unidos a la proteína no estructural 2B (NS3-NS2B). Los estudios *in vitro* revelaron que los compuestos **1a** y **1b** reducen la expresión de *Renilla* luciferasa en un 44.2 y 31.6%, respectivamente. Adicionalmente, estos compuestos redujeron la carga viral, revelando así su actividad potencial contra el virus del Dengue serotipo 4. Derivado de las simulaciones *in silico*, se obtuvo un modelo homólogo para NS3-NS2B, el cual fue considerado como blanco de las moléculas estudiadas. Los resultados computacionales correlacionan con los experimentales, mostrando que **1a** es el mejor ligando. Finalmente, se generó un modelo farmacofórico para NS3-NS2B, el cual muestra que los ligandos necesitan dos fragmentos hidrofóbicos y uno hidrofílico. Estos resultados demuestran que dos de los seis compuestos que se estudiaron presentan actividad antiviral *in vitro*.

Palabras clave: Replicón del virus del dengue; serotipo 4 del virus del dengue; ensayos *in vitro*; simulaciones *in silico*; docking; pirrolo[3,4-*b*]piridin-5-onas; reacción de Ugi-Zhu.

Introduction

Dengue virus (DENV) belongs to the genus *Flavivirus* and the family of *Flaviviridae* [1]. DENV comprises four serotypes, namely DENV1-4, that are genetically similar but antigenically distinct. However, all serotypes are infectious and pathogenic, and their circulation patterns fluctuate based on both geographical location and time [2]. DENV infection is a prevalent mosquito-borne disease occurring in tropical and subtropical regions. Globally, DENV infection cases range from 100 to 400 million and, 25,000 deaths [3], ranked second only for SARS-CoV-2, the causative agent of COVID-19 [4]. DENV infection manifests in various clinical conditions, including Dengue fever, Dengue hemorrhagic fever, and the highly dangerous Dengue shock syndrome [5,6]. In 2020, the vaccine Dengvaxia[®] (CYD-TDV) against DENV received approval. Developed by Sanofi-Pasteur, the vaccine aimed to alleviate the impact of DENV infection and its associated complications. As per the World Health Organization (WHO), Dengvaxia[®] demonstrated a reduction in morbidity of at least 25%, and its effectiveness and safety are influenced by previous exposure to the virus [7]. Given the suboptimal nature of current preventive measures and treatments for DENV, there is a genuine need to explore novel therapeutic alternatives to mitigate and potentially eradicate this disease.

Throughout the various stages of the DENV life cycle, several structural (S) and non-structural (NS) proteins play critical roles. The NS proteins found in DENV, including NS1, NS2A, NS2B, NS3, NS4A, NS4B, and NS5, are essential for viral genome replication, translation, viral polyprotein processing, encapsidation, and proper folding of viral proteins [2]. Among these NS proteins, those of utmost relevance due to their catalytic role are NS3, coupled with NS2B, as they are responsible for cleaving the polyprotein, a critical step in the DENV life cycle [8]. Consequently, NS3-NS2B emerges as an attractive target for the development of new drugs.

Subgenomic replicon systems are useful for identifying potential therapeutic molecules through efficient and high-throughput testing without extraneous and labor-intensive techniques [9,10]. In these systems, generally the genes that codify for the structural proteins of the virus are removed, preventing the generation of viral particles. Additionally, a reporter gene is inserted in the viral genome, enabling the monitoring of the replication process. The replicons follow the natural replicative cycle of the virus. Within the *Flavivirus* family, once inside the cell, the viral genome is translated into a polyprotein, which undergoes processing by cellular proteases and viral proteases. The proteolytic processing generates individual and functional viral proteins that facilitate the replication of the viral genome. Subsequently, copies of the viral genome initiate a new cycle [11] (Fig. 1). The interruption of any step of the cycle will be reflected in the reduction of the expression of the reporter gene. Replicons have been employed in the study of various *Flaviviruses* such as Yellow Fever [12,13], Hepatitis C Virus [14], West Nile [15,16], DENV [17,5] and Zika [18], including the assessment of the antiviral activity of a diversity of compounds, underscoring the value of these systems.

In a previous work [19], we reported the synthesis of a series of six new *bis-furyl-pyrrolo[3,4-*b*]pyridin-5-ones*, which exhibited moderate activity against human SARS-CoV-2. By evaluating the efficacy of these compounds in the Dengue replicon system and DENV4 infection, we aim to investigate their potential as antiviral agents against DENV. This research carries significance as it offers an opportunity to explore the antiviral effectiveness of the initially investigated polyheterocycles against SARS-CoV-2. Understanding their effectiveness in inhibiting the replication of the DENV could provide valuable insights into the design of future therapeutics targeting this global health concern.

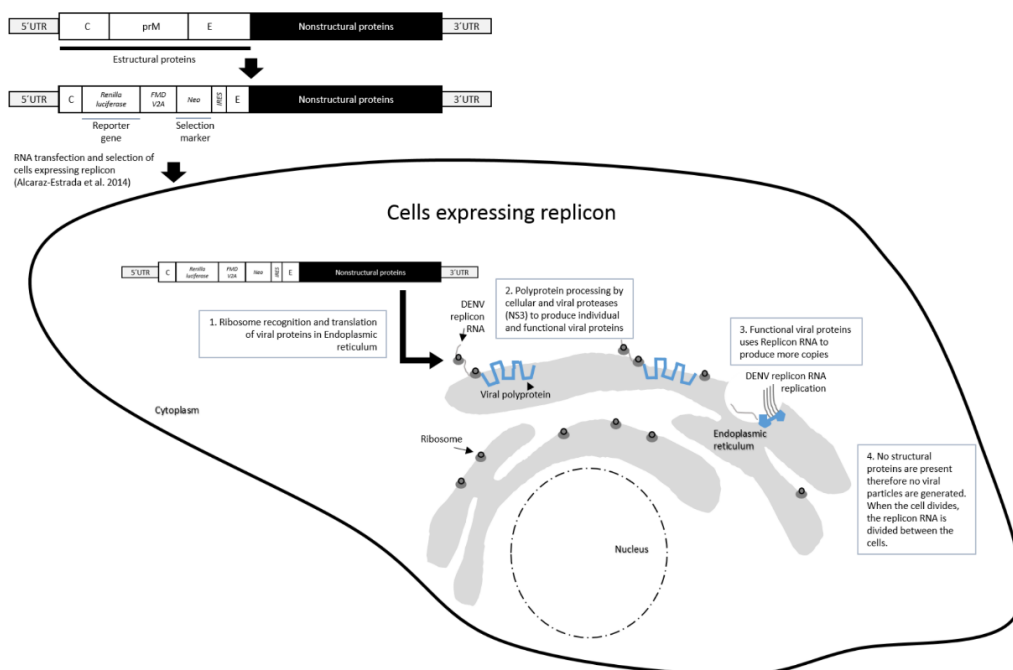


Fig. 1. Schematic representation of the replicon model. The DENV viral genome was modified to remove most of the structural viral proteins which were then replaced with the *Renilla* luciferase reporter gene and a selection gene. The RNA is transfected and once it reaches the cytoplasm, it is immediately recognized by ribosomes that generate the nascent viral polyprotein, which will be further processed by cellular proteases and by the viral protease (NS3) to produce individual and functional viral proteins. These proteins, in turn, will drive the replication of the viral genome.

Experimental

Materials

Synthesis

All starting reagents and solvents were used as received (without further purification, distillation, nor dehydration).

Cell line

Vero (African green monkey kidney) CCL-81 cells expressing DENV serotype 4 replicons were used [5]. Vero cells were cultured in Dulbecco's Modified Eagle's Medium high glucose (DMEM) (Gibco™) supplemented with 10 % fetal bovine serum (FBS) (Gibco™), glutamine 2 mM (Sigma-Aldrich-Merck) and G418 300 µg/mL (Gibco™) and placed in 5 % CO₂ atmosphere at 37 °C.

Instrumentation

Microwave-assisted reactions were performed in closed-vessel mode on a CEM Discover SP MW-reactor. Reaction progress was monitored by thin-layer chromatography (TLC) and the spots were visualized under ultraviolet (UV) light (254 or 365 nm). Flash columns packed with silica-gel 60, 230–400 mesh particle size and glass preparative plates (20 × 20 cm) coated with silica-gel 60 doped with UV indicator (F₂₅₄) were used to purify the products.

General method for the preparation of the assayed *bis*-furyl-pyrrolo[3,4-*b*]pyridin-5-ones **1a–f**

The corresponding *bis*-furyl-pyrrolo[3,4-*b*]pyridin-5-ones **1a–f** were synthesized using the methodology reported by us [19]. Thus, in a sealed CEM Discover microwave reaction tube (10 mL) containing a stirring bar, corresponding aldehydes (1.00 equiv.) and amines (0.10 mmol, 1.00 equiv.) were diluted in dry toluene (1.00 mL). These mixtures were stirred and heated using microwave irradiation (65 °C, 100 W) for 5 minutes. Then, ytterbium(III) triflate (0.03 equiv.) was added and heated using microwave irradiation (65 °C, 100 W) for 5 minutes. The corresponding isocyanides (1.20 equiv.) were added and again heated using microwave irradiation (70 °C, 150 W) for 15 minutes. Finally, maleic anhydride (1.40 equiv.) was added, and the new reaction mixture was stirred and heated using microwave irradiation (80 °C, 150 W) for 15 minutes. At the end of the reaction time, the solvent was removed to dryness under vacuum. Then, extractions of the crude were carried out using dichloromethane (3 × 25 mL) to collect the organic phases, which were washed with brine (3 × 25 mL), dried in anhydrous Na₂SO₄, filtered, and concentrated to dryness. The new crude was purified by column chromatography using as stationary phase silica-gel followed by preparative TLC (20 x 20 cm) plates. The solvent mixtures of *n*-hexane (Hex) and ethyl acetate (EtOAc) in 1:1 or 1:2 (*v/v*) proportions were employed as mobile phase in both chromatography procedures to isolate the corresponding *bis*-furyl-pyrrolo[3,4-*b*]pyridin-5-ones **1a–f** in 45 to 82 % overall yields (Fig. 2).

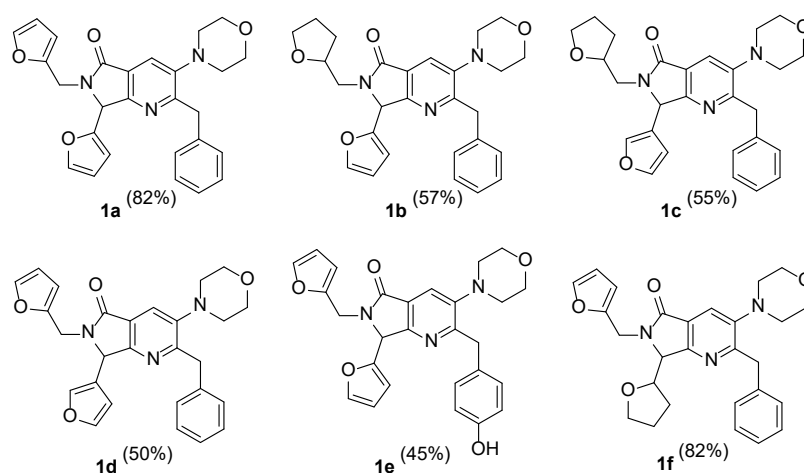


Fig. 2. Series of *bis*-furyl-pyrrolo[3,4-*b*]pyridin-5-ones **1a–f** synthesized via MCRs and *in vitro* assayed against DENV.

In vitro assays

Vero CCL-81 cell viability

The effect of the six *bis*-furyl-pyrrolo[3,4-*b*]pyridin-5-ones **1a–f** on Vero CCL-81 cell viability was determined as previously described [19]. Briefly, 24 h before the experiment 25000 cells/per well were placed in a 96-well plate using DMEM supplemented with 8% of FBS and glutamine in an incubator under 5% CO₂ atmosphere at 37 °C. The compounds were added at concentrations of 0.1, 1, 10, 100 μM in a final volume of

100 μ L of medium. After 48 h, media was removed and, 100 μ L of crystal violet (0.1% crystal violet, 3.7% formaldehyde) were added. After 1 h at room temperature, plates were washed and 100 μ L of 10% of acetic acid was added release to the dye. Plates were placed in an absorbance reader at a wavelength of 590 nm (Sunrise, TECAN) and cell viability was determined with respect to the vehicle control (DMSO). The experiments were performed three times in duplicates ($n = 6$). The vehicle refers to cells that were cultured in DMEM medium plus 0.5 % DMSO, which was the DMSO volume used in the diluent to solubilize the compounds.

Antiviral assay in DENV4 replicon system

The DENV4 replicon reporter assay was performed as previously described [5]. Briefly, 24 h before the assay, 25000 cell/per well of Vero cells were seeded in a 96-well plate. 10 μ M of the compounds were added and after 48 h, the cells were lysed and *Renilla* luciferase was detected using *Renilla* Luciferase Assay System (Promega) and then measured using Luciferase reader (GloMax 20/20 Luminometer, Promega). Percent of expression was calculated normalizing the luciferase signal with the cells treated with vehicle (DMSO) (100 % of expression). Graph and statistical analysis were calculated using in GraphPad Prism version 9.5.1 (San Diego, CA, USA). p-Value was calculated using ordinary one-way-ANOVA test.

Antiviral assay Inhibition of DENV4 infection

For the infection inhibition assays of the Dengue virus serotype 2 and 4, 25000 Vero cells were seeded 24 h before infection. Infection was carried out at a multiplicity of infection (MOI) of 0.1 at 37 °C for 1 h. The addition of the compounds is as described above. Carnosine (L-CAR) was used as a positive control for replication inhibition since its direct interaction with the viral protein NS3-NS2B of DENV2 has been reported [20]. 24 h later, RNA was extracted from the collected supernatant using QuickExtract RNA Extraction Kit (Lucigen) following the supplier's recommendations. Briefly, the medium was removed from the cells, washed with 1x PBS, 50 μ L cold Quick Extract RNA Extraction Solution was added, and the lysate was transferred to a 1.5 mL, vortexed for 1 min and heated for 2 min at 65 °C. Afterwards, 5.5 μ L of DNase Buffer 1, 1.25 μ L of RiboGuard RNase Inhibitor, 2.5 μ L of RNasefree DNase were added and heated for 15 min at 37 °C. Finally, 2 μ L of Stop Solution was added and incubated for 10 min at 65 °C. Subsequently, the RT-qPCR was carried out in CFX96 Touch Real Time PCR Detection System (Bio-Rad) using OneStep RT-PCR Kit (Qiagen) to determine viral load following the supplier's recommendations. Briefly, 10 μ L of 5x QIAGEN OneStep RT-PCR Buffer, 2 μ L of dNTP Mix, 0.6 μ M of forward primer 5'-TTGAGTAAACYRTGCTGCCTGTAGCTC-3' and 0.6 μ M of reversed primer 5'-GAGACAGCAGGATCTCTGGTCTYTC-3'[21], 2 μ L of OneStep RT-PCR Enzyme Mix, 50 μ g of RNA and 1 μ L of Eva Green (Biotium). The RT-qPCR conditions were 50 °C for 30 min and 95 °C for 15 min, followed by 40 cycles of 94 °C for 30 sec, 55 °C for 30 sec and 72°C for 30 sec. Fluorescence quantification was performed during the extension step. The viral load of the dengue virus was obtained with the $-2^{\Delta\Delta CT}$ method [22] and analyzed by two-way Anova in the Graph Pad V5 software using, p-values ≤ 0.05 w. The decrement of the viral load in each assay was compared to the vehicle, which was DMSO and was used as the negative control.

In silico studies

The *in silico* analyzes were carried out specifically on the protein used in the *in vitro* assays. A homology model of the DENV4 replicon has been computed using the Swiss-model server [23] and their sequence of amino acids, and so called NS3-t4. Also, it was considered the NS3-NS2B protein with their cofactor (NS2b) for the serotype-4 (PDB code: 2FOM, NS3/NS2B-t4). On the other hand, the *bis*-furyl-pyrrolo[3,4-*b*]pyridin-5-ones **1a-f**, as well as a control molecule (carnosine) [20] were modeled using the Avogadro package [24] and optimized through the generalized gradient approximation functional development by Perdew, Burke, and Erzerhof (PBE) [25] in the Gaussian 09 software [26].

The molecular docking was carried out using the Moldock [27] scoring function implemented in the Molegro Virtual Docker (MVD) package [28]. Finally, with ZincPharmer software [29] a pharmacophoric model was computed.

Results and discussion

In vitro assays

The compounds under investigation were the six *bis*-furyl-pyrrolo[3,4-*b*]pyridin-5-ones **1a-f** that have previously shown moderate activity against the human SARS-CoV-2 [19]. By evaluating the efficacy of these compounds in the Dengue replicon system and using the viral particle, their potential as antiviral agents against DENV 4 were herein assessed.

The Vero cell line is considered as the standard model cell in dengue studies due to its infectability in response to dengue infection. This cell line is derived from African green monkey (*Chlorocebus sabaues*) renal are classified into four major cell lineages: Vero JCRB0111, Vero CCL-81, Vero 76, and Vero E6. Each one of this cell lineages display specific features making them suitable for the propagation of certain viruses. For example, Vero CCL-81 is capable of propagating the Japanese encephalitis virus under prolonged culture conditions [12], West Nile Virus [30], Zika virus and DENV2 [31], while Vero E6 is used to propagate SARS-CoV-2 more efficiently [32]. The cell line expression in DENV replicon and infection used in this study was Vero CCL-81. As each subline has phenotypic and genetic differences [33]. It was relevant to determine the effect of the compounds on the Vero CCL-81 viability, despite their effect on Vero E6 viability was already investigated [19].

We observed a viability greater than 80% when Vero cells, expressing the DENV4 replicon, were exposed to the series of six compounds at the concentration of 10 μM (Fig. 3). At 100 μM , cell viability was reduced significantly, with the exception of compound **1f**. To note, these results align with the previous findings reported [19].

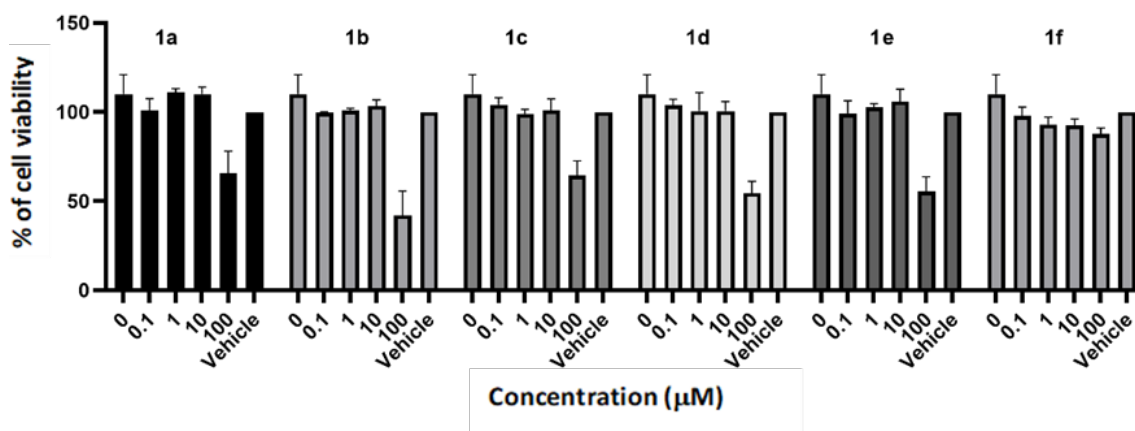


Fig. 3. Vero CCL-81 cell viability assays. The experiment was performed two independent times in triplicate and the bars depict the standard deviation of the mean ($n = 6$).

Antiviral activity on the Dengue virus replicon system

The antiviral activity on the DENV4 replicon of heterocyclic compounds was studied at 10 μM as this concentration did not affect the viability of Vero CCL-81 cells. Fig. 4 expresses the percentage of luciferase activity in y-axis that is a direct measurement of the viral genome translation and replication. Compounds **1c-f** did not reduce the expression of *Renilla* luciferase. On the other hand, compounds **1a** and **1b** showed a considerable reduction of the expression of the reporter gene, 44.2 % and 31.6 % respectively.

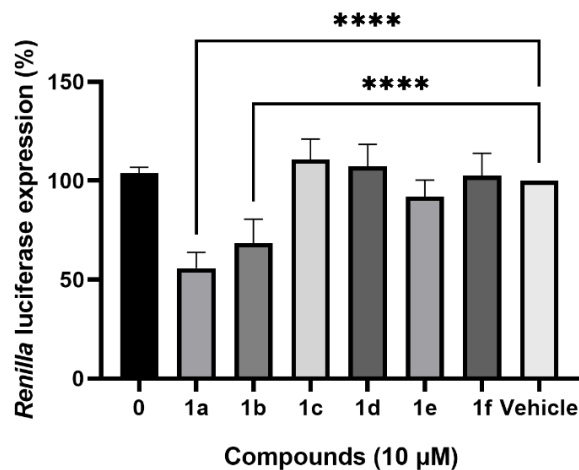


Fig. 4. Inhibition of DENV serotype 4 replicon replication and translation in Vero CCL-81 cells. The experiment was performed two independent times in triplicate and the bars depict the standard deviation of the mean ($n = 6$). **** p -Value = < 0.0001 using ordinary one-way-ANOVA test.

Antiviral activity on Dengue virus serotype 4

In this regard, DENV2 and DENV4 infection inhibition tests were carried out at 10 μ M of the compounds (Fig. 5). In the case of DENV2, **1a** and **1b** did not reduced viral load, nevertheless with L-CAR we observed a reduction as reported (Figure S1 of Supplementary Materials File). The result obtained was that for DENV2 there is no reduction in viral load measured through RT-qPCR. Whereas that, **1a** y **1b** reduce in the viral load of DENV4 with respect to compounds **1c-1e**, L-CAR and negative control, although this trend was observed, it was not statistically significant (Fig 5).

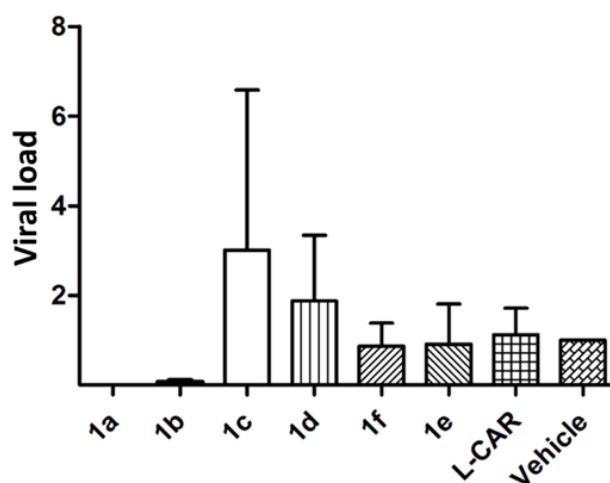


Fig. 5. Inhibition of DENV4 serotype 4 infection in Vero CCL-81 cells. The experiment was performed three independent times in duplicate and the bars depict the standard deviation of the mean ($n = 6$).

The results indicate that compounds **1a** and **1b** have an antiviral effect in the replicon model and DENV4 infection. The specific inhibition observed in **1a** and **1b** could be due to the genome variability between serotypes and particularly for NS3, the conserved regions of the protein are few [34]. The same behavior can be observed for the positive control L-CAR that reduces the viral load specifically for DENV2 in our results but not DENV4.

As **1a** is the one with the highest activity, which may be due to interactions directed by the furane heterocycle in compound **1a**. Differences between compounds **1a** and **1b** are found in the furan and tetrahydrofuran heterocycles that decorates pyrrolo[3,4-*b*]pyridin-5-one core.

This result seems to be in contrast when the series were evaluated against SARS-CoV-2 [19], in which **1a** and **1b** did not affect the viral infection. We must take into account that there are structural differences between the two proteases, where the SARS-CoV-2 protease requires its dimeric form to be active, DENV protease requires a protein cofactor (NS2B) to be active. Hence, the active sites differ, and for this reason, we see a difference between the preference of compounds with inhibitory capacity according to the viral protease [35]. Compounds of a similar nature have been tested against other members of the *Flaviviridae* family *e.g.* Zika virus and have been shown to interact with and affect the viral protease NS3-NS2B of this flavivirus [36]. Therefore, performed an *in silico* study to delve into the possible interactions between **1a** and **1b** and the viral proteases mentioned above.

In silico studies

The first results regarding the docking studies are presented in Fig. 6, which demonstrates that the synthesized molecules are docked into the NS3 and NS3-NS2B DENV4 serotype.

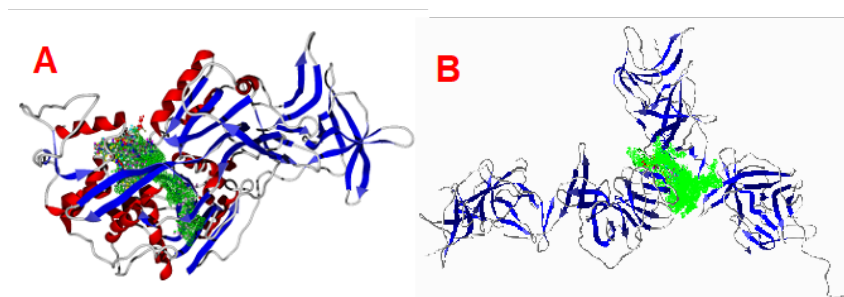


Fig. 6. Studied molecules docked into the (A) modeled NS3 DENV4 serotype-4 surface, (B) the NS3-NS2B DENV4 serotype-4.

Table 1. Ligand efficiency (LE) of the NS3-NS2B DENV4 serotype-4. All the values are in kcal/mol.

Molecule	LE	
	NS3-t4	NS3/NS2B-t4
1a	-4.95	-4.57
1b	-4.68	-4.36
1c	-4.84	-4.33
1d	-4.85	-4.57
1e	-4.90	-4.52
1f	-4.92	-4.30
Carnosine	-6.32	-6.39

Analyzing the results of Table 1, the interactions between the selected ligands and the NS3-t4 and the NS3/NS2B-t4 correlated with the experimental results, considering that the best ligand is **1a**. In this order, the best interactions were between **1a** and NS3-t4, which present -4.95 kcal/mol, compared with the value of NS3/NS2B-t4, -4.57 kcal/mol. In this order, it was decided to analyze the interactions with NS3-t4 with the studied molecules.

The results agree with the experimental data, see Table 2, mainly considering the better interacting molecule **1a**. Highlight that these results were computed using the NS3 free protein, without the possible co-factor, proving that this is a possibility of interaction between **1a-f** compounds with the NS3, which interacts before coupling NS3 with the co-factor.

Table 2. Principal interacting energies between the studied molecules and the NS3 protein. All the values are in kcal/mol.

Ligand	LE	Hbond	Electro	VdW
1a	-4.95	-1.63	-0.67	9.44
1b	-4.68	-3.94	0.09	-37.15
1c	-4.84	-0.76	-1.67	-25.29
1d	-4.85	0.00	-1.30	-43.35
1e	-4.90	-4.05	-1.15	-51.50
1f	-4.92	-1.68	0.47	-47.30
Carnosine	-6.32	-6.70	-0.91	-20.93

*LE is the ligand efficiency (LE = Energy/# heavy atoms). Hbond is the hydrogen bond interaction. Electro is the electrostatic interactions, and VdW is the Van der Waals interactions.

Regarding the kind of interactions between **1a** and NS3-t4, Fig. 7 shows the key interactions. As well as Fig. 8 shows the interactions between NS3 protein and carnosine. Carnosine presents better interactions than **1a** because the last presents few steric interactions, see Fig. 7 and 8. At the same time, Carnosine presents more hydrogen bond interactions than **1a**.

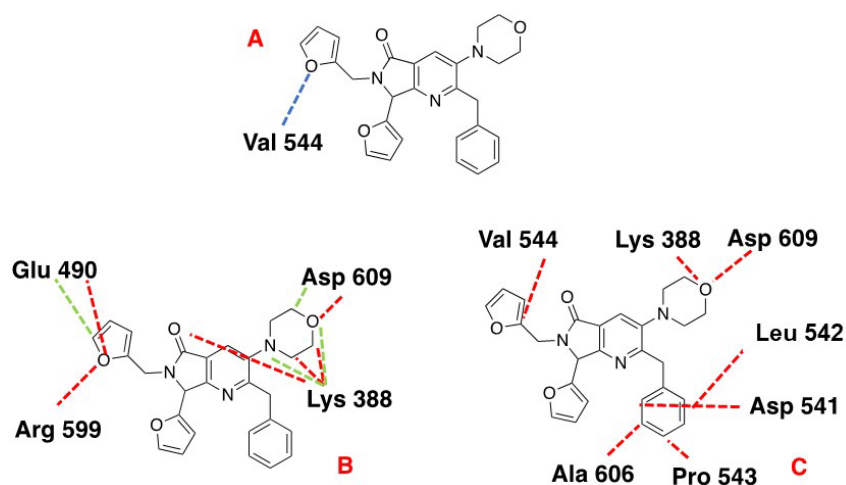


Fig. 7. (A) Hydrogen bond, (B) Electrostatic, and (C) Steric interactions between NS3 and **1a**. Blue lines depict the Hydrogen bond interactions, and Red and green dotted lines show the repulsive and attractive interaction, respectively.

Fig. 8 shows that carnosine presents electrostatic interactions only with Lys 388, in contrast to **1a**, which presents electrostatic interactions with Asp 609, Arg599, and Glu490; see Fig. 6.

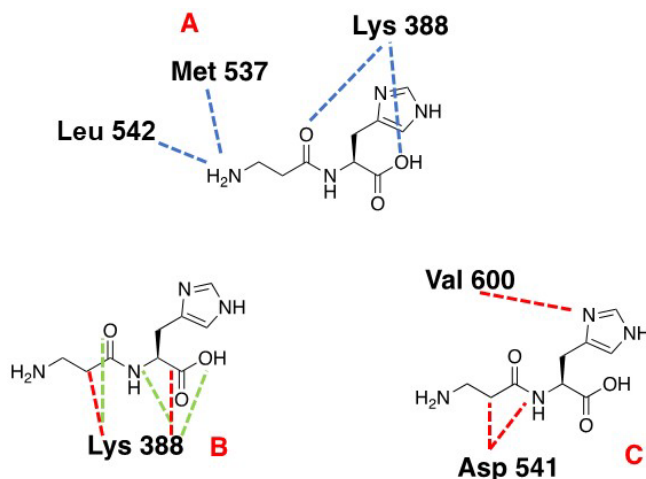


Fig. 8. (A) Hydrogen bond, (B) Electrostatic, and (C) Steric interactions between NS3 and carnosine. Blue lines depict the Hydrogen bond interactions, and Red and green dotted lines show the repulsive and attractive interaction, respectively.

In the case of hydrophobic interactions, the better-interacting cavity presents two hydrophobic surfaces surrounding a hydrophilic surface, see Fig. 9 **1a** presents interactions with both surfaces (hydrophobic) and, in the center, interacts with the hydrophilic surface (Fig. 9(A)). Carnosine only interacts with one hydrophobic surface and the hydrophilic surface in the center of the cavity, see Fig. 9(B). The last can be the cause of finding a higher inhibitory effect with **1a** against serotype DENV4, which is more clearly shown in Fig. 9(C), founding that carnosine, despite presenting a higher Ligand efficiency in the case of the hydrophobic interactions, needs some hydrophilic fragment to promote a better target-ligand interaction.

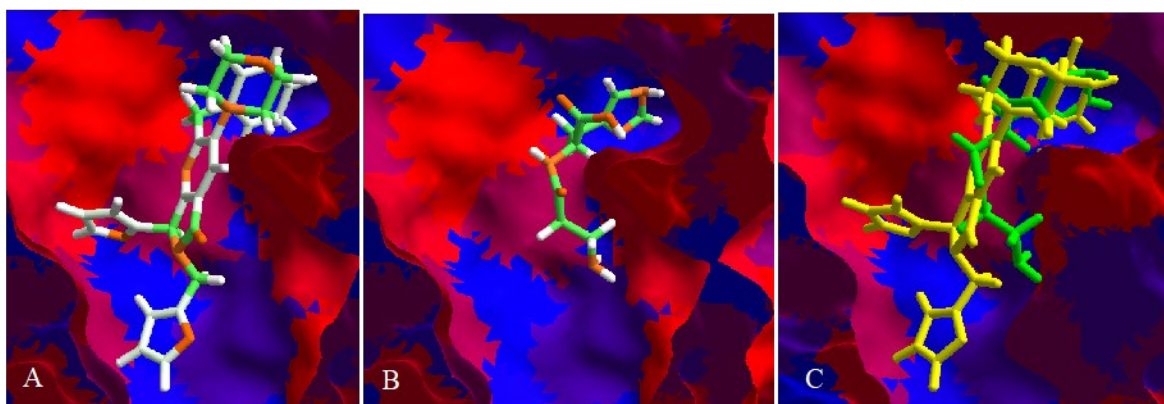


Fig. 9. Hydrophobic interactions between NS3 and A) **1a**, B) carnosine, and C) both molecules. Red surfaces show hydrophilic interactions and blue surfaces show hydrophobic interactions.

Finally, a pharmacophoric model based on **1a** interactions was performed considering the whole ligand-receptor interactions. Fig. 10 shows that one molecule needs mainly six zones to better interact with NS3, these two hydrophobic-aromatic sites, other hydrophilic, and three hydrogen acceptor fragments. In agree with Fig. 9, one ligand proposed to link with NS3 needs only two hydrophobic fragments and one hydrophilic. Besides, Fig. 10 depicts carnosine and **1a** (Fig. 9(B), and 10(D), respectively) over pose into the pharmacophoric model, highlighting the need for two hydrophobic sites in the molecule to better interact with the NS3 target. Note that compounds that present higher LE and are not active can be due to the hydrophilic interactions and the need to modify their bioactive structure to interact with the pharmacophoric sites, such as the aromatic-hydrophobic site. Also, the bioactive pose is proposed around some factors, such as the whole functional groups of the molecule and the interactions of this with the target.

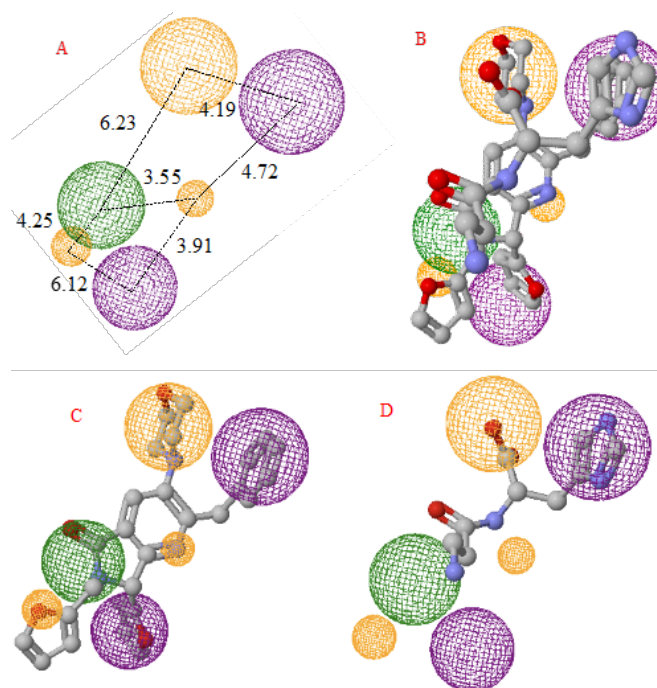


Fig. 10. (A) Pharmacophoric model for NS3 receptor (B) Pharmacophoric model with **1a**, and carnosine overlapping (C) **1a**, and (D) Carnosine into the pharmacophoric model. The purple sphere depicts the hydrophobic-aromatic fragments, the orange sphere is the hydrogen acceptor fragments, and the green sphere is the hydrophilic fragments.

Conclusions

The results indicate that compounds **1a** and **1b** have an antiviral effect in the replicon model of DENV4 and DENV4 infection. The *in vitro* results showed that the compounds **1a** and **1b** exhibit antiviral effect (44.2 and 31.6 % respectively) in Vero cells that express DENV-4 virus. Commonly, replicon results are extrapolated to other DENV serotypes or even to other flaviviruses such as Zika. Interestingly, we show that the inhibition of compounds **1a** and **1b** are specific to DENV4, thus revealing their potential activity against DENV4.

An NS3 model was obtained *via* a homology model and used as a target for the studied molecules. Computational results agree with experimental data, which shows that the polyheterocycle **1a** is the best ligand. Finally, a pharmacophoric model was computed for NS3, which demonstrates that the ligands need two hydrophobic and one hydrophilic fragment.

Acknowledgements

I.M.-S. thanks CONAHCYT – México for her PhD scholarship (947606). A.I.-J. acknowledges “Proyecto Apoyado por el Fondo Sectorial de Investigación para la Educación CONACyT-SEP CB-2017-2018 (A1-S-32582)” for financial support. E.D.-C. acknowledge to Dirección de Apoyo a Investigación y al Posgrado through the Convocatoria Institucional de Investigación Científica (CIIC) 2023, by the financed project 270/2023. Y.R.-A acknowledges to PAPIIT-UNAM IA200821.

References

1. Alcaraz-Estrada, S. L.; Manzano, M. I. M.; Del Angel, R. M.; Levis, R.; Padmanabhan, R. *J. Gen. Virol.* **2010**, *91*, 2713–2718. DOI: <https://doi.org/10.1099/vir.0.024083-0>.
2. Yung, C. F.; Lee, K. S.; Thein, T. L.; Tan, L. K.; Gan, V. C.; Wong, J. G. X.; Lye, D. C.; Ng, L. C.; Leo, Y. S. *Am. J. Trop. Med. Hyg.* **2015**, *92*, 999–1005. DOI: <https://doi.org/10.4269/ajtmh.14-0628>.
3. Bhatt, S.; Gething, P. W.; Brady, O. J.; Messina, J. P.; Farlow, A. W.; Moyes, C. L.; Drake, J. M.; Brownstein, J. S.; Hoen, A. G.; Sankoh, O.; Myers, M. F.; George, D. B.; Jaenisch, T.; William Wint, G. R.; Simmons, C. P.; Scott, T. W.; Farrar, J. J.; Hay, S. I. *Nature*. **2013**, *496*, 504–507. DOI: <https://doi.org/10.1038/nature12060>.
4. Kok, B. H.; Lim, H. T.; Lim, C. P.; Lai, N. S.; Leow, C. Y.; Leow, C. H. *Virus Res.* **2022**, *324*, 199018. DOI: <https://doi.org/10.1016/j.virusres.2022.199018>.
5. Alcaraz-Estrada, S. L.; del Angel, R.; Padmanabhan, R., in: *Dengue. Methods in Molecular Biology*, Vol. 1138, Padmanabhan, R., Vasudevan, S., Eds., Humana Press, New York, NY, **2014**, 131–150. DOI: <https://doi.org/10.1007/978-1-4939-0348-1>.
6. Alcaraz-Estrada, S. L.; Yocupicio-Monroy, M.; Del Angel, R. M. *Future Virol.* **2010**, *5*, 575–592. DOI: <https://doi.org/10.2217/FVL.10.49>.
7. World Health Organization, <https://www.who.int>, accessed in June 2023.
8. Li, Z.; Zhang, J.; Li, H. in *Viral proteases, and their inhibitors*, Gupta, S. P., Ed., Academic Press, **2017**, 163–188. DOI: <https://doi.org/10.1016/B978-0-12-809712-0.00007-1>.
9. Hannemann, H. *Drug Discov. Today* **2020**, *25*, 1026–1033. DOI: 10.1016/j.drudis.2020.03.010.
10. Fernandes, R. S.; Freire, M. C. L. C.; Bueno, R. V.; Godoy, A. S.; Gil, L. H. V. G.; Oliva, G. *Viruses* **2020**, *12*, 598. DOI: <https://doi.org/10.3390/v12060598>.
11. Patil, V. M.; Balasubramanian, K.; Masand, N., in: *Dengue Virus Polymerase: A Crucial Target for Antiviral Drug Discovery*, Gupta, S. P., Ed., Academic Press, **2019**, 387–428. DOI: <https://doi.org/10.1016/B978-0-12-815422-9.00014-0>.
12. Saito, K.; Shimasaki, K.; Fukasawa, M.; Suzuki, R.; Okemoto-Nakamura, Y.; Katoh, K.; Takasaki, T.; Hanada, K. *Virus Res.* **2022**, *322*, 198935. DOI: <https://doi.org/10.1016/j.virusres.2022.198935>.
13. Jones, C. T.; Patkar, C. G.; Kuhn, R. J. *Virology*. **2005**, *331*, 247–259. DOI: <https://doi.org/10.1016/j.virol.2004.10.034>.
14. Satoh, S.; Mori, K.; Ueda, Y.; Sejima, H.; Dansako, H.; Ikeda, M.; Kato, N. *Plos one*. **2015**, *10*, e0118313. DOI: <https://doi.org/10.1371/journal.pone.0118313>.
15. Puig-Basagoiti, F.; Deas, T. S.; Ren, P.; Tilgner, M.; Ferguson, D. M.; Shi, P. Y. *Antimicrob. Agents Chemother.* **2005**, *49*, 4980–4988. DOI: <https://doi.org/10.1128/aac.49.12.4980-4988.2005>.
16. Alcaraz-Estrada, S. L.; Reichert, E. D.; Padmanabhan, R., In: *Antiviral Methods and Protocols. Methods in Molecular Biology*, Vol. 1030, Gong, E. Eds., Humana Press, Totowa, NJ, **2013**, 283–299. DOI: https://doi.org/10.1007/978-1-62703-484-5_22.
17. Kato, F.; Hishiki, T. *Viruses*. **2016**, *8*, 122. DOI: 10.3390/v8050122.
18. Li, J. Q.; Deng, C. L.; Gu, D.; Li, X.; Shi, L.; Zhang, Q. Y.; Zhang, B.; Ye, H. Q. *Antivir. Res.* **2018**, *150*, 148–154. DOI: <https://doi.org/10.1016/j.antiviral.2017.12.017>.

19. Morales-Salazar, I.; Montes-Enríquez, F. P.; Garduño-Albino, C. E.; García-Sánchez, M. A.; Ibarra, I. A.; Rojas-Aguirre, Y.; García-Hernández, M. E.; Sarmiento-Silva, R. E.; Alcaraz-Estrada, S. L.; Díaz-Cervantes, E.; González-Zamora, E.; Islas-Jácome, A. *RSC Med. Chem.* **2023**, *14*, 154–165. DOI: <https://doi.org/10.1039/d2md00350c>.
20. Rothan, H. A.; Abdulrahman, A. Y.; Khazali, A. S.; Nor Rashid, N.; Chong, T. T.; Yusof, R. *J. Pep. Sci.* **2019**, *25*, e3196. DOI: <https://doi.org/10.1002/psc.3196>.
21. García-Ruiz, D.; Martínez-Guzmán, M. A.; Cárdenas-Vargas, A.; Marino-Marmolejo, E.; Gutiérrez-Ortega, A.; González-Díaz, E.; Morfín-Otero, R.; Rodríguez-Noriega, E.; Pérez-Gómez, H.; Elizondo-Quiroga, D. *Springerplus.* **2016**, *5*, 1–9. DOI: <https://doi.org/10.1186/s40064-016-2318-y>.
22. Rao, X.; Huang, X.; Zhou, Z.; Lin, X. *Biostat. Bioinforma. Biomath.* **2013**, *3*, 71–85.
23. Waterhouse, A.; Bertoni, M.; Bienert, S.; Studer, G.; Tauriello, G.; Gumienny, R.; Heer, F. T.; de Beer, T. A. P.; Rempfer, C.; Bordoli, L.; Lepore, R.; Schwede, T. *Nucleic Acids Res.* **2018**, *46*, W296–W303. DOI: <https://doi.org/10.1093/nar/gky427>.
24. Hanwell, M. D.; Curtis, D. E.; Lonie, D. C.; Vandermeersch, T.; Zurek, E.; Hutchison, G. R. *J. Cheminform.* **2012**, *4*, 17. DOI: <https://doi.org/10.1186/1758-2946-4-17>.
25. Perdew, J. P.; Burke, K.; Ernzerhof, M. *Phys. Rev. Lett.* **1997**, *78*, 1396. DOI: <https://doi.org/10.1103/PhysRevLett.77.3865>.
26. Gaussian 09, Frisch, M. J.; Trucks, G. W.; Schlegel, H. B.; Scuseria, G. E.; Robb, M. A.; Cheeseman, J. R.; Scalmani, G.; Barone, V.; Mennucci, B.; Petersson, G. A.; Nakatsuji, H.; Caricato, M.; Li, X.; Hratchian, H. P.; Izmaylov, A. F.; Bloino, J.; Zheng, G.; Sonnenberg, J. L.; Hada, M.; Ehara, M.; Toyota, K.; Fukuda, R.; Hasegawa, J.; Ishida, M.; Nakajima, T.; Honda, Y.; Kitao, O.; Nakai, H.; Vreven, T.; Montgomery, J. A., Jr.; Peralta, J. E.; Ogliaro, F.; Bearpark, M.; Heyd, J. J.; Brothers, E.; Kudin, K. N.; Staroverov, V. N.; Kobayashi, R.; Normand, J.; Raghavachari, K.; Rendell, A.; Burant, J. C.; Iyengar, S. S.; Tomasi, J.; Cossi, M.; Rega, N.; Millam, J. M.; Klene, M.; Knox, J. E.; Cross, J. B.; Bakken, V.; Adamo, C.; Jaramillo, J.; Gomperts, R.; Stratmann, R. E.; Yazyev, O.; Austin, A. J.; Cammi, R.; Pomelli, C.; Ochterski, J. W.; Martin, R. L.; Morokuma, K.; Zakrzewski, V. G.; Voth, G. A.; Salvador, P.; Dannenberg, J. J.; Dapprich, S.; Daniels, A. D.; Farkas, Ö.; Foresman, J. B.; Ortiz, J. V.; Cioslowski, J.; Fox, D. J. Gaussian, Inc., Wallingford CT, **2009**.
27. Thomsen, R.; Christensen, M. H. *J. Med. Chem.* **2006**, *49*, 3315–3321. DOI: <https://doi.org/10.1021/jm051197e>.
28. Yang, J. M.; Chen, C. C. *Proteins* **2004**, *55*, 288–304. DOI: <https://doi.org/10.1002/prot.20035>.
29. Koes, D. R.; Camacho, C. J. *Nucleic Acids Res.* **2012**, *40*, W409–W414. DOI: <https://doi.org/10.1093/nar/gks378>.
30. McAuley, A. J.; Beasley, D. W. C. in: *West Nile Virus. Methods in Molecular Biology*, Vol. 1435, Colpitts, T., Ed., Humana Press, New York, **2016**, 19–27. DOI: https://doi.org/10.1007/978-1-4939-3670-0_3.
31. De Castro Barbosa, E.; Alves, T. M. A.; Kohlhoff, M.; Jangola, S. T. G.; Pires, D. E. V.; Figueiredo, A. C. C.; Alves, É. A. R.; Calzavara-Silva, C. E.; Sobral, M.; Kroon, E. G.; Rosa, L. H.; Zani C. L.; de Oliveira, J. G. *Virol. J.* **2022**, *19*, 31. DOI: <https://doi.org/10.1186/s12985-022-01751-z>.
32. Harcourt, J.; Tamin, A.; Lu, X.; Kamili, S.; Sakthivel, S. K.; Murray, J.; Queen, K.; Tao, Y.; Paden, C. R.; Zhang, J.; Li, Y.; Uehara, A.; Wang, H.; Goldsmith, C.; Bullock, H. A.; Wang, L.; Whitaker, B.; Lynch, B.; Gautam, R.; Schindewolf, C.; Lokugamage, K. G.; Scharton, D.; Plante, J. A.; Mirchandani, D.; Widen, S. G.; Narayanan, K.; Makino, S.; Ksiazek, T. G.; Plante, K. S.; Weaver, S. C.; Lindstrom, S.; Tong, S.; Menachery, V. D.; Thornburg, N. J. *Emerg. Infect. Dis.* **2020**, *26*, 1266. DOI: <https://doi.org/10.3201/eid2606.200516>.
33. Konishi, K.; Yamaji, T.; Sakuma, C.; Kasai, F.; Endo, T.; Kohara, A.; Hanada, K.; Osada, N. *Front. Genet.* **2022**, *13*, 801382. DOI: <https://doi.org/10.3389/fgene.2022.801382>.
34. Ayub, A.; Ashfaq, U. A.; Idrees, S.; Haque, A. *BioResearch Open Access.* **2013**, *2*, 392–396.
35. A) Lee, J.; Worrall, L. J.; Vuckovic, M.; Rosell, F. I.; Gentile, F.; Ton, A. T.; Caveney, N. A.; Ban, F.; Cherkasov, A.; Paetzl, M.; Strynadka, N. C. *Nat. Commun.* **2020**, *11*, 5877. DOI:

- <https://doi.org/10.1038/s41467-020-19662-4>. B) Lee, W. H. K.; Liu, W.; Fan, J. S.; Yang, D. *Biophys. J.* **2021**, 120, 2444–2453. DOI: <https://doi.org/10.1016/j.bpj.2021.04.015>.
36. Soto-Acosta, R.; Jung, E.; Qiu, L.; Wilson, D. J.; Geraghty, R. J.; Chen, L. *Molecules.* **2021**, 26, 3779. DOI: <https://doi.org/10.3390/molecules26133779>.

